



HAL
open science

Rôle des Méninges et des Péricytes dérivés de la Crête Neurale dans les Altérations Cognitives à la Naissance

Emmanuel Bruet

► **To cite this version:**

Emmanuel Bruet. Rôle des Méninges et des Péricytes dérivés de la Crête Neurale dans les Altérations Cognitives à la Naissance. *Development Biology*. Université Paris-Saclay, 2023. English. NNT : 2023UPASL059 . tel-04643382

HAL Id: tel-04643382

<https://theses.hal.science/tel-04643382v1>

Submitted on 10 Jul 2024

HAL is a multi-disciplinary open access archive for the deposit and dissemination of scientific research documents, whether they are published or not. The documents may come from teaching and research institutions in France or abroad, or from public or private research centers.

L'archive ouverte pluridisciplinaire **HAL**, est destinée au dépôt et à la diffusion de documents scientifiques de niveau recherche, publiés ou non, émanant des établissements d'enseignement et de recherche français ou étrangers, des laboratoires publics ou privés.

Role of the Neural Crest-derived Meninges and Pericytes in Cognitive Impairment at Birth

*Rôle des Méninges et des Péricytes dérivés de la Crête Neurale
dans les Altérations Cognitives à la Naissance*

Thèse de doctorat de l'université Paris-Saclay

École doctorale n°568 : signalisations et réseaux intégratifs en biologie (Biosigne)
Spécialité de doctorat : Biologie moléculaire et cellulaire
Graduate school : Life Sciences and Health
Réfèrent : Faculté de médecine

Thèse préparée dans l'unité de recherche **Institut des Neurosciences Paris-Saclay
(NeuroPSI, CNRS, Université Paris-Saclay)**,
sous la direction de **Sophie CREUZET**, Directrice de Recherche, CNRS, Neuro-PSI

Thèse soutenue à Paris-Saclay, le 19 juin 2023, par

Emmanuel BRUET

Composition du Jury

Jean-Loup DUBAND Directeur de recherche, Université Pierre et Marie Curie	Président
Farida DJOUAD Directrice de recherche, Institute for Regenerative Medicine and Biotherapy	Rapporteur & Examinatrice
Heather ETCHEVERS Directrice de recherche, Marseille Medical Genetics	Rapporteur & Examinatrice
Eric BELLEFROID Professeur, Université Libre de Bruxelles	Examineur
Christelle GOLZIO Directrice de recherche, Institut de Génétique et de Biologie Moléculaire et Cellulaire	Examinatrice
Salvador MARTINEZ PEREZ Professeur, Instituto de Neurociencias UMH-CSIC	Examineur

Title: Role of the Neural Crest-derived Meninges and Pericytes in Cognitive Impairment at Birth

Keywords: Behavior, Brain, Vascularization, Meninges, Neural Crest

Abstract: The neural crest is an embryonic multipotent cell population deriving from the neuroectoderm during the neurulation. These cells migrate to colonize the embryonic body and generate different lineages. More specifically in the cephalic region, the cephalic neural crest (CNC) plays a leading morphogenetic role in development. They give rise to the pericytes composing the meninges of the developing forebrain and the stroma of the choroid plexus (CP). Previous work done by the group has shown that the absence of CNC coincides with anencephaly and an absence of CP. Furthermore, the mutations of certain genes identified in humans are correlated to neurodevelopmental syndromes and have neurocristopathy manifestations taking place before cognitive impairment. Altogether, these observations suggest that the CNC can control the homeostasis of the central nervous system, by regulating the biology of the CP through the production of the cerebrospinal fluid and the repertoire of cytokines involved in the brain immunity. In addition to a mechanical protection, we investigate the role of the CNC cells and the meninges in the immunosurveillance of the embryonic brain. More specifically, we investigate the hypothesis that the deregulation of the CNC and their immune functions may cause neurodevelopmental defects associated with cognitive defects and behavioral impairments at birth. To explore this question, we use the chick embryo as a model in which the social interactions can be modelled and analyzed using "filial imprinting".

Due to the accessibility of the avian embryo at all developmental stages, microsurgery is performed in a stage-, space- and tissue-specific manner. In vivo experiments were performed using immunohistochemistry on histological sections of the brain or on whole-mount brains using Light sheet microscopy. To analyze the effect of valproic acid (VPA), an anticonvulsant known to

cause cognitive disorders, on the brain at a cellular level, *in vitro* experiments were performed using immunocytochemistry. Gene expression profiling was also carried out on meninges and pericytes, grown *in vitro*.

When chick embryos are treated with VPA, they exhibit severe alterations in their social interactions after birth and hypervascularization in the brain. Furthermore, pericytes acquire macrophage features. By using an antiangiogenic drug called Sunitinib (Suni) on VPA-treated chicken embryos, a significant rescue of social behavior and hypervascularisation in the brain is observed.

By characterising the phenotype of CNCs, it was possible to describe the ability of these cells to decondense their nuclear material and form extracellular DNA traps. This process called ETosis was first described for neutrophils and circulating blood cells as a defence mechanism against pathogens but has never been described in mesenchymal cells, nor in embryos. When pericytes come into contact with VPA, they generate a decondensation of their DNA, which is found in large proportions in the cytoplasm. DNA filaments are also observed in the extracellular compartment. VPA also tends to inhibit pericyte migration, leading to cooperating cells that produce cytokines and assist VPA-affected cells. With the application of VPA+Suni, migration is partially rescued and is completely rescued with the presence of Suni alone. Our data show that CNC-derived pericytes are professional immune cells that express inflammatory molecules and deregulation of this inflammation would suggest possible adverse effects on the development of cognitive functions in the embryo. This work can open new avenues to further explore the role of CNC-derived pericytes in the aetiology of developmental encephalopathies.

Titre : Rôle des Méninges et des Péricytes dérivés de la Crête Neurale dans les Altérations Cognitives à la Naissance

Mots clés : Comportement, Cerveau, Vascularisation, Méninges, Crête Neurale

Résumé : La crête neurale (CN) est une population de cellules multipotentes issues du neurectoderme, à la neurulation, à l'origine de nombreux lignages. Au niveau céphalique, la CN céphalique (CNC) forme les péricytes qui composent les méninges et le stroma des plexus choroïdes (PC) du cerveau antérieur. Les travaux antérieurs de l'équipe ont montré que l'absence de CNC coïncide avec des anomalies cérébrales, consistant en une anencéphalie sévère et une absence de PC. De plus, certains gènes liés chez l'homme à des syndromes neurodéveloppementaux sont soit régulés précocement par la CNC, soit exprimés par les méninges dérivées de la CNC.

Nous avons exploré le lien entre les altérations de méninges et les troubles du comportement à la naissance, et posé l'hypothèse que la CNC contrôle l'homéostasie et l'immunité intracérébrale du cerveau antérieur. Pour explorer ces questions, nous utilisons l'embryon de poulet comme modèle : nous avons mis au point un ensemble de tests comportementaux reposant sur le réflexe de "l'empreinte filiale". Grâce à l'accessibilité de l'embryon aviaire à tous les stades de développement, des expériences de micro-injection ont été réalisées et analysées par immunohistochimie sur des coupes histologiques, et sur cerveaux entiers clarifiés, en utilisant la microscopie à feuillets de lumière. Un profil transcriptomique a également été réalisé sur des méninges et des péricytes, cultivés *in vitro*.

Lorsque des embryons de poussins sont traités au VPA, un anticonvulsivant connu pour provoquer des troubles cognitifs de type autistiques, ils présentent des altérations sévères de leurs interactions sociales après la naissance et une hypervascularisation dans le cerveau. De plus, nous montrons l'implication de cellules dérivées de la CNC dans la veille immunitaire du cerveau en développement : ces cellules sont capables d'intercepter des agents pathogènes, et confèrent un privilège immunitaire au cerveau. Nos analyses fonctionnelles révèlent que les péricytes dérivés

de la CNC sont des cellules immunitaires professionnelles qui expriment des récepteurs immunitaires et des molécules inflammatoires. Une dérégulation de cette fonction immunitaire par le VPA entraîne des effets néfastes sur l'élaboration des fonctions cognitives. De plus, nous montrons que les cellules périvasculaires sont capables de former des pièges d'ADN qui peuvent s'avérer nocifs en provoquant une réaction inflammatoire incoercible. Les péricytes entrant en contact avec le VPA génèrent une décondensation de leur ADN qui se retrouve en grande proportion dans le cytoplasme. Des filaments d'ADN sont aussi observés dans le compartiment extracellulaire. Le VPA tend également à empêcher la migration des péricytes, conduisant à des cellules coopérantes qui produisent des cytokines et aident les cellules affectées par le VPA.

L'utilisation d'un médicament antiangiogénique, le Sunitinib (Suni) permet un sauvetage significatif du comportement social, de l'hypervascularisation dans le cerveau, et de la fonction immunitaire des cellules méningées.

En révélant que ces cellules sont dotées de capacités macrophagiques, et capable de phagocyter des agents pathogènes, nous montrons l'implication des péricytes comme cellules immunocompétentes dans la surveillance immunitaire du cerveau en développement. Nos travaux introduisent un nouvel acteur cellulaire, les cellules périvasculaires dérivées de la CNC, dans la défense du cerveau contre les intrusions pathogènes. Comprendre ces mécanismes présente des implications biomédicales qui revêtent une importance toute particulière pour éclairer l'origine de troubles du comportement, considérés jusqu'à présent comme « cerveau autonome » mais dont nous montrons qu'ils peuvent impliquer des cellules méningées défectueuses.

ACKNOWLEDGEMENTS

First and foremost, I would like to express my sincere gratitude to my Thesis supervisor, Dr. Sophie Creuzet. I am extremely honored to have had the opportunity to work in her laboratory since the first year of my Master's degree. During my academic studies, I have had the chance to benefit not only from her immense scientific knowledge, particularly in developmental biology, but also from her invaluable advice in improving my lab skills and presenting my work to the scientific community. I am also incredibly grateful for her continuous support in every step of my PhD journey.

I would also like to express my deepest appreciation to all the members of my Thesis jury, especially to Dr. Farida Djouad and Dr. Heather Etchevers for accepting to read my research work, as well as Dr. Eric Bellefroid, Dr. Jean-Loup Duband, Dr. Salvador Martinez Perez and Dr. Christelle Golzio.

I also appreciate all the support from my defence committee, Dr. Christelle Golzio and Dr. Sylvie Granon, who generously provided knowledge and expertise to improve my work.

I am deeply indebted to both the previous and the actual CNRS / Neuro-PSI directors, Dr. Philippe Vernier and Dr. François Rouyer, for trusting and accepting me in their Institute. Similarly, this endeavour would not have been possible without the generous support from the University of Paris-Saclay and from the Doctoral School Biosigne, directed by Dr. Oliver Nüsse. I am extremely grateful for their IDEX funding.

This journey would never have been possible without my Master 2 directors, Dr. Hervé Daniel and Dr. Karim Benihoud, who gave me the opportunity to find Dr.

Creuzet's lab, trusted me in their course and made me discover the world of neuroscience.

I would like to extend my sincere thanks to Jérôme Bignon and Laurie for their help in carrying out the Western-Blot experiments, as well as to Dr. Anne Poliard, Dr. Lotfi Slimani and Jérémy Sadoine for their help with the micro-computed tomography (micro-CT). Moreover, I am extremely grateful to Aurélie Heuzé for sharing her knowledge in Light sheet microscopy with me, to Dr. Juliette Bitard for her patience in explaining all the rules of the culture room and to Hélène Faure for all her help with the epifluorescence microscopy.

A special thanks to my lab colleagues. To Alexandra Vargas, my thesis partner, thank you for always giving me useful advice and for supporting me when I was feeling down. This thesis would definitely have not been the same without you. To Diego Amarante, thank you for sharing with me all your scientific knowledge and experience, and it was a real pleasure sharing this fascinating work with you. To Tatiana Gorojankina, thank you for always giving me feed-back on my work. To Rémy Gars, I could not thank you enough for your input with analyzing the chick behavioral tests. I would also like to thank our previous colleagues, Antonia Amicone, Margaux Piechon, Caroline Gora and Fanny Detroyat for all the great times we had together.

During my PhD course, I have had the pleasure of meeting so many fascinating people including my Master's colleagues with whom we have done our PhD together, Catherine Hottin and Elie Partouche, and my Italian colleagues and car-poolers Mariagiovanna Russo and Giovanni Usseglio. I'd also like to thank Nastasia Mirofle, Dylan Manceau, Laurine Gonzalez and Maxime Lehman for the fun breaks we had after work.

My appreciation also goes out to my family for their encouragement and support all through my studies. I cannot express how grateful I am for my parents who have encouraged and supported me endlessly during my entire studies and who have always been present, especially at the most difficult times. I specifically want to thank my father for all his help in analyzing the chicks' behavioral tests. I could not have asked for better brothers, Julien and Shaam thank you for always encouraging me to do my best. Charlotte and Mathilde, I am so pleased to call you my family and you are an inspiration for my professional life. Romane and Gabrielle, you have brought so much joy in my life since a year!

Lastly, I could not be luckier to have such supporting friends, especially "Les 6 compagnons", Julie and Théo, Etienne and Deb, Gwen and Mathieu, Alex and Philipine, I hope to spend many more holidays with you in the future. I'd finally like to thank my friends from school, Hortense, Marie-Cécile and Rémy, Paul-Eloi and Jordan, Gabrielle and Francky.

ABBREVIATIONS

°C	Degrees Celsius
%	Percent
αSMA	α-smooth muscle actin
μg	Microgram
μL	Microliter
μm	Micrometer
2D	Two-dimensional
3D	Three-dimensional
3DISCO	Three-dimensional imaging of solvent-cleared organs
3V	Third ventricle
4V	Fourth ventricle
Aβ	Amyloid β-peptide
AD	Alzheimer's disease
ANR	Anterior neural ridge
APP	Amyloid-beta precursor protein
ASD	Autism spectrum disorder
BA	Branchial arch
BBB	Blood brain barrier
BMP	Bone morphogenetic protein
bp	Base pair
BSA	Bovine serum albumin
Ca²⁺	Calcium ion
CAMs	Non-parenchymal CNS-associated macrophages
CCL2	C-C motif chemokine ligands 2
CCR2	C-C chemokine receptors 2
CD	Cluster of differentiation
cDNA	Complementary deoxyribonucleic acid
Cit-H3	Citrullinated histone 3
Cit-H4	Citrullinated histone 4
Cl⁻	Chloride ion
CMV	Cytomegalovirus
CNC	Cephalic neural crest
CNS	Central nervous system
CP	Choroid plexus
CPMs	Choroid plexus macrophages
CS	Carnegie stage

CSF	Cerebrospinal fluid
CSF-1R	Colony stimulating factor 1 receptor
CTL	Control
DBE	Benzyl ether
DCM	Dichloromethane
DKK	Dickkopf-related protein
DLHP	Dorsal lateral hinge points
DMEM/F-12	Dulbecco's Modified Eagle Medium/Nutrient Mixture F-12
DNA	Deoxyribonucleic acid
E	Embryonic day
<i>E. coli</i>	Escherichia coli
EMPs	Erythromyeloid progenitors
EMT	Epithelial-to-mesenchymal transition
EMX	Empty spiracles homeobox
EtOH	Ethanol
FBS	Fetal bovine serum
FGF	Fibroblast growth factor
FLT-3	Fms-like tyrosine kinase 3
FOXG	Forkhead box G
FSNC	Facial Skeletogenic Neural Crest
Fung	Amphotericin B anti-fungal
GABA	γ -aminobutyric acid
GABA_AR	GABA _A receptor
GAD	Glutamic acid decarboxylase
GS	Goat serum
h	Hours
HAT	Histone acetyl transferase
HDAC	Histone deacetylase
HDM	Histone demethylase
HH	Hamburger-Hamilton stages
HIV	Human Immunodeficiency Virus
HMT	Histone methyltransferase
Hox	Homeobox gene
HSV-1	Herpes Simplex Virus
Iba1	Ionized calcium binding adaptor molecule 1
ID	Inhibitor of DNA binding protein
IFN	Interferon
IL	Interleukin
K⁺	Potassium ion
Kg	Kilogramme

KIT	Stem cell factor receptor
LAS AF	Leica Application Suite, Advanced Fluorescence
LC-MS	Liquid chromatography–mass spectrometry
LPS	Lipopolysaccharide
LTA	Lipoteichoic acid
LV	Lateral ventricles
M	Molar
MAC1	Macrophage-1 antigen
MECP	Methyl CpG binding protein
MeOH	Methanol
mg	Milligram
MHC	Major histocompatibility complex
MHP	Medial hinge point
MIA	Maternal immune activation
Micro-CT	Micro-computed tomography
min	Minutes
mL	Milliliter
mM	Millimolar
mm²	Square millimeter
MMs	Meningeal macrophages
MPO	Myeloperoxidase
mRNA	Messenger ribonucleic acid
ms	millisecond
Msh	Muscle segment homeobox gene
MSX	Homeobox protein (vertebrate homologous to the <i>Drosophila</i> msh)
mTORC1	Mammalian target of rapamycin complex 1
Na⁺	Sodium ion
NC	Neural crest
NCC	Neural crest cells
NE	Neutrophil elastase
NET	Neutrophil extracellular trap
NG	Neural/glial antigen
ng	Nanogram
NOX	NADPH oxidase
NT	Neural tube
NVU	Neurovascular unit
OTX	Orthodenticle homeobox
PAMPs	Pathogen associated molecular patterns
PAX	Paired box protein
PBS	Phosphate-buffered saline

PDGF	Platelet-derived growth factor
PDGFR	Platelet-derived growth factor receptor
PK	Protein kinase
PMA	Phorbol 12-myristate 13-acetate
PNS	Peripheral nervous system
PP	Protein phosphatase
PRRs	Pattern recognition receptors
PS	Penicillin-streptomycin antibiotic
pS6	Phosphorylated ribosomal protein S6
PVMs	Brain perivascular macrophages
QCPN	Quail non-Chick Peri-Nucleolar
r	Rhombomere
RNA	Ribonucleic acid
RTK	Receptor tyrosine kinase
s	Second
scRNA-seq	Single cell RNA sequencing
SEM	Standard error of the mean
SHANK	SH3 And Multiple Ankyrin Repeat Domains
SHH	Sonic hedgehog
SIX	Sine oculis homeobox
SLC	Solute carrier
Smad	Small mothers against decapentaplegic
SMC	Smooth muscle cells
ss	Somites stage
Suni	Sunitinib
SVZ	Subventricular zone
TFM	Tissue freezing medium
TLR	Toll-like receptor
TNC	Truncal neural crest
TNF	Tumor necrosis factor
VEGF	Vascular endothelial growth factor
VEGFR	Vascular endothelial growth factor receptor
VPA	Valproic acid
vSMC	Vascular smooth muscle cells
VSU	Valproic acid + Sunitinib
VZ	Ventricular zone
WNT	Wingless
ZEB	Zinc finger E-box binding homeobox
ZIC	Zinc finger protein

CONTENTS

Acknowledgements	4
Abbreviations	7
Contents	11
Figures	16
Preamble and objectives of this PhD project	19
Introduction.....	22
I. Neural crest implication in the evolution of the anterior central nervous system ..	22
1. Deuterostome evolution.....	22
2. Neural crest and vertebrate evolution.....	22
3. Gene regulatory network and vertebrate evolution	27
II. Early development of the central nervous system	29
1. Gastrulation	29
2. Vertebrate neurulation and neural crest emergence.....	30
3. Formation of the brain vesicles.....	32
4. NC emigration along the antero-posterior axis.....	36
5. Identification of the NCC fate	36
6. Regionalization of the neural crest.....	40
III. Singularity of the cephalic neural crest.....	42
1. Morphogenetics of the craniofacial and brain development	42
2. Neural crest contribution to the branchial vascular sector	49
3. NC contribution to the meninges	51
4. NC contribution to the pericytes.....	53
5. Pericyte identifications, structural and surface markers.....	54
IV. Vascular network development	60
1. Vasculogenesis	62
2. Angiogenesis.....	62
V. Contribution of the meninges to the choroid plexus.....	65
1. Formation of the falx cerebri.....	66
2. Choroid plexus functions and development.....	68
3. CSF in the homeostasis of the brain	70
4. Early roles of the CSF.....	72
5. CSF movement and outflow	75
6. CSF barriers and immune functions.....	75
7. Kolmer's cells, choroid plexus macrophagic cells.....	78

VI. Cephalic meninges and CP physiopathology during development	81
1. Falx cerebri malformation	81
2. Syndrome/disorders with neurocristopathy manifestations	83
VII. Infection impact on cognitive behavior at birth.....	85
1. Maternal infections impact fetal neurodevelopment	85
2. Molecular impact on fetal neurodevelopment	87
3. The macrophages of the embryonic brain	90
VIII. ETosis, a defence mechanism involving extracellular DNA traps.....	92
1. Core histones and epigenetic modifications	92
2. PAD4 generates citrullination of histones	93
3. NETs and ETosis	94
IX. In utero valproic acid (VPA) generates autistic behaviors in neonates	99
1. VPA, a widely used anticonvulsant	99
2. VPA, a potent teratogen when administrated in utero.....	101
3. Anti-angiogenic effect of VPA in neonates.....	104
4. VPA effect on embryonic brain vascularization	104
X. Sunitinib, an anti-angiogenic used in cancer treatments	105
1. Sunitinib exhibits anti-angiogenic effects.....	105
2. Sunitinib is an anti-tumoral target.....	105
3. Sunitinib used to counteract VPA-induced phenotypes	106
Specific objectives and hypotheses	107
Methods and Material	110
I. Microsurgery in chick embryos	110
1. Chick embryo model.....	110
2. Stage-specific embryos	110
II. Embryo manipulation and VPA injection	110
III. Histological preparations.....	112
1. Embedding and microtome sections	112
2. Immunohistochemistry.....	112
3. Confocal microscopy	113
IV. Immunofluorescence markers used for the study of meninges and pericytes	113
V. Brain dissection and immunohistochemistry for Light sheet microscopy.....	113
1. Whole-brain dissections and fixation.....	113
2. Immunohistochemistry.....	115
3. Whole-mount brain clearing using the 3DISCO protocol	115
4. Light sheet microscopy	116
VI. In vitro experimental design: meningeal cell cultures	116

1.	Pericytes culture using inserts	116
2.	Immunocytochemistry	118
3.	Cell analysis	118
VII.	3D ex vivo system: choroid plexus explants	119
1.	CP development in a dish	119
2.	Immunohistochemistry of CP.....	120
VIII.	Morphometric analyses and 3D rendering.....	120
1.	Lugol staining and Micro-computed tomography acquisition (Micro-CT).....	120
2.	Cephalic and facial measurements	121
3.	Brain's ventricle measurements	121
4.	Measurements of the blood vessels	122
5.	CP explant analysis	122
IX.	RNA sequencing: transcriptomic analysis on meninges and pericyte cultures	123
X.	Proteomic analysis on CSF	125
1.	Preparation of samples and dosage	127
2.	Preparation of samples before gel deposition	127
3.	Liquid transfer	129
4.	Membrane blocking and antibody incubation.....	129
5.	Revelation by chemoluminescence	129
XI.	Behavioral tests	129
XII.	Statistical analysis	131
Results	132
I.	Analyses of the prosencephalic vascular network.....	132
1.	VPA induces hypervascularization in brain parenchyma	135
2.	Sunitinib tends to limit brain hypervascularization yielded by VPA	136
II.	Cephalic and facial morphometric analyses	136
1.	VPA impacts the facial and brain morphologies of E8 embryos	140
2.	Sunitinib does not restore facial and brain morphologies in VPA-treated embryos. 141	
III.	Filial imprinting to model the elaboration of social interactions at birth.....	143
1.	Video recording tracking to study social interactions at birth	143
2.	VPA generates severe alterations in social interactions at birth	143
3.	Sunitinib tends to restore social behavior at birth.....	146
4.	Behavioral scoring to study social interactions at birth	146
5.	VPA increases aversive behaviors at birth.....	154
6.	Sunitinib tends to normalize attachment behaviors at birth.....	154
IV.	The cephalic neural crest-derived pericytes harbour immune capacities	155
1.	Pericytes exhibit high migration capacity in vitro, hindered by VPA.....	156

2.	The pro-immune properties of pericytes are enhanced with VPA.....	157
3.	The phagocytosis capacities of pericytes are exacerbated with VPA	161
4.	VPA deregulates the expression of macrophage-related genes in pericytes	162
5.	Toxic or septic insults toward pericytes yield distinct immuno-responsive profiles.	163
V. The cephalic neural crest-derived pericytes are an active component of the neurovascular unit.....		166
1.	VPA impairs the expression of genes involved in neural control of vasomotricity ...	166
2.	VPA targets glutamatergic and GABA-ergic signaling	167
3.	VPA affects gene expression of ion channels regulating vasomotricity	170
4.	Divergent neurovascular unit in embryos versus adults.....	172
5.	VPA impacts neurodevelopmental genes.....	173
6.	VPA enhances neurodegenerative targets	174
VI. The cephalic neural crest-derived pericytes can promote DNA shedding and generate ETosis to form DNA traps.....		175
1.	Chromatin decondensation from noxious insults.....	175
2.	Chromatin decondensation from septic insults	179
3.	VPA interferes in genes coding for chromatin remodeling proteins	179
4.	Noxious insults affect ETosis effectors, PAD4, Cit-H4 and Cit-H3	180
5.	VPA deregulates the expression of genes coding for ETosis markers.....	181
VII. DNA shedding and ETosis occur <i>in vivo</i>		182
1.	Pericytes disperse DNA in the parenchyma of VPA-treated brains	182
2.	Pericytes may disperse DNA and proteins in the CSF of the LV	182
3.	Choroid plexus may have a role in brain immunity by conditioning the CSF.....	186
Discussion		196
I. PhD overview: achievements and significance.....		196
1.	The development of social behavior at birth can be modeled by studying imprinting reflex	196
2.	Aberrant meningeal and intracerebral vascular network precede behavioral disorders	197
3.	Anti-angiogenic treatments restore social behavior at birth.....	197
4.	Embryonic perivascular cells are endowed with immune properties	198
5.	Perivascular cells develop DNA traps in response to pathogenic stimuli	198
II. NC-derived meninges' role in social behavior at birth.....		199
III. NC-derived meninges' role in craniofacial development.....		203
IV. NC-derived meninges' pro-neurogenic role.....		206
V. NC-derived meninges' role in immune surveillance		207
VI. NC-derived meninges' plausible role in carbohydrate metabolism		210
Conclusion and future directions		213

References 216
Review 245

FIGURES

INTRODUCTION

Figure 1. Deuterostome phylogeny.	23
Figure 2. The GRN underlying NC development.	28
Figure 3. . Migration of endodermal and mesodermal cells through the primitive streak.	31
Figure 4. Scanning electron microscopy of the origin of the NC.	33
Figure 5. Primary and secondary neurulation and the transition zone between them.	34
Figure 6. Brain vesicles and the origin of meninges.	35
Figure 7. Derivatives of the NC according to their level of origin along the anteroposterior axis.	37
Figure 8. Quail-chick chimeras for investigating the fate of avian NCC.	39
Figure 9. Overview of NC subpopulations along the anteroposterior axis.	41
Figure 10. The CNC: fate map and <i>Hox</i> gene expression.	43
Figure 11. Contribution of the NC to head development.	45
Figure 12. The FSNC controls cephalic neural tube closure.	46
Figure 13. The FSNC regulates the morphogenetic activity of brain organizing centers.	48
Figure 14. Role of the <i>Six</i> genes in cephalic development.	48
Figure 15. Contribution of the CNC to the cardiovascular system.	50
Figure 16. Anatomy of the meninges surrounding the anterior brain.	52
Figure 17. Pericyte Anatomy.	55
Figure 18. The meninges and brain vasculature.	57
Figure 19. Schematic representing the differential distribution of mural cell markers in the vascular tree.	61
Figure 20. Seven critical steps of the angiogenic response.	64
Figure 21 The NC-derived meninges form the falx cerebri.	67
Figure 22. 3D <i>ex vivo</i> explant of a CP.	69
Figure 23. Contribution of the CNC to the CP.	69
Figure 24. Representative 3D image of the CP.	71
Figure 25. Summary of histological findings of CP between CS18 and CS23.	73
Figure 26. Comparison of T2-weighted images.	73
Figure 27. Mass Spectrometry reveals dynamic changes in CSF proteome as it differentiates from E8.5 amniotic fluid (AF) to E14.5 CSF.	74
Figure 28. Schematic representation of the major CSF pathways.	76
Figure 29. Directionality of CSF movement is partially dependent on heartbeat at early larval stage.	76
Figure 30. Schematic diagram of the blood–CSF barrier.	77
Figure 31. Kolmer’s cell	79

Figure 32. Elongated falx cerebri, separating the two brain hemispheres in the forebrain leads to a total absence of corpus callosum.	82
Table 1. Mutations in specific genes generate neurocristopathy manifestations taking place before cognitive impairment.	84
Figure 33. Physical barriers of the brain in normal physiology and infection.	86
Table 2. Inflammatory signatures of viruses and their neurological consequences.	88
Figure 34. MIA as a disease primer.	91
Figure 35. Citrullination (deimination) of peptidylarginine by PAD.	95
Figure 36. Scanning electron micrograph of purified human neutrophils.	96
Figure 37. NET formation pathways.	98

METHODS AND MATERIAL

Table 3. List of antibodies used in immunofluorescence.	114
Table 4. List of samples analyzed for bulk RNA sequencing.	124
Table 5. List of samples analyzed for Nanostring.	124
Table 6. List of 40 genes selected for Nanostring.	126
Table 7. List of CSF samples collected for proteomic analysis.	128

RESULTS

Figure 38. Sunitinib limits hypervascularization in brain parenchyma induced by VPA.	133
Figure 39. Sunitinib does not restore microcephaly induced by VPA.	138
Figure 40. Sunitinib tends to restore social interactions at birth altered by VPA.	144
Figure 41. Sunitinib tends to restore attachment behaviors and reduce aversive behaviors of newborn chicks treated with VPA.	148
Figure 42. Sunitinib tends to restore socialization compared to VPA-treated chicks.	150
Figure 43. Sunitinib tends to reduce anxiety compared to VPA-treated chicks.	152
Figure 44. The CNC-derived pericytes harbour immune capacities.	159
Figure 45. The CNC-derived pericytes are an active component of the NVU.	168
Figure 46. The CNC-derived pericytes promote DNA shedding and generate ETosis to form DNA traps.	177
Figure 47. DNA shedding and ETosis occur <i>in vivo</i>	184
Figure S1. Morphometric analyses of the face.	187
Figure S2. Meningeal NC-derived pericytes provide a homogeneous α SMA(+) cell population under fibronectin-coated cell culture plates and co-express specific pericyte markers.	188
Figure S3. Meningeal NC-derived pericytes present a macrophage-like and immune profile and VPA treatment modulates this profile.	189
Figure S4. Meningeal spinal cord mesoderm-derived pericytes express macrophage markers at a lower level than meningeal prosencephalon NC-derived pericytes.	191

Figure S5. Pericytes present DNA decondensation and produce ETosis *in vitro*. Noxious insults increase the inflammatory profile of pericytes. **193**

Figure S6. 3D *ex vivo* system to develop CP in a Petri dish. **195**

DISCUSSION

Figure 48. The CNC-derived meninges and pericytes' roles in brain homeostasis during development and in neonatal behavior. **200**

Figure 49. The CNC-derived meninges regulate the insulin pathway and VPA modulates this pathway. **212**

Figure 50. Multi-systemic role of the CNC-derived meninges and pericytes..... **215**

PREAMBLE AND OBJECTIVES OF THIS PHD PROJECT

Phylogenetically, among the chordates, the vertebrates undergo an evolutionary transition from the protochordates as they are characterized by the spectacular formation of a “New Head” (Aguiar et al., 2014). Specifically, vertebrates are distinguished by the development of the forebrain, the emergence of craniofacial and associated sense organs (Garcez et al., 2014), and the acquisition of myelin (for review, Zalc, 2016). This process of encephalization, allowing the development of cognitive functions in vertebrates, coincides with the appearance of the neural crest (NC) (Creuzet et al., 2006). The NC cells (NCC), first appearing during neurulation at the lateral borders of the neural plate, delaminate and migrate along the antero-posterior axis of the vertebrate body to differentiate into a large variety of cell types (Williams et al., 2022). Depending on their anatomical destination, the NCC can be divided in four distinct groups, including the cephalic NC (CNC) (Gilbert, 2019). At the cephalic region, the CNC give rise, inter alia, to the meninges covering the forebrain and specifically to the pericytes underlying the blood vessels (Couly et al., 1995; Etchevers et al., 1999). Moreover, the CNC also gives rise to pericytes underlying the blood vessels in the stroma of the choroid plexus (CP) contained in the brain’s ventricles.

During the embryonic development, the cerebrospinal fluid (CSF) is separated by the blood system by the CSF-blood interface. This interface, lacking real blood-brain barrier (BBB), leads to the possible entrance for infection or intoxication from the CSF to the brain via the CP (Llovera et al., 2017). Thus, in case of maternal infection during pregnancy, several pathogens infecting pregnant mothers can cross the fetal BBB to infect the developing central nervous system (CNS). This

infection could lead to an inflammatory response sufficient to generate developmental abnormalities in the fetus (for review, Ganguli and Chavali, 2021). Before I arrived in the laboratory, the team had investigated the role of the CNC, besides its structural role in craniofacial structures, in the formation of the brain. Precisely, they had studied the precocious potent morphogenetic and paracrine CNC effect on the development of the brain and sense organs (for review, Creuzet, 2009a; Creuzet et al., 2002, 2006; for review, Le Douarin et al., 2012; Garcez et al., 2014). Even though the control of the CNC cells on the vertebrate encephalization had been studied at embryonic stages, the possible role of the CNC cells on brain homeostasis, at later fetal stages, has never been examined.

Several neurodevelopmental syndromes and disorders involving gene mutations have neurocristopathy manifestations taking place before cognitive impairment at birth (Brunelli et al., 1996; Gregory et al., 2021; for review, Kyle et al., 2018; Papa et al., 2008). We hypothesized that these neurodevelopmental syndromes and disorders involve genes regulated by CNC cells or expressed later in development in CNC-derived meninges. We investigated the hypothesis that the deregulation of the CNC may cause neurodevelopmental defects associated with cognitive defects and behavioral impairments at birth.

The goal of this PhD project is to explore how the NC and more specifically the CNC, implicated in the early development of the anterior CNS and providing the meninges, its pericytes and the stromal CP of the developing vascular network, exerts a deterministic and biological role in brain development and homeostasis. To this purpose, we test the insults induced by valproic acid (VPA) on CNC-derived meninges function, alterations in the vascularization and brain homeostasis. More precisely, using experimental models that mimic developmental autistic disorders, we elucidate the involvement of CNC-derived meninges in social impairments at

birth. In addition, we characterize the immunosurveillance role of the CNC-derived pericytes during early development. When exposed to septic insults, *Escherichia coli* (*E. coli*), CNC-derived pericytes trigger a defense mechanism similar to neutrophil extracellular traps (NET) or ETosis ([Brinkmann et al., 2004](#)). Finally, we found that application of another drug, Sunitinib (Suni) together with VPA partly suppress VPA-induced defects.

INTRODUCTION

I. Neural crest implication in the evolution of the anterior central nervous system

1. *Deuterostome evolution*

The deuterostomes are characterized by the formation of the posterior blastopore, by the formation of a mouth at the opposite end of the embryo and by a digestive tract developed in the middle, connecting the two (for review, Baker and Bronner-Fraser, 1997). These invertebrates possess three germ layers: ectoderm, mesoderm and endoderm. However, they are characterized by the lack of the notochord, a flexible rod-like structure of mesodermal origin, and are therefore defined as non-chordates deuterostomes (Hall, 1999).

Unlike non-chordates deuterostomes, chordates possess a dorsal hollow nerve cord, a notochord, a muscular post-anal tail and a perforated muscularised pharynx, with pharyngeal ciliated slits modified for gill-based respiration and suction feeding (Baker, 2008; for review, Baker and Bronner-fraser, 1997; Hall, 1999). In addition to the protochordates body plan, chordates contain a CNS. The protochordates, non-vertebrate chordates, include urochordates (tunicates and ascidians) and cephalochordates (amphioxus) (Baker, 2008) (Fig. 1).

2. *Neural crest and vertebrate evolution*

Among the chordates, vertebrates are specifically characterized by the appearance of the NC (Fig. 1). The emergence of the NC is responsible for the formation of a “New Head” (Gans and Northcutt, 1983; Le Douarin, 1982) characterized by the spectacular development of the forebrain, the emergence of

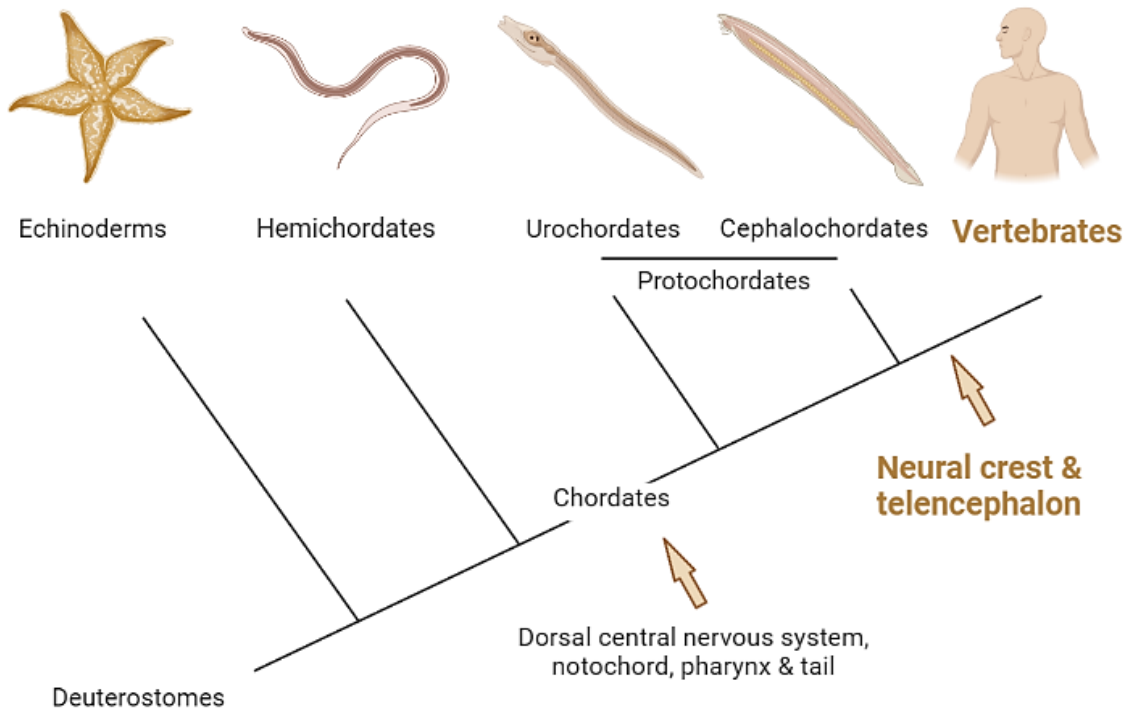


Figure 1. Deuterostome phylogeny. The deuterostomes are characterized by the formation of the posterior blastopore, by the formation of a mouth at the opposite end of the embryo and by a digestive tract developed in the middle, connecting the two. Unlike non-chordates deuterostomes (echinoderms and hemichordates), chordates possess a dorsal hollow nerve chord, a notochord, a perforated pharynx, and a muscular post-anal tail. Vertebrates are specifically characterised by the simultaneous appearance of the neural crest and the anterior brain called the telencephalon. [Created with Biorender.com.](#)

craniofacial and associated sense organs (Garcez et al., 2014), and the acquisition of myelin (for review, Zalc, 2016).

a. Expansion of the anterior forebrain

The development of the CNC coincides with the process of encephalization, characterizing the evolution transition from the protochordates to the vertebrates (Martínez-Cerdeño et al., 2018; Northcutt, 2002). More specifically the CNC enhances the development of the most evolutionarily recent part of the CNS, the telencephalon (Aguiar et al., 2014; Creuzet, 2009a; Garcez et al., 2014). During the early embryonic stage in vertebrates, the CNC migrates along the antero-posterior axis to regulate the expression of morphogens for the organization of the CNS and more specifically in brain organizers for the development of the anterior forebrain. These morphogenetic factors determine the spatial specification of the CNS. The ventro-dorsal axis of the embryo is determined by the inhibition of ventralizing factors such as Sonic hedgehog (SHH) at the basal plate and by the activation of dorsalizing factors like bone morphogenetic proteins (BMPs) and Wingless (WNT) at the dorsal midline. The antero-posterior specification is determined by the regulation of fibroblast growth factor (FGF) 8 in secondary organizers: the anterior neural ridge (ANR) at the anterior end of the neural plate and the isthmus organizer at the mid – hindbrain transition (for review, Echevarría et al., 2003). FGF8, initially in the ANR, initiates a signaling pathway by interacting with CNC-derived small mothers against decapentaplegic (SMAD) 1. This interaction leads to the expression of *Dickkopf-related protein 1 (dkk1)* acting upstream of *Noggin* and *Gremlin* for the induction of *Forkhead box G (foxd) 1* expression in the telencephalon. The *FoxG1* transcription factor is essential for the differentiation of the prosencephalon between telencephalon and diencephalon (Aguiar et al., 2014; Creuzet, 2009a).

b. Emergence of the craniofacial organs

In addition to an increased forebrain, the specification of the NC coincides with the emergence of the face and associated sense organs (Garcez et al., 2014). The contribution of the CNC predominates in the development of the cephalic region by giving rise to the musculo-conjunctive, skeletogenic, perivascular, and meningeal structures of the cranio-facial region (Le Douarin and Kalcheim, 1999). In the rest of the body, these derivatives develop from the mesoderm origin. During the evolution, NCC overtake mesodermal tissues to develop the cranio-facial structures of the vertebrates (for review, Creuzet, 2009a). In comparison the amphioxus, devoid of NCC, lacks a craniofacial skeleton and has a very rudimentary anterior CNS (Creuzet, 2009b). Even the most primitive living vertebrates, cyclostomes (lampreys and hagfish), already have most of the NC and placode derivatives but not all. The emergence of craniofacial bone, such as the upper and lower jaws of gnathostomes (jawed vertebrates) from the first branchial arch, and the development of sensory placodes have led to the adaptation of the environment by facilitating predator behavior. Thus, the sophistication of specialized senses and the integration of sensory information may have coincided with the growth of the forebrain and craniofacial structures (Bronner and LeDouarin, 2012).

Interestingly, the migrating NC marker HNK1 present in vertebrates did not recognize any cells in amphioxus embryos (Holland and Holland, 2001). However, even though no intermediate forms of rudimentary NC and placodes were found, NC and placodes cannot have appeared spontaneously. Thus, their precursors must have evolved from a common deuterostome ancestor and whereas they have persisted and developed in vertebrates, these precursors must have disappeared in urochordates and cephalochordates (for review, Baker and Bronner-Fraser, 1997; Medeiros, 2013). Therefore, potential NC- and placodes-like precursors present in the common ancestor of the chordates must exist in non-

vertebrate chordates and/or in non-chordate deuterostomes. Although NC marker genes were expressed at the edges of the neural plate and/or adjacent nonneural ectoderm of protochordates, these cells do not present the multipotency and migratory characteristics of NCC (Holland and Holland, 2001). Therefore, despite presenting the beginnings of a genetic programme for NC formation, unlike in the protochordates, the programme allowed the development of definitive NC in the vertebrates. This suggests that some of the genetic machinery for generating NC was already in place in the common ancestor of the protochordates and the vertebrates (Holland and Holland, 2001), and even in invertebrates (Medeiros, 2013; for review, York and Mccauley, 2020).

c. The acquisition of myelin

During development, the NC gives rise to the Schwann cells. These glial cells form the myelin sheaths surrounding neuronal axons in the peripheral nervous system (PNS) (Armati and Mathey, 2013). The myelin sheaths have three major roles in the nervous system: they protect the neuronal axons of the nervous system, they accelerate the conduction of nerve influx (for review, Zalc, 2016) and they support the integrity of neurons by providing nutrient (Morrison et al., 2013).

The speed of the nerve influx transmission can only be accelerated either by increasing the diameters of the neuronal axons or by surrounding these axons with a myelin sheath (Morrison et al., 2013). In invertebrates, the increase of the axonal diameter, observed in cephalopods (squid and octopus), is limited to the neurons involved in the rapid escape response. However, in vertebrates, the whole CNS is confined to the skeletal structure, the brain in the skull and the spinal cord in the vertebrae, limiting its expansion and the increase of the axon diameter. Therefore, the acquisition of myelin sheaths has allowed to increase nervous

influx speed without increasing the axon's diameter. The increase of axons has led to the expansion of their body size (for review, Zalc, 2016).

Zalc suggested that the acquisitions of myelin and the hinged jaw were coupled in evolution and that myelin would have appeared with the oldest jawed fish during the Devonian period, the placoderms (Grassé, 1975; for review, Zalc, 2016). Overall, the acquisition of myelin from NC-derived Schwann cells has allowed the increase in body size and specifically the expansion of the face and of the anterior CNS (Zalc and Colman, 2000).

3. Gene regulatory network and vertebrate evolution

During vertebrate development, the NC undergoes a series of events occurring from gastrulation to late organogenesis: initial induction of the NC at the neural plate border between future neural and non-neural ectoderm, epithelial-to-mesenchymal transition (EMT), NC survival, migration and differentiation. Each of these events is controlled by multiple regulatory modules involving transcription factors and ribonucleic acid (RNA) binding proteins interacting with each other. These interactions generate a specific spatial and temporal regulation of the NC along each step of their development (Peter, 2017). This complex network is orchestrated by a gene regulatory network (GRN), guiding the ability of NCC to acquire specific capacities (for reviews, Meulemans and Bronner-Fraser, 2004; Sauka-Spengler and Bronner-Fraser, 2008) (Fig. 2). With the recent discoveries using single cell RNA sequencing (scRNA-seq), Di Gregorio et al. suggest that the GRN could involve thousands of genes to complete all the steps of the NC development (Di Gregorio, 2020). For example, as cited previously, the induction of the NC involves morphogens such as WNTs, BMPs and FGFs and the specification of the neural plate border includes expression of homeobox proteins MSX1, MSX2 (homologous to the *Drosophila* muscle segment homeobox gene

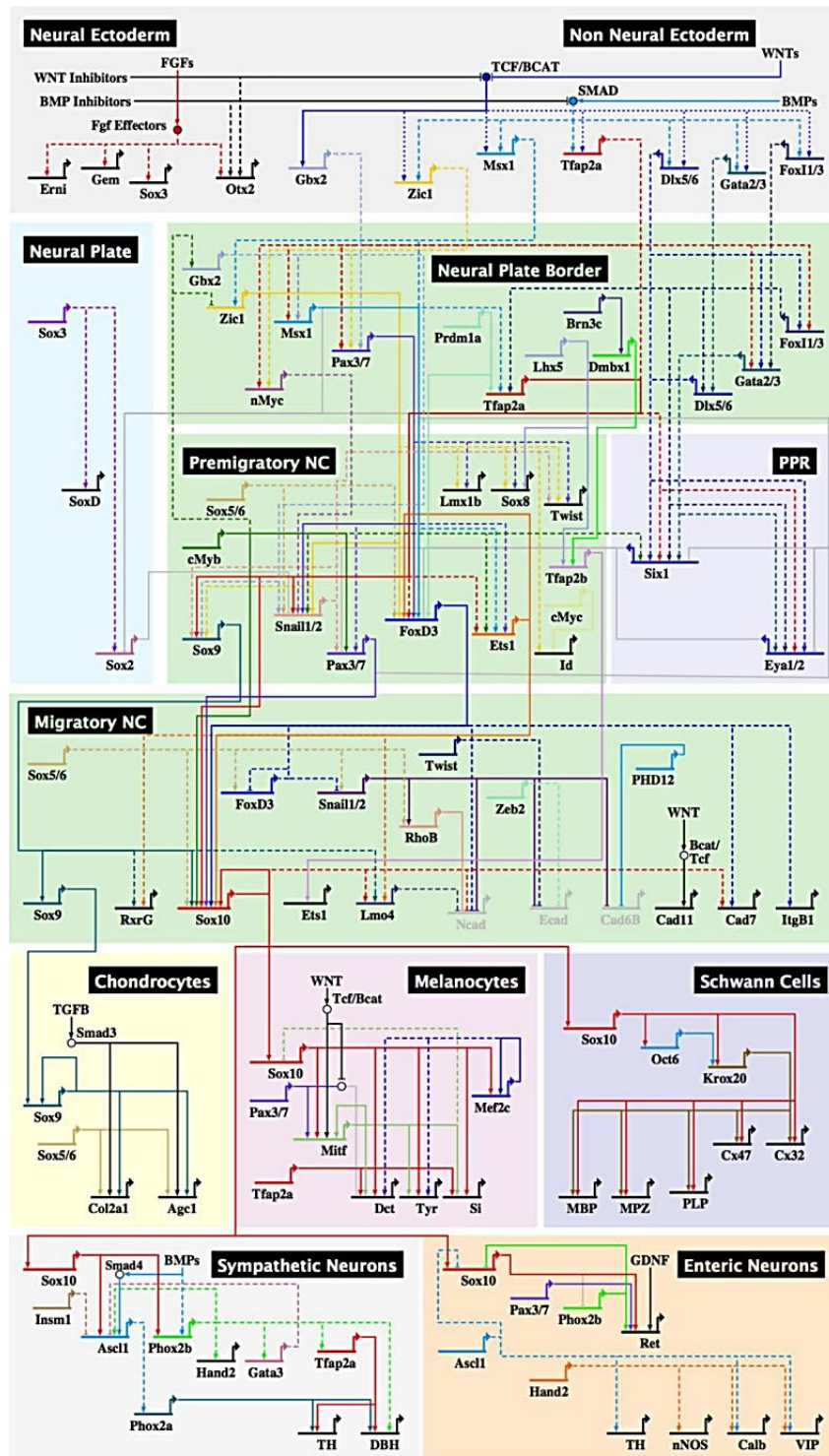


Figure 2. The GRN underlying NC development. The complexity of the NC GRN is comprised of sequential regulatory modules, focusing on transcription factors and signaling molecules for each stage of NC formation: induction, specification, delamination, migration, and differentiation. Differentiation gene batteries for five representative NC derivatives are placed downstream in the GRN hierarchy. The GRN is largely conserved across vertebrates with some variation between species. For example, *Twist1* is part of the NC specification module in frog and zebrafish, but missing in amniotes. From Martik and Bronner, 2017.

(*Msh*) (for review, Alappat, et al., 2003), paired box proteins PAX3, PAX7 and zinc finger protein ZIC1 (for review, Sauka-Spengler and Bronner-Fraser, 2008). Following the initial NC specification, *Snail* and *Sox* family of genes, as well as FOXD3, inhibitor of deoxyribonucleic acid (DNA) binding (ID) 3 and TWIST are involved in NCC survival (for review, Steventon, et al., 2005). However, the expression of the genes along the developmental process is not linear as genes involved at an early stage of NC induction are also expressed in later steps of the development (for review, Steventon et al., 2005).

So, evolutionary appearance of the NC in vertebrates allowed development of the forebrain and emergence of the face and associated sense organs. The main contribution in the development of the cephalic region belongs to the CNC, which gives rise to the musculo-conjunctive, skeletogenic, perivascular, and meningeal structures of the craniofacial region. These changes are accompanied by development of a GRN, guiding the ability of NCC to acquire specific capacities. We will follow NC formation in vertebrate embryo development.

II. Early development of the central nervous system

1. Gastrulation

During early development, at the blastocyst stage, the cells of the inner cell mass form two layers, an upper layer called the epiblast and a lower layer called the hypoblast. The epiblast is thought to contain the cells that will generate the actual embryo while the hypoblast contributes to the extraembryonic membranes. Then occurs the gastrulation between days 13 and 19 in humans and between 12 and 22 hours of development, corresponding to 3-5HH in chicks (for review, Martinsen, 2005). Gastrulation begins at the site of a node, or primitive knot, consisting of an

enlarged group of cells located in the anterior portion of the primitive streak in a developing gastrula. In the chick embryo, the node was discovered by Viktor Hensen, hence calling it the Hensen's node (Hensen, 1876). The node, with similar characteristics, was later discovered in xenopus, calling it "the Spemann-Mangold organizer" (Spemann, 1924) and in fish, calling it the "Kupffer's vesicle" (Kupffer, 1868).

During gastrulation, the primitive streak first appears at the caudal end of the embryo and grows cranially. The epiblast cells migrate through the groove to become layers of endoderm and mesoderm (Fig. 3). The gastrulation leads to the formation of three germ layers: the endoderm, the mesoderm and the ectoderm. Ventrally the endoderm generates the epitheliums lining the visceral and respiratory cavities. The dorsal outer-layer called the ectoderm becomes segregated into the neural plate and the surrounding non-neural ectoderm. The neural plate ultimately generates the CNS, whereas the surrounding non-neural ectoderm forms the epidermis of the skin as well as the epithelial lining of the mouth and nasal cavities (Couly and Le Douarin, 1985). The intra-embryonic mesoderm derives from the invagination of ectoderm cells at the level of the primitive streak, and its condensation gives rise to the notochord, limited anteriorly by the prechordal plate. On either side of the notochord, the paraxial mesoderm is the site of segmentation which also takes place in the rostro-caudal direction to give rise to metameric structures: the somites, at the origin of the vertebrae and skeletal muscles of the body.

2. Vertebrate neurulation and neural crest emergence

From 23 to 26 hours of development, corresponding to 6-7HH in chick embryos (Hamburger and Hamilton, 1951; for review, Martinsen, 2005), the embryo called neurula goes through the process of neurulation, consisting in the distinction of

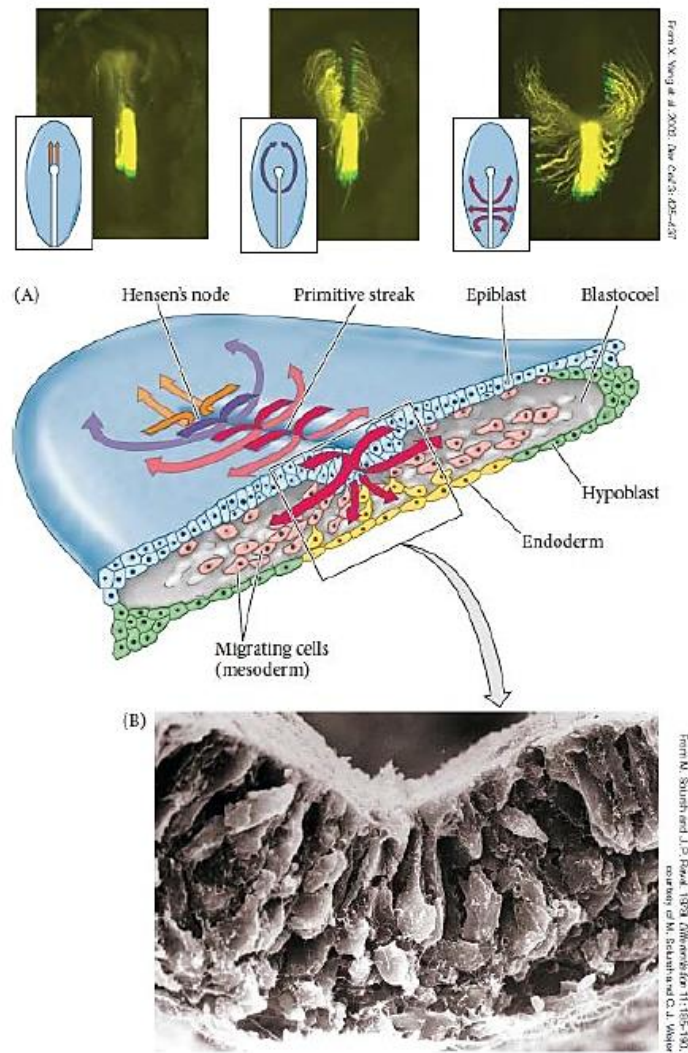


Figure 3. Migration of endodermal and mesodermal cells through the primitive streak. (A) Stereogram of a gastrulating chick embryo, showing the relationship of the primitive streak, the migrating cells, and the hypoblast and epiblast of the blastoderm. The lower layer becomes a mosaic of hypoblast and endodermal cells; the hypoblast cells eventually sort out to form a layer beneath the endoderm and contribute to the yolk sac. Above each region of the stereogram are micrographs showing the tracks of GFP-labeled cells at that position in the primitive streak. Cells migrating through Hensen's node travel anteriorly to form the prechordal plate; those migrating through the next anterior region of the streak travel laterally but converge near the midline to make notochord and pre-somitic mesoderm. Farther posterior, the cells migrating through the primitive streak make up the extraembryonic mesoderm (not shown). (B) This scanning electron micrograph shows epiblast cells passing into the blastocoel and extending their apical ends. [From Gilbert, 2019.](#)

three ectodermal regions from one another: the neural plate giving rise to the neural tube (NT), the surface nonneural ectoderm giving rise to the epidermis and the NC rising from the borders of the neural plate (**Fig. 4**).

The distinction between the three regions is regulated by the levels of BMPs on the epidermal cells. The notochord, underneath the neural plate, secretes signals such as SHH to form the medial hinge point (MHP) and Noggin to form the dorsal lateral hinge points (DLHPs) by inhibiting BMPs, allowing the neural plate to fold by invagination, giving rise to a neural groove and in fine a NT ([Charrier et al., 1999](#); [Zohn, 2012](#)). The neural folds converge and its lateral ridges fusion along the dorsal midline to form the NT, and allow the emergence of the NC ([Donoghue et al., 2008](#)). In amniotes, the process of neurulation proceeds along the anterior-to-posterior axis. Therefore, in chick embryos, while the neurulation is well advanced in the cephalic region, the caudal region is still undergoing gastrulation (**Fig. 5**).

3. Formation of the brain vesicles

While the NT is still closing in the posterior region of the embryo, three primary vesicles forming the initial brain are developed in the anterior region: 1) the forebrain, called prosencephalon, forms the brain hemispheres, 2) the midbrain, called mesencephalon, and 3) the hindbrain, called rhombencephalon, forms the cerebellum, the pons and the medulla oblongata. By the time the posterior NT has closed, secondary vesicles are formed in the anterior region: 1) the forebrain gives rise to the telencephalon and the diencephalon, 2) the midbrain becomes the mesencephalon and 3) the hindbrain becomes the metencephalon and the myelencephalon (**Fig. 6**). In fine, the telencephalon generates the cerebral hemispheres and the hippocampus. The diencephalon becomes the optic vesicle, the epithalamus, the thalamus and the hypothalamus. The metencephalon gives rise to the cerebellum and the pons. The myelencephalon becomes the medulla

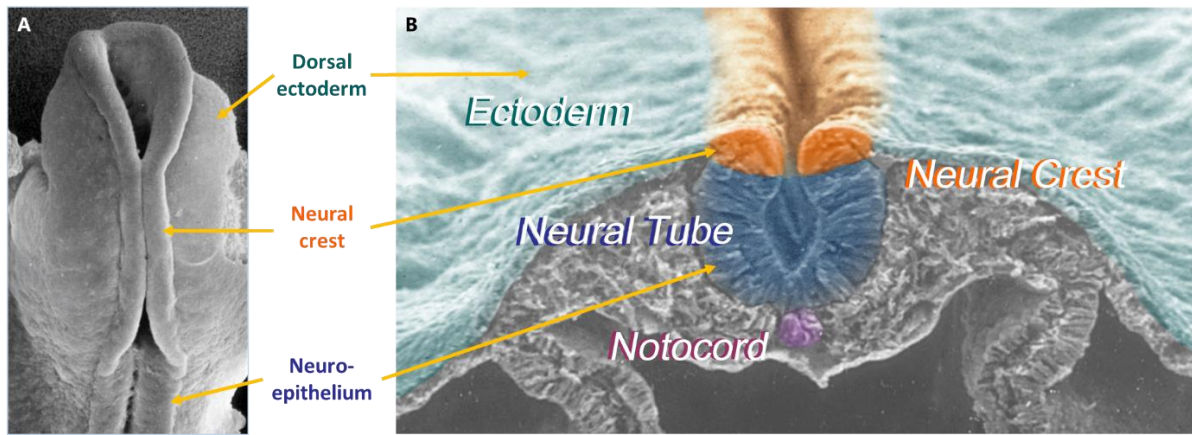


Figure 4. Scanning electron microscopy of the origin of the NC. (A) Scanning electron microscopy of the dorsal view of the embryo during the closing of the neural tube. The three steps of the neurulation are shown: the neural plate caudally, the neural groove cranially and the neural folds in between. (B) During neurulation, at the closure of the neural tube (in blue), the NC (in orange) will derive from the neural folds of ectodermal origin (in green). Adapted from Nogent Institute, Le Douarin's lab.

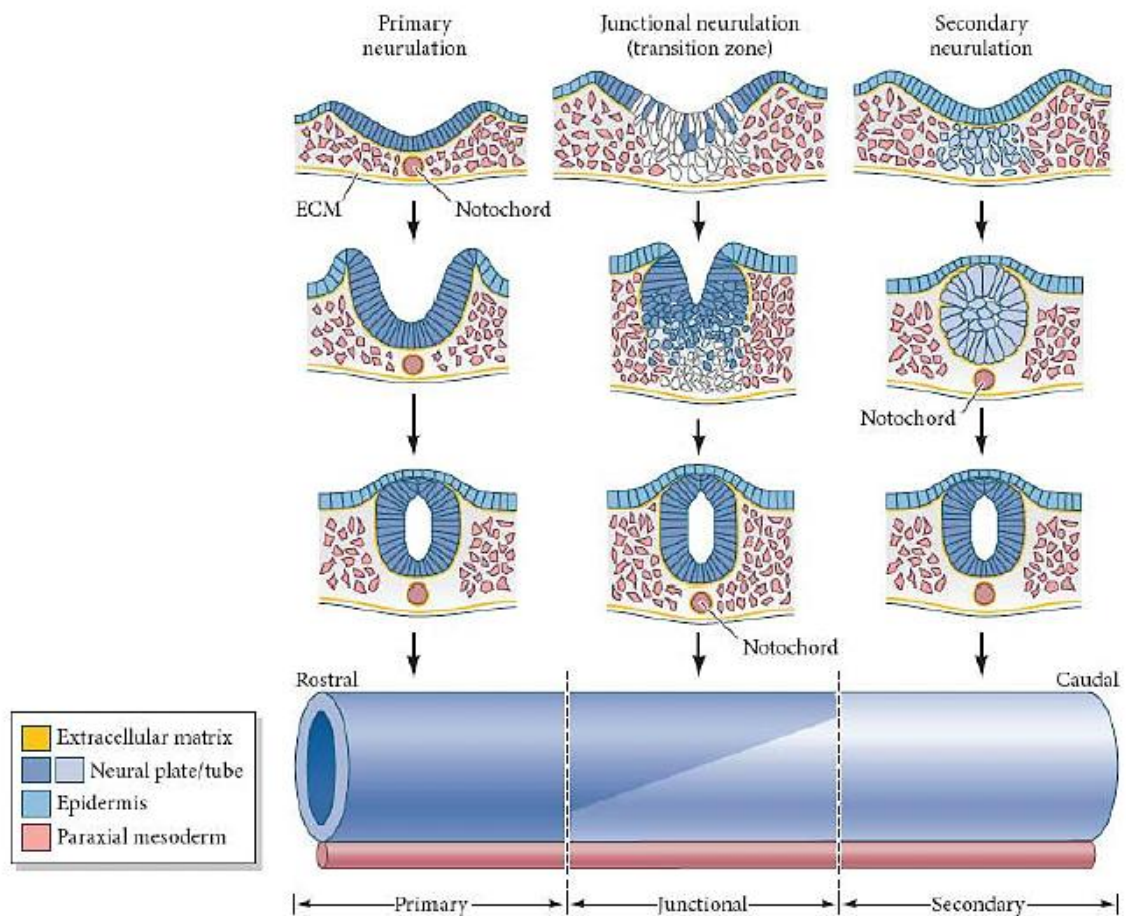


Figure 5. Primary and secondary neurulation and the transition zone between them. The bottom image is a lateral view of the neural tube surface. The illustrations above the neural tube correspond to transverse sections through the axial level indicated as the neural tube forms in a rostral-to-caudal direction. Different cell types are represented in different colours, as indicated in the key. [From Gilbert, 2019.](#)

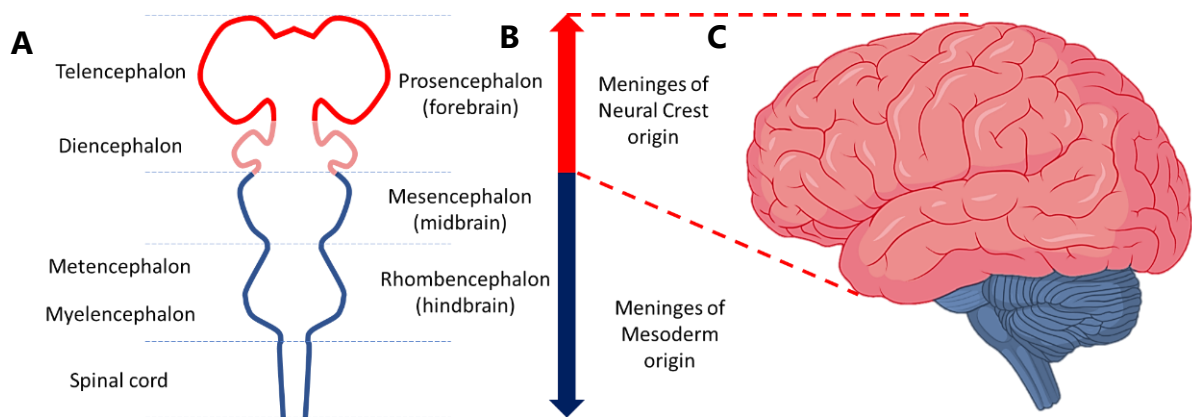


Figure 6. Brain vesicles and the origin of meninges. (A) Diagram representing a dorsal view of the main subdivisions composing the embryonic vertebrate brain. (B) The meninges covering the telencephalon and diencephalon (forebrain), from prosencephalon origin, are derived from CNC cells (in red). However, the meninges covering the mesencephalon, the rhombencephalon and the spinal cord are derived from the mesoderm (in blue). (C) Schematic representation of the developed human brain: the telencephalon and diencephalon, are covered by CNC-derived meninges (in pink). The midbrain (mesencephalon) and the hindbrain (rhombencephalon) are covered by mesoderm-derived meninges. [Created with Biorender.com](https://www.biorender.com).

(for review, Gupta and Sen, 2016).

4. NC emigration along the antero-posterior axis

The NC also start emerging cranially and migrate lastly from the caudal region along the antero-posterior axis (Creuzet et al., 2005; Donoghue et al., 2008; Grapin-botton et al., 1998). At the extremities of both cranial and caudal regions, the NT remains open to give rise to the anterior and posterior neuropores (Gilbert, 2019). In addition, while the NT closure starts at the level of the midbrain in chick embryos and proceeds in both cranial and caudal directions, in humans there are probably five sites of NT closure ignition (Bassuk and Kibar, 2009; Gilbert, 2019; Nakatsu, 2000; O’Rahilly and Müller, 2002). The NC is a transient, multipotent and highly migratory cell population discovered in the trunk by the Swiss embryologist Wilhelm His (His, 1868). This tissue was later renamed NC by Arthur Milnes Marshall (Marshall, 1879) with a more precise description of its anatomical position. The NC was first described in the chick embryo as a band of cells lying between the NT and the future epidermal ectoderm (His, 1868). During neurulation, the NCC, located dorsally to the NT, detach from the neural epithelium and undergo an EMT. Then they delaminate and migrate on either side of the NT along the anterior-posterior axis to invade the whole embryo (Le Douarin et al., 2004) (Fig. 7).

5. Identification of the NCC fate

To identify the fate and differentiation of the NCC during development, different techniques were developed in the XXth century: vital staining (Detwiler, 1937; Hilber, 1942; Hörstadius and Sellman, 1946), xenoplastic grafting of amphibian cells with nuclear size markers (Raven, 1936), ectopic grafting and explantation (Dorris, 1938; DuShane, 1935; Koecke, 1960; Rawles, 1940; Willier and Rawles, 1940), and finally excision or ablation followed by analysis of the resulting

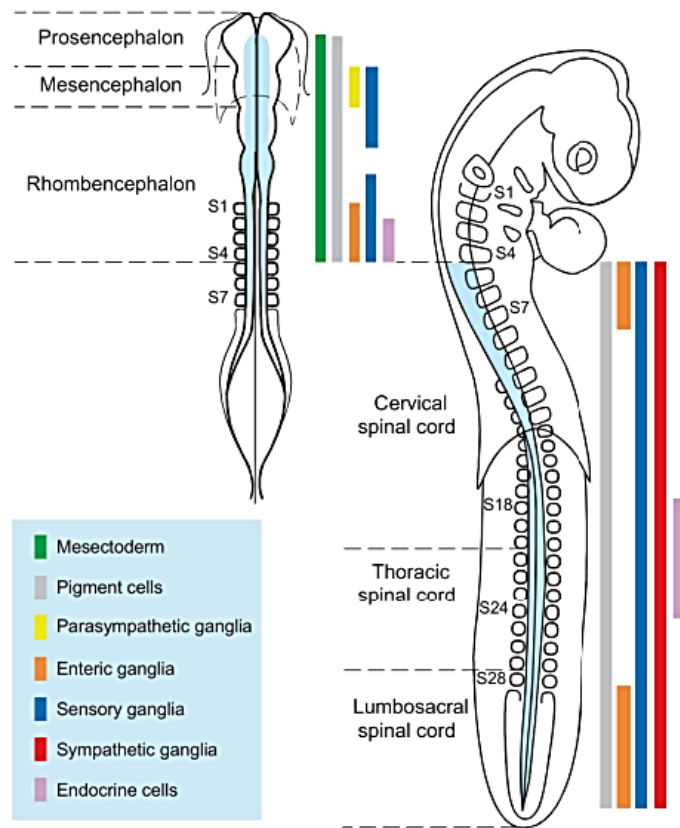


Figure 7. Derivatives of the NC according to their level of origin along the anteroposterior axis. At the cephalic level, the NC forms mesectodermal derivatives (green) comprising skeletogenic, connective, adipose and perivascular cells. Glial and melanocytic phenotypes represent a basic trait produced throughout the neuraxis. The rhombencephalic and sacral NC provides the enteric neurons. As for the neurendocrine, calcitonin and adrenomedullary cells, they derive from the posterior rhombencephalic (r8) and thoracic levels, respectively, between S18 and S24. [From Le Douarin et al., 2004.](#)

deficiencies (DuShane, 1935; Hammond and Yntema, 1947; Harrison, 1924; Hörstadius and Sellman, 1946; Nawar, 1956; Yntema and Hammond, 1945). However, none of these techniques allowed the mapping of NCC migration but concerned with the result of migration. For example, the technique of vital staining does not allow a precise identification of each individual cells' migration as the staining transfers to neighbouring tissues.

In the 1960s, Weston and Chibon suggested a cellular marking technique by using radioactive tritiated thymidine *in vivo* and tracing the radioactivity by autoradiography (Chibon, 1964; Weston, 1963) to reveal the migration pathways of the NCC (Johnston, 1966). However, this technique is limited in time due to the dilution of the staining as the marked cells go through their division cycle.

In 1969, Nicole Le Douarin developed the quail-chick chimera model to investigate the migration pathway of the NCC along the anterior-posterior axis, as well as their fate and differentiation during development (Le Douarin, 1969). This technique consists of xenografting NCC before the onset of their migration between a quail and a chick embryo at a same developmental stage (Fig. 8). These two avian species are very similar from a taxonomic point of view and share very similar developmental morphological traits during the first half of ontogenesis (Alrajeh, 2018). However, a very distinct characteristic differs between the two avian species: while the heterochromatin is uniformly spread in the nucleoplasm of the interphase nucleus in chick embryos, the quail cells contain very condensed heterochromatin accumulated in the nucleolus (Le Douarin, 1969). This specificity of the quail nucleus allows the recognition of quail cells in chick-quail chimeras by histological staining of the nucleus (Le Lievre and Le Douarin, 1975). The use of a monoclonal antibody specifically directed against quail nuclei, called Quail non-Chick Peri-Nucleolar (QCPN), prepared by B. Carlson and J. Carlson (University of Michigan, USA), allows to identify the quail cells from all the cell lineages,

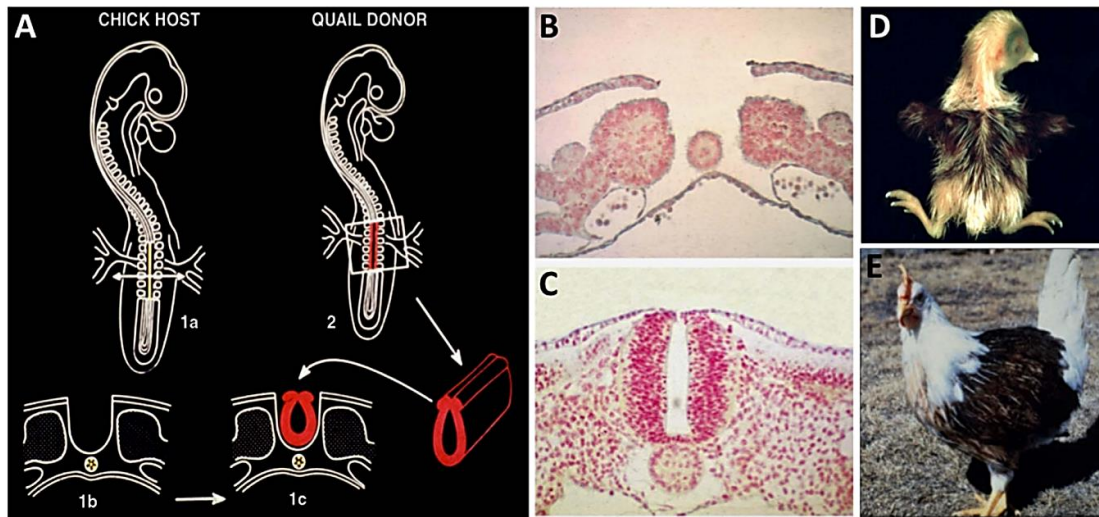


Figure 8. Quail-chick chimeras for investigating the fate of avian NCC. (A) Schematic of the construction of quail-chick chimeras of the neural tube at “adrenomedullary” trunk level (somites 18–24). The neural tube was removed from the chick host (1a, 1b) and replaced by its equivalent neural tube (1c), previously taken at the same level from a quail donor of the same developmental stage (2). (B, C) Transversal sections of chick host embryo (as indicated in A) stained with Feulgen, after removal of the neural tube (B) and when removal was followed by quail neural tube grafting (C). (C) Resulting chimeric birds at post-hatching stage (C) and at three months old (D), which exhibit quail-specific pattern of brown pigmentation at brachial level, due to colonization of the host skin by the grafted NC-derived melanocytes. [From Le Douarin and Dupin, 2018.](#)

independently from their differentiation state This technique was highly used to identify the fate and differentiation of the NCC during development (Le Douarin, 1982; Le Douarin and Kalcheim, 1999).

6. Regionalization of the neural crest

Depending on their anatomical destination, the NCC can be divided in four distinct groups, each with characteristic derivatives and functions. 1) The vagal and sacral NCC give rise to the parasympathetic (enteric) ganglia of the gut (Le Douarin and Teillet, 1974). 2) The trunk NCC either migrating along the ventrolateral pathway to differentiate into the sensory neurons of the dorsal root ganglia, or form the sympathetic ganglia, the adrenal medulla, and the nerve clusters surrounding the aorta, or migrate along the dorsolateral pathway to develop into pigment cells. 3) The cardiac NCC extend from the level of otic placodes down to the third somites (Kirby, 1988; Kirby and Waldo, 1990). Cardiac NCC differentiate into melanocytes, neurons, cartilage, and connective tissue of the 3rd, 4th and 6th pharyngeal arches (Gilbert, 2019). 4) The cranial, or cephalic, NC (CNC) cells give rise to the mesenchymal cell population of the developing vertebrate head. These cells differentiate into the cartilage, bone, cranial neurons, glia, pigment cells, and connective tissues of the face (for review, Creuzet, 2009a; Gilbert, 2019) (**Fig. 9**). Thus, NC emerges from the neural fold borders during vertebrate embryo neurulation. The NC is a transient, multipotent cell population which undergoes EMT and migrates to invade the whole embryo. Anterior-posterior origin of NCC determines their destination and derivatives they give rise to. We will concentrate our attention on the CNC.

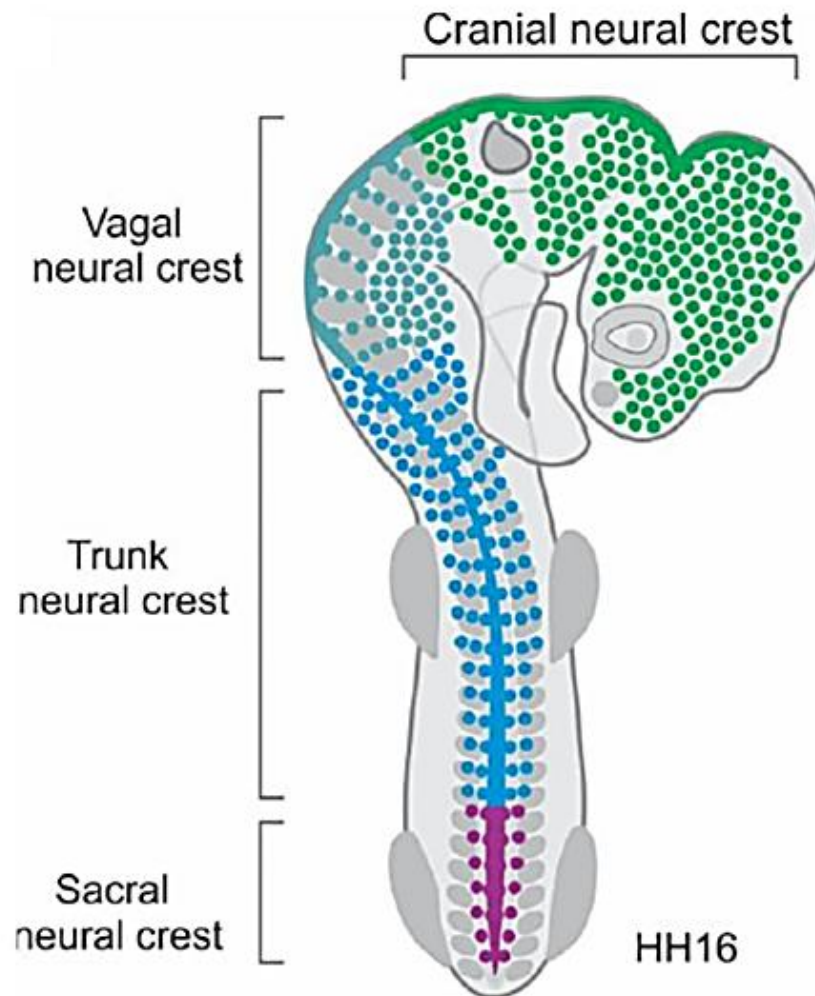


Figure 9. Overview of NC subpopulations along the anteroposterior axis. Diagram of NC subpopulations in an HH16 chick embryo. The CNC subpopulation includes NCC that are formed between the forebrain and the 6th rhombomere (r6) of the hindbrain. The vagal NC is adjacent to the first seven somites. The trunk NC spans from the 8th to the 27th somite, while the sacral NC is positioned posterior to this boundary. HH: Hamburger and Hamilton developmental stages. [From Rothstein et al., 2018.](#)

III. Singularity of the cephalic neural crest

At the cephalic level, CNC from the anterior to the posterior brain differ from the truncal NC (TNC) as they give rise to a broad range of derivatives and specifically mesenchymal cells. Katschenko was the first to claim the participation of the NC in some of the head mesenchyme (Katschenko, 1888). Goronowitsch confirmed the NC origin in cephalic mesenchymal structures by observing teleosts and birds (Goronowitsch, 1893). Around this time Julia Platt, one of the rare women involved in research, showed that mesenchymal cells giving rise to bone and cartilage structures of the visceral arches were of ectodermal and more specifically NC origin (Platt, 1893; 1897). Platt categorized the mesenchyme in two entities: the “mesectoderm” or “ectomesenchyme” for the mesenchyme originating from the ectoderm via the NC, versus the “mesoderm”. The NC derivatives, can be grouped in two categories: 1) the ectomesenchymal derivatives including bone, cartilage and dentine, specifically yielded by CNC, and 2) the non-ectomesenchymal derivatives giving rise to neurons, glia and diverse pigment cells such as melanocytes, yielded by CNC and TNC (Le Douarin, 1982).

1. Morphogenetics of the craniofacial and brain development

The entire facial skeleton and most of the skull (except of the occipital region) are derived from the NC domain of the posterior diencephalon, mesencephalon and rhombomeres 1 and 2 (r1, r2). This region is referred as the Facial Skeletogenic Neural Crest (FSNC). In a 5-somites stage (ss) embryo, corresponding to 8-9HH, the NC contributing to the FSNC lacks homeobox (*Hox*) gene expression (Fig. 10).

Therefore, in the cephalic region up to the first maxillo-mandibular arch of the vertebrate embryo, corresponding to r2, the genes of the four Hox-clusters are not expressed. r3 forms the intermediate zone between a rostral Hox-negative

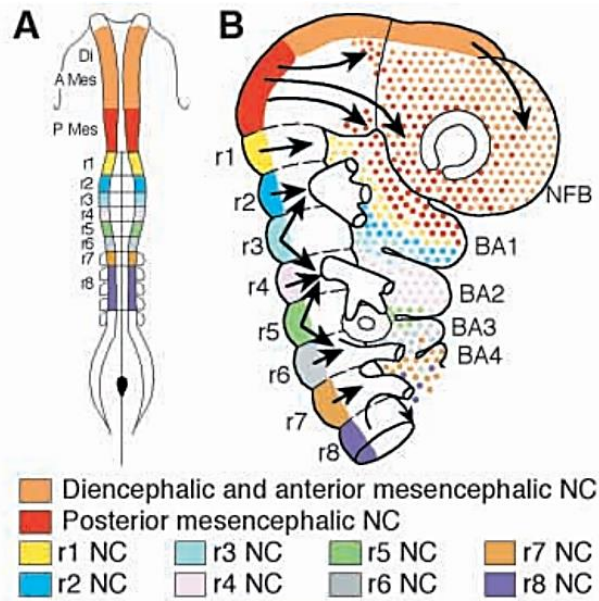


Figure 10. The CNC: fate map and *Hox* gene expression. (A) Presumptive diencephalic, mesencephalic and rhombencephalic territories of the neural fold in the avian embryo at 5 ss. (B) Migration map of CNC cells in the avian embryo. The origin of NCC found in the nasofrontal and periorbital regions and in the branchial arches is color-coded as in A. NCC arising from the posterior diencephalon and mesencephalon populate the nasofrontal and periorbital region. Posterior mesencephalic NCC also participate in these structures, but in addition populate the anterodistal part of the first branchial arch. The complementary portion of the first branchial arch derives from r1/r2, together with a small contribution from r3. The major contribution to the second branchial arch comes from r4. NCC arising from r3 and r5 split into strains participating to two adjacent arches: r3 cells migrate to the first and second branchial arches; r5 cells migrate to the second and third branchial arches. r6 cells migrate to the third and fourth branchial arches, r7- and r8- derived cells migrate to the third and to the more caudal branchial arches. [From Creuzet et al., 2002.](#)

and a caudal Hox-positive domain of the NC. Hox-negative neural folds are compulsory for the development of the skull and facial structures and behave like a « morphogenetic field » (Fig. 11). The NCC from the FSNC are competent to produce facial and skull structures and a smaller fraction of this field has the capacity to replace the whole in building the NC-derived portion face and part of the skull. Brain development depends upon the signaling activity of the « secondary brain organizers » producing *Fgf8* during the early stage of neurogenesis: the isthmus, or midbrain-hindbrain boundary which patterns the cerebellum and the optic tectum, and the ANR also designated as « telencephalic organizer » (Cobos et al., 2001; Crossley et al., 2001). *Fgf8* expression in the prosencephalon and in the branchial arch (BA) ectoderm depends upon an interaction with the migratory NCC. The latter are responsible for inducing and maintaining the expression of *Fgf8* by the superficial ectoderm and the neuroepithelium of the forebrain, via the secretion of BMP antagonists. In turn, foci of *Fgf8* expression impose the directionality of the NCC migration streams (for review, Creuzet, 2009a).

By removing the FSNC, the level of *Fgf8* transcripts is reduced in the ectodermal components of the developing head (Creuzet, 2009a). The absence of these NCC causes brain and facial defects: prosencephalic anencephaly or exencephaly, partitions into telencephalon, diencephalon and mesencephalon are no longer recognizable, facial processes devoid of NCC mesenchyme (except in trigeminal root ganglia) (Creuzet et al., 2006), lack of skeletal structures such as a complete loss of maxillo-mandibular structures (agnathia), severe eye defects and atrophied CP (for review, Creuzet, 2009a; Creuzet et al., 2002). When FSNC-deprived embryos are stimulated with exogenous FGF8 in the ANR, NT closure occurs and brain regionalization is restored (Creuzet et al., 2006) (Fig. 12).

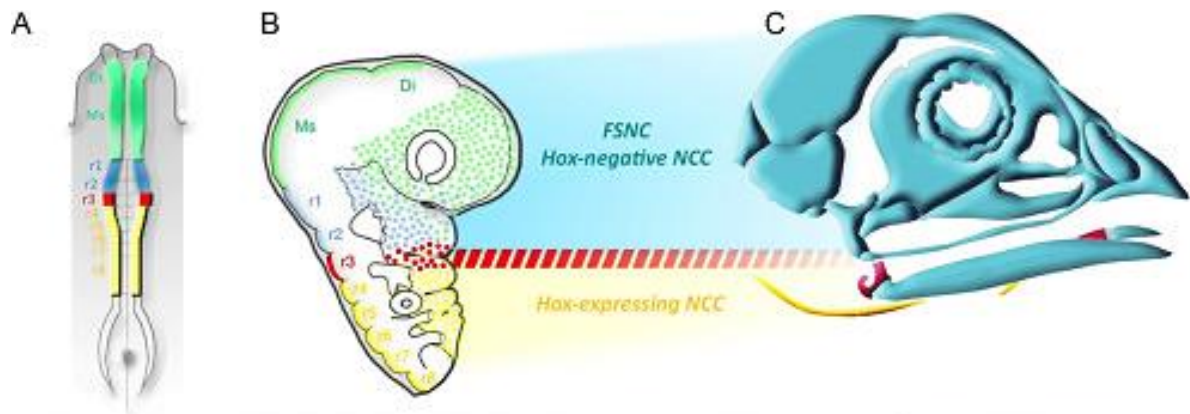


Figure 11. Contribution of the NC to head development. (A) The color-coded representation of the cephalic neural fold in a 5-ss embryo: the di- and mesencephalic NC appears in green, the first and second rhombomeres (r1-r2) NC in cyan, the r3 NC in red, and the r4-r8 NC in yellow. (B) Colonization of the facial processes and branchial arches by the NCC according to their level of origin. (C) The skull vault, nasal and orbital capsules, jaws and entoglossum are derived from the Hox-negative FSNC. The hypobranchial skeleton corresponding to the posterior part of the hyoid bone is derived from Hox-expressing NCC (in yellow). Interposed between these two domains, r3 NCC contribute to the retro-articular and to the medial third of the basihyal (in red). [From Le Douarin et al., 2012.](#)

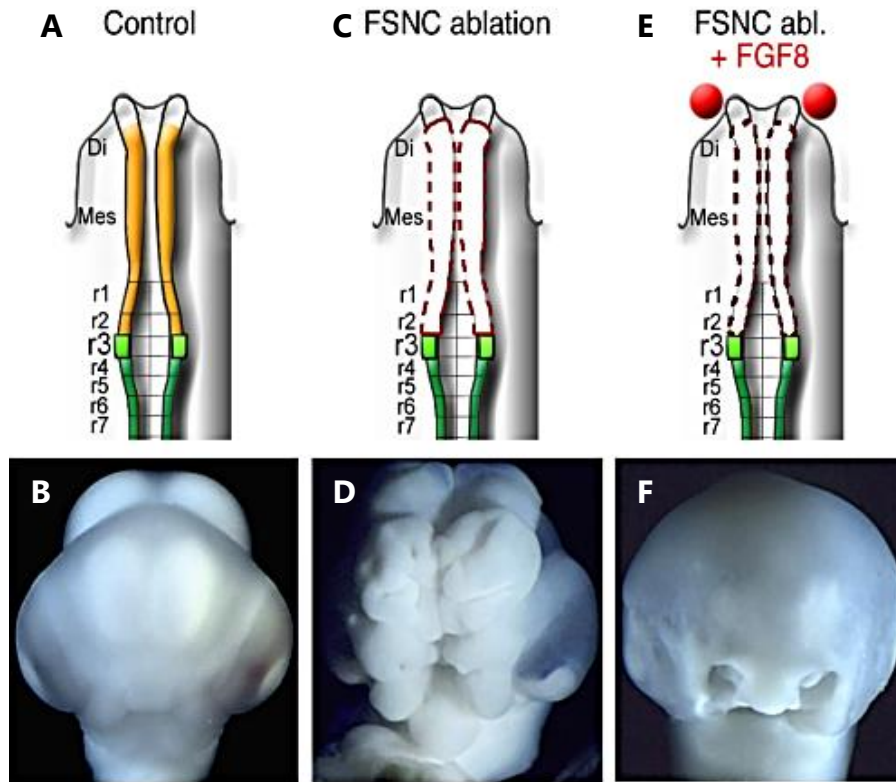


Figure 12. The FSNC controls cephalic neural tube closure. (A,B) At E5, when the FSNC (A, in yellow) is intact, (B) anterior and middle cephalic vesicle formation is normal. (C,D) Removal of the FSNC (C), from the middle diencephalon to r2, leads to extensive anencephaly (D). (E,F) Implantation of Fgf8-soaked beads (E, in red) allows closure of the tube (F). [From Creuzet et al., 2006.](#)

The defects observed by removing the FSNC are also observed with an overexpression of either *Hoxa2* alone or a combination of *Hoxa3* and *Hoxb4* in FSNC cells. The expression of *Hox* genes in the Hox-negative neural folds prevents the development of the head and facial skeleton. By engrafting 5-6 ss embryos with neural folds expressing *Hoxa2* in the entire Hox-negative neural fold, the embryos present severe facial and forebrain malformations. They lack facial structures such as the upper and lower jaws and the frontonasal structures. Their pre-otic brain vesicles are also strongly shrunk. However, the neural derivatives of the anterior CNC are well developed: the mesenchymal cells of NC origin are present and participate in the formation of the blood vessel walls and the NCC give rise to the pericytes of the forebrain vasculature (Creuzet et al., 2002; Etchevers et al., 1999; 2001). *Hoxa2* activation in the FSNC leads to a downregulation of *Fgf8* in the ANR, the isthmus and the BA ectoderm, altering prosencephalon and mesencephalon development, a downregulation of *Wnt8b* in the prosencephalon and rhombencephalon, altering the CP development, and a lateral expansion of *Shh*, decreasing the size of the prosencephalic and mesencephalic alar plates (Creuzet et al., 2002; 2006) (Fig. 13).

Furthermore, *Hoxa2* expression in the Hox-negative neural fold downregulates the sine oculis homeobox (*Six*)2, strongly expressed in the Hox-free NCC. *Six* genes have complementary roles in the head skeletogenic patterning and a silencing of these genes give rise to severe cephalic and facial malformations. *Six2* silencing results in the loss of the CP at both prosencephalic and rhombencephalic levels and gives rise to defects of the nasofrontal skeleton, joint and of the mandibular symphysis development. *Six4* silencing perturbs the formation of the septum pellucidum (resembling lobar holoprosencephaly) and leads to defects of the nasofrontal and mandibular skeletons. *Six1* silencing affects the diverticulation of the prosencephalon (flagrant alobar holoprosencephaly). A silencing of all three *Six* genes triggers an overall reduction of the head skeleton (Garcez et al., 2014)

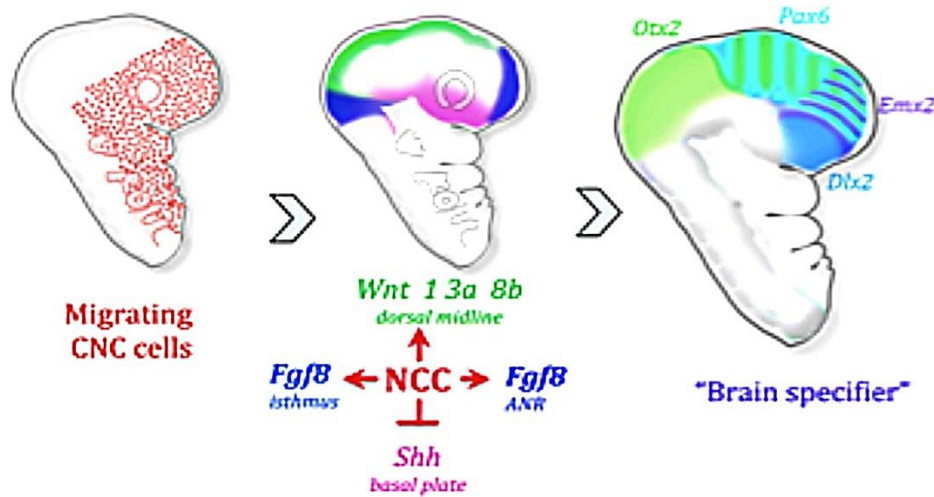


Figure 13. The facial NC regulates the morphogenetic activity of brain organizing centers. During their migration, NC cells stimulate *Fgf8* activity in the ANR and isthmus, as well as *Wnt* activity along the dorsal midline. At the same time, they limit *Shh* expression to the basal lamina. From Creuzet et al., 2006; Bruet, Amarante-Silva, Gorojankina and Creuzet, 2023.

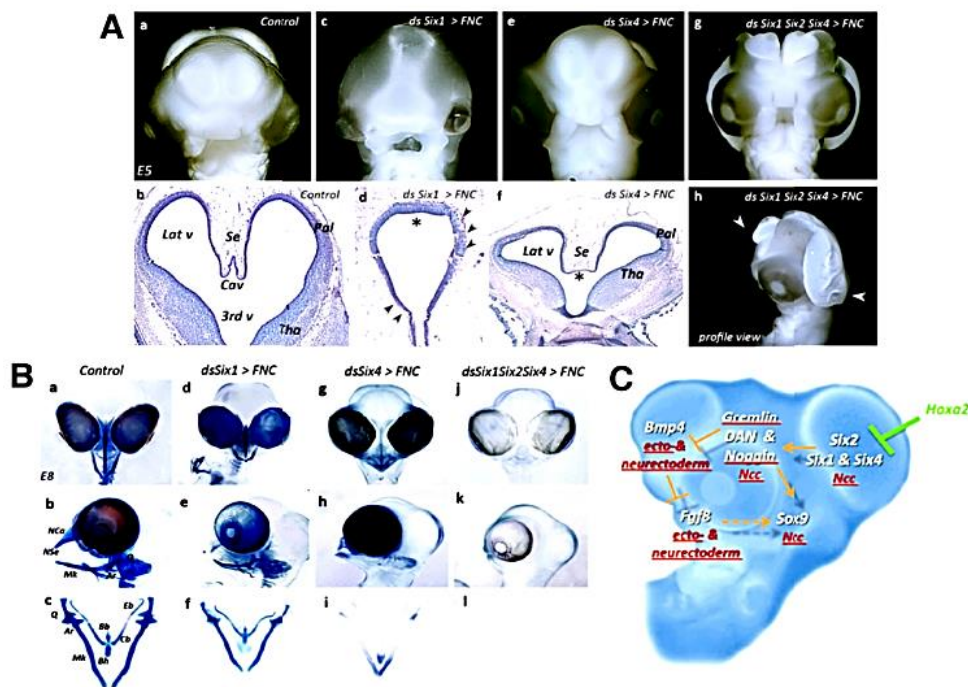


Figure 14. Role of the *Six* genes in cephalic development. (A) Deficits induced at E5 by selective inactivation of *Six1*, *Six2*, *Six4* affect the development of the midline structures of the brain, leading to lobar or alobar holoprosencephaly. Triple silencing leads to extensive anencephaly. (B) Inhibition of each *Six* gene leads to partial skeletal defects at E8, but triple silencing leads to skeletal defects. (C) Interaction model where *Six1*, *Six2* and *Six4* genes regulate *Noggin* and *Gremlin* activity for brain development and, via *Sox9*, for skeletal development. From Garcez et al., 2014.

(Fig. 14).

By expressing *Hoxa3* in the Hox-negative neural fold, the skeleton derived from the first BA is absent with a reduced nasofrontal bud (with persistence of the nasal septum), an absence of the anterior hyoid and sclerotic cartilages, and an absence of the lower jaw skeleton and the entoglossum. Besides, the head blood vessels, lined by endothelial cells, lack NC-derived pericytes and form large blood lacunae. The expression of *Hoxb4* in the Hox-negative neural fold leads to the total absence of the nasal bud-derived skeleton, the upper beak and the sclerotic cartilage. However, development of the neural derivatives persists with the presence of Schwann cells in peripheral cranial nerves, pericytes in the choroid membrane and around the endothelial wall of blood vessels. Naturally, by co-transfecting *Hoxa3* and *Hoxb4*, embryos fail to develop the skeletal structures of the upper and lower beaks, the nasofrontal, maxillary and mandibular buds and cartilage. Even though the pericytes persist in the choroid membrane, the choroid vessels form large blood lacunae around the optic vesicles (Creuzet et al., 2002).

2. Neural crest contribution to the branchial vascular sector

NC deriving from the pharyngeal arches 3, 4 and 6 (Le Lievre and Le Douarin, 1975; Sizarov et al., 2012) produce the entire muscular-connective tissue wall of the large arteries down to the heart, where they contribute to the semilunar valves (Etchevers et al., 2002) and to the conotruncus, the septum separating the truncus arteriosus into the pulmonary artery and the aorta, along with the inter-ventricular septum (Kirby, 1988; Nishibatake et al., 1987; Waldo et al., 1998) (Fig. 15).

For these reasons, the caudal subregion of the CNC is referred as the cardiac NC: the bilateral defect of any segment leads to irreversible cardiovascular malformations (Kirby, 1988; Kirby and Waldo, 1990), which accounts for congenital disorders.

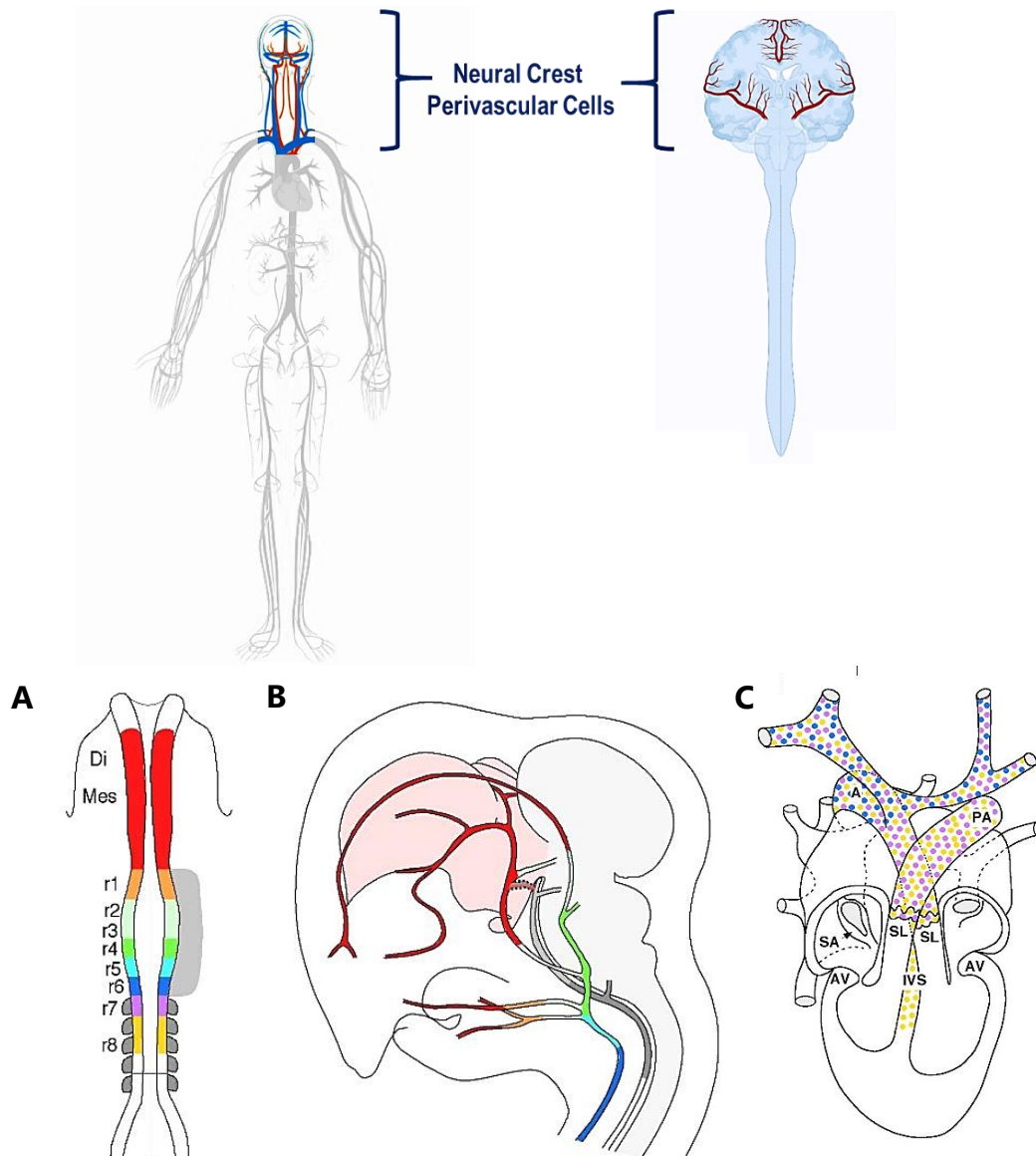
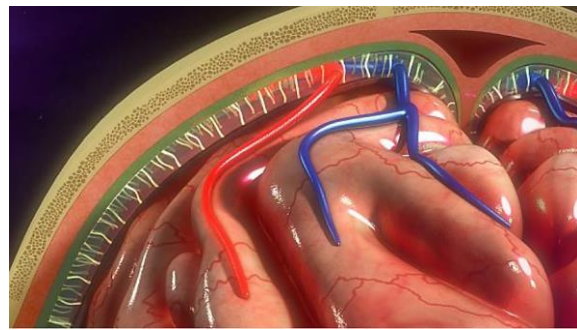
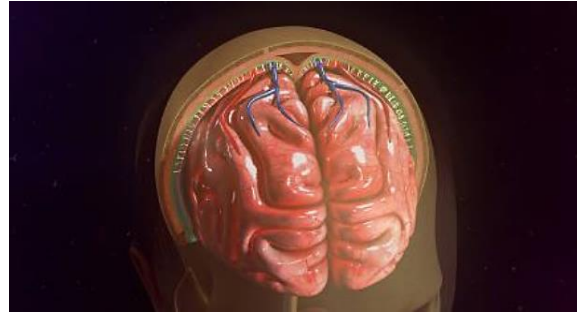
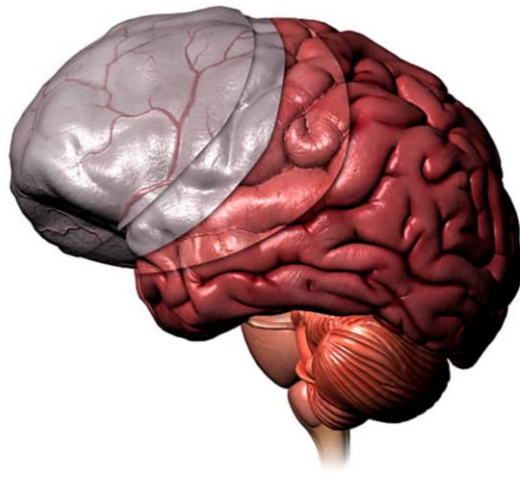
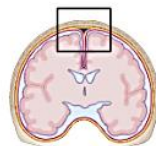


Figure 15. Contribution of the CNC to the cardiovascular system. The NC-derived pericytes give rise to the vascular network from the cranial cardiovascular network to the meninges covering the telencephalon. (A) Schematic representation of CNC cells according to their level of origin. (B) Contribution of the FSNC to the prosencephalic meninges (pink) and the facial and cerebral vascular network. (C) Contribution of the cardiac NCC to the wall of the large arteries, the conotruncus, and the sigmoid valves. Created with Biorender.com and adapted from Etchevers et al., 1999; 2001.

Therefore, in the cephalic region, the wall of blood vessels harbors two linings of different embryonic origin and distinct vascular circuits: 1) the “branchial vascular sector” originates from the ventral aorta and branchial arches, and terminates in the venous return to the heart. Its ramifications irrigate the ventral and anterior head. 2) The second vascular sector of non-branchial arteries, entirely originating from the cephalic and somatic mesoderm, irrigates the dorsal and posterior head, including the midbrain, cerebellum, and hindbrain. These two sectors join behind the optic chiasm at the circle of Willis, an anastomosis surrounding the hypophysis, where mesoderm versus NC-derived vascular circuits abut to each other. From this region onward, the meninges covering the forebrain are from NC origin, while downward, the meninges covering the rest of the CNS derive from the mesoderm (Etchevers et al., 2001; Etchevers et al., 2002).

3. NC contribution to the meninges

The meninges form a vascular network irrigating the brain. They are composed of three layers surrounding the CNS: 1) an outer dura mater, lining the inner surface of the cranium’s bone and the bones of the vertebral column, 2) an arachnoid mater in the middle, composed of trabeculae, thin strands of connective tissue that extend from the arachnoid mater to the pia mater and help to keep the brain suspended in place and 3) an inner pia mater, outlining the shape of the brain (Bailey, 2021) (Fig. 16). Each layer of the forebrain meninges derives from the CNC (Etchevers et al., 1999). More specifically, the NC give rise to the pericytes and the connective tissue cells of the blood vessels in the leptomeninx. However, the endothelial cells of the blood vessels derive from mesoderm origin (Couly et al., 1995). The double origin of the leptomeninx is only found in the meninges surrounding the prosencephalon. The meninges surrounding the caudal part of the CNS are entirely of mesodermal origin (Le Lievre, 1976). Thus, the endothelial cells found in the blood vessels of the head and the body originate strictly from

A**B**

Cranial Meninges

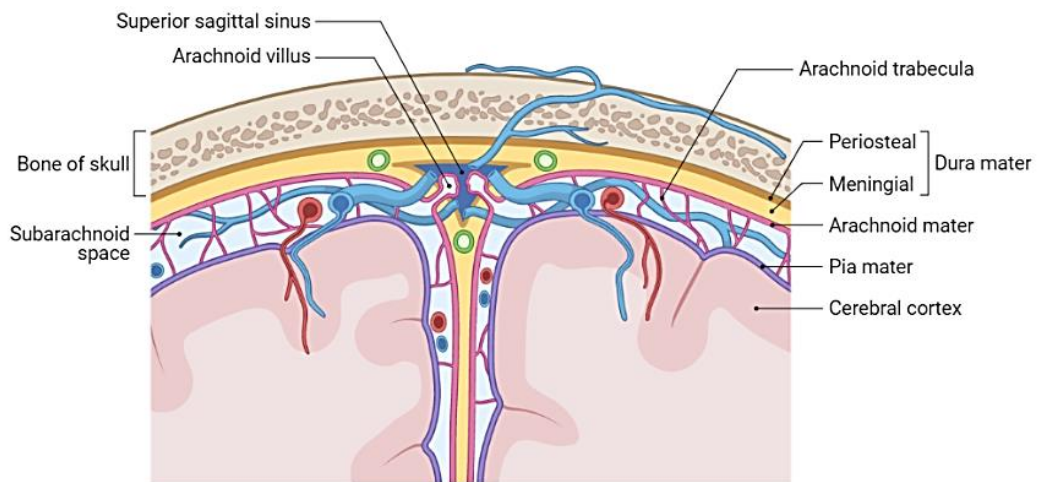


Figure 16. Anatomy of the meninges surrounding the anterior brain. (A) The meninges, formed of the dura mater, the arachnoid and the pia mater, enclose the entire central nervous system (CNS). The meninges covering the anterior brain derive from the NC whereas the meninges surrounding the posterior CNS derive from the mesoderm. [From Kenhub.com](https://www.kenhub.com). (B) The dura mater lines the interior portion of the skull whereas the pia mater surrounds all the circumconvolutions of the CNS and isolates arachnoidal blood vessels from the neuroepithelium. [Created with Biorender.com](https://www.biorender.com).

the mesodermal. However, the pericytes have a double origin: the pericytes found in the meninges covering the forebrain originate from the NC whereas the pericytes found in the meninges covering the rest of the CNS (midbrain, hindbrain and spinal cord) derive from the mesoderm (Le Douarin, 1982).

The coincidence between the emergence of the forebrain and the meningeal construction leads to exploring the role of the NC-derived meninges and its pericytes in the development of the forebrain (Etchevers et al., 1999).

4. NC contribution to the pericytes

Pericytes were first called Rouget cells as they were described by the French physiologist Charles-Marie Benjamin Rouget in 1873 (Dore-Duffy and Cleary, 2011). These cells were later referred as pericytes in 1923 by Zimmermann. Pericytes are vascular cells surrounding the endothelial cells of the micro vessels (precapillary arterioles, capillary and postcapillary venules) with which they have extensive contacts (for review, Girolamo et al., 2021) and are retained within the basal membrane of the blood vessels (for review, Rustenhoven et al., 2017). The pericyte-to-endothelial cell ratio along the blood vessels varies among the species but also between the different organs of a given species: the highest pericyte-to-endothelial cell ratio observed among all the organs is in the brain (for review, Rustenhoven et al., 2017). The average pericyte-to-endothelial cell ratio observed in humans is 1:3-4 (Dore-Duffy and Cleary, 2011). A deficiency of pericytes in the brain could lead to severe neurological pathologies such as Alzheimer's disease (AD) (Winkler et al., 2014).

The vascular vessels are composed of an inner layer of endothelial cells, closely interacting with an outer sheath of mural cells. Among the mural cells are either found smooth muscle cells (SMC) or pericytes, depending on the type of vessel in which they are found. While vascular SMC (vSMC) are found in large vessels, pericytes are associated with arterioles, venules and capillaries (Ozerdem et al.,

2001). Pericytes are described as contractile and motile cells, projecting their cytoplasmic protrusions around the blood vessels (Ding et al., 2004).

Pericyte morphology varies depending on the 5 types of blood vessel they are attached to, from arteriole to venule. In arterioles and precapillary arterioles, a single pericyte layer encircles the entire abluminal side of the endothelium. 1) In arterioles, the pericytes are flattened and spindle-shaped, with few cytoplasmic processes, whereas in 2) precapillary arterioles, the cell bodies are distinctly protruding and extend several processes encircling the endothelium. 3) In the capillaries, the pericytes contain round cell bodies and protrude a few primary processes along the capillaries, giving rise to secondary perpendicular processes in order to maintain a firm joint with the endothelium. Both cells keep contact via a “peg-socket” system where pericyte cytoplasmic fingers (pegs) are inserted into endothelial invaginations (sockets). The pericytes start flattening again around 4) postcapillary venules and give rise to many slender, branching processes. Pericytes covering 5) the venules have large stellate shaped cell bodies with several branching processes. However, unlike arteriolar pericytes, they do not wrap circularly around the endothelium (for review, Armulik, et al., 2011) (Fig. 17).

5. Pericyte identifications, structural and surface markers

a. α -Smooth Muscle Actin

Depending on their IgG fraction, Vandekerckhove and Weber differentiate six individual actin isoforms: four muscular actin isoforms and two non-muscle actin isoforms. Two isoforms found in skeletal and cardiac muscles are referred as α -skeletal and α -cardiac actin, two isoforms specific of SMC are called α - and γ -smooth muscle actins (α -SMA and γ -SMA). All cells contain the two non-muscle actin isoforms in their cytoplasm, β - and γ -cytoplasmic actins (Vandekerckhove and Weber, 1978a; Vandekerckhove and Weber, 1978b; Vandekerckhove and

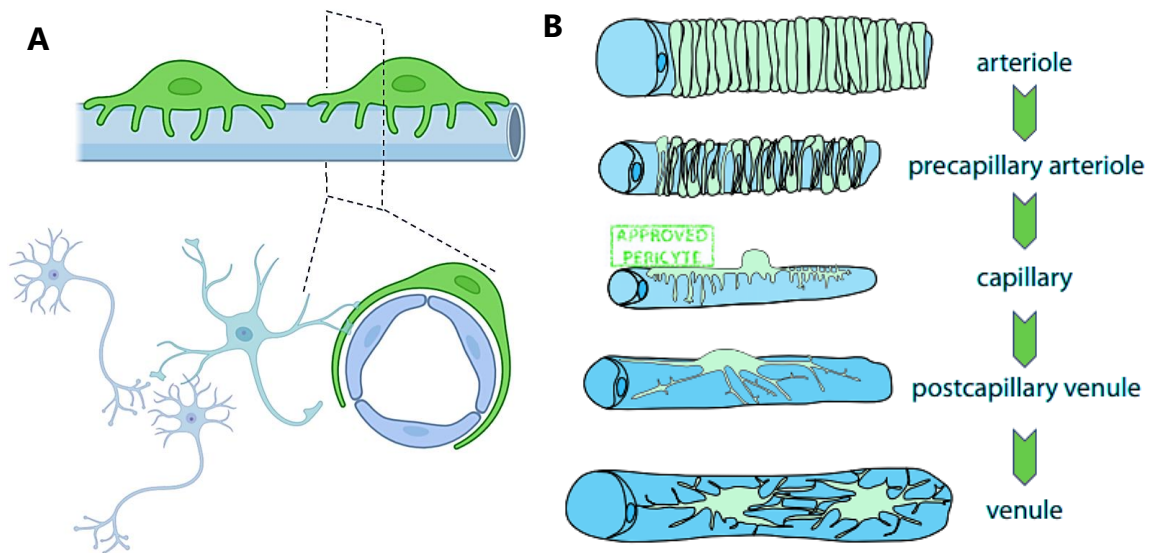


Figure 17. Pericyte Anatomy. (A) Pericytes (in green) surround the endothelial cells of the blood vessels to contain their circular form. They are connected to the neurons via astrocytes. This group of closely related cells forms the neurovascular unit. (B) A continuum of mural cell cyto-architecture from arteriole to venule. A single vSMC layer around arterioles and precapillary arterioles encircles the entire abluminal side of the endothelium. vSMCs around arterioles have a flattened, spindle-shaped appearance with few cytoplasmic processes, whereas around precapillary arterioles the cell bodies are distinctly protruding and extend several processes encircling the endothelium. Pericytes investing capillaries have a nearly rounded cell body that gives rise to a few primary processes running on the endothelium in the length of the capillary. The primary processes give rise to secondary perpendicular processes. The tips of secondary processes attach firmly to the endothelium. On postcapillary venules the mural cell body flattens and gives rise to many slender, branching processes. vSMCs covering venules have a relatively big, stellate shape cell body with many branching processes, which, unlike arteriolar vSMCs, do not wrap circularly around the endothelium. [Adapted from Armulik et al., 2011 with Biorender.com.](#)

Weber, 1981). In 1989, Skalli and colleagues detected the presence of α -SMA in pericytes using immunogold electron microscopy on Lowicryl-embedded tissues with an anti- α -SMA antibody raised against the NH₂-terminal decapeptide of α -SMA. Gold particles were observed in SMC, myoepithelial cells and pericytes. However, they were absent in endothelial cells (Skalli et al., 1986; Skalli et al., 1989). Skalli and colleagues recognized the pericytes by their proximity to endothelial cells and by their basal lamina. In their cytoplasmic portion facing endothelial cells, α -SMA was observed in microfilamentous bundles (Skalli et al., 1989). Due to their contractile properties by the presence of contractile proteins (myosin, tropomyosin and high expression of α -SMA) and their intermediate filament compositions (vimentin and desmin) (Fujimoto and Singer, 1987; Fujimoto et al., 1987), pericytes are compared to the vSMC (Gabbiani et al., 1981; Skalli et al., 1989) (Fig. 18). Thus, pericytes have a double role providing support to vasculature: 1) a structural role maintaining the circular shape of blood vessels and 2) a contracting mechanical role to regulate blood flow (Kelley et al., 1987; Schor and Schor, 1986; Tilton et al., 1979).

b. Platelet-Derived Growth Factor Receptor β

During the development of the vascular network, platelet-derived growth factor (PDGF) β , expressed by endothelial cells, bind to tyrosine kinase PDGF receptors (PDGFR) β , exclusively expressed on the surface of pericytes (Hellström et al., 1999; Lindahl et al., 1997). The PDGF β /PDGFR β recognition leads to a dimerization of the PDGFR β , followed by autophosphorylation of cytoplasmic tyrosine residues and binding of SH2 domain. Ultimately, a multitude of signal transduction pathways allows the proliferation, migration and recruitment of pericytes to the vascular wall of newly formed blood vessels for further angiogenesis sprouting (for review, Armulik et al., 2011; Hellström et al., 1999; Lindahl et al., 1997). Complete knock-down of *Pdgfb* or *Pdgfrb* genes, observed in mice, leads to embryonic lethality resulting from haemorrhages and oedemas due to mural cell deficiency

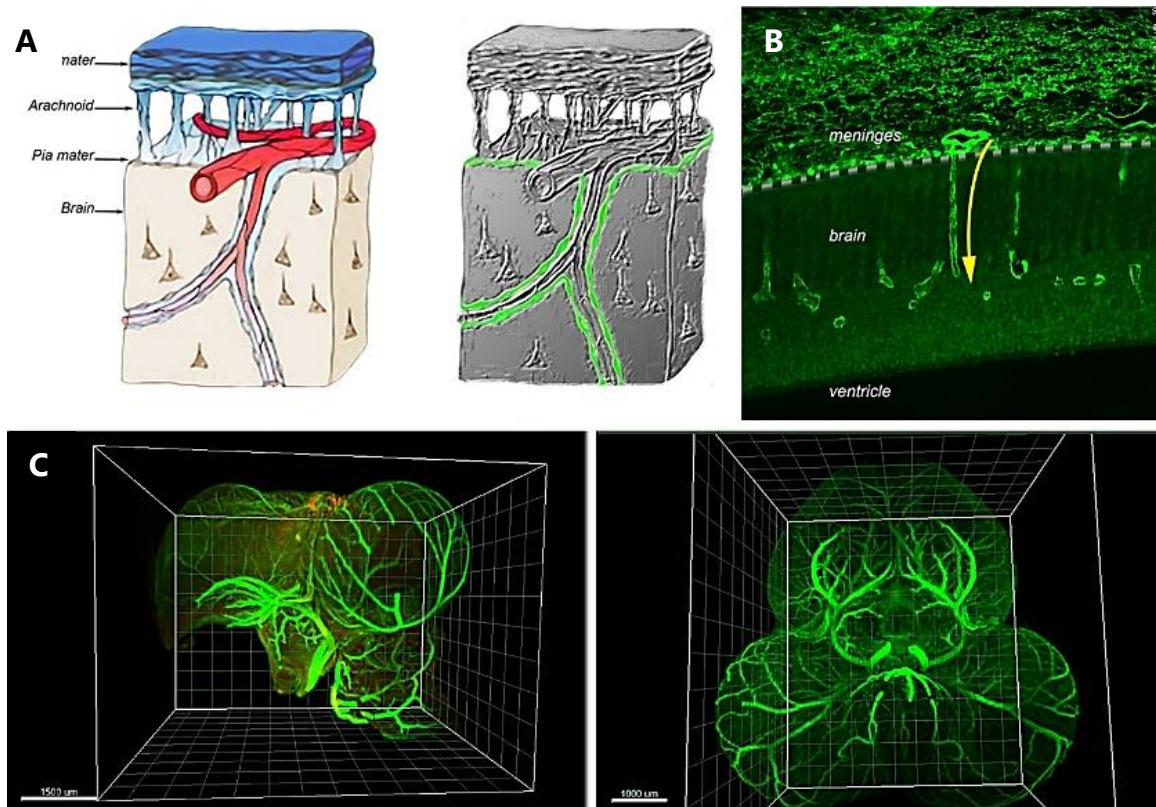


Figure 18. The meninges and brain vasculature. (A) Schematic representation of the different layers of the meninges (dura mater, arachnoid and pia mater). And the pericytes lining the capillaries in the brain (in green). (B) Histological section representing the macrophage-like pericytes invading the brain parenchyma (yellow arrow). On histological section (B) and the 3-dimensional rendering of the whole-brain vasculature imaging (C), an anti-smooth muscle actin (α -SMA) antibody is used to evidence pericytes. [From Creuzet's lab.](#)

(for review, Armulik et al., 2011; Levéen et al., 1994; Lindahl et al., 1997; Soriano, 1994). Thus, the PDGF β /PDGFR β recognition and the endothelial cells/pericytes interaction is compulsory for embryonic vascular development.

c. CD13/aminopeptidase N

CD13, a member of the zinc-binding metalloproteinase superfamily (Uzunalli et al., 2021), is localized essentially at the plasma membrane, especially on the side facing the brain parenchyma rather than on the endothelial side, and more in the soma than in the processes of pericytes (Alliot et al., 1999). CD13, also known as aminopeptidase N or ANPEP, has a role in signal transduction, differentiation and tumor metastasis (Uzunalli et al., 2021). CD13 is highly expressed in vSMC, especially of larger brain, and in pericytes, especially of small capillaries vessels (Alliot et al., 1999; Armulik et al., 2010; Bourassa et al., 2020). However, CD13 does not label endothelial cells (Alliot et al., 1999; Kunz et al., 1994). Furthermore, CD13 is also present in pericytes of meningeal and CP vessels (Alliot et al., 1999). CD13 is therefore used as a marker for brain capillary pericytes (for review, Armulik et al., 2011; Paul et al., 2012; Uzunalli et al., 2021).

d. Desmin and vimentin

In all eukaryotic cells, the cytoskeleton is made up of three major cytoskeletal elements: intermediate filaments, microtubules and microfilaments. Intermediate filaments are specific to each cell type. In muscle cells, the intermediate filaments contain mainly desmin and vimentin (Schmid et al., 1982).

In post-natal chickens, desmin and vimentin characterize the pericytes and SMC of several organs: chicken gizzard smooth muscle, differentiated SMC of the digestive and urogenital tracts, skeletal and cardiac muscles, exocrine pancreas, kidney, liver, and spleen (Fujimoto and Singer, 1987; Gabbiani et al., 1981). In all layers of the large arteries, including the aorta, the vast majority of cells contain vimentin, the predominant intermediate filament protein. On the contrary,

desmin is only found in some SMC of the aorta (Schmid et al., 1982).

In contrast, during chicken embryonic development, desmin is highly found in various organs and tissues: in the somites and all skeletal muscle, all visceral and vascular SMC, and the tracheoesophageal mesenchyme (Beall and Rosenquist, 1990). Expressions of desmin and vimentin vary during embryonic development. While desmin is increased in cardiomyocytes all along the chick embryonic development, the quantity of vimentin varies depending on the embryonic stage. Vélez and colleagues show a peak of vimentin at HH29, followed by a decrease up to HH39 in chick cardiomyocytes (Vélez et al., 2000).

An affinity-purified antibody raised against chicken gizzard desmin is used as a marker for selective staining of microvascular pericytes in several studies, differentiating them from endothelial cells and quiescent fibroblasts. However, this marker does not allow recognition of immature pericytes (Jindatip et al., 2012; for review, Nehls and Drenckhahn, 1993).

e. Neural/glial antigen 2

The neural/glial antigen (NG) 2 proteoglycan is a cell surface component found prominently in pericytes, contributing to their recruitment and to pericyte/endothelial cell interaction during vascular development of large vasculogenic vessels such as the aorta and in angiogenic micro vessels of the CNS (Huang et al., 2011; Ozerdem et al., 2001). Regardless of the type of vasculature, NG2 is expressed by mural cells of the blood vessels and is therefore used as a marker of the vSMC and especially of the developing pericytes in micro vessels (Ozerdem et al., 2001).

However, in 1987, Levine and Card identified the NG2 antigen at the surface of smooth protoplasmic astrocytes (Levine and Card, 1987). Since, the NG2 marker has been used to characterize other type of glial cells, especially the oligodendroglial precursor cells. These cells differentiate into oligodendrocytes,

glial cells found in the grey and white matter of the CNS, along with other glial cells, astrocytes and microglia (Bell et al., 2020; He et al., 2022; Reynolds and Hardy, 1997). Since the NG2 marker is a marker of glial cells in the CNS, it is not specific to pericytes and perivascular cells: it prevents differentiation between these cells and glial cells (Fig. 19).

Thus, CNC contributes to the morphogenetics of craniofacial and brain development and in particular to the development of branchial vascular sector, forebrain meninges and pericytes. Pericytes can be characterised by their position around vessels, by their morphology and by the expression of several surface markers. These cells have a double role: 1) providing support to vasculature and 2) a contracting mechanical role to regulate blood flow.

IV. Vascular network development

During embryonic development, blood vessels form via two distinct processes: vasculogenesis and angiogenesis. During vasculogenesis, mesodermal precursor cells, called angioblasts, differentiate into endothelial cells. This process establishes the first major vascular structures in the developing embryo, such as the dorsal aorta or the cardinal vein (Fruttiger, 2002). Angiogenesis generates new vessels from pre-existing ones, like capillaries and venules, without involving the angioblasts to extend the vascular network (Fruttiger, 2002). Angiogenesis is the principle process by which certain organs, such as the embryonic brain and kidney, become vascularized (Breier and Risau, 1996; for review, Ferrara and Alitalo, 1999; Ozerdem et al., 2001; Risau, 1997).

1. Vasculogenesis

Initially, vascularization develops via a mechanism called vasculogenesis where mesoderm-derived angioblasts differentiate to form the primitive blood vessels, also known as primitive vascular plexus. These angioblasts, originally devoid of a lumen, give rise to the vascular endothelial cells (Risau, 1997). Later, the endothelial channels form a vascular tree-like network composed of mature vessels (for review, Ferrara and Alitalo, 1999).

To initiate angioblastic differentiation, the endoderm produces vascular endothelial growth factors (VEGF) that will recognise in a paracrine manner their VEGF receptors (VEGFR) 2, expressed by mesoderm-derived angioblasts (Risau, 1997). Since embryos lacking VEGFR2 or losing a single *VEGF* allele results in embryonic lethality with a defect in angioblastic lineage and an insufficient development of the vascular system, VEGF is essential for the development and differentiation of the vascular system (for review, Ferrara and Alitalo, 1999; Shalaby et al., 1995). Later in development, angioblasts express a second receptor for VEGF, VEGFR1 (previously known as FLT-1), to form the functional blood vessels by assembling together. Overall, the quantity and activity of both VEGF ligands and receptors determine angioblast differentiation and survival during vasculogenesis (Risau, 1997).

2. Angiogenesis

Unlike vasculogenesis forming new blood vessels, angiogenesis develops new capillaries from pre-existing blood vessels (Egginton and Gerritsen, 2003). Once the primitive vascular plexus is formed, the endothelial cells can generate new capillaries via two angiogenesis processes: either by sprouting from pre-existing vessels or by splitting from their vessel of origin (called intussusception or non-sprouting angiogenesis) (for review, Colville-Nash and Willoughby, 1997; Risau, 1997).

Sprouting angiogenesis occur either in the embryo (particularly in the brain) or in the yolk sac. Seven critical steps take place during sprouting angiogenesis: 1) angiogenesis is initiated by a number of growth factors, 2) endothelial cells secrete proteases to disintegrate the basement membrane and extracellular matrix, 3) the cells migrate to form a capillary sprout, 4) the endothelial cells proliferate to increase the capillary sprout, 5) forming a lumen and new basement membrane, 6) two capillary sprouts join to form a capillary loop and 7) form a second-generation capillary sprout. This sprouting angiogenesis gives rise to a functional maturation of the endothelium (for review, Colville-Nash and Willoughby, 1997; Risau, 1997). In fine, the collateral sprouts invade the neighbouring tissues (Ozerdem et al., 2001) (Fig. 20).

During non-sprouting angiogenesis, endothelial cells proliferate in the lumen of a pre-existing vessel, forming slender transcapillary tissue pillars which increase in size by intussusception (Burri and Djonov, 2002).

Similarly to vasculogenesis, angiogenesis is controlled by a variety of mediators, such as peptide growth factors. For example, VEGF (Breier and Risau, 1996) and tumour necrosis factor (TNF) α are powerful angiogenic mediators enhancing the sprouting of neural capillaries in vivo. Extracellular matrix components such as hyaluronan, various collagens and fibrin also control angiogenesis in vivo (for review, Colville-Nash and Willoughby, 1997). Canonical and non-canonical Wnt signalling pathways, regulated by SFRP family proteins, are implicated in angiogenesis (Scholz et al., 2016; Vanhollebeke et al., 2015; Zhou & Nathans, 2014) and are specifically essential for vascular endothelial cells growth through transcriptional regulation of VEGF. Defects in β -catenin and Wnt signalling can lead to over-expression of VEGF (Jun Olsen et al., 2017). Wnt7a/b binds to Fzd4 to initiate the activation of the canonical Wnt/ β -catenin signalling (Posokhova et al., 2015; Zhou & Nathans, 2014). The activation of the co-receptors GPR124 and LRP5

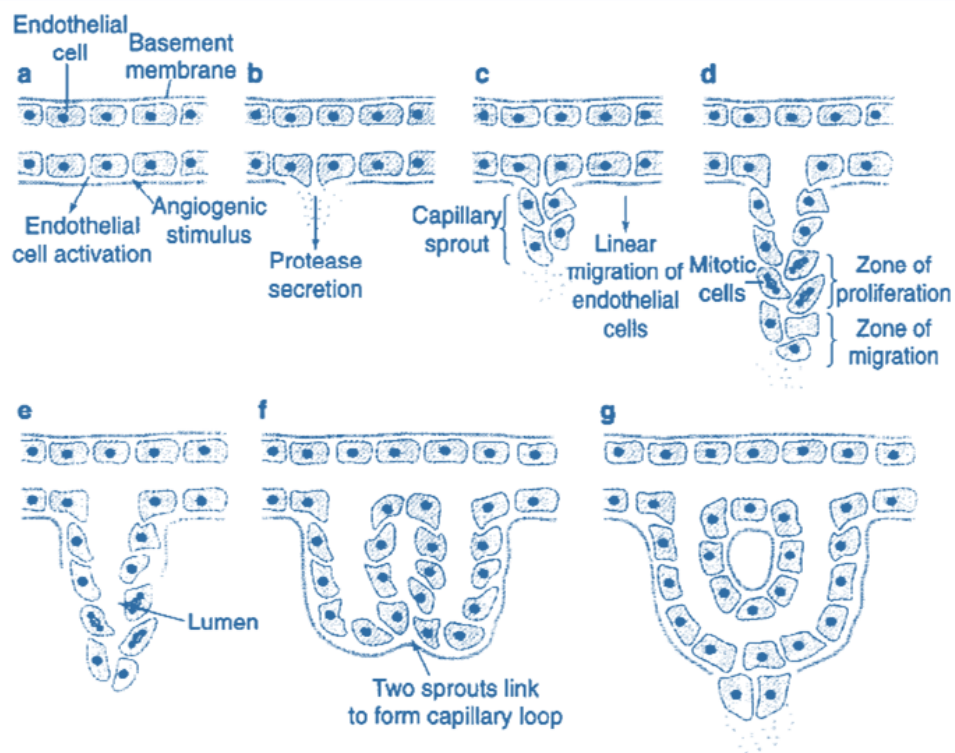


Figure 20. Seven critical steps of the angiogenic response. (a) Endothelial cells are activated by an angiogenic stimulus; (b) the endothelial cells secrete proteases to degrade the basement membrane and extracellular matrix and (c) a capillary sprout is formed by directed migration of endothelial cells. (d) The capillary sprout grows and (e) forms a lumen and new basement membrane. (f) Two sprouts become linked to form a capillary loop and (g) second-generation capillary sprouts begin to form. Adapted from Colville-Nash and Willoughby, 1997.

leads to a destabilization of the Axin, GSK3 β , CK1 α/ϵ complex). β -catenin is stabilised, allowing its translocation to the nucleus, where it can bind to TCF/LEF transcription factors, leading to vascularisation and angiogenesis ([Jun Olsen et al., 2017](#)).

V. Contribution of the meninges to the choroid plexus

The CSF constitute the immediate environment of the brain and the spinal cord ([for review, Fame and Lehtinen, 2020](#)). The CSF was first known by the Egyptians and the Greeks during the antiquity to fill the brain. In the course of the XVth and XVIth centuries, anatomists such as DaVinci (1500s) and Vesalius (1543) described the ventricular system of the CNS in which the CSF circulates. During the XXth century, the neurosurgeons Harvey Cushing first described the production of the CSF by the CP in adults ([Cushing, 1914](#)) and Walter Dandy modelled the CSF circulation in the ventricles ([Dandy, 1919](#)). However, till 1919, the CSF was mostly recognized as a protective fluid cushion, an ionic buffer and a sink for waste. More recent studies have shown the importance of the CSF as an integral CNS component with dynamic and diverse roles emerging in parallel with the developing CNS. For instance, recent discoveries have shown that embryonic and adult neural precursors harbour primary cilia that protrude into the CSF, that CSF components can exchange with the interstitial fluid of the brain parenchyma, and that the CSF contents can reflect brain states including satiety, sleep, and disease ([for review, Fame and Lehtinen, 2020](#)). The rapidly evolving area and complexity of the CSF system leads to controversial neurobiology at the crossroad of CSF system barriers ([for reviews, Abbott et al., 2018; Saunders et al., 2018](#)), CP fluid production and detoxifying functions ([for review, Gherzi-Egea et al., 2018; Praetorius and Damkier, 2017](#)), brain vasculature development ([Chow and Gu,](#)

2015), glymphatic system function (Jessen et al., 2015; Louveau et al., 2017), ependymal cell development and function (for review, Spassky and Meunier, 2017) and meningeal lymphatic function (Louveau et al., 2015; Raper et al., 2016).

1. Formation of the falx cerebri

During the development of the meninges development, the dura mater invaginates along the longitudinal fissure of the brain to separate both cerebral hemispheres. Specifically, the dura mater invaginates between brain regions to form dural partitions: the falx cerebri, the falx cerebelli, the tentorium cerebelli, and the sellar diaphragm (Bair and Munakomi, 2022).

The falx cerebri is a sickle-shaped structure, anchored posteriorly to the internal occipital protuberance, travels superiorly to the corpus callosum, and anchors anteriorly to the crista galli which sits above the ethmoid bone (Bair and Munakomi, 2022; KostECKI et al., 2022). Two vessels irrigate the falx cerebri: the anterior meningeal artery, also known as the anterior falx artery or anterior falcine artery, arises from the ethmoidal artery and irrigates the anterior falx cerebri. The posterior falx cerebri receives its blood supply from the posterior meningeal artery, arising from the ascending pharyngeal artery (Bair and Munakomi, 2022; Pollock and Newton, 1968). The falx cerebri then drains blood and brain CSF from the arachnoid granulation via dural sinuses (superior and inferior sagittal sinuses). The blood from these sinuses drains into the internal jugular veins and finally into the systemic circulation (Bayot et al., 2022) (**Fig. 21**). The falx cerebri is a common site for various pathologies. Falx cerebri agenesis leads to developmental complications with neural symptoms (Ryu, 2010). Its development is correlated to brain development: semi-lobar holoprosencephaly can prevent appropriate formation of the dural partitions (Cayea et al., 1984). The falx cerebri structure is also related to post-natal pathologies such as falcine meningiomas and age-related calcification (Welikala, 1947).

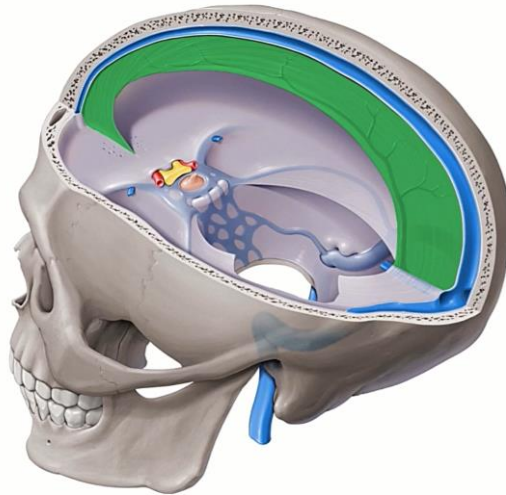


Figure 21. The neural crest-derived meninges form the falx cerebri. The falx cerebri (in green) is a sickle-shaped structure, anchored posteriorly to the internal occipital protuberance, travels superiorly to the corpus callosum, and anchors anteriorly to the crista galli which sits above the ethmoid bone. The falx cerebri drains blood and brain CSF from the arachnoid granulation via dural sinuses (superior and inferior sagittal sinuses). [From Kenhub.com](https://www.kenhub.com).

2. Choroid plexus functions and development

The CP is essential for the healthy development of the brain. It produces the majority of CSF. Genetic factors control CP progenitor cell proliferation and differentiation, and a loss of these genetic factors could lead to a reduction of all CP tissues (Langford et al., 2020), a reduction of CSF production (Lindvall et al., 1978), a collapse of the brain ventricles (Dandy, 1919), and a shrinkage of the brain (Monuki et al., 2001).

The CP is a three-dimensional (3D) organ system composed of the ependyma, an outer-layer of epithelial cells of neuroepithelial origin, and the stroma, a vascular network including stromal cells of meningeal origin (Catala, 1998) (Fig. 22). The ependymocytes participate in the formation of the ependyma whereas the CNC cells contribute to the formation of the stroma (Creuzet, unpublished) (Fig. 23). During its development, the CP emerges by invagination of the dorsal midline and rhombic lip lineages (Monuki et al., 2001). A CP is formed in each ventricle and starts emerging around embryonic day (E) 11 in mice and between Carnegie stages (CS) 18 and 19 in humans (O'Rahilly and Müller, 1990; Shiraishi et al., 2013). Each CP is a distinct tissue emerging overtime, starting with the fourth ventricle (4V) CP emerging from the rhombencephalon and roof plate (Hunter and Dymecki, 2007; Nielsen and Dymecki, 2010), followed by the lateral ventricles (LV) CP in the telencephalon and the third ventricle (3V) CP in the diencephalon.

The LV and 3V CP eventually connect but maintain distinct identities (Currele et al., 2005). Each CP has a distinct anatomical origin and gene expression profile (Dani et al., 2021). The LV and 3V CP start arising from the interventricular foramen at CS18. The growth of the LV CP follows the expansion of the LV, forming a C-shape between CS18 and CS23. The CP first develop laterally and caudally towards the inferior horn of the LV up to CS20, then develop in all directions after CS21, especially dorsally after CS22. Finally, at CS23, the CP grow frontally, filling one-

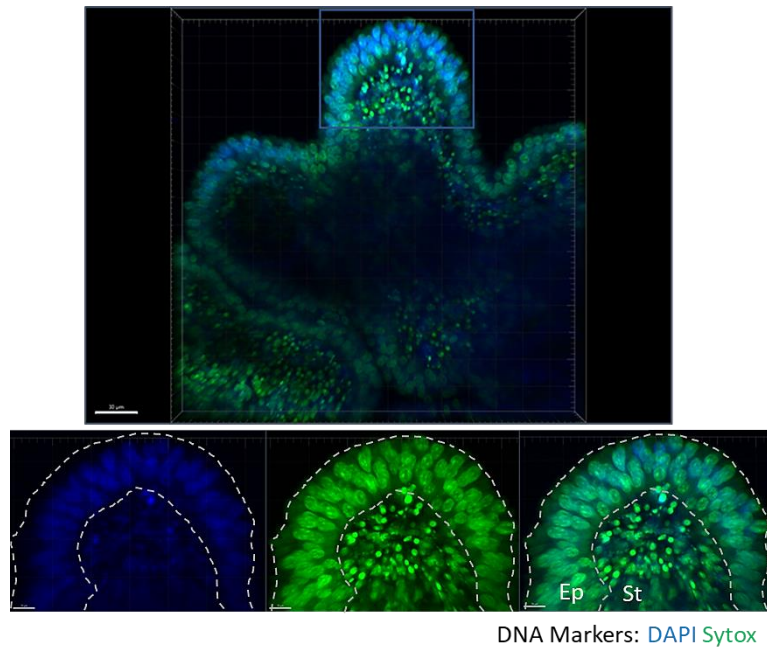


Figure 22. 3D *ex vivo* explant of a CP. The ependyma (Ep) separating the vascular system from the CSF, is composed of epithelial cells while the stroma (St), containing the blood vessels, derives partly from the CNC. Explants are stained with two separate DNA markers: DAPI in blue and Sytox in green. [Confocal imaging, Bruet, unpublished.](#)

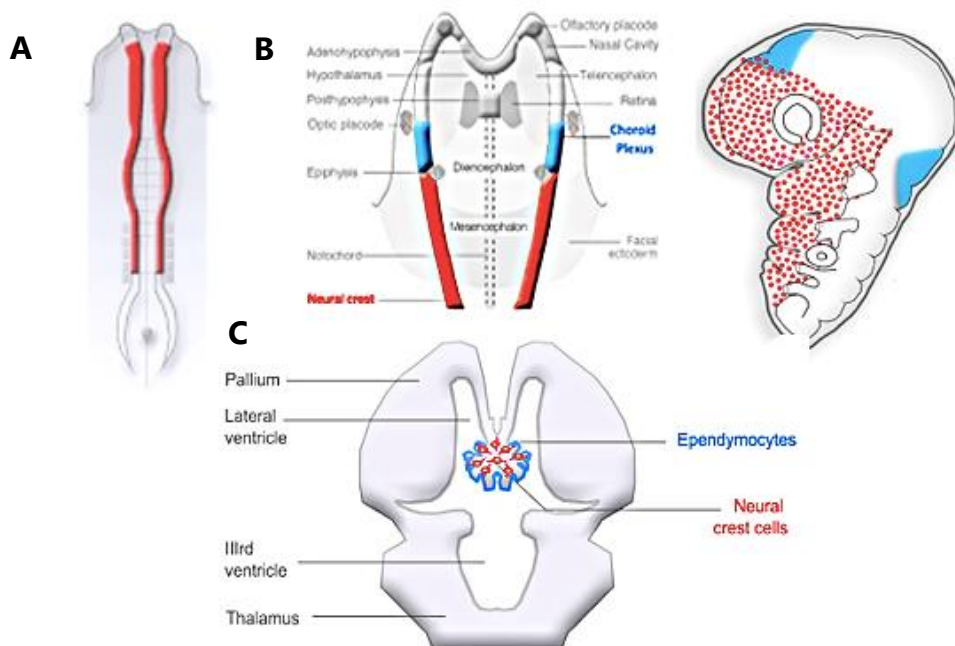


Figure 23. Contribution of the CNC to the CP. (A) NC domain during the neurulation stage. (B) Topography of the presumptive NC territories (in red) and prosencephalic CP (in blue), before CNC cells migration. (C) Respective contribution of the neuroepithelium (in blue: ependymocytes) and of the CNC (in red) in the formation of the CP. [From Creuzet.](#)

fourth of the LV. The volume ratio of CP to LV increases by approximately 5-fold from CS19 to CS23 so the CP increase its volume relatively faster than the LV. No morphological or volumetric difference is observed between the left and right CP (Shiraishi et al., 2013) (Fig. 24).

Even though the embryonic origin of the meninges and stromal CP varies across species, in birds (and probably in mammals), the meninges covering the spinal cord and the rhombencephalon, as well as the 4V stromal CP derive from the somitic mesoderm, whereas the diencephalic and telencephalic meninges, LV and 3V stromal CP derive from the NC (Catala, 1998). As the CP develop, they undergo specific maturation with an increase in microvilli surface, allowing more interaction with the CSF, an increase in basal surface through fenestrated capillaries, allowing more interaction with systemic blood, and metabolic shifts, with higher glycogen stores in CP epithelial cells (Keep and Jones, 1990). The mature CP is specialized to secrete CSF in response to osmotic gradient. The role of the epithelial layer is to selectively secrete neurotransmitters, transferrin and insulin, leptin, folate copper, growth factors or morphogens including retinoic acid, Fgf2, Wnt5a and Shh and other components from the blood supplies via the fenestrated capillaries of the basal surface into the CSF. The secretion of ions depends on the Na^+ gradient generated by the Na^+/K^+ pump and the balance between osmotic gradient and protein secretion. H_2O is secreted through aquaporin1 (AQP1) (Karimy et al., 2016).

3. CSF in the homeostasis of the brain

Regulation of CSF volume, osmolality and pH is essential for a healthy brain. On the one hand, the absence of CSF, with depressurization in the ventricles, leads to neural progenitor apoptosis. The CSF regulates neuroepithelial survival, proliferation, and differentiation of neuroepithelial stem cells during development

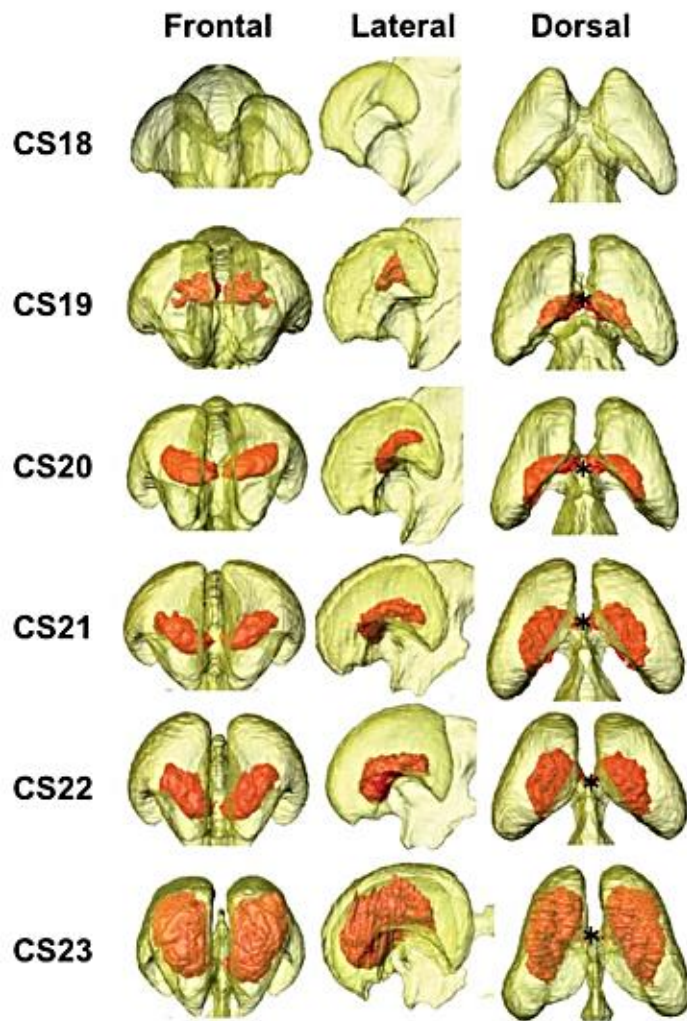


Figure 24. Representative 3D image of the CP (red) within the lateral ventricles (yellow). Frontal, lateral, and dorsal view between CS18 and CS23 are shown. [From Shiraishi et al., 2013.](#)

(Gato et al., 2005). On the other hand, an increased CSF volume with a high pressure in the brain leads to a debilitating and life-threatening condition called hydrocephalus, causing in fine brain herniation, learning and memory deficits, and epilepsy (for review, Bräutigam et al., 2019; Karimy et al., 2016). Cases of hydrocephalus have also led to AD (for review, Reeves et al., 2020). In addition, elevated extra-axial CSF surrounding the brain in the subarachnoid space has been shown to be predictive of later development in infants and young children of autism spectrum disorder (ASD) (Shen et al., 2013) (Fig. 26). Thus, CSF disturbances are most probably the origin of disease, and neurodegeneration is rather a consequence than a pathogenetic factor.

4. Early roles of the CSF

The CSF plays an important role during neurodevelopment as it provides a diverse array of molecules (e.g., proteins, neuropeptides, membrane-bound vesicles) to the embryonic CNS progenitors. The neuroepithelial cells contact the CSF via their apical surface, which also harbors primary cilia, contributing to retained stemness of these cells (Paridaen et al., 2013). The adult neural stem cells of the subventricular zone (SVZ) also maintain contact with the CSF, which functions as a stem cell niche in this context (Kokovay et al., 2012; Silva-Vargas et al., 2016). During early development, CSF maturation goes through three successive stages: the amniotic fluid trapped in the brain vesicles during NT closure (E8.5), the nascent CSF leading to the expansion of the ventricular system following neurulation (E10.5) and the mature CSF produced by the CP (E14.5) (Chau et al., 2015). During these stages, CSF undergoes a dynamic transition with a substantial divergence of the proteomic composition, stage-specific for the normal development of the brain (Fig. 27). These changes include essential signaling molecules such as Shh, Bmps, and retinoic acid (Chau et al., 2018). CSF supports neuron viability and network function in a way that cannot be achieved with

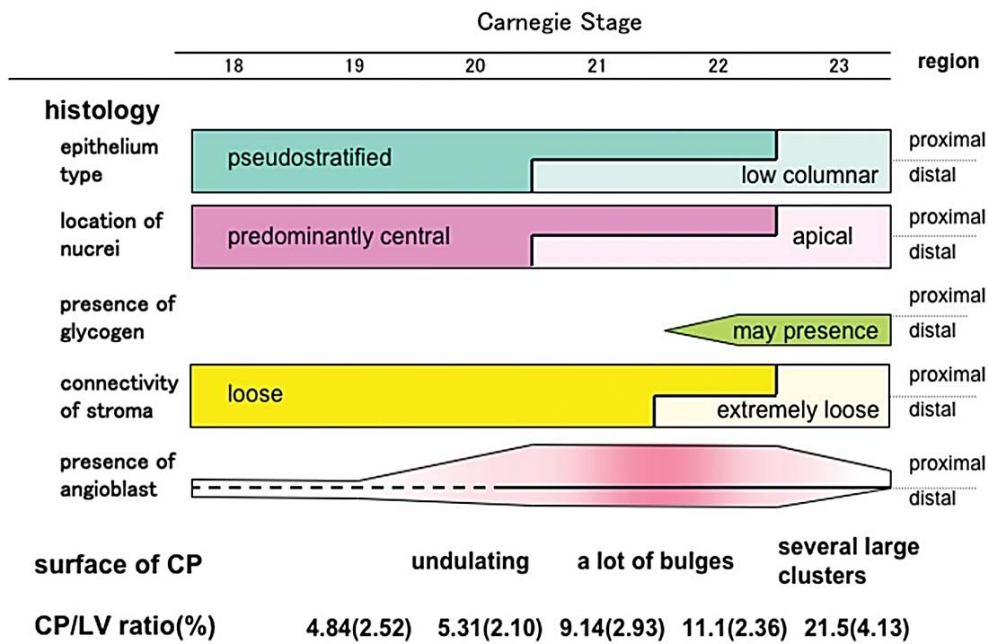


Figure 25. Summary of histological findings of CP between CS18 and CS23. CP/LV ratio: ratio of volume of CP to volume of lateral ventricles (LV). Standard deviation of them is in parentheses. From Shiraishi et al., 2013.

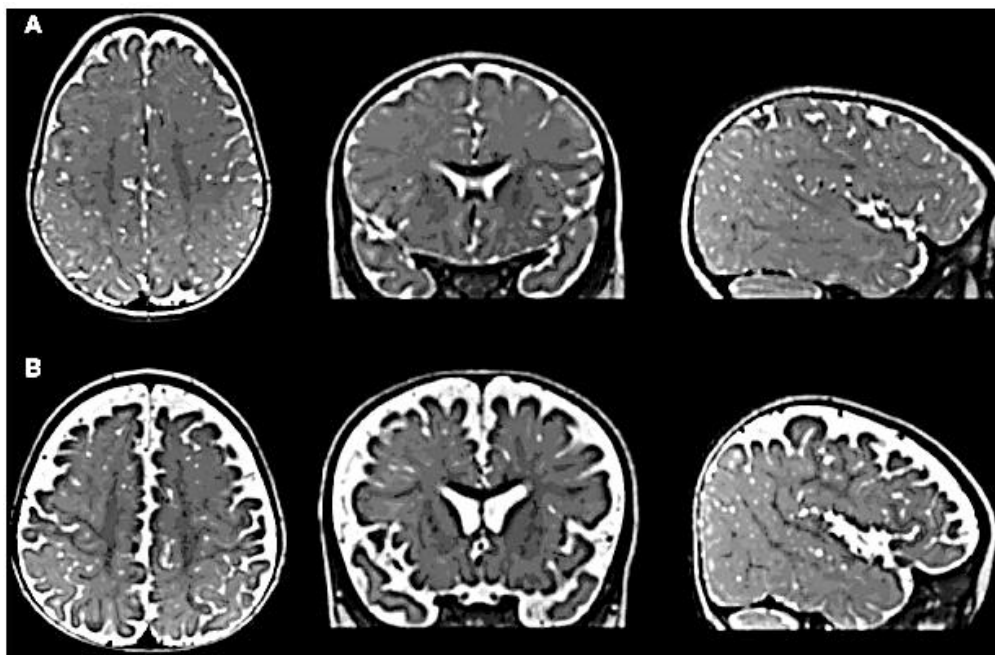


Figure 26. Comparison of T2-weighted images. (A) T2-weighted image of a low-risk infant with normal MRI at 9 months, confirmed as having typical development at 36 months. CSF is indicated as brighter regions in these images. Images are of a horizontal section (left) coronal section (middle) and sagittal section (right) through the brain. (B) Similar T2-weighted images of a high-risk infant with excessive extra-axial fluid at 9 months, diagnosed with ASD at 36 months. From Shen et al., 2013.

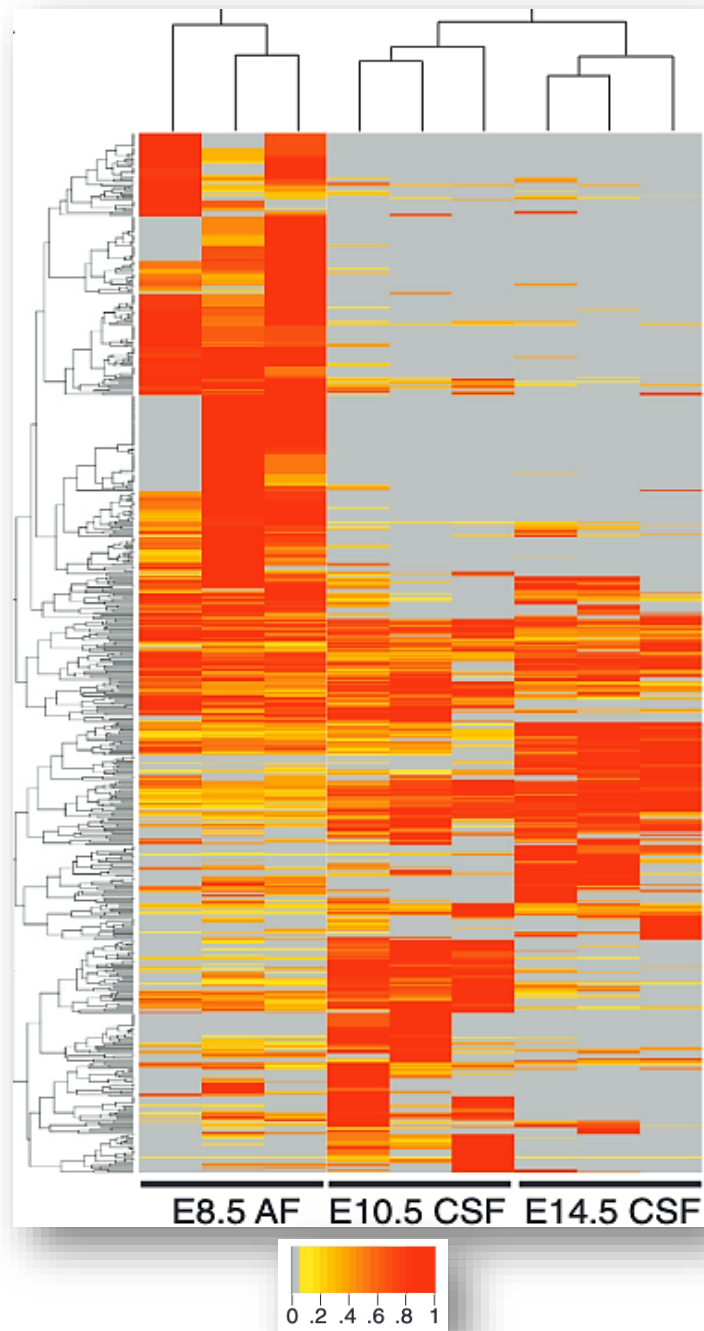


Figure 27. Mass Spectrometry reveals dynamic changes in CSF proteome as it differentiates from E8.5 amniotic fluid (AF) to E14.5 CSF. Heatmap of normalized spectral counts reveals differential protein availability between E8.5 AF, E10.5 CSF, and E14.5 CSF. The unsupervised hierarchical clustering grouped the three biological replicates of each fluid together. Each replicate contains 30 mg total CSF protein pooled from multiple embryos. The spectral counts were scaled such that for each protein, the sample with the highest spectral count is set as one. The grey indicates undetected protein (i.e., 0 spectral counts). Proteins with peptides detected in at least two samples were included in the heatmap. [From Chau et al., 2015.](#)

common culture media or artificial CSF (Chau et al., 2015).

5. CSF movement and outflow

The CSF generally flows from the CP secretion sites to the extracranial lymphatics and is drained by distinct anatomical structures: in the subarachnoid space through the arachnoid villi (Weed, 1914), through the meningeal lymphatic vessels (for reviews, Cserr et al., 1992; Pollay, 2010), through the cranial and spinal nerve sheaths into the lymphatic system (Brierley and Field, 1948; Ma et al., 2019), through the olfactory nerve sheaths, draining into the nasal cavity and through the cribriform plate (Mollanji et al., 2002). The cardiorespiratory system modules the CSF movement through the ventricles and spinal canal. During systole, when the heart muscle exhibit pressure, the CSF flows from the LV to the 3V by the foramina of Monro, and into the 4V through the aqueduct of Sylvius. The CSF then gains the subarachnoid space by the foramina of Magendie and Luschka before being drained. During diastole, when the heart muscle is relaxed, the CSF flows in the opposite direction (Casaca-Carreira et al., 2018) (Fig. 28). Therefore, the CSF movement is dependent on the onset of heartbeat, linking the circulatory and CSF developmental systems (Fame et al., 2016) (Fig. 29).

6. CSF barriers and immune functions

The CSF is compartmentalized both from the brain parenchyma (CSF-Brain barrier) and from the blood system (Blood-CSF barrier). The CSF-Brain barrier is composed by a layer of neuronal progenitors joined by adherent junctions along the ventricular surface. The Blood-CSF barrier is composed by a layer of ependymal cells joined by tight junctions along the CP epithelium (Fig. 30). The ependymal cells express stage-specific transporters as mentioned previously. In both barriers,

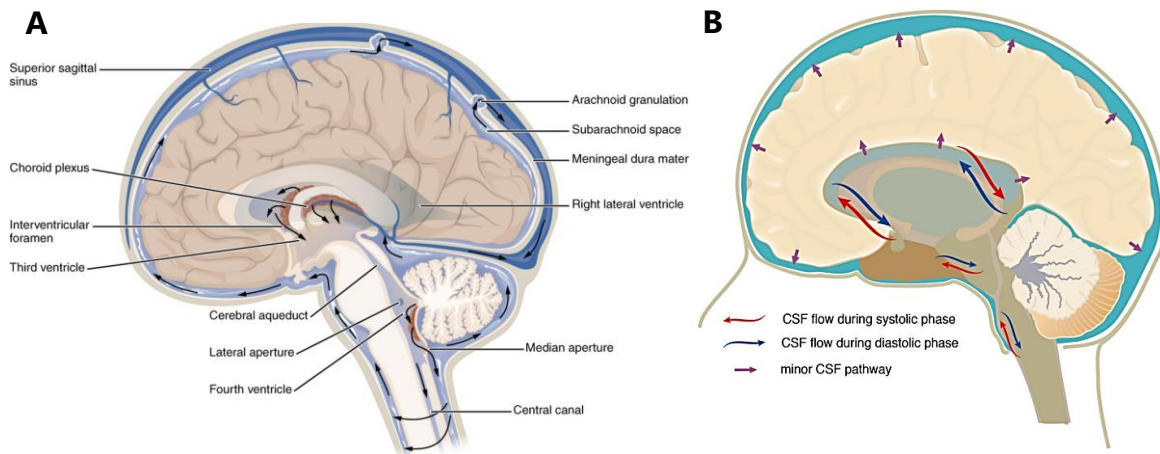


Figure 28. Schematic representation of the major CSF pathways. (A) The CSF flows from the CP secretion sites to the extracranial lymphatics and is drained by distinct anatomical structures: in the subarachnoid space through the arachnoid granulations, through the meningeal lymphatic vessels, through the cranial and spinal nerve sheaths into the lymphatic system, through the olfactory nerve sheaths, draining into the nasal cavity and through the cribriform plate. [From Wikimedia.org](#). (B) The major pathway follows the cardiac rhythm, while the minor pathway is described as a constant flow of CSF through the ependyma towards the subarachnoid space. [From Casaca-Carreira et al., 2018](#).

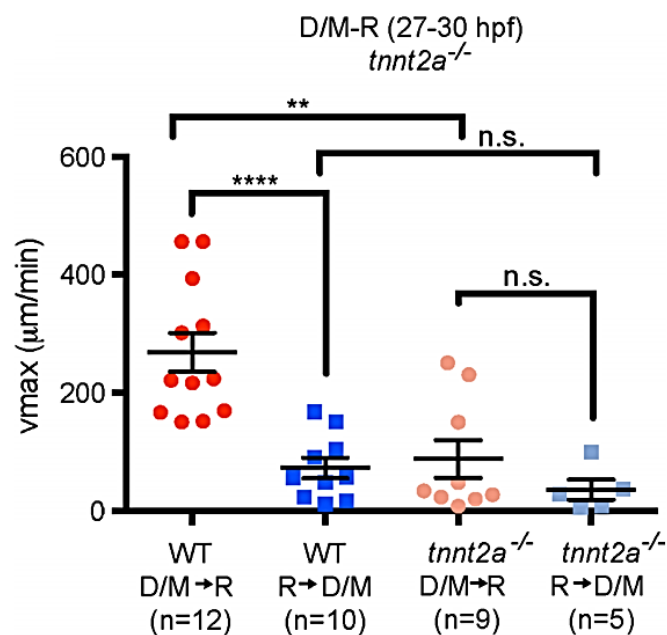


Figure 29. Directionality of CSF movement is partially dependent on heartbeat at early larval stage. In *tnnt2a*^{-/-} mutant fish there is no directionality of CSF movement observed through the diencephalic/mesencephalic to rhombencephalic aqueduct. Horizontal lines represent average v_{max} and error bars denote SEM. p value calculated using unpaired Student's t test, **p < 0.001; ****p < 0.0001; n.s. not significant, D/M diencephalic/mesencephalic ventricle, R rhombencephalic ventricle, hpf hours post-fertilization. [From Fame et al., 2016](#).

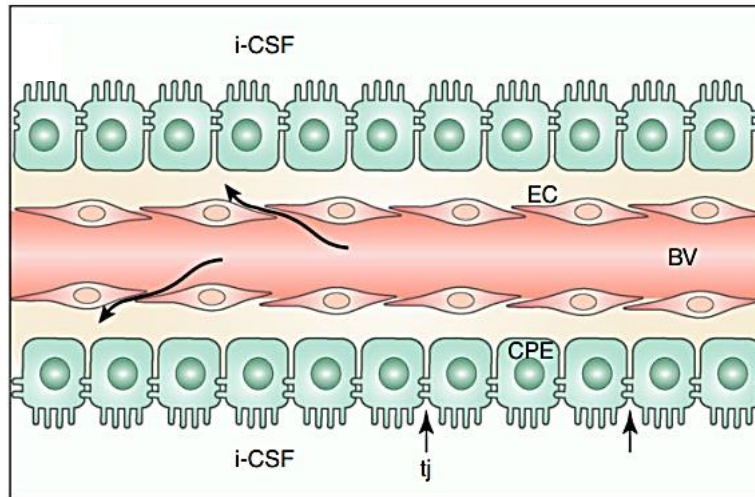


Figure 30. Schematic diagram of the blood-CSF barrier. The blood-CSF barrier is situated in the CP within each brain ventricle. Barrier-forming cells are the epithelial cells (CPE), which have tight junctions at their apical side (CSF facing, arrowheads). Blood vessels (BV) are fenestrated and do not form a barrier (arrows); apical microvilli increase exchange surface of epithelial cells to the internal CSF (i-CSF). [From Saunders et al., 2018.](#)

only the apical surface is in contact with the CSF, preventing exchange of large molecules (for review, [Saunders et al., 2018](#)).

The CP is a critical and active interface between the brain and circulating immune cells (for reviews, [Engelhardt and Ransohoff, 2005](#); [Kierdorf et al., 2019](#)). The separation of the CSF from the blood system is precisely called the CSF-blood interface. Thus, there is no real blood-brain barrier and it leads to the possible entrance for infection or intoxication from the CSF to the brain via the CP. The CP is the interface between the brain and the circulating immune cells. During neuroinflammation, specific CP permeability changes allow immune cells entry into the CNS through the CP: tight junctions breakdown, expression of immune adhesion molecules like selectins (L-selectin (leucocytes), P-selectin (platelets) and E-selectin (endothelial cells), and positive attraction through chemokines or cytokines ([Llovera et al., 2017](#)). Therefore, immune surveillance is probably mediated by other mechanisms at the CSF-blood interface. However, CNC-derived pericytes, so far characterized by their structural role in vasculature ([Appaix, 2014](#)), have never been categorized as immune cells in embryos.

7. Kolmer's cells, choroid plexus macrophagic cells

In 1921, Kolmer described specific cells of the CP called Kolmer's cells. These cells are attached to the ventricular surface of CP epithelial cells by its pseudopodal cytoplasmic processes ([Nakamura et al., 1982](#)) (**Fig. 31**). In 1953, Ariëns-Kappers renamed these Kolmer's cells "epiplexus cells" ("Epiplexuszellen") to emphasize their epi-epithelial position ([Carpenter et al., 1970](#); [Nakamura et al., 1982](#)). The epiplexus cells are in close apposition to the brush border of the choroidal epithelium. Microvilli and cilia of epithelial cells penetrate the pit-like invaginations found at the plasma membrane of epiplexus cells ([Carpenter et al., 1970](#)).

Ariëns-Kappers described the phagocytic behavior of epiplexus cells. Like other type of macrophages, the epiplexus cells move actively. They are polymorphic,

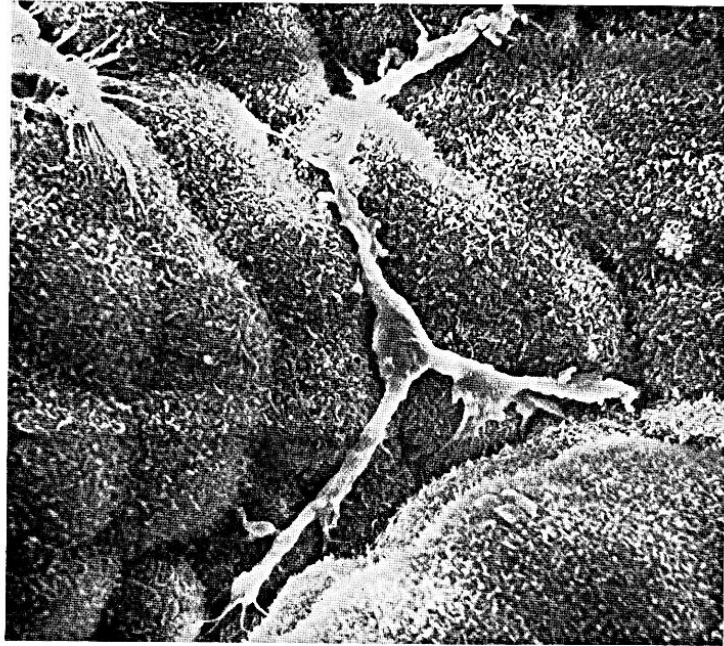


Figure 31. Kolmer's cell. Triangular cell body and three pseudopod-like processes are seen. Fibrous processes emerge from the sides or tips of the pseudopod-like processes. ×3,600. [From Hosoya and Fujita, 1973.](#)

ranging from round to polar and stellate and their shape varies from cell to cell. They also display both microvilli and pseudopodal processes. Their phagocytic role is emphasized by the presence of numerous lysosomes and vacuoles, and a moderate number of mitochondria, as well as clusters of free ribosomes in proximity of agranular and granular endoplasmic reticulum (Carpenter et al., 1970; Hosoya and Fujita, 1973; Joukal et al., 2016). Additionally, epiplexus cells are actively recruited and may play a significant immune role in inflammation in case of infection or hemorrhagic strokes, such as subarachnoid hemorrhage. Activation of Kolmer's cells leads to hypersecretion of CSF from the CP and is often associated with spontaneous hydrocephalus (Joukal et al., 2016; Koduri et al., 2020).

Kolmer's cells were first observed in amphibians and further confirmed in other vertebrates such as salamander and guinea pigs by Ariëns-Kappers, cats (Carpenter et al., 1970), rodents (Koduri et al., 2020), *Cebus apella apella* monkeys (Tamega et al., 2000) and humans (Biondi, 1934). However, even though their role in immune defence has been studied since the 1950s, the origin of these cells has not yet been identified and could probably derive from NCC.

The CP, present in all brain ventricles, are essential for the healthy development of the brain. They produce the majority of CSF which volume, osmolality and pH is critical for a healthy brain. The CSF flows to the extracranial lymphatics and is drained by distinct anatomical structures. CSF has multiple roles in the brain, participating in 1) brain protection, 2) homeostasis and 3) clearing wastes. The CP serve an interface between the brain and circulating immune cells. Immune surveillance is also provided by Kolmer's cells, CP macrophagic cells.

VI. Cephalic meninges and CP physiopathology during development

1. *Falx cerebri malformation*

An inbred mouse strain, the BTBR T+ tf/J mouse, is characterized by an abnormal development of the meninges, with meningeal extension atrophied in adult mice and an altered trajectory of the meninges coursing beneath the hippocampal formation. These mice present an abnormally small hippocampal commissure and a total absence of corpus callosum (Wahlsten et al., 2003) due to an elongated falx cerebri, separating the two brain hemispheres in the forebrain (Fig. 32). Besides, BTBR T+ tf/J mice's LV are shrunk and their CP, although thicker, are reduced in length. Enlarged arteries are also observed in the ventral extremity of the falx cerebri (Mercier et al., 2011).

The BTBR T+ tf/J mouse is studied as a model of autism as they acquire the three diagnostic symptom domains of autistic behavior, as described previously : social deficit interaction, repetitive behavior and impaired communication (American Psychiatric Association, 2013; Nicolini and Fahnstock, 2018). The BTBR mice lack social interaction as they spend more time with non-social novel objects than stranger mice, less time in engaged social interactions and sniffing of each other than B6 control mice. They have unusual spontaneous repetitive behavior patterns with high level of repetitive self-grooming and lack in communication as they sniff their cage mates' whiskers and mouth less and for a shorter time than B6 control mice (McFarlane et al., 2008). Thus, the malformation of the falx cerebri, and more generally of the meninges, could impact the social behavior at birth, leading to autistic symptoms.

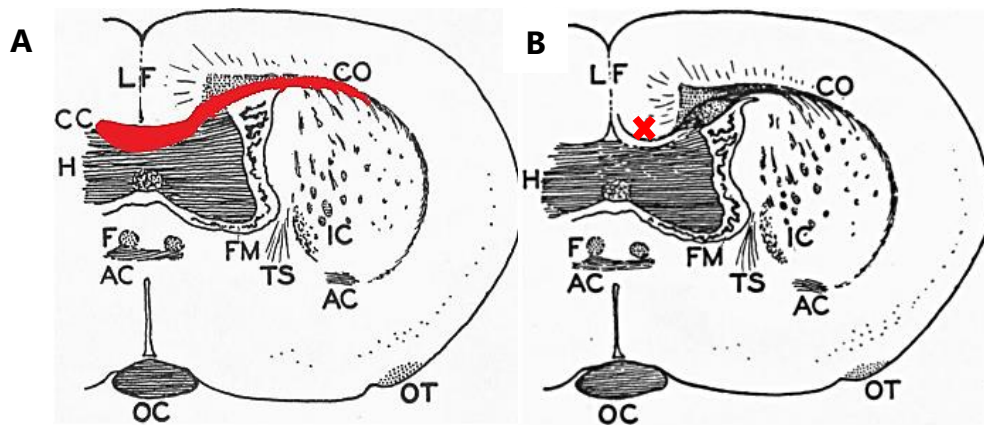


Figure 32. Elongated falx cerebri, separating the two brain hemispheres in the forebrain leads to a total absence of corpus callosum. (A) Cross-section through the cerebral hemispheres of the normal mouse, at the level of the foramen of Munro (FM). All three commissures of the forebrain are shown. The anterior commissure (AC) is cut twice, once in its central portion, surmounted by the descending columns of the fornix (F), and also in the temporal limb. The hippocampal commissure (H) with the corpus callosum (CC, in red) above it, display the structure typical of rodents. In addition, the section shows the centrum ovale (CO), internal capsule (IC), terminal striae (TS), lateral olfactory tract (OT) and optic chiasm (OC). (B) Cross-section through the cerebral hemispheres of the abnormal brain. The corpus callosum is absent (red cross). The longitudinal fissure (LF) extends down to the hippocampal commissure, with no dorsal connection of the hemispheres. [Adapted from King and Keeler, 1932.](#)

2. Syndrome/disorders with neurocristopathy manifestations

A series of epidemiological studies in humans have highlighted that several syndromes or disorders, involving gene mutations, generate neurocristopathy manifestations taking place before cognitive impairment at birth. For instance, *Foxg1* mutations are responsible for microcephaly and mild facial dysmorphisms in the atypical form of Rett syndrome and 14q12 microdeletion (Papa et al., 2008). Septo-Optic Dysplasia (De Morsier, 1956), caused by mutations in the Orthodenticle Homeobox 2 (*Otx2*) gene, triggers syndromic phenotypes including midline defects. These include agenesis of the interhemispheric septum, and/or corpus callosum, and lead to cortical malformations, microphthalmia or anophthalmia and intellectual deficits (Gregory et al., 2021; Ragge et al., 2007).

Mutations in the homeobox gene Empty spiracles Homeobox 2 (*Emx2*) gene led to the observations of severe schizencephaly in humans, characterized by full-thickness cleft within the cerebral hemispheres (Brunelli et al., 1996). Several gene mutations including methyl CpG binding protein 2 (*Mecp2*) leading to typical Rett syndrome (Jeffrey L. Neul et al., 2010; for review, Kyle et al., 2018), SH3 And Multiple Ankyrin Repeat Domains 3 (*Shank3*) generating ASD (Mei et al., 2016; O'Farrell et al., 2003) and Zinc finger E-box-binding homeobox 2 (*Zeb2*) gene associated with Mowat-Wilson syndrome (for reviews, Epifanova et al., 2019; Garavelli and Mainardi, 2007) were all linked to neurocristopathy manifestations such as microcephaly. Specifically, Mowat-Wilson syndrome generated by *Zeb2* mutation is associated with an absence of the corpus callosum. Finally, a mutation observed in the Actin Beta (*Actb*) or the Actin Gamma 1 (*Actg1*) genes leads to Baraitser-Winter syndrome with notably anterior predominant lissencephaly and ocular coloboma (Table 1).

Syndrome /Disorder	Gene involved	Neurocristopathy manifestations	CNC status (hypothesis)
Atypical RETT syndrome <i>(Aguiar, 2014; Papa, 2008)</i>	FOXP1	Microcephaly mild facial dysmorphisms	regulated by CNC expressed in CNC meninges
SEPTO-OPTIC Dysplasia (SOD) <i>(Gregory, 2021)</i>	OTX2	Microphthalmia anophthalmia	regulated by CNC
SCHIZENCEPHALY <i>(Brunelli, 1996)</i>	EMX2	Full-tickness cleft within the cerebral hemispheres	regulated by CNC
GILLESPIE syndrome <i>(Glaser, 1994)</i>	PAX6	Partial anerdia cerebellar ataxia	regulated by CNC
RETT syndrome <i>(Kyle, 2018; Neul, 2010)</i>	MECP2	Microcephaly	expressed in CNC meninges
AUTISM spectrum disorder (ASD) <i>(Mei, 2016; Manning, 2004)</i>	SHANK3	Microcephaly or macrocephaly <i>(specific cases)</i>	expressed in CNC meninges
MOWAT-WILSON syndrome <i>(Epifanova, 2019; Garavelli, 2007)</i>	ZEB2	Microcephaly , absence of corpus callosum , distinct facial phenotype	expressed in CNC meninges
WILSON-TURNER syndrome <i>(Harakalova, 2012; Wilson, 1994)</i>	HDAC8	Coarser face with larger head and chin	expressed in CNC meninges
BARAITSER-WINTER syndrome <i>(Zhang, 2020; Rivière, 2013)</i>	ACTB ACTG1	Anterior predominant lissencephaly and ocular coloboma	expressed in CNC meninges

Table 1. Mutations in specific genes generate neurocristopathy manifestations taking place before cognitive impairment. A serie of studies have registered the implication of gene mutations leading to neurodevelopmental syndromes or disorders. This table lists examples of diseases with neurocristopathy manifestations taking place during development, before cognitive impairment at birth. We hypothesize that either the CNC plays a key role in regulating these genes' expression or these genes are expressed later in development in CNC-derived meninges. The CNC regulation of these genes is crucial for early brain development. [Bruet, unpublished](#).

VII. Infection impact on cognitive behavior at birth

1. Maternal infections impact fetal neurodevelopment

The first studies linking maternal immune response to pathogens and fetal brain development began in the late 1960s - early 1970s during the rubella epidemic. During this outbreak, both infant mortality and children born with developmental deficits and cognitive impairments increased (Chess, 1971; Stern et al., 1969). Affected children were diagnosed with microcephaly or ASD (for review, Ganguli and Chavali, 2021). Since then, the link between the maternal immune system and the fetus CNS development has been highly reported in a variety of pathological infections. For instance, a maternal immune activation (MIA) generated by several different viruses in pregnant mothers could lead to neurological dysfunction and behavioural deficits in newborns and to neurodegenerative and psychiatric disorders in mothers (Patterson, 2009; Scola and Duong, 2017) (Fig. 33). Among the DNA viruses, the Herpes Simplex Virus (HSV-1) affects almost a quarter of pregnant women worldwide, leading to neurodevelopmental disabilities in children (for review, Straface et al., 2012) and AD later in adults (for review, Ganguli and Chavali, 2021). The second large DNA virus, the Cytomegalovirus (CMV), leads to disorders in mothers (Patterson, 2009; Scola and Duong, 2017) (Fig. 33). Among the DNA viruses, the Herpes Simplex Virus (HSV-1) affects almost a quarter of pregnant women worldwide, leading to neurodevelopmental disabilities in children (for review, Straface et al., 2012) and AD later in adults (for review, Ganguli and Chavali, 2021). The second large DNA virus, the Cytomegalovirus (CMV), leads to lifelong latent infection generating neurodevelopmental deficits such as microcephaly and hearing loss, and neuropsychological disorders such as ASD and schizophrenia in infants (Adler et al., 2007; Cheeran et al., 2009; for review, Ganguli and Chavali, 2021). The Human Immunodeficiency Virus (HIV) can also generate microcephaly and trigger neurodevelopmental and neuropsychiatric disorders

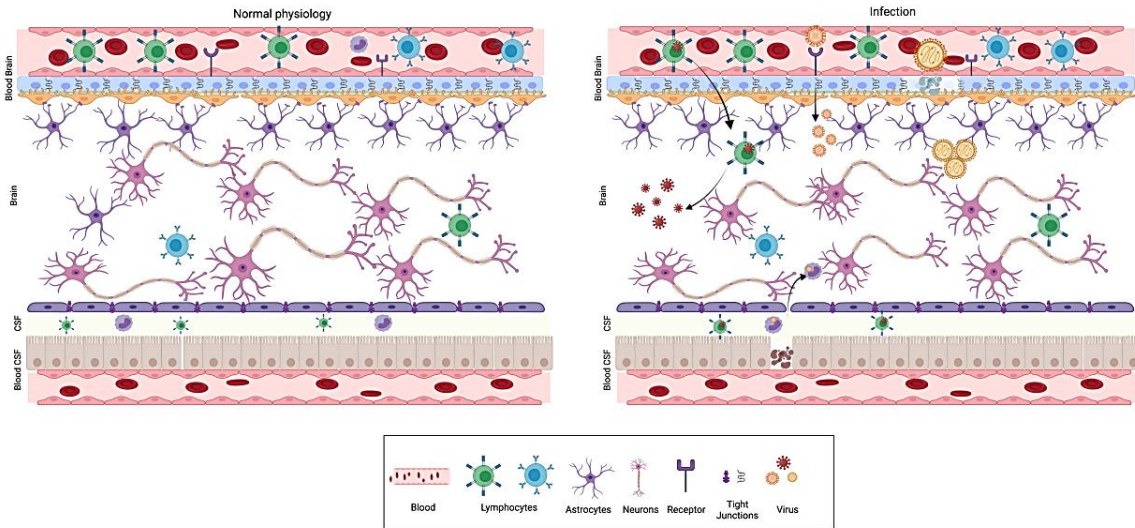


Figure 33. Physical barriers of the brain in normal physiology and infection. The major physical barriers to enter the brain are: Blood Brain Barrier (BBB) and Blood CSF (BCSF) Barrier. BBB is composed of endothelial cells, pericytes and glial cells. The endothelial cells are held together by tight junctions, which prevent permeability and acts as a barrier. The BCSFB is composed of epithelial cells of the CP and ependymal cells. Under normal physiological conditions (left panel), pathogens, toxins, several immune modulatory molecules are barred from entering the brain by the presence of these barriers. Neurotropic viruses can breach the BBB using different mechanisms as depicted from left to right. (i) Trojan horse mechanism—virus infects peripheral immune cells, followed by the infected cell crossing BBB ultimately resulting in CNS infection. (ii) Receptor mediated transcytosis—several viruses can directly bind to receptors and cross the BBB by transcytosis. (iii) Some viruses are capable of dissolving tight junctions and compromise BBB’s protective function. [From Ganguli and Chavali 2021.](#)

such as schizophrenia (for reviews, Ganguli and Chavali, 2021; Ghafouri et al., 2006; Van Rie et al., 2008). Among the RNA viruses, the Zika Virus generates microcephaly and ASD in children (Ganguli and Chavali, 2021; Krauer et al., 2017; Rasmussen et al., 2016) and the Influenza Virus generates NT defects, hydrocephaly and increased risk of ASD and schizophrenia in adult life (Ganguli and Chavali, 2021; Kendell, 1989; Mednick, 1988) (**Table 2, cf. columns boxed in red**).

2. Molecular impact on fetal neurodevelopment

While the adult BBB is composed of various cells including endothelial cells, pericytes, astrocytes, microglia and neurons, the early embryonic BBB is devoid of astrocytes and microglia (for review, Abbott et al., 2010; Daneman and Prat, 2015). Several viruses, infecting pregnant mothers, migrate to the fetus and breach the BBB to infect the developing CNS. Three different mechanisms to cross the BBB are observed: 1) the Trojan Horse mechanism (once the virus infects peripheral immune cells, these cells cross the BBB to infect the CNS), 2) the receptor mediated transcytosis (the virus binds to a receptor and crosses the BBB by transcytosis), and 3) the tight junctions dissolving (the virus compromises the BBB's protective function by eliminating the tight junctions and allowing gaps between the cells to cross the BBB) (for review, Ganguli and Chavali, 2021).

Although specific pathogens cross the fetal BBB to infect the developing CNS, maternal infection leading to an inflammatory response is sufficient to generate developmental abnormalities in the fetus. Each pathogen has unique small membranous motifs called pathogen associated molecular patterns (PAMPs). These PAMPs are recognized by pattern recognition receptors (PRRs), such as toll-like receptors (TLRs), present on host immune cells to trigger an inflammatory response by secreting pro- or anti-inflammatory cytokines. The major anti-inflammatory cytokines regroup the IL family (IL-4, IL-6, IL-10 and IL-13). Among

Virus	Host Cell entry receptor	Major CNS cells affected	Cytokine signature post infection	Neurological consequences
Cytomegalovirus (CMV)	Platelet-Derived growth factor, Neuropilin2, Olfactory receptor 1411, Epidermal growth factor receptor (EGFR), Tetherin	Neurons, Glia, Ependymal cells, Choroid plexus	Monocyte chemoattractant protein 1 (MCP1) IL8, TNF α , IL6, CXCL11/ITAC, and CCL5/Regulated on Activation, Normal T Expressed and Secreted (RANTES), IL1B, IL10	Neurosensory loss, Focal encephalitis, Microcephaly, Seizures, Paralysis, Mental retardation, Autism spectrum disorder
Herpes Simplex Virus 1 (HSV-1)	Myelin-associated glycoprotein (MAG), Sialic-acid-binding Ig-like lectin, Non-muscle myosin heavy chain (NMHC)-IIA, Nectin 1	Hippocampal neurons, Brain stem neurons	Macrophage inflammatory protein1a (MIP1a), IL1 β , TNF α , IL6, IL8, CCL5, CXCL10	Necrotizing encephalitis, Multiple sclerosis, Alzheimer's disease
Epstein-Barr virus (EBV)	CD21, CD35	Astrocytes and Microglia	IL2, IFN γ , TNF, LT α , LT β , CXCL10-CXCR3, CCL5-CCR5	Encephalitis, Meningitis, Cerebellitis, Polyradiculomyelitis, Transverse myelitis, Cranial and Peripheral neuropathies, Schizophrenia, Psychiatric abnormalities
Varicella-zoster virus	Mannose-6-phosphate receptor, Myelin associated glycoprotein (MAG)	Neurons	IL1, IL6, IL8, and Tumor necrosis factor alpha (TNF α)	Aseptic meningitis, Encephalitis, Cerebral infarction associated with granulomatous vasculitis, Myelitis, and Cranial polyneuropathy.
Rubella virus	Myelin oligodendrocyte glycoprotein (MOG), Signaling lymphocytic activation molecule (SLAMF1), CD46	Astrocytes, Neural progenitor cells	IL1 β , IL6, TNF α	Congenital Rubella syndrome, Microcephaly, Encephalitis, Panencephalitis, Autism spectrum disorder
Mumps virus	Trisaccharide containing -2,3-linked sialic acid	Ependymal cells that line the ventricles, pyramidal cells in the cerebral cortex and hippocampus	TNF α , IL6, MCP1, CXCL10	Encephalitis, Aseptic meningitis
Influenza virus	Sialic acids (SAs) of cell surface glycoproteins and glycolipids	Hippocampal neurons in the CA1 and dentate gyrus	IL8, RANTES, MCP1, MCP3, MIP1 α , IFNG induced protein 10 (IP-10) IL8, IL1B, IL6, IL18, TNF α and IFN α/β	Neural tube defects, Hydrocephaly, Schizophrenia, Autism spectrum disorder
Human Immunodeficiency Virus 1 (HIV1)	CD4, CCR5, CXCR4	Microglia	TNF α , IFN α , IL6, IL8, IL1 β , CCL2 and CCL5	Microcephaly, Slow neurodevelopment, Dementia, Increased risk of schizophrenia
Polio virus	Human poliovirus receptor (PVR) or CD155	Motor neuron cells in CNS	IL6, IL8, CXCL10, IFN β	Paralytic poliomyelitis
Severe acute respiratory syndrome coronavirus 2 (SARS-CoV-2)	Angiotensin-converting enzyme 2 (hACE2), Transmembrane protease serine 2 (TMPRSS2)	Choroid plexus cells, neurons	IL17, IL1, IL6, TNF α , IL15, IFN γ	Neurodevelopmental disorders?
Japanese Ecephalitis Virus (JEV)	Plasmalemma Vesicle Associated Protein (PLVAP), Gastrokine-3 precursor (Gkn3), C-Type Lectin Domain Containing 5A (CLEC5A), Heparansulfate, Glucose regulatory protein 78 (GRP78), Scavenger receptor I	Pyramidal neurons of the cerebrum, Purkinje cells of the cerebellum	IFN α , IL8, RANTES, IL6	Encephalitis, Paralysis, Seizures, Inability to speak, Memory loss, Impaired cognition, and other Mental disorders
Zika virus (ZKV)	TAM (AXL), Dendritic Cell-Specific Intercellular adhesion molecule-3-Grabbing Non-integrin (DC SIGN), Neural cell adhesion molecule 1 (NCAM1), Tyro 3	Neural Stem Cell (NSC), Neural Progenitor Cell (NPC)	IL1 β , IL2, IL9, IL15, IFN γ , CXCL10, CXCL9	Microcephaly, Autism spectrum disorder
West Nile Virus (WNV)	TLR3, C type lectins, T cell Ig- and mucin domain-containing, molecule (TIM), and Tyro3, Axl, and Mertk (TAM), Natural Killer p44 (NKP44)	Neurons, Bovine microvascular endothelial (BMVE), Astrocytes, Microglia, Endothelial cell (EC)	IL1 β , IL2, TNF α	Encephalitis, Depression, Memory loss and Motor dysfunction
Dengue Virus (DENV)	C-type lectin domain containing 5A (CLEC5A), TIM and TAM, Heparan sulfate, GRP78, Scavenger receptor I, Integrin $\alpha\beta$ 3, Claudin 1, Nkp44, Laminin	Neurons, Astrocytes	IL8, IL13, MCP3, Granulocyte-macrophage colony-stimulating factor(GM-CSF) IL10, MIP1B, IFN γ , TNF α , RANTES, IL6, IL10	Encephalopathy, Acute disseminated encephalomyelitis, Myelitis, Neuritis brachialis, Stroke, Neuro thalamic complications acute hypokalemic paralysis

Table 2. Inflammatory signatures of viruses and their neurological consequences. Many epidemiologic studies in humans highlight the detrimental neurological consequences of viral infections. [Adapted from Ganguli and Chavali, 2021.](#)

the pro-inflammatory cytokines are the TNF α , interferon (IFN) γ , IL-1, IL-2 and IL-8. A high exposure of these cytokines found in the maternal blood and amniotic fluid and reaching the fetal CNS can generate neurodevelopmental disorders like microcephaly, lissencephaly and ASD, as well as neuropsychiatric disorders such as schizophrenia (for review, Ganguli and Chavali, 2021).

During early development, cytokines regulate the expression of other immune molecules such as major histocompatibility complex (MHC) class I molecules (Estes and McAllister, 2016). MHC class I, located on neurons, negatively regulate synapse formation and plasticity required for synaptic pruning (Glynn et al., 2012; Shatz, 2009). High level of cytokines, deregulating MHC class I molecules, could lead to altered synaptogenesis and pruning, causing ASD or schizophrenia in newborns (Sekar et al., 2016).

Cui and colleagues have induced MIA in pregnant dams at E12.5 by intra-peritoneal delivery of polyinosinic: polycytidylic acid (poly(I:C)) to observe inflammation effects on the embryonic brain. MIA triggers increasing levels of C-C motif chemokine ligands 2 (CCL2), as well as other pro-inflammatory cytokines and chemokines in the CSF, allowing recruitment of C-C chemokine receptors 2 (CCR2)-expressing cells to the CP. These cells are round, ionized calcium binding adaptor molecule 1 (Iba1)⁺ and positive for the phagocytic marker CD68. They migrate to the apical, CSF-facing surface of the CP. MIA also allow CCL2 upregulation in the meninges and increase of Iba1⁺ macrophages in the ventricular zone (VZ) of the developing cortex. Thus, MIA triggers a global immune reaction in the fetal brain (Cui et al., 2020).

However, MIA seems to act as the first from a series of risk factors required to trigger disease-related symptoms later in life. Multiple risk factors along the developing CNS (pre- and post-natal) may be required for disease induction, such as genetic mutations and other environmental exposures. MIA affects brain

development by interacting with mutations in cognitive diseases-associated genes. Therefore, the risk of maternal infection triggering schizophrenia is greater in families with a history of schizophrenia and, more generally, families with autoimmune disorders have a much higher risk of causing ASD or schizophrenia (Estes and McAllister, 2016) (Fig. 34).

3. The macrophages of the embryonic brain

During embryonic development, the CNS starts harboring an immune system against pathogens (Oschwald et al., 2020) composed of 1) microglia colonizing the parenchymal brain and 2) non-parenchymal CNS-associated macrophages (CAMs), also known as Border-associated macrophages (BAMs), located in the CNS interfaces such as the perivascular space, the meninges, and the CP of the brain (Faraco et al., 2017; Gerganova et al., 2022; Karam et al., 2022). Starting from E9,5 in mice and around gestational week 4,5 in humans, erythromyeloid progenitors (EMPs) from the yolk sac colonize the brain to give rise to the parenchymal microglia (Chen et al., 2017; Ginhoux et al., 2010; Mehl et al., 2022). From E12,5 in mice and around gestational week 11, a second wave of EMPs migrate to colonize their specific niche in the CNS interfaces, giving rise to the CAMs (Goldmann et al., 2016; Mehl et al., 2022). Depending on their location, at the border regions which form barriers and interfaces between the brain and the periphery, CAMs are composed of three defined macrophages: 1) the brain perivascular macrophages (PVMs), 2) the meningeal macrophages (MMs) and the CP macrophages (CPMs) (Gerganova et al., 2022). In comparison to the parenchymal microglia, CAMs represent only 10% of total leukocytes in the homeostatic murine brain (Gerganova et al., 2022; Mrdjen et al., 2018). However, their distinct position at the border of the CNS compared to the parenchymal microglia could point out a specific role in brain homeostasis. Indeed, as PVMs are found around the vessel walls, between the endothelium and the parenchyma, MMs are found alongside

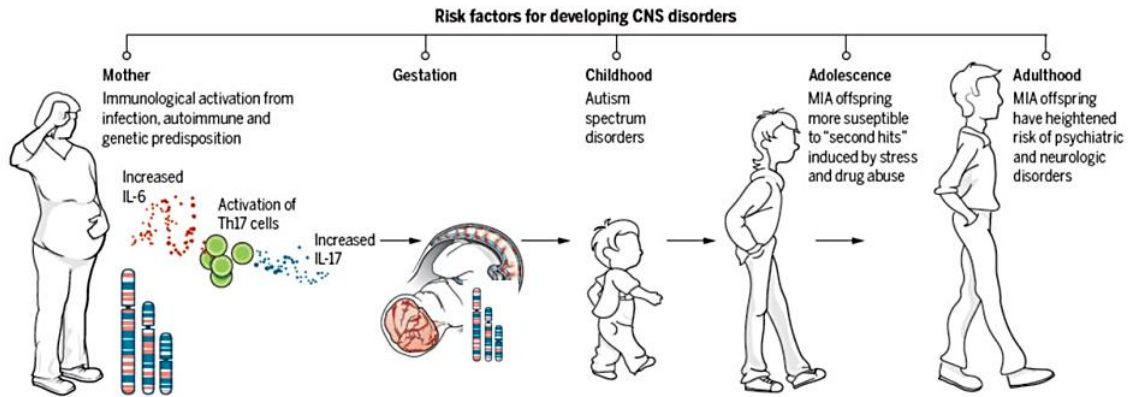


Figure 34. MIA as a disease primer. This schematic depicts the current model for how MIA leads to psychiatric disorders in offspring. Infection leads to release of pro-inflammatory cytokines and activation of T-helper cells in the mother's bloodstream. A combination of genetic background, autoimmune status, and second hits during childhood and adolescence (including stress and drug abuse) combine with the consequences of maternal infection to increase the likelihood of offspring developing psychiatric disorders as adults. [From Estes and McAllister, 2016.](#)

pial and subpial vessels of the meninges border, and CPMs are found at the border between the stromal CP and the CSF, they have a specific immune-surveillance and fluid homeostasis roles, different from the parenchymal microglia (Karam et al., 2022).

The CAMs are commonly discriminated from parenchymal microglia by their cell surface marker expression using immunohistochemistry techniques. For instance, they are identified by their high expression of CD11b (also known as Macrophage-1 antigen, MAC1), and the glycoprotein F4/80, as well as their low expression of Iba1 relative to microglia (Gerganova et al., 2022). They also express Colony Stimulating Factor 1 Receptor (CSF-1R) for their normal proliferation, maturation and survival (Gerganova et al., 2022; Mehl et al., 2022; Oswald et al., 2020). More specifically, PVMs are identified by their high expression of lymphatic vessel endothelial hyaluronan receptor 1 (LYVE-1) (Karam et al., 2022).

VIII. ETosis, a defence mechanism involving extracellular DNA traps

1. Core histones and epigenetic modifications

At a molecular level, epigenetic mechanisms are biochemical modifications of the DNA and histone proteins, the major constituents of chromatin (for review, Gräff and Mansuy, 2008). In eukaryotic cells, The DNA measures 147 bp and is compressed around a core histone, composed of pairs of each of the histones H2A, H2B, H3 and H4, to form a nucleosome core particle (Li et al., 2010; Wang et al., 2009). Nucleosomes are the basic structural units of chromatin and are around 11 nm in diameter (Richmond and Davey, 2003). The nucleosomes are stabilized and maintained compacted by H1 linker histones (Brown et al., 2006).

Histones are basic proteins consisting of a core and an N-terminus tail composed of a loosely-structured sequence of amino acids. Post-translational histone

modifications occur primarily on the N-terminus tail, and include acetylation, methylation, phosphorylation, ubiquitination and sumoylation. Because of their chemical properties, these modifications influence the condensation of chromatin, and thereby modulate the accessibility of DNA to the transcriptional machinery (for review, Gräff and Mansuy, 2008).

These modifications are governed by specific enzymes, allowing chromatin accessibility or inaccessibility for the transcriptional machinery. Acetylation, phosphorylation or methylation (depending on the methylated residue) of histones are modulated by histone acetyl transferase (HAT), protein kinase (PK) and histone methyltransferase (HMT)/histone demethylase (HDM) respectively, which results in a less condensed chromatin structure giving access to the transcriptional machinery. On the contrary, in the absence of acetylation and phosphorylation, and when certain histone residues are methylated, by histone deacetylase (HDAC), protein phosphatase (PP) and HMT/HDM respectively, chromatin structure is compact, preventing the transcriptional machinery's accessibility and results in transcriptional silencing (for review, Gräff and Mansuy, 2008).

2. PAD4 generates citrullination of histones

An intriguing epigenetic modification observed on the nucleosome is citrullination of the histones. The peptidyl-arginine deiminase 4 (PAD4), also called PADI4/PADV, converts arginine (Arg) to citrulline (Cit), a nonconventional amino acid in proteins (for review, Vossenaar et al., 2003) that lacks arginine's positive charge (Neeli et al., 2008). PAD4, a member of the PAD family of enzymes, was first identified in human HL-60 leukemia cells upon differentiation along granulocyte lineage (Nakashima et al., 1999). PAD4 is an abundant component of cytoplasmic granules (Asaga et al., 2001) and its activation leads to a transfer in the nucleus and targets histones H2A, H3 and H4 for citrullination (Wang et al., 2009). PAD4 converts arginine 2, 8

and 17 of histone H3 and arginine 3 of histone H4 to citrulline. PAD4-catalyzed histone hypercitrullination plays a critical role in chromatin decondensation, observed in granulocytes and peripheral blood neutrophils (Nakashima et al., 2002; Wang et al., 2009) (Fig 35).

3. NETs and ETosis

In response to inflammation, neutrophils migrate from the circulating blood to infected tissues to defend the organism against potential bacteria. Activated neutrophils generate several defence mechanisms: they phagocytose bacteria that are killed by proteolytic enzymes, antimicrobial proteins and reactive oxygen species or they degranulate, releasing antimicrobial factors into the extracellular medium (Brinkmann et al., 2004). In 2004, Brinkmann and colleagues described a novel antimicrobial mechanism of these neutrophils where upon activation they release extracellular traps to disarm and kill bacteria extracellularly. These traps are composed of extremely decondensed chromatin to form 15-25 nm chromatin fibers (Fig. 36). Even though the majority of DNA released in the extracellular compartment originates from the nucleus, mitochondrial DNA was also observed in these structures (Lood et al., 2016). This mechanism is called NET (Brinkmann et al., 2004). The presence of NETs seems to be crucial for the immune defence during development and in newborns: impaired NET formation predisposes newborn infants to bacterial infection (Yost et al., 2009). Naïve neutrophils are round with some membrane folds. However, when activated in response to infection or sterile inflammatory process (Hirose et al., 2014), such as calcium ionophore, phorbol 12-myristate 13-acetate (PMA), lipopolysaccharide (LPS), inflammatory cytokines such as interleukin (IL)-8 and others (Li et al., 2020), they become flat and form membrane protrusions (Brinkmann et al., 2004). In addition, they form NETs, fibrous structures composed mainly of DNA and the 5 histones (H1, H2A, H2B, H3 and H4) (Brinkmann et al., 2004), as well as other components such as neutrophil elastase (NE) and myeloperoxidase (MPO) (Hirose et al., 2014).

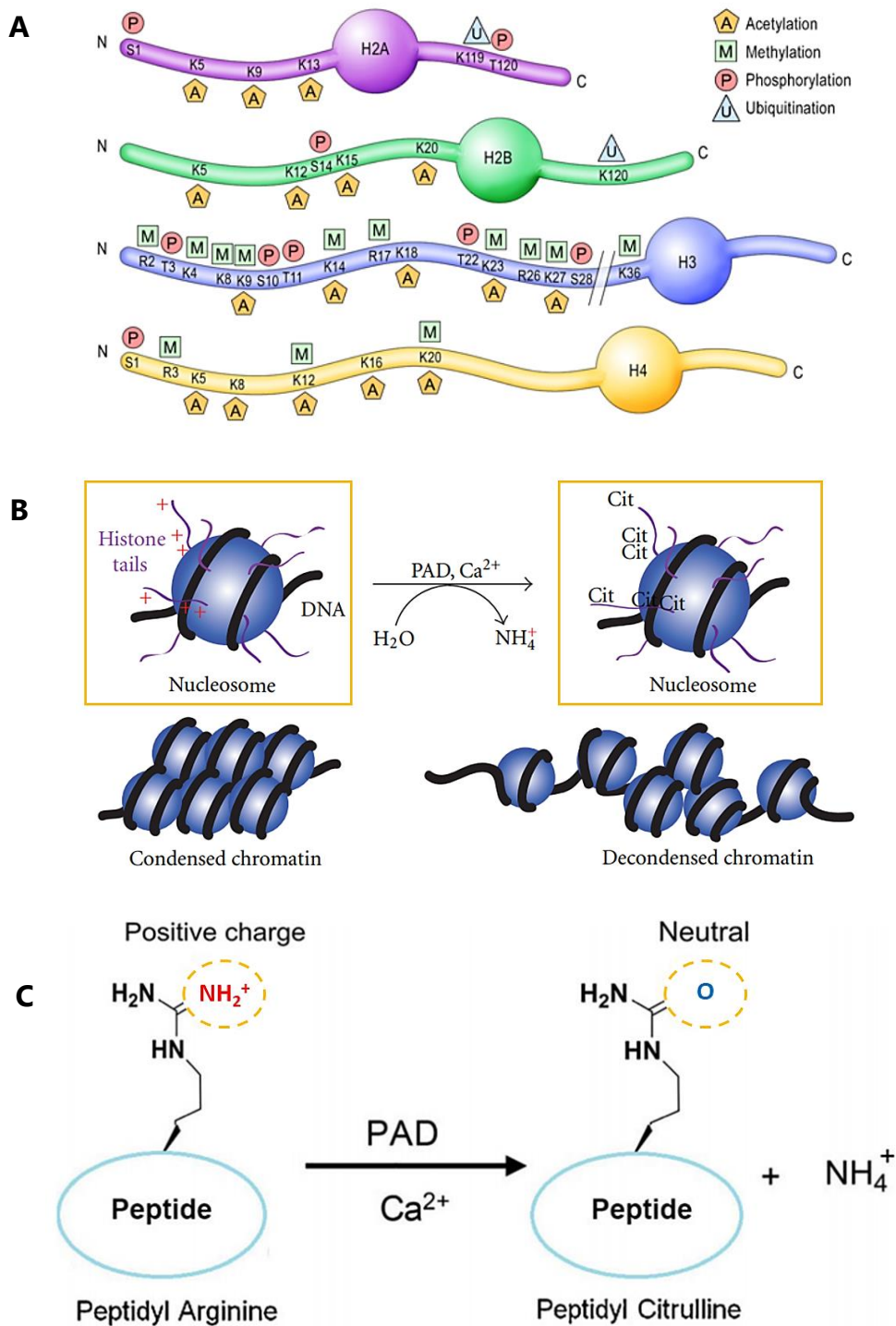


Figure 35. Citrullination (deimination) of peptidylarginine by PAD. (A) Schematic representation of the four-nucleosome core histones, H2A, H2B, H3 and H4, the N- and C-termini of the core histones and their residue-specific epigenetic modifications. [From Gräff and Mansuy, 2008.](#) (B) PAD-mediated histone tail citrullination leads to chromatin decondensation. [Adapted from Mohanan et al., 2012.](#) (C) The guanidinium group of arginine is hydrolyzed yielding a ureido group and ammonia. [Adapted from Zhu et al., 2021.](#)

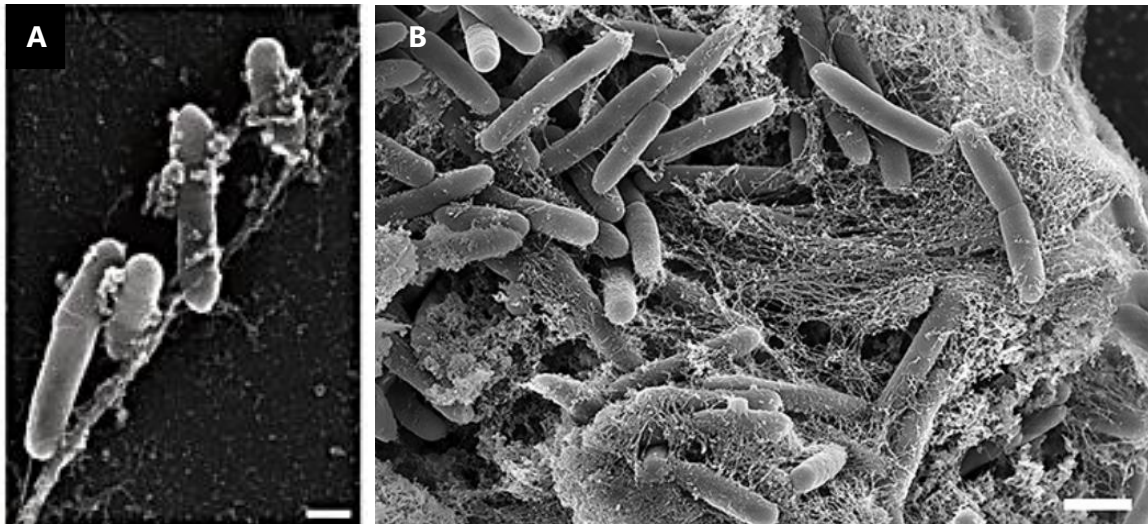


Figure 36. Scanning electron micrograph of purified human neutrophils that have produced NETs after cocultivation with *S. typhimurium* (A) and *P. aeruginosa* (B). Scale bar, 500 nm (A) and 1 μ m (B). From Brinkmann, 2018; Brinkmann et al., 2004.

Due to a long list of proteins found in these NET structures, the composition of NETs could vary depending on the stimulus (for review, Papayannopoulos, 2018). The classification of NET as a cell death process is very controversial. For certain scientists, even though DNA is released in the extracellular compartment, the process of releasing NETs, called NETosis for neutrophils or ETosis for any type of cells, differs from apoptosis and necrosis. In the cell death processes, disintegration of the nuclear envelope and mixing of nuclear and cytoplasmic material, loss of internal membranes, and disappearance of cytoplasmic organelles are observed. In comparison, in cells forming NETs, the nuclear membrane remains intact and clearly separate nucleoplasm from cytoplasm. The structure of organelles is not affected as well. In addition, formation of NETs does not require caspases (Fuchs et al., 2007; Hirose et al., 2014; Neeli et al., 2008). For other scientists, NET release occurs primarily through a cell death process (Fuchs et al., 2007). Papayannopoulos and colleagues have described two different pathways for NET formation: 1) a cell death pathway called NETosis and 2) a rapid release from live cells pathway called Non-lytic NETosis (for review, Papayannopoulos, 2018) (Fig. 37). During the first pathway, the nuclear envelope disintegrates to release decondensed chromatin into the cytoplasm, mixing cytoplasmic and granule components. The plasma membrane then ruptures to release NETs into the extracellular compartment 3 to 8 h after cell activation. In the second pathway, nuclear chromatin is rapidly released within minutes, accompanied by the release of granule proteins through degranulation. These components assemble extracellularly to form NETs and leave behind active anucleated cytoplasts that continue to ingest microorganisms (Christensen et al., 2013).

During NETosis, neutrophils' nuclear chromatin structure is highly decondensed, allowing the release of DNA in the extracellular compartment. This decondensation is due to hypercitrullination of histone H3 by PAD4 (Neeli et al.,

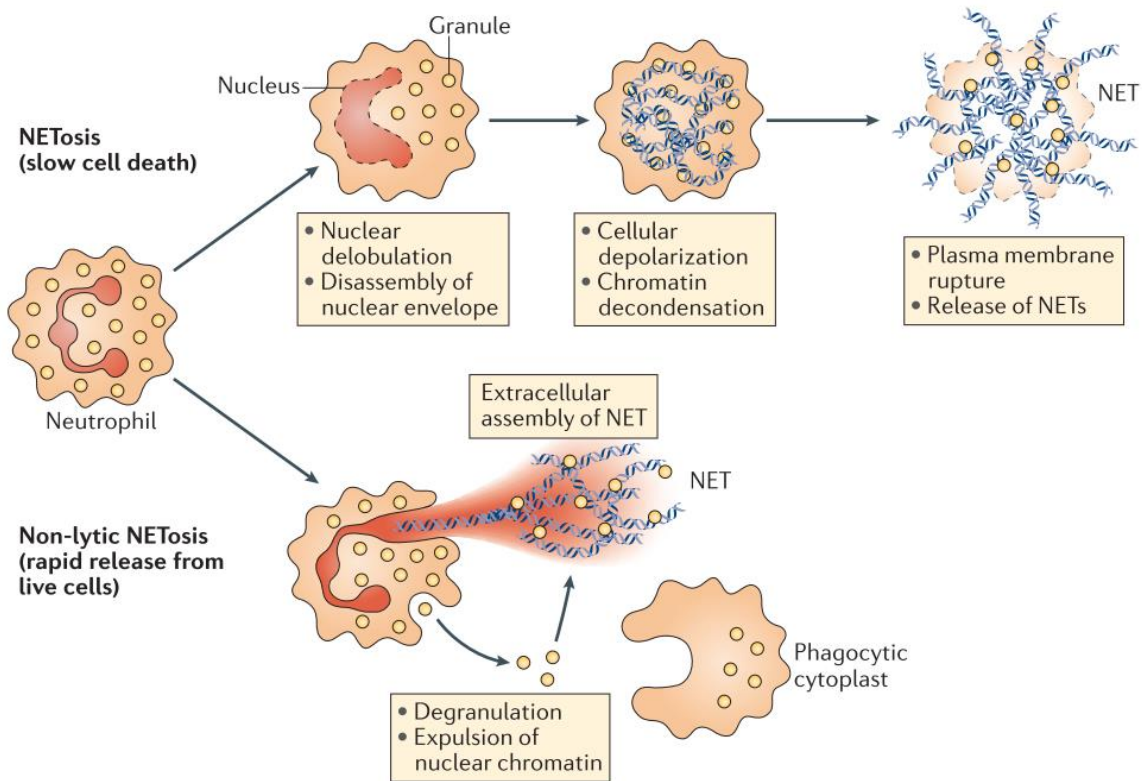


Figure 37. NET formation pathways. Neutrophil extracellular traps (NETs) form via two pathways. The first is a cell death pathway termed NETosis that begins with nuclear delobulation and the disassembly of the nuclear envelope and continues with loss of cellular polarization, chromatin decondensation and plasma membrane rupture. The second is a non-lytic form of NETosis that can occur independently of cell death and involves the secreted expulsion of nuclear chromatin that is accompanied by the release of granule proteins through degranulation. These components assemble extracellularly and leave behind active anucleated cytoplasts that continue to ingest microorganisms. [From Papayannopoulos, 2018.](#)

2008; for review, Remijnsen et al., 2011; Wang et al., 2009). PAD4 translocates from the cytoplasm to the nucleus and mediates citrullination of histones. For example, citrullination of histone H3 at arginine residues R2, R8 and R17 by PAD4 results in a reduction of the positive charge and decondensation of chromatin (Li et al., 2020; Neeli et al., 2008; Wang et al., 2009). Thus, measuring the presence of citrullinated histone H3 (Cit-H3) allows to identify cells performing ETosis (Hirose et al., 2014). The presence of Cit-H3 bound to cell-free DNA forming NETs has been documented from neutrophils from tumor-bearing hosts, hosts with bacterial infections (Li et al., 2020) and *in vitro* in response to varying stimuli such as LPS, tumor necrosis factor (TNF), lipoteichoic acid (LTA), f-MLP and hydrogen peroxidase (H₂O₂) (Neeli et al., 2008).

IX. *In utero* valproic acid (VPA) generates autistic behaviors in neonates

1. VPA, a widely used anticonvulsant

VPA, also called valproate or 2-propylpentanoic acid, is a short-chained fatty acid commonly used as a broad-spectrum anticonvulsant drug in the management of epilepsy (for review, Löscher 2002) but also migraines (for review, Evers, 2008), bipolar disorders (for review, Bowden, 2009), schizophrenia (Nevo et al., 2020), and mood stabilizer (Emrich et al., 1980; Lambert et al., 1975). Among all antiepileptic medications, VPA remains the most efficient drug to provide adequate epileptic seizure control (Thomas, 2018). Two well-known mechanisms of actions for VPA include the potentiation of γ -aminobutyric acid (GABA) signalling and the inhibition of class I and II histone deacetylases (HDAC). 1) VPA's antiepileptic action is mediated by the inhibition of the enzymes involved in GABA degradation, GABA transaminases, and promotes the activity of GABA synthesizing enzymes, glutamic acid decarboxylases (GAD). Thus, overall, VPA results in an elevation of GABA levels (Kukino & Deguchi, 1977). The regulation of GABA level is critical to maintain the

maturation of neural network in the developing brain (Baltz et al., 2010; Ben-Ari et al., 2007; for review, Sernagor et al., 2010) and a change in GABA levels could therefore disrupt this developing neuronal circuitry.

Indeed, a dysregulation of the inhibitory GABA system has been associated with ASD (Blatt and Fatemi, 2011). Precisely, copy number variations (CNVs) of the chromosome 15q11-13 region has been observed in ASD. The prevalence of 15q11-13 duplications in the population of individuals with ASD has been estimated at 0,5-3% (for review, Bolton et al., 2001). This region contains several genes coding for the GABA_A receptor subunits such as GABRB3, GABRA5 and GABRG3, and a duplication of this region leads to excessive inhibitory neurotransmission, and affected cell migration and maturation (Delahanty et al., 2011).

The mutations of several GABA subunits were associated with ASD such as GABRB3 (Delahanty et al., 2011), GABRA4 and GABRB1 (Ma et al., 2005), leading to a reduction of these proteins, notably in the cingulate cortex (Thanseem et al., 2012) and the cerebellar vermis (Delahanty et al., 2011). Overall, a decreased level of GABA and GABA receptor density is observed in the cerebellum of ASD patients. Moreover, the GAD enzyme catalysing the transformation of glutamate into GABA is also decreased in the cerebellum, especially the GAD types 65 and 67 (GAD65, GAD67) (Blatt and Fatemi, 2011).

In addition, VPA plays a role in the blockage of voltage-dependent Na⁺ channels, preventing the activation of neurons in the brain (Cao and Peng, 1993; Emrich et al., 1980; Kukino and Deguchi, 1977). Finally, by activating the β -catenin-Ras-ERK-p21 pathway (Jung et al., 2008) and inhibiting GSK3 β , VPA increases the level of β -catenin, therefore promoting Wnt signaling (for review, MacDonald et al., 2009). The activation of β -catenin leads to the regulation of Ras, increasing the levels of phosphorylated ERK (pERK) and in fine modulating p21, leading to a stimulation of

neural cell progenitor differentiation and inhibition of their proliferation. Thus, VPA affects differentiation and proliferation of neural cell progenitors and impacts axonal remodelling in developing neurons (Hall et al., 2002). 2) The second action of VPA is its capacity to generate epigenetic modifications, such as DNA methylation, modulating gene expression. VPA exposure leads to histone hyperacetylation by directly inhibiting class I and II HDACs (Tung and Winn, 2010). Histone acetylation is correlated with a significant increase in the expression of di- and trimethylated histone 3 lysine 4 (H3K4), associated with gene transcription (for review, Berger, 2007), and significant decrease in the expression of monomethylated histone H3K9, associated with gene silencing (for review, Berger, 2007; Tung and Winn, 2010). Epigenetic modifications on histones regulate gene expression by controlling interactions between DNA and transcription factors. Acetylation of lysine residues on histone tails reduces their overall positive charge, thus weakening their interaction between DNA and histone proteins and consequently facilitating the binding of transcription factors to DNA, through permissive or open chromatin (for review, Eberharter and Becker, 2002). In addition, acetylated histones are recognized by other proteins that allow recruitment of ATP-dependent chromatin remodelling complexes which consequently may lead to gene activation (Grant et al., 1999). Studies have shown that H3 and H4 histones hyperacetylation induced by VPA exposure *in utero* (Kataoka et al., 2013; Moldrich et al., 2013) and HDAC inhibition during a critical window of embryonic brain development (Nicolini and Fahnestock, 2018) are associated with post-natal autistic-like behavioral impairments.

2. VPA, a potent teratogen when administrated in utero

VPA exposure during the first trimester of pregnancy could lead to “fetal valproate syndrome”, a VPA-induced embryofetopathy (Clayton-Smith and Donnai, 1995) with an increased risk of congenital malformations, cognitive impairments and behavioral deficits in newborns. Prenatal VPA exposure leads to approximately

10% of all major congenital malformations (Tomson et al., 2018). The developing nervous system is particularly sensitive to VPA as it could result in NT defects leading to spina bifida aperta and exencephaly (for reviews, Nau et al., 1991; Ornoy, 2009). Newborns exposed to VPA have a 10 to 20 times higher risk of NT defects compared to the general population (for review, Ornoy, 2009). Other organ malformations are observed due to VPA exposure: craniofacial abnormalities such as craniosynostosis and cleft palate, heart defects such as atrial septal defect, skeletal and limb defects such as polydactyly and hypospadias (Jentink et al., 2010; for review, Nau et al., 1991; Werler et al., 2011). In 1986, Mast and colleagues treated pregnant rhesus monkeys with 10x human clinical doses of VPA (20 mg/kg/day for common dosages in children) and observed craniofacial and skeletal defects in the newborns (Mast et al., 1986). Gurvich and colleagues had observed other organ malformations in xenopus and zebrafish embryos exposed to VPA during the early gastrula stage: growth retardation, defect in gut coiling, and eye, heart and tail defects (Gurvich et al., 2005).

In 1996, Rodier and colleagues were the first to create a VPA model by injecting pregnant rats, dams, with a 350 mg/Kg single dose of VPA by intraperitoneal on either day 11.5, 12, or 12.5 of gestation (Rodier et al., 1996). However, the first detailed behavioral studies after VPA exposure were performed by Schneider and Przewlocki after injecting a single dose of VPA on day 12.5 of gestation, corresponding to the early/middle fetal life in humans (Schneider and Przewlocki, 2005). Several behavioral characteristics were observed in newborn rodents following VPA exposure *in utero*. Rodents showed a deficit in social functioning (Christianson et al., 1994; Williams and Hersh, 1997; Williams et al., 2001), recognition and interaction due to sensory system deficits (Schneider and Przewlocki, 2005) such as impaired olfaction and communications deficits with reduced distress pup calls and adult pre-mating vocalizations (Gandal et al., 2010; Gąssowska-Dobrowolska et al., 2020), reduced number of calls per minute and in

complex call types in mouse pups (Moldrich et al., 2013). Play behavior and exploration were also decreased in VPA induced pups (Gąssowska-Dobrowolska et al., 2020; Melo et al., 2006; Shah et al., 2002; for review, Wilson and Sullivan, 1994). Other behavioral impairments were observed in newborn rodents such as delayed neurodevelopment and impaired cognitive functions (Nicolini and Fahnestock, 2018), increased repetitive behavior and increased anxiety (Gąssowska-Dobrowolska et al., 2020; Markram et al., 2008; Schneider and Przewłocki, 2005; Schneider et al., 2006; Schneider et al., 2008) or abnormal fear processing (Markram et al., 2008). In 2015, Zimmermann and al. performed the first study of VPA exposure in zebrafish, a common model used in social behavioral studies, especially social interaction in an interdependence group (Gerlai, 2014; for review, Kalueff et al., 2014; Saverino and Gerlai, 2008). VPA exposed during the first 48h of life exhibit anxiety, locomotor activity changes and social interaction deficits (Zimmermann et al., 2015). These behavioral impairments characterised by three symptom domains, social deficit interaction, repetitive behavior and impaired communication, are clinically relied on to diagnose autism (American Psychiatric Association, 2013; Nicolini and Fahnestock, 2018). Symptoms in at least 1 area must manifest before age 3 years (Christensen et al., 2013). Thus, newborn rodents previously injected with VPA *in utero* show behavioral and cognitive characteristics resembling symptoms of autism (Christianson et al., 1994; Williams and Hersh, 1997; Williams et al., 2001). Even though 25% of children are diagnosed with a gene-related autism (for review, Miles, 2011), a variety of environmental factors could lead to the risk of autism (Gardener et al., 2011), including VPA as previously shown. Therefore, ASD regroups several different syndromes and disorders depending on their origin: childhood autism (autistic disorder), Asperger syndrome, atypical autism (Christensen et al., 2013), pervasive developmental disorder, childhood disintegrative disorder and Rett's disorder (for review, Grzadzinski et al., 2013).

3. Anti-angiogenic effect of VPA in neonates

In addition to the action of VPA in GABA signaling and in the inhibition of HDAC, Michaelis and colleagues have demonstrated an anti-angiogenic effect of VPA (Michaelis et al., 2004). *In vitro* experiments have shown an inhibition of endothelial cell proliferation, migration and tube formation in human umbilical vein with VPA, preceded by hyperacetylation on histone H4 and therefore an inhibition of HDAC. *In vivo* experiments showed disturbance of vessel formation in mice embryos and angiogenesis inhibition in the chicken chorioallantoic membrane assay both treated with VPA.

Iizuka and colleagues suggest an anti-angiogenic action of VPA by interfering with the vascular endothelial growth factor-mammalian target of rapamycin complex 1 (VEGF-mTORC1) pathway in endothelial cells. In the neonatal mouse retina, VEGF binds to the VEGFR to activate the mTORC1-dependent pathway, leading to a phosphorylation of the ribosomal protein S6 (pS6). This signaling pathway activated in endothelial cells leads to angiogenesis (for review, Nakahara et al., 2017). *In vitro*, VPA inhibits endothelial cell proliferation and exhibits anti-angiogenic effects *in vivo*. Several possible mechanisms of VPA could lead to anti-angiogenic effects in endothelial cells: 1) VPA may decrease the expression of VEGFR-2 and VEGF production, attenuating the response of endothelial cells to VEGF or 2) VPA may decrease pS6, blocking the VEGF-mTORC1 pathway (Iizuka et al., 2018). Thus, VPA has been proposed in anti-cancer therapy for its anti-angiogenic properties (Nilubol et al., 2017).

4. VPA effect on embryonic brain vascularization

In this PhD project, VPA was used to perform microinjections directly in the cephalic vesicles of chick embryos, before the development of the vascular network, in order to decipher the effect of VPA on CNC-derived meninges and pericytes in brain vascularization during embryonic development. Behavioral

assays were then performed on newborn chicks treated with VPA to generate a new model of VPA-induced autism. Thus, this PhD project tends to investigate the impact of toxic insults and the role of CNC-derived meninges on social behaviour at birth.

X. Sunitinib, an anti-angiogenic used in cancer treatments

1. Sunitinib exhibits anti-angiogenic effects

Suni (or SU11248) is a multitargeted receptor tyrosine kinase (RTK) inhibitor (Dib et al., 2022), studied as a potential agent in the treatment of metastatic solid tumors (Gridelli et al., 2007). This small molecule targets proliferation and survival of tumor cells by inhibiting RTKs such as PDGFR α and β , VEGFR 1, 2 and 3, stem cell factor receptors (KIT) and fms-like tyrosine kinase 3 (FLT-3). FLT-3 is an RTK mainly expressed in hematopoietic cells (O'Farrell et al., 2003). RTKs play major roles in angiogenesis, tumor growth and metastasis (Faivre et al., 2006). In addition, Sunitinib (suni) exhibits antiangiogenic properties, thus preventing the formation of new blood vessels (Seiwert and Cohen, 2008), by inhibiting VEGFR and PDGFR signaling in tumoral cells (Gridelli et al., 2007; Mendel et al., 2003; O'Farrell et al., 2003) but also in endothelial cells and pericytes (Bozec et al., 2009; Gridelli et al., 2007).

By blocking RTKs, suni inhibits Ras that functions downstream of several RTKs and thus inactivates the RAF/mitogen-activated protein kinase kinase (MEK)/extracellular signal-regulated kinase (ERK) cascade. In fine, the MAPK/ERK pathway is unable to achieve angiogenesis (Gridelli et al., 2007).

2. Sunitinib is an anti-tumoral target

Bozec and colleagues have demonstrated that suni, combined or not with

cetuximab, decreases tumor growth and produced a significant tumor mass decrease in CAL33 cells, cells giving rise to head and neck cancer. In addition, the suni-cetuximab combination significantly reduces cell proliferation. Furthermore, suni alone or in combination with cetuximab significantly reduces the number of vessels in tumors (Bozec et al., 2009). Mendel and colleagues used mouse xenograft models to study the efficacy of suni using human and rat tumor cell lines derived from various different tumor types (colon, epidermoid, glioma, melanoma, breast and non-small cell lung cancer). They show that suni was efficacious against all tumor types tested by exhibiting antitumor activity: tumor regression, destruction of the tumor mass and growth arrest (Mendel et al., 2003).

3. Sunitinib used to counteract VPA-induced phenotypes

Surprisingly, as VPA induces hypervascularization in embryonic brains, Suni was used in this PhD project as an anti-angiogenic drug with the aim to compensate this phenotype and as a way to revert social impairments observed at birth on VPA-treated chicks.

SPECIFIC OBJECTIVES AND HYPOTHESES

This PhD project opens a new dimension by studying the effects of the NC at a behavioral level. In addition, the absence of both BBB at the CSF-blood interface and immune cells at an early stage of the developmental embryo led to the hypothesis that the CNC-derived pericytes exert an immunosurveillance role at an early stage in the embryonic brain, before the emergence of microglial cells.

The goals of this PhD are:

- 1) to decipher the roles of the CNC-derived meninges and pericytes in brain vascularization and homeostasis,
- 2) to characterize the consequences of defective NC-derived meninges and CP on the CSF regulating the whole CNS,
- 3) to investigate the impacts of toxic insults on social behavior at birth.

In order to fulfil these objectives, we used the avian chicken embryos as a model and performed precise microsurgery in a stage-specific manner due to the accessibility of the avian embryo at any stage of its development and in a space-specific manner as microinjections are directly performed in the brains' vesicles of the CNS. As the chick embryos are not connected to their maternal progenitor via a placenta, the pathogen effect is analyzed by directly introducing *E. coli* particles to the embryos, allowing a direct and specific effect of pathogenic infection on the cerebral structures of the embryo and avoiding MIA on the whole embryo.

The avian embryo, and especially the use of the quail-chick chimeras, is a powerful model to analyze transcriptomic studies as the chick genome has been totally sequenced. Likewise, as the GRN of the NCC has been fully mapped,

morphogenetic analyses allow functional studies implicating gene expression modulations and their consequences at molecular, cellular and anatomical levels.

This behavioral level, and more specifically social interactions, has many drawbacks when using the mouse pups as the experimental models since they should be weaned from their mothers between 21 and 26 days of age. Besides, mouse pups only open their eyes around 13 days, complicating any observational behavior of the mouse model. Finally, exploratory studies are also biased with the use of mouse pups as they have difficulties moving during the first days after birth. Indeed, they are only able to crawl till 5 days after birth and start walking between 5 to 10 days after birth. Thus, the newborn chick can be modelled and analyzed for behavioral studies using “filial imprinting”, a complex reflex in which learning capabilities, memory, and empathy are integrated ([Bateson, 1969](#)). When newborn chicks hatch, they follow their congeners. If isolated from their congeners, they adopt the first moving object as their maternal substitutes. This behavior is called “filial imprinting”. So far, “filial imprinting has never been exploited as a behavioral assay to uncover the possible impact of neurodevelopmental defects, resulting from genetic impairments or environmental changes, on the elaboration of postnatal behaviors.

VPA, a widely used anti-convulsant drug, is known to trigger autistic manifestation in newborns when administrated during the first trimester of pregnancy. VPA exposure leads to embryofetopathy with an increased risk of congenital malformations, cognitive impairments and behavioral deficits in newborns ([Clayton-Smith and Donnai, 1995](#)). Thus, we decided to use VPA to generate our experimental models and observe its effects on social behavior at birth, on the development of NC-derived meninges, on regulation of the CSF and on NC-derived

pericytes. With the intention to limit VPA defects on NC-derived meninges, an anti-angiogenic drug called Sunitinib was used for the rescue model.

In 2004, Brinkmann and colleagues described a defense mechanism against pathogens in adults called NET or ETosis. As neutrophils are activated upon infected pathogens, they release extracellular DNA traps to disarm and kill them (Brinkmann et al., 2004). However, this process has never been described in mesenchymal cells or embryos. To our surprise, by characterizing the phenotype of CNC cells, it was possible to describe the ability of these cells to decondense their nuclear material and form extracellular DNA traps. Thus, these observations lead to another hypothesis that aseptic toxicities such as VPA and septic toxicities such as *E. coli* can lead to DNA decondensation and ETosis in CNC-derived pericytes as a defense mechanism to regulate the brain's homeostasis. Therefore, we hypothesize that CNC-derived pericytes have a protective role in brain immunity through the ETosis process.

METHODS AND MATERIAL

I. Microsurgery in chick embryos

1. Chick embryo model

Precise microsurgery in chick embryos was performed in a stage-specific manner due to the accessibility of the avian embryo at any stage of its development and in a space-specific manner as microinjections were directly performed in the brains' vesicles of the CNS. The injections were performed during the 21 HH stage, corresponding to 3,5 days of incubation (E3,5). At this stage, the three vesicles of the brain (telencephalon, diencephalon, and mesencephalon) were clearly visible.

2. Stage-specific embryos

The eggs were weekly delivered to the laboratory by the breeders (Earl Les Bruyères, Dangers), and stored in a cold room at 16°C to avoid any development of the embryos. To obtain the necessary stage of embryo development for experiments, the eggs were horizontally placed in an incubator at 38±0,5°C, the top of the shell previously marked with a pencil as the embryo shifts to the top of the yolk. The stage of the embryo was defined using the Hamburger-Hamilton (HH) stages ([Hamburger and Hamilton, 1951](#)).

II. Embryo manipulation and VPA injection

To perform the injections, a hole was created at the smallest end of the egg to extract 2-4 mL of albumin, allowing the yolk and the embryo to detach from the shell ([Alrajeh et al., 2019](#)). At this stage, the three vesicles of the brain (telencephalon, diencephalon and mesencephalon) were individualized but not

fully segregated, so it allowed the expansion of the experimented solutions in the three compartments. As the meninges covering the forebrain are derived from NC and those covering the rest of the CNS derive from the mesoderm (Etchevers et al., 1999; 2001), the injection of experimental solutions in the mesencephalon emphasized the role of the NC-derived meninges on the anterior CNS.

Four experimental groups were performed in parallel: the control group was injected with a vehicle solution consisting of Phosphate-Buffered Saline (PBS) supplemented with vital dye called Fast Green FCF (Sigma-Aldrich), to facilitate the injection. For experimental series, embryos were injected with a VPA solution (Sigma-Aldrich) diluted to 0,17 M with PBS from a stock solution of 1,7 M adjusted to 240 µg/µL to match with doses reported in other models (Markram et al., 2007). In a third series of experiments, we challenged the detrimental effect of VPA by injecting at once both VPA and Sunitinib (Cell Signaling Technology, #12328) at a concentration of $3 \cdot 10^{-6}$ M from a stock solution of $3 \cdot 10^{-2}$ M (Guo et al., 2006; Mendel et al., 2003; O'Farrell et al., 2003). Finally, a fourth group of embryos was injected with a solution of Sunitinib only, at a concentration of $3 \cdot 10^{-6}$ M diluted with PBS. The microinjections were performed in the three cephalic vesicles of E3,5 embryos in order to fill the cephalic compartment. Thus, the quantity injected was proportional to the size of each embryo.

After injection, a transparent tape was used to reseal the egg, before replacing the egg in the incubator, allowing it to develop till the desired stage for analysis. The embryos were then harvested at 32 HH, corresponding to 8,5 days of incubation, in sterile PBS 1X and fixed in 4% formaldehyde until used for further experiments. At this stage, the vascularization was sufficiently developed to observe the vascular network of the whole brain.

III. Histological preparations

1. Embedding and microtome sections

Once the embryos were fixed in a new solution containing 60% EtOH, 10% formaldehyde and 10% acetic acid for a few days, they were dehydrated in 100% EtOH (Prolabo) and then impregnated with Toluene (Fisher) for permeabilization, the duration being proportional to the stage of the embryo. Embryos were then placed on the surface of solid paraffin (Paraplast, Sigma) and left for incubation overnight at 65°C. The following day, the embryos were permanently embedded in liquid paraffin with a precise orientation, allowing selected plans passing through the structures of interest. After hardening, 7 µm sections were obtained by using a microtome (LEICA) and placed on Superfrost® slides (ThermoFisher Scientific). The slides were finally dried at 37°C in an incubator for 48h before being used for immunocytochemistry.

2. Immunohistochemistry

Slides were dewaxed in two baths of Toluene, dehydrated in two baths of 100% EtOH and rinsed in two baths of PBS 1X. They were then incubated with the primary antibodies. Each antibody was diluted at 1: 500 in PBS 1X and 120 µL was deposited on each slide. The slides were then covered by a coverslip and stocked in a humid chamber overnight at room temperature. The next day, the slides were washed three times 10 min in baths of PBS 1X, and incubated overnight with the secondary antibodies diluted at 1: 1000. After three final rinses in PBS 1X, Slides were mounted with 80 µL of DAPI + Fluoromount-G® (SouthernBiotech). Slides were observed under a DM 6000B microscope (LEICA) using the Leica Application Suite, Advanced Fluorescence (LAS AF) software. Mosaics of the sections are performed using the Tile Scan tool to create high-resolution images under a x20 focus. Images taken with different fluorescent channels were combined using the

Adobe Photoshop® CS4 software.

3. Confocal microscopy

Microtome and cryostat slides were also observed under a confocal microscope (LEICA TCS SP8) using the LAS AF software. A series of 1 µm thickness for 7 µm slides and 2,5 µm thickness for 20 µm slides were captured and assembled to obtain 3D reconstructions of the slides.

IV. Immunofluorescence markers used for the study of meninges and pericytes

For the analysis of the meninges and pericytes, several immunofluorescence markers were used to perform immunohistochemistry on histological sections, whole-mount brains and choroid plexus explants, and immunocytochemistry on pericyte cultures: αSMA (α-Smooth Muscle Actin) or phalloidin were used to detect the pericytes and the vascular network in the brain. Sytox™ green was used to detect DNA, especially extracellular DNA strands. CSF-1R, MAC1 and F4/80 antibodies were used to detect macrophage cells. Cit-H3, Cit-H4 and PAD4 are used to detect proteins implicated in the decondensation of DNA (**Table 3**).

V. Brain dissection and immunohistochemistry for Light sheet microscopy

1. Whole-brain dissections and fixation

To bypass the tissue being damaged by the blades during the brain slices, immunohistochemistry was performed on whole-mount brains to visualize the 3D structures of the brain. To do so, 32 HH embryo heads were dissected to isolate the brain. The eyes are first removed using Pascheff's scissors. The dorsal skin of

Table 3. List of antibodies used in immunofluorescence

Acronym	Primary antibody	Manufacturer	Secondary antibody	Fluorophore
α-SMA	α Smooth Muscle Actin	Sigma-Aldrich®	Goat Anti- Mouse monoclonal IgG2α	Alexa Fluor® 594/488
CSF-1R	Colony Stimulating Factor 1 Receptor	Santa Cruz Biotechnology®	Goat Anti- Rabbit polyclonal IgG	Alexa Fluor® 594
MAC1	Macrophage-1 antigen	Novus Biologicals®	Goat Anti- Rabbit polyclonal IgG	Alexa Fluor® 594
F4/80	(C-7)	Santa Cruz Biotechnology®	Goat Anti- Mouse monoclonal IgG1	Alexa Fluor® 594
Cit-H3	Citrullinated histone 3	Abcam®	Goat Anti- Rabbit polyclonal IgG	Alexa Fluor® 633
Cit-H4	Citrullinated histone 4	Merck®	Goat Anti- Rabbit polyclonal IgG	Alexa Fluor® 633
PAD4	Peptidyl Arginine Deiminase 4	Abcam®	Goat Anti- Rabbit polyclonal IgG	Alexa Fluor® 633

the head, the epidermis, was then delicately removed starting by the mesencephalon region all the way to the telencephalon. Curved scissors were then used to remove the ventral region of the head and isolate the brain. The brain was then refixed in 4% formaldehyde.

2. Immunohistochemistry

For the immunohistochemistry, the brains were placed in 1 mL wells each and incubated with 50% PBS 1X – 50% methanol (MeOH, Prolabo) for 15 min, and twice 15 min with 100% MeOH. A cold shock was then performed with 100% MeOH at -20°C for 45 min. The brains were then rehydrated with three times 15 min baths of PBS 1X before being incubated with the primary antibodies at 1: 500. The wells were then placed at 37°C on rotation overnight. The following day, the brains were washed 4 times 1h in rotation at room temperature with PBS 1X + 0,5% triton + 0,2% bovine serum albumin (BSA, ThermoFisher Scientific). The brains were left in the rinsing solution overnight 1h in rotation at room temperature. On the third day, the wells were first rinsed with a solution of PBS 1X + 0,5% triton + 0,2% BSA + 1% goat serum (GS, Gibco, ThermoFisher Scientific) for 1h before being incubated with the second antibodies diluted at 1: 1000. The wells were place at 37°C on rotation, without light, overnight. On the next day, the brains were washed 4 times 1h in PBS 1X + 0,5% triton + 0,2% BSA at room temperature on rotation, without light, and left overnight in a new solution of PBS 1X + 0,5% triton + 0,2% BSA at room temperature on rotation, without light, overnight. On the last day, the brains are rinsed in a new solution of PBS 1X + 0,5% triton + 0,2% BSA at room temperature on rotation, without light, for 1h. The brains were then placed in 15 mL tubes surrounded by aluminium to avoid light.

3. Whole-mount brain clearing using the 3DISCO protocol

The three-dimensional imaging of solvent-cleared organs (3DISCO) method

described by Vigouroux et al. was used to make the brains transparent ([for review, Vigouroux et al., 2017](#)). To do so, the brains were dehydrated for 1h with 50 % PBS 1X / 50 % MeOH, 1h with 20% PBS 1X/80% MeOH and 2h with 100% MeOH. They were then delipidated all afternoon in 1h baths of Dichloromethane (DCM, Sigma-Aldrich). Finally, the brains were cleared in a solution of Benzyl ether (or Dibenzyl ether, DBE, Sigma-Aldrich) for the week-end and stored in a new solution of DBE.

4. Light sheet microscopy

The brains were observed under an UltraMicroscope II (Miltenyi Biotec), a Light sheet microscope, using the ImspectorPro software. The brains were stabilized on a round platform using liquid glue to position the samples: the mesencephalon and spinal cord were stuck to the platform and the telencephalon was positioned to allow the crossing of the microscope's lasers. The platform was then plunged in DBE before microscopy acquisition.

VI. *In vitro* experimental design: meningeal cell cultures

1. Pericytes culture using inserts

To mimic the *in vivo* experiment and analyze the effect of VPA on the brain at a cellular level, *in vitro* experiments were performed by adding pericyte cultures in inserts containing two distinct wells. Beforehand, round coverslips placed in Nunc IVF 4-well dishes (ThermoFisher Scientific), were coated with human plasma fibronectin (Gibco, ThermoFisher Scientific) for 1h, rinsed 3 times with 70 μ L of distilled water and dried for at least 1h. The fibronectin allows pericytes adhesion to the coverslip by excluding all circulating cells. 1 mL of distilled water was first added to the 5 mg of stock solution and was kept at -20°C. The final solution was prepared by adding 9,8 mL of PBS 1X to 200 μ L of fibronectin. Two-well culture inserts (Ibidi) were then attached to the cover slips. 32 HH non-injected embryos

were collected in PBS 1X + 1% antibiotic penicillin-streptomycin (PS, Sigma-Aldrich) + 1% anti-fungal amphotericin B (fung for Fungizone, Gibco, ThermoFisher Scientific). Dissection was then performed on the heads of E8.5 embryos to isolate the meninges. At this stage, the pericytes are mature, the meninges are sufficiently developed and easy to isolate. First the dorsal skin of the head, the epidermis, was delicately removed starting with the mesencephalon region all the way to the telencephalon. Then the meninges covering the diencephalon and the telencephalon was collected in 200 μ L of PBS 1X + 1% PS + 1% fung. The tubes containing the meninges were centrifuged to remove the PBS 1X and 300 μ L of TrypLE™ Express (Gibco, ThermoFisher Scientific), pre-heated at 37°C, was added to the meninges. Homogenization using a 200 μ L pipette was performed every 10 min for 30 min to dissociate the tissues in individual cells. 500 μ L of culture medium (Dulbecco's Modified Eagle Medium/Nutrient Mixture F-12 (DMEM/F-12, Gibco, ThermoFisher Scientific) + 10% foetal bovine serum (FBS, Sigma) + 1% PS + 1% fung was added to the meninges to stop the enzyme's reaction. To count the number of cells in suspension in the solution and obtain the same proportion of cells in each culture well, 13 μ L of the solution was placed on a Malassez counting chamber (Marienfeld). The number of cells on three horizontal lines were counted and the average of the three lines was calculated and multiplied by 10 to obtain a total number of cells per μ L of solution. The solution was then diluted in cell culture medium to obtain a total of 5000 cells in 20 μ L of cell culture medium for each culture well. In the first well of the insert, 20 μ L of the solution containing the pericytes was added. After 1 h at 37°C to allow the cells to attach to the fibronectin, 50 μ L of culture medium was added. 400 μ L of culture medium was also added in the well surrounding the insert to allow a humid environment for the cells. The pericytes proliferate for 3 days at 37°C and the second well was filled with the conditioned solutions at 1 mM from a stock solution of 1,7 M (culture medium for control, VPA, VPA+Suni or Suni). After 3 days, the inserts were removed, allowing

the solutions to be in contact with the cells and the latter were then fixed 24h later. Immunocytochemistry was then performed and analyzed under an epifluorescence microscope to allow wide-field images using the mosaic acquisition and a confocal microscope to perform z-stack images and observe co-localization of double markers in a 3D structure.

2. Immunocytochemistry

Wells containing the coverslips were first incubated with 0,1% of Triton™ X-100 (Sigma-Aldrich) for 15 min to permeabilize the cells and rinsed three times 10 min in baths of PBS 1X. They were then incubated with the primary antibodies. Each antibody was diluted at 1: 500 in PBS 1X and 250 µL was deposited in each well. The plates were surrounded by paraffin and left overnight in rotation at room temperature. The next day, the wells were washed three times 10 min in PBS 1X, and incubated with the secondary antibodies diluted at 1: 1000, in rotation at room temperature for the day. To perform deoxyribonucleic acid (DNA) staining, after 7h, wells were either incubated with Sytox™ green nucleic acid stain (Invitrogen) diluted at 1: 30000 for 30 min, rinsed three times in PBS 1X and the coverslips were mounted with a drop of Fluoromount-G® (SouthernBiotech) on slides or the wells were directly rinsed three times in PBS 1X and the coverslips mounted with DAPI + Fluoromount-G®. Slides were observed under a DM 6000B microscope (LEICA) using the LAS AF software.

3. Cell analysis

The pericytes morphology and density was analyzed with the α -smooth muscle actin (α -SMA) marker under a confocal microscope using the LAS AF software. Pericytes migration was analyzed by quantifying the cells present in the 500 µm gap between both wells of the insert. To analyze DNA decondensation process, the Imaris Viewer software 9.7.2 was used to observe the Sytox™ green nucleic

acid stain marker. Each individual cell was categorized in three distinct grades of DNA condensation: a cell containing condensed DNA in the nucleus, a cell containing decondensed DNA present in the nucleus and the cytoplasm, and a cell presenting an ETosis phenotype.

VII. 3D ex vivo system: choroid plexus explants

1. CP development in a dish

To decipher differential expression between the ependyma and the stroma of CP, *ex vivo* experiments were performed on CP. 4-well dishes were previously coated with fibronectin for 1h, rinsed 3 times with 70 μ L of distilled water and dried for at least 1h. 100 μ L of each conditioned solution was then added to the wells. Dissection was performed on the heads of the embryos to isolate the CP. First the dorsal skin of the head, the epidermis, was delicately removed starting with the mesencephalon region all the way to the telencephalon. Then the meninges were removed from the diencephalon and the telencephalon. The 3V CP was extracted from the diencephalon and the LV CP was extracted by performing incisions with forceps in the telencephalon. The CP were then placed on the coverslips. After 1 h at 37°C to allow the CP to attach to the fibronectin, 200 μ L of conditioned solution was added to the wells. In addition, septic experiments were performed by adding 3 % of *E. coli* diluted in cultured medium. 300 μ L of the *E. coli* solution was added for 1h or 3h before rinsing with PBS 1X. After 24 h in the incubator at 37°C with the conditioned solutions, the CP were fixed by adding 200 μ L of 4% formaldehyde for another 24 h. Finally, the CP were rinsed three times with PBS 1X and stored in PBS 1X at 4°C.

2. Immunohistochemistry of CP

The CP were first incubated with 0,1% of Triton™ X-100 (Sigma-Aldrich) for 25 min to permeabilize the cells and rinsed three times with PBS 1X. They were then incubated with the primary antibodies. Each antibody was diluted at 1: 500 in PBS 1X and 200 µL was deposited in each well. The plates were surrounded by paraffin and left overnight in rotation at room temperature. The next day, the wells were washed three times 10 min in PBS 1X, and incubated with the secondary antibodies diluted at 1: 1000, in rotation at room temperature for the day. After 7 h, the wells were rinsed three times 10 min in PBS 1X and the coverslips were mounted between a slide with a cavity (Carl Roth) containing two drops of DAPI + Fluoromount-G® and a slide using Aquatex (Merck). Slides were observed under a confocal microscope using the LAS AF software and an Axio Imager Z1 Upright Trinocular Fluorescence microscope equipped with apotome (Zeiss) to perform a z-stack, allowing the observation of co-localizations between two markers. The images were visualized and analyzed with the Imaris Viewer software 9.7.2.

VIII. Morphometric analyses and 3D rendering

1. Lugol staining and Micro-computed tomography acquisition (Micro-CT)

Embryos were analyzed by Micro-CT scanning (Quantum FX Caliper; <http://www.perkinelmer.com>) hosted by the IDV Platform (EA2496; IDV Solutions, <http://www.idvsolutions.com>). Samples were scanned after staining for 72H in Lugol solution (Sigma), used as a contrast agent. Three-dimensional (3D) images were acquired. Full 3D high-resolution raw data were obtained from a series of 2-dimensional (2D) projections by rotating both the x-ray resource and the flat panel detector 360° around the sample (scanning time, 3 minutes) (Boerckel et al., 2014). 3D renderings were subsequently extracted from Digital Imaging and Communications in Medicine data frames using the open-source OsiriX imaging

software, version 3.7.1 (Dr A. Rosset, Geneva, Switzerland). Delineations of the brain structures (telencephalon, diencephalon and mesencephalon) were first performed before quantifying the brain surface and volume for each series using CTscan Analyzer software (SkyScan, Kontich, Belgium, <http://www.bruker-microct.com>).

2. Cephalic and facial measurements

Embryos were harvested in sterile PBS 1X then fixed in 4% formaldehyde. Photos taken to illustrate the gross anatomy, were performed using a WILD M10 microscope (LEICA) and the QCapPro60 software with a x10 focus. One frontal and two profile (left and right) photos were taken per embryo. The embryos were then fixed in 60% ethanol (EtOH), 10% formaldehyde and 10% acetic acid for wax embedding. To measure the morphology of the embryos' heads, the ImageJ software was used. For each embryo, cephalic vesicles and facial structures were measured as previously described (Creuzet, 2009b) and the ANOVA test was used to compare the variation between control (n = 9), VPA-treated (n = 6) and VPA+Suni-treated (n = 8) embryos.

3. Brain's ventricle measurements

To compare the area of the cephalic LV in the different conditions (control, VPA and VPA+Suni), the histological sections of the fixed E8 brains were performed under a microtome. To compare brain structures at a precise anatomical level, we selected sections where the CP were visible in the LV of the brains. Immunohistochemistry was then performed with DAPI to visualize the different structures of the brain and differentiate the parenchyma from the LV. For each slide analyzed under an epifluorescence microscope, the parenchyma and LV areas were measured in square millimetres (mm²) using the ImageJ software and the ventricle area/parenchyma area ratios were then calculated and expressed in

percentage (%).

4. Measurements of the blood vessels

The vascularization in the brain parenchyma was characterized and quantified by using Imaris Viewer 9.7.2 images from Light sheet microscopy acquisition and the ImageJ software. Once the images were converted into 8-bit, the threshold was adjusted to select all the blood vessels. Then by using the “Analyze Skeleton (2D/3D)” plug-in with the “shortest branch” option, the data was collected on Excel and a scatter plot was created using “Skeleton ID” as the abscissa axis (referring to the number of branches) and “Branch length” as the ordinate axis (referring to the length of each branch). The plug-in also generated the image color-coded by junctions count: end-point voxels were displayed in blue, slab voxels in orange and junction voxels in purple.

5. CP explant analysis

The intensity of the immunomarkers was measured in E8 CP explants using the ImageJ software. For each channel, the z-stacks were summed up using “z-project”. For each image, the scale was then adjusted by measuring the scale bar on the image and using the option “set scale” on ImageJ. Then ependyma and stroma of each CP were redefined using “free-hand selections” to differentiate both regions. The intensity of each marker was finally measured in fluorescence intensity/ μm^2 via the mean in “analyze” and “measure” options.

The number of *E. coli* particles and their average size were measured using the Imaris analysis software 9.9.1. For each CP, the *E. coli* particles were detected with the “add new spots” option. First the *E. coli* channel was selected and the estimated *E. coli* spots diameter was calculated with “slice” by measuring the diameter of one *E. coli* particle (5 μm). The selection of the *E. coli* particles for each image was

adjusted manually and the software regenerated the number of *E. coli* particles and the average *E. coli* particles size per image.

IX. RNA sequencing: transcriptomic analysis on meninges and pericyte cultures

To identify the gene expression profiling of perivascular cells, ribonucleic acid (RNA) sequencing was performed both on meninges (*in vivo*) and on pericyte cultures (*in vitro*). The injections with the conditioned solutions (PBS for the control group, VPA, VPA+Suni and Suni) were performed during the 21 HH stage. In addition, septic experiments were performed by adding 100 μ L of *E. coli* on VPA-treated embryos 24h before collecting the meninges. *E. coli* solution was prepared by adding 2 mL of PBS 1X in 2 mg of pHrodo™ *E. coli* BioParticles™ for phagocytosis (Invitrogen, ThermoFisher Scientific). Sonication was then performed for 15 min. For the *in vivo* experiment, the meninges were collected at 34 HH and placed in tubes containing 200 μ L of TRI Reagent® (Sigma) to isolate the RNA. For the *in vitro* experiment, the meninges were collected at 34 HH. After 3 days of culture, the cells were collected in tubes containing 200 μ L of TRI Reagent® (Sigma-Aldrich) to isolate the RNA. The tubes were then stored at -80°C.

Both bulk RNA sequencing in collaboration with the Novogene Company Limited (Cambridge, England) (**Table 4**) and specific transcriptomic analysis in collaboration with the Nanostring platform (**Table 5**) were performed. The Nanostring method counts individual messenger ribonucleic acid (mRNA) transcripts using an amplification-free and enzyme-free technology, without any reverse transcription. The Nanostring technology uses fluorophore barcoding to label individual mRNA transcripts. These barcodes are then mobilized to a slide surface and a picture of the slide is taken. Gene expression from a list of 40 genes

Table 4. List of samples analyzed for bulk RNA sequencing

Experiment	Conditions	Samples
<i>In vivo</i>	CTL	3
	VPA	3
	VPA+Suni	3
	Suni	3
	VPA+ <i>E. coli</i>	1
<i>In vitro</i>	CTL	3
	VPA	3
	<i>E. coli</i>	3
	VPA+ <i>E. coli</i>	3

Table 5. List of samples analyzed for Nanostring

Experiment	Conditions	Samples
<i>In vivo</i>	CTL	7
	VPA	7
	VPA+Suni	7
	Suni	7
	CTL+ <i>E. coli</i>	7
	VPA+ <i>E. coli</i>	8
<i>In vitro</i>	CTL	4
	VPA	4
	VPA+Suni	4
	Suni	4
	CTL+ <i>E. coli</i>	4
	VPA+ <i>E. coli</i>	4

(Table 6) is detected and transcripts are quantified in each sample by directly counting each barcode. The Nanostring technology allows an absolute quantification of each condition without comparing the conditions between each other, therefore allowing an exact quantification of the gene profiling expressed by the meninges and the pericytes.

In parallel, transcriptomic analyses on bulk RNA was also performed using Novogene (Cambridge, UK) sequencing services. Before exportation to the Novogene company, RNA extraction was performed using TRI Reagent® (Sigma) according to manufacture protocol. Briefly, dissected tissues were homogenised in TRI Reagent® supplemented with 0,2 mL of chloroform for 1 mL of TRI Reagent®. After centrifugation, aqueous phase was transferred into new tubes and precipitated with 2-propanol. RNA pellets were washed with 75% EtOH and after air drying were dissolved in DEPC-H₂O (Sigma-Aldrich). RNA concentration was adjusted to 200 ng/μL for each sample. The samples were then exported to the Novogene company where the first complementary DNA (cDNA) strand synthesis was synthesized randomly by hexamer primer M-MuLV reverse transcriptase and the second cDNA strand was synthesized using DNA polymerase I and RNase. Libraries fragments were purified and sequenced on Illumina Novaseq platform, and 150 base pair (bp) paired ends reads were generated. Gene model annotation files were downloaded from genome website directly using genome *Gallus gallus* (genome ID: ensemble_gallus_gallus_grcg6a_gca_000002315_5) as a reference.

X. Proteomic analysis on CSF

To analyze the secretion induced by the CP, proteomic analysis was performed on the cerebrospinal fluid (CSF) of E8 embryos. The injections with the conditioned solutions (PBS for the control group and VPA) were performed during the 21 HH stage. In addition, septic experiments were performed by adding 100 μL of *E. coli*

Table 6. List of 40 genes selected for Nanostring

Pericyte	NCC/Myeloid	ETosis
α SMA	CD14	MPO variant 3
CD13 ANPEP	CD18	NOX2
PDGFR β	CD44	
Cytokine	HDAC	TLR
TNF α	HDAC1	TLR1A
NF- κ B1	HDAC2	TLR1B
PDGF β	HDAC3	TLR2A
CTNNB1	HDAC8	TLR2B
		TLR3
MHC class I	MHC class II	TLR4
BF1	HLA-DMA	TLR5
BF2	HLA-DMB	TLR7
	HLA-DRA	TLR15
		TLR21
Interleukin	Housekeeping genes	Other targets
IL1B	GAPDH	FOXG1
IL6	MRSP27	RUNX1
IL10	RPL19	
	YWHAZ	

on control or VPA-treated embryos 24h before collecting the CSF. Syringes were used to extract the CSF directly from the prosencephalic vesicles. 3 samples containing between 150-300 μ L were collected for each condition (CTL, VPA, *E. coli* and VPA+*E. coli*) (**Table 7**). The tubes were then stored at -80°C.

The samples were sent to the proteomic platform of Paris Descartes University (3P5) for analysis. Liquid chromatography–mass spectrometry (LC–MS) analyses were performed using a TIMS TOF Pro mass spectrometer. Chromatographic time was 120 min. The mass spectrometry data were analyzed using Maxquant version 2.0.3.0. and Perseus version 1.6.15.0. The database used was uniprot_gallus_gallus_reviewed_fev2022.

CSF samples were also sent to the CIBI platform (Gif-sur-Yvette, France) for Western-blot analyses.

1. Preparation of samples and dosage

Samples were slowly defrosted in ice and sonicated, with 3,4 power for 5 seconds on/off, using the Sonicator[®] Ultrasonic Liquid Processor. Samples were then centrifuged at 5000g for 10 min at 4°C. The supernatant was diluted 10 to 50 times in cold PBS and was dosed for proteins using the Pierce[™] BCA Protein Assay Kit (#23225, Thermofisher Scientific).

2. Preparation of samples before gel deposition

Before gel deposition, 20 μ g of the samples were boiled with 5X Laemmli blue sample buffer for 5 min at 96°C. The samples were then cooled down, centrifuged and homogenized. Pre-cast SDS-PAGE, 4–20% Mini-PROTEAN[®] TGX[™] gels (10 wells, 50 μ L) (#4561094, Biorad) were used. 20 μ g of proteins per well and 3 μ L of molecular weight marker Precision Plus Protein[™] Standards, Dual color (#1610374, Biorad) were charged. The gel migrated in TGS 1X migration buffer at

Table 7. List of CSF samples collected for proteomic analysis

Conditions	Samples
CTL	3
VPA	3
<i>E. coli</i>	3
VPA+ <i>E. coli</i>	3

150V for approximately 1h.

3. Liquid transfer

Liquid transfer was performed by activating the PVDF - Immun-Blot® Low Fluorescence PVDF Membrane (#1620264, Biorad) membrane in EtOH at 96°C for 5 min. Foam and Watmann papers were balanced in transfer buffer. The gel, membrane, Watmann and foam papers were then assembled in the transfer tank Invitrogen XCell II™ Blot Module (#EI9051, Thermofisher Scientific). The transfer was performed at 20V for 2h at room temperature.

4. Membrane blocking and antibody incubation

The membrane was blocked by incubating with 5% BSA-Tris Buffered Saline Buffer with Tween 20 (TBST) for 2h at room temperature under agitation. Primary antibodies were diluted in TBST and incubated all night at 4°C under agitation. The next day, the membranes were rinsed with TBST 5 times 5 min. Second antibodies were diluted in TBST and added for incubation for 2h at room temperature, under agitation and hidden from light exposure. Finally, the membranes were rinsed with TBST 5 times 5 min.

5. Revelation by chemoluminescence

The membrane was incubated under agitation at room temperature in enhanced chemiluminescence (ECL) for 1 to 1.30 min, revealed and analyzed with the Chemidocs XRS+ and the ImageLab software (V 6.0.0).

XI. Behavioral tests

To test the elaboration of social interactions at birth using filial imprinting, behavioral tests were performed in newborn chicks. Filial imprinting is a process

in which newborn birds can be isolated from their congeners at birth and are prone to adopt any mobile object as a congener substitute (Bateson, 1979; 1990; Lorenz, 1935). Filial imprinting, first evidenced and described in birds, has also been characterized in other species, like mammals, primates, and even in humans (Lemche, 2020; Scott, 1962). Therefore, we believe that using the filial imprinting as a testable behavioral assay is a relevant and promising approach to model the impact of inherited genetic defects or noxious exposure to environmental insults happening during development on the elaboration of social interactions in neonates. By comparison, current social behavioral tests performed on juvenile mice are biased since mice pups grow up in direct contact with their progenitors and can only be isolated after weaning, corresponding to 3 weeks after birth. In addition, mice pups are blind and mostly crawl at birth. Moreover, testing their capacity to actively interact with congeners is also limited since they only start walking from 5 to 10 days after birth.

Once the chicken embryos were injected at 3,5 days of incubation, they were left in the incubator till they hatched (at around 21 days). Each egg was isolated in a humid box to prevent the chicks from seeing each other. Newborn chicks were subjected to behavioral tests for three days. During the test, the chicks were placed in an open field heated at 37°C with an object, representing a puppet, suspended from a wind up mobile. Before each video, the chick was first placed in the center of the field: once the video started, the object rotated around the chicken. A resting period of 3h was required between each test. To analyze the videos, every second was observed to notice and compare 9 different types of behavior classified in two groups: the first group containing the positive behaviors (if the chick was singing, gazing at, or pursuing the object, and if the chick was in contact with the object), if the chick was self-pecking (unidentified in both groups), and the second group containing the negative behaviors (if the chick was calling

for other chicks, visually avoiding the object, trying to escape the box or aggressively pecking the object). Videos were then analyzed second per second to score each behavioral component. The trajectories of both the newborn chicks and the objects were also tracked using the Kinovea software (0.9.5) to obtain for both of them: the trajectory paths, the distance travelled during the video, the distance between the chick and the object every ms, the velocity and the thigmotaxis (Walz et al., 2016), referring to the specific behavior when the individual stands at distance. In our behavioral approach, the thigmotaxis refers to the chick staying at distance, outside the path designated from the mobile object.

XII. Statistical analysis

The values are expressed as \pm SEM (standard error of the mean). Statistical analyses are performed with the Graph-Pad Prism 8.4.0 software with a confidence interval of 95%. As the data are quantitative continuous, and follow a normal distribution, the results collected from the independent observations are compared two conditions at a time using the paired parametric t-test (p-value $**\leq 0.01$ and $*\leq 0.05$; ns for non-significant).

For the comparison of the vascular branching (the length of the branches and the number of branches) and for the surface + volume of the cerebral vesicles, as the data do not follow a normal distribution, the non-parametric test Kruskal-Wallis was used (p-value $**** p \leq 0.0001$, $***p \leq 0.0005$, $**p \leq 0.005$, $*p \leq 0.05$); ns: non-significant.

The genes compared in the bulk RNA sequencing analyses were selected depending on a significant difference between the control and VPA-treated conditions (p-value $**\leq 0.01$ and $*\leq 0.05$).

RESULTS

I. Analyses of the prosencephalic vascular network

The contribution of the CNC to the development of the meningeal and vascular network in the prosencephalon (comprising the telencephalon and the diencephalon) was analyzed on paraffin sections and on whole-mount dissected E8 brains by immunolabeling CNC-derived perivascular cells with an anti- α SMA antibody. In anticipation of experimental approaches consisting in the injection of molecules of interest in the cephalic vesicles, control embryos were injected at 21 - 22 HH with PBS + Fast Green. Injected embryos were then harvested at 32 - 34 HH and fixed for paraffin embedding or for whole-mount dissection and ultramicroscopy. Histological microtome sections were examined under epifluorescence and confocal microscopes.

In controls at E8, the CNC contribution to the prosencephalic vascularization consists of the meninges surrounding the brain and in the stroma of the CP. Moreover, capillary branches of the meningeal vessels also penetrate the brain parenchyma and vascularize the neural tissue of the pallium from the pial to the ventricular side, except the ependymal layer of VZ which remains avascular (**Fig 38A**).

On E8 whole-mount dissected brains, the 3DISCO technique was used for clearing samples before imaging under Light sheet microscopy and 3D rendering of the vascular network. In control brains, the normal vascular network is mainly found in the meninges covering the exterior surface of the brain. Arterioles are also observed in the brain's parenchyma but the length of their vascular branches does not exceed 160 μ m (**Fig 38D**). Also, these capillaries only contain a single layer of

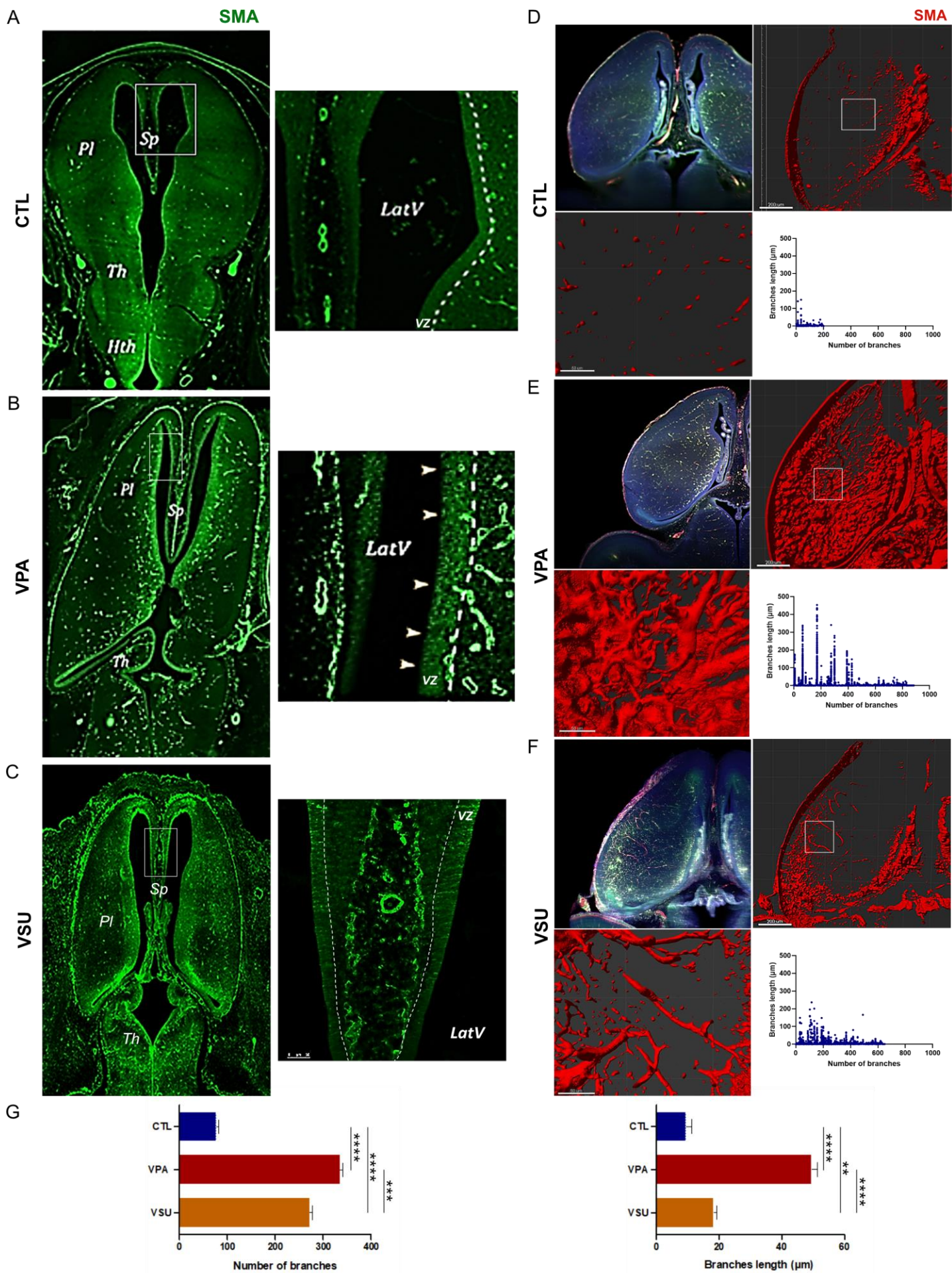


Figure 38. Sunitinib limits hypervascularization in brain parenchyma induced by VPA. (A-C) 2D paraffin-embedded sections of **(A)** a control, **(B)** a VPA-treated and **(C)** a VPA+Suni-treated E8 chick brains visualized with the α -SMA marker (in green) to analyze brain vascularization. **(A)** The vascularization of the control brain is limited at the edge of the ventricular zone (VZ), indicated by the dotted line. **(B)** Hypervascularization is observed in VPA-treated brain parenchyma, especially near the lateral ventricles where arterioles expand into the VZ, indicated by the dotted line (white arrows). **(C)** Sunitinib tends to limit the vascular expansion observed with VPA, especially in the VZ indicated by the dotted line. Hth, hypothalamus, LatV, lateral ventricle, Pl, pallium, SMA, smooth muscle actin, Sp, inter-ventricular septum, Th, thalamus. **(D-F)** Light sheet 3D reconstruction of **(D)** a control, **(E)** a VPA-treated and **(F)** a VPA+Suni-treated E8 chick brains visualized with the α -SMA marker (in red) to analyze brain vascularization. **(D)** The vascularization is limited in control brains with a few arterioles observed in the brain parenchyma (in the lower left panel). The number of vascular branches and their length (μm) were measured using the ImageJ software. The length of the vascular branches does not exceed $160 \mu\text{m}$. **(E)** Hypervascularization is observed in the VPA-treated brain parenchyma leading to more anastomotic and curvier blood vessels with higher ramifications (in the lower left panel) compared to control brains. The number of vascular branches increases in VPA-treated brains compared to control brains and their length measures up to $460 \mu\text{m}$. **(F)** The hypervascularization observed in VPA-treated brains is reduced with VPA+Sunitinib. The number of vascular branches decreases with VPA+Sunitinib compared to VPA-treated brains and their length do not exceed $250 \mu\text{m}$. Scale bars: $200 \mu\text{m}$ (in the upper right panels) and $50 \mu\text{m}$ (in the lower left panels). **(G)** The number of branches (left panel) and the length of the branches in μm (right panel) were compared between the three conditions CTL, VPA and VPA+Sunitinib. Error bars represent \pm SEM. **** $p \leq 0.0001$, *** $p \leq 0.0005$, ** $p \leq 0.005$.

pericytes surrounding the endothelium.

1. VPA induces hypervascularization in brain parenchyma

Embryos were injected at 21 – 22 HH with VPA for experimental models and harvested at 32 - 34 HH for paraffin embedment and histological microtome sections. Immunostaining of CNC-perivascular cells with α SMA antibody in VPA-treated embryos reveals an early expansion and densification of the vascular network in the brain parenchyma. At the level of the meninges surrounding the brain, large vascular lacunae are present in the pericytes. The hypervascularization is especially observed in the dorsal pallium, the region of the brain mediating cognition in birds (Güntürkün et al., 2021), and along the interventricular septum. Interestingly, the blood vessels cross the SVZ and the VZ to invade the LV (Fig 38B), probably disrupting proliferation, migration and maturation of neural stem cells by generating an early normoxic environment. The hypervascularization is also observed in the CP, where the blood vessels from the stroma cross the ependyma to invade the LV. The emphasized vascularization, reaching the LV either via the VZ or via the ependymal layer of the CP, could lead to a change in the composition of the CSF contained in the LV.

By analyzing 32 - 34 HH VPA-injected brains under Light sheet microscopy using the 3DISCO technique, the vascularization is intensified with VPA. The meninges extend their blood vessels across the brain's parenchyma, leading to more anastomotic and curvier blood vessels with higher ramifications. The number of branches is increased by 2.5 times in $280 \mu\text{m}^2$ of the VPA-induced parenchyma compared to control brains. The vascular expansion favors the interconnexion between the blood vessels. VPA also extends the diameters of their lumen. The length the blood vessels measure up to $460 \mu\text{m}$ (Fig 38E,G). Besides, while the control capillaries contain a single layer of pericytes surrounding the endothelium,

with VPA the pericytes aggregate to form multilayers, thus increasing the blood vessels' diameters. VPA could therefore have a double effect on the vascularization: 1) an increase of the vasculogenesis by expanding the size of the blood vessels in the parenchyma and, 2) an increase of the angiogenesis at the expense of the avascular VZ which becomes vascularized, and through the ependymal layers of the CP in order to reach the LV of the brain.

2. Sunitinib tends to limit brain hypervascularization yielded by VPA

When injecting Suni with VPA at 21 – 22 HH chick embryos, a significant rescue of the vascular expansion is observed. The vascular network is especially limited beyond the SVZ and totally absent in the VZ lining the LV of the brain. The vascular network is also retracted from the ependymal layer of the CP (**Fig 38C**).

When embryos are injected with both molecules VPA+Suni, Suni partially reverses the phenotype provoked by VPA and tends to normalize the vascularization. Indeed, the blood vessels are less anastomosed and ramified. Moreover, the diameter of the blood vessels decreases, as well as the length of vascular branches that does not exceed 250 μm . In addition, in 280 μm^2 of the brain parenchyma, the number of branches decreases from 900 for VPA-treated embryos to 650 in VPA+Suni-treated embryos (**Fig 38F,E**).

II. Cephalic and facial morphometric analyses

In parallel, we performed a morphometric analysis to characterize the cephalo-facial morphology of embryonic chicks. The measurements of the face and the brain were carried out on 9 control embryos. The embryos were collected and measured at E8. For each embryo, four measurements were performed to analyze

the facial morphology, as described previously (Creuzet, 2009b): 1) the outer inter-canthal distance, 2) the inter-alar distance, 3) the inter-commissural distance, and 4) the mandibular arch length (**Fig S1A**). In addition, four measurements were performed to analyze the brain morphology: 1) the lens-dorsal telencephalon distance, 2) the lens-epiphysis distance, 3) the lens-optic tectum distance, and 4) the optic vesicle diameter.

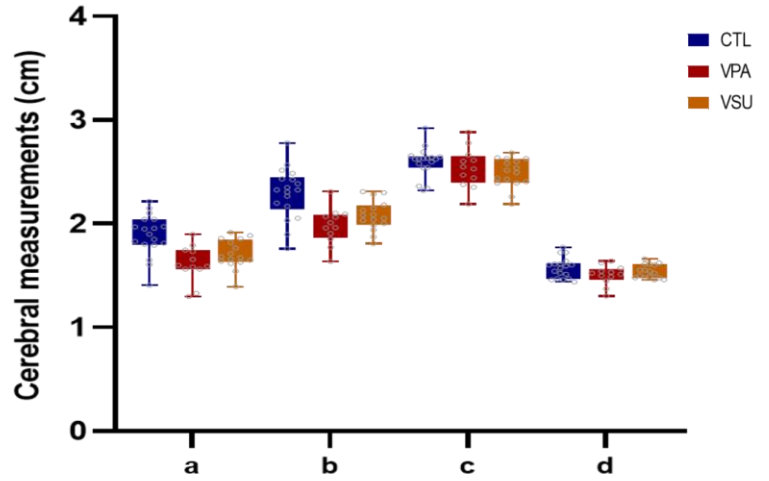
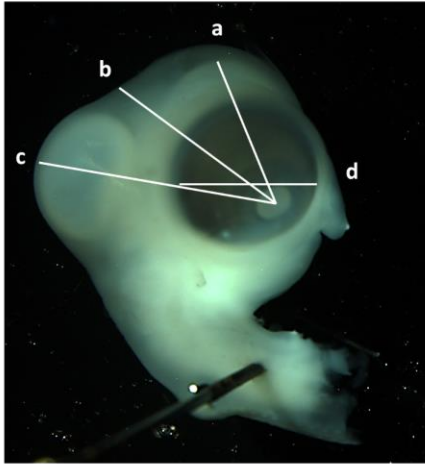
On average out of the 9 embryos, the outer inter-canthal distance measures 3,27 cm, the inter-alar distance 0,38 cm, the inter-commissural distance 0,95 cm and the mandibular arch length 0,64 cm (**Fig S1A**). For the brain morphology, on average of left and right sides of the head, the lens-dorsal telencephalon distance measures 1,89 cm, the lens-epiphysis distance 2,29 cm, the lens-optic tectum distance 2,59 cm and the optic vesicle diameter 1,57 cm (**Fig 39A**).

To measure the surface and the volume of the brain, micro-CT analysis was performed on 7 control embryos. The E8 embryos were collected and stained in Lugol solution for 72h before being scanned by x-rays to obtain high-resolution 3D reconstructions from a series of 2D projections. The brain surface's average, including the telencephalon, diencephalon and mesencephalon is 1971,24 mm² and the brain volume's average is 78,85 mm³ (**Fig 39B**). The average surface of the eyes is 1309,32 mm² and average volume is 52,38 mm³ (**Fig S1B**).

We also performed quantitative analyses to segment and measure the relative size of the brain parenchyma and the LV on histological microtome sections of E8 embryos using DAPI staining. The segmented surface areas of the parenchyma and of the LV was compared using ImageJ.

The parenchyma of control embryos measures 3,48 mm² and the LV 0,49 mm². Thus, the proportion between the LV and the parenchyma surfaces is 14,3% in control brains (**Fig 39C**).

A

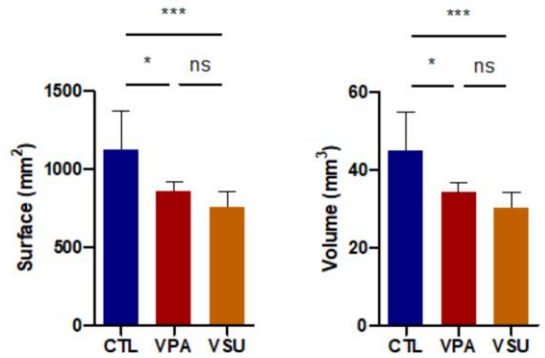
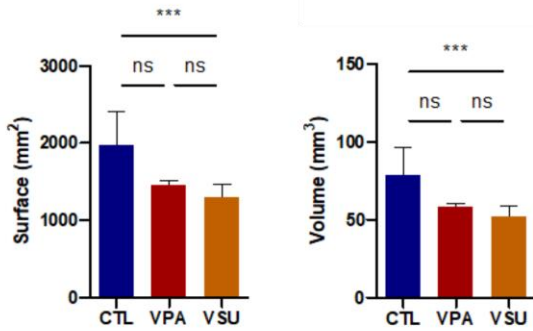


B

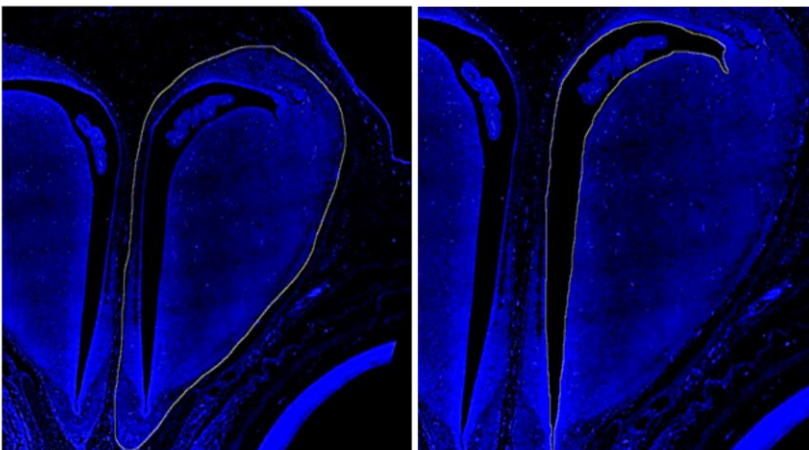


Cerebral vesicles

Telencephalon + diencephalon vesicles



C



Parenchyma and ventricular areas

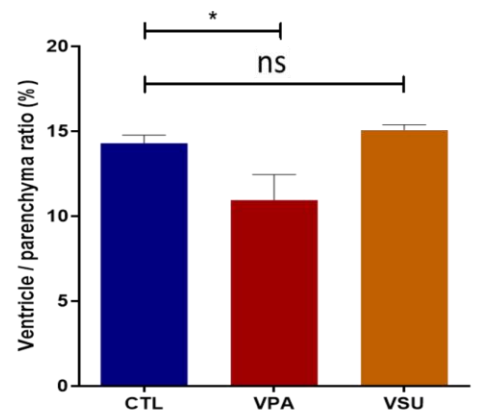


Figure 39. Sunitinib does not restore microcephaly induced by VPA. (A) Morphometric analyses of the cerebral morphology on control, VPA-treated, and VPA+Suni-treated E8 chick heads using ImageJ. a) lens-dorsal telencephalon distance, b) lens-epiphysis distance, c) lens-optic tectum distance, and d) optic vesicle diameter. The four cerebral measurements of VPA-treated embryos decrease compared to the control embryos. For all the measurements performed on the control, VPA- and VPA+Suni-treated embryos, some subtle differences persist but there is no significant difference observed on the overall cranio-facial measurements **(B)** 3D reconstruction on the whole brain of control, VPA-treated and VPA+Suni-treated E8 chick embryos imaged by micro-computed tomography: 2D section of the whole embryo (in the left panel), cranial view (in the middle panel) and lateral view (in the right panel). Scale bars: 0,10 cm. The surface and volume were both measured for the three cerebral vesicles together (telencephalon, diencephalon and mesencephalon) and for the telencephalon and diencephalon vesicles together. All measurements decrease for the VPA-treated brains compared to the control brains. The surface and volume of the VPA+Suni-treated brains continue to decrease compared to the VPA-treated brains. **(C)** The parenchyma and the lateral ventricle areas of E8 chick brains were measured using the ImageJ software. The ratio of the ventricle area on the parenchyma was calculated. This ratio is significantly decreased in VPA-treated brains compared to control brains but there is no significant difference between the control and VPA+Suni-treated brains. Error bars represent \pm SEM. *** $p \leq 0.0005$, ** $p \leq 0.005$, * $p \leq 0.05$; ns: non-significant.

1. VPA impacts the facial and brain morphologies of E8 embryos

To analyze the impact of VPA on the morphology of the face and the brain, morphometric analyses were performed to compare cephalic and facial variations. The measurements of the face and the brain were performed on 6 VPA-treated embryos. The embryos were collected and measured at E8. When the embryos are injected with VPA, the general morphology of the face and the brain decreases when compared to the control group. The outer inter-canthal distance varies from 3,27 cm to 3,10 cm, the inter-alar distance decreases from 0,38 cm to 0,34 cm, the inter-commissural distance from 0,95 cm to 0,79 cm. However, the mandibular arch length increases from 0,64 cm to 0,68 cm (**Fig S1A**). This difference could be due to the relative expansion of the brain in control embryos, which limits the frontal space for the mandibular to grow. As far as the brain morphology is concerned, the average of left and right sides of the head varies between individuals: we calculated an asymmetry index (mean of Δ left-right measurements / mean of left+right measurements). We noticed an increase by 3,3% of brain asymmetry in VPA compared to control, meaning that upon VPA insult, facial and brain development gains in asymmetry, as observed in human patients (Boutrus et al., 2019; Tan et al., 2021). Moreover, the lens-dorsal telencephalon distance decreases from 1,89 cm for control brains to 1,61 cm for VPA-treated brains. In addition, the lens-epiphysis distance decreases from 2,29 cm to 1,98 cm, the lens-optic tectum distance varies from 2,59 cm to 2,54 cm and the optic vesicle diameter decreases from 1,57 cm for control embryos to 1,52 cm for VPA-treated embryos (**Fig 39A**).

The percentage of changes observed between the two groups of embryos was performed. When comparing the control to the VPA, the facial and brain morphogenesis is decreased up to 20% for most measurements (-20,62% for the lens dorsal telencephalon distance), excepting the mandibular arch length (+5,88%) and non-significantly the right lens-optic tectum distance (+0,88%).

Altogether, these results show an overall reduction in size of the both the brain and the face with VPA treatment.

Micro-CT analysis was performed on 8 VPA embryos, collected and analyzed at E8. When embryos are treated with VPA, the surface and the volume of the cerebral vesicles (telencephalon + diencephalon and mesencephalon) decrease significantly compared to control brains. The brain's surface decreases from 1971,24 mm² to 1459,16 mm² and the brain's volume decreases from 78,85 mm³ to 58,37 mm³ compared to the control brain. The anterior brain of VPA-treated embryos, thus excluding the mesencephalon also shrinks compared to control brains as the surface decreases from 1127,38 mm² to 855,82 mm² and the volume from 45,10 mm³ to 34,23 mm³ (**Fig 39B**). VPA also decreases the average volume of the eyes from 52,38 mm³ to 22,17 mm³ and the surface from 1309,32 mm² to 554,18 mm² compared to the control eyes (**Fig S1B**).

While the areas of the parenchyma and of the LV show no significant difference between the three groups, the parenchyma of VPA-treated embryos tends to develop (from 3,48 mm² for control brains to 3,85 mm² for VPA-treated brains) whereas the LV tends to shrink (from 0,49 mm² for control brains to 0,43 mm² for VPA-treated brains). However, when comparing the proportion between the LV and the parenchyma surfaces in VPA-treated embryos, it decreases from 14,3% to 10,94% compared to control embryos (**Fig 39C**). These results confirm the reduction in ventricular size observed in patients with autism compared to control subjects ([Vidal et al., 2008](#)).

2. Sunitinib does not restore facial and brain morphologies in VPA-treated embryos

The measurements of the face and the brain were performed on 8 VPA+Suni-treated embryos. Surprisingly, when the embryos are injected with VPA+Suni, Suni

does not restore the overall morphology of the face and the brain altered by VPA. For all the measurements performed on the CTL, VPA and VPA+Suni-treated embryos, some subtle differences persist but there is no significant difference observed on the overall cranio-facial measurements (**Fig 39A; S1A**). However, we noticed a rescue by 37% of brain asymmetry in VSU compared to VPA embryos. These asymmetric measurements could suggest an important marker in the diagnosis of ASD.

The Micro-CT analysis was performed on 8 VPA+Suni embryos, collected and analyzed at E8. The Suni does not seem to restore the effect of VPA on brain morphology as the surface (1301,48 mm²) and the volume (52,06 mm³) of the cerebral vesicles: both decreases compared to the VPA-treated group (1459,16 mm² and 58,37 mm³ respectively) (**Fig 39B**). However, the average volume and surface of the eyes and is almost restored with VPA+Suni (50,6 mm³ and 1265,04 mm² respectively) compared to the volume of the control eyes (52,38 mm³ and 1309,32 mm² respectively) and significantly increased compared to VPA-treated embryos (22,17 mm³ and 554,18 mm² respectively) (**Fig S1B**).

When analyzing the surfaces of the brain parenchyma and the LV, the application of VPA+Suni tends to rescue the brain morphology with a decrease of the parenchyma surface measuring 3,33 mm² (3,85 mm² for VPA-treated brains) and an increase of the LV measuring 0,50 mm² (0,43 mm² for VPA-treated brains). However, the application of VPA+Suni rescues the proportion between the parenchyma and the LV surfaces up to 15,07% compared to VPA-treated embryos (**Fig 39C**).

III. Filial imprinting to model the elaboration of social interactions at birth

1. Video recording tracking to study social interactions at birth

We tested the relevance of the filial imprinting to model the elaboration of social behavior at birth. Newborn chicks injected with PBS at E3,5 were isolated from their congeners. Few hours after hatching, the chicks were placed in an open field with an object, representing a decoy, used as the congener substitute, suspended from a wind up mobile, for short video-recorded training session of 3,5 min each (**Fig 40A**). Filial imprinting was observed by analyzing the interactions between the chick and the object. By using the Kinovea software to track the trajectories of both the newborn chick and the object (**Fig 40A,B**), the distance between both of them at every second of the video was calculated (**Fig 40C**). Distance categories were analyzed between the chick and the object: 1) when the chick is far from the object, above 40 cm, referring to a disinterest or avoidance of the chick towards the object, 2) when the chick is between 5 and 20 cm of the object, referring to an attachment of the chick towards the object and, 3) when the chick is less than 5 cm away from the object, referring to a close contact between both of them (5 cm representing the distance between the barycentre of the chick and the object). The control chick spent a majority of the time (more than 45%) close to the object with a distance oscillating between 5 and 20 cm, and less than 7% of the time further than 40 cm away from the congener. Moreover, both were in contact for 0,7% of the behavioral test (**Fig 40D**).

2. VPA generates severe alterations in social interactions at birth

With the aim of investigating the effects of VPA on social behavior at birth, E3,5 chick embryos were injected with VPA and left until hatching at E21. By using the Kinovea software to track the trajectories of both the newborn chick and the object (**Fig 40A**), the VPA-treated chick spends less time in the circumference of the circle

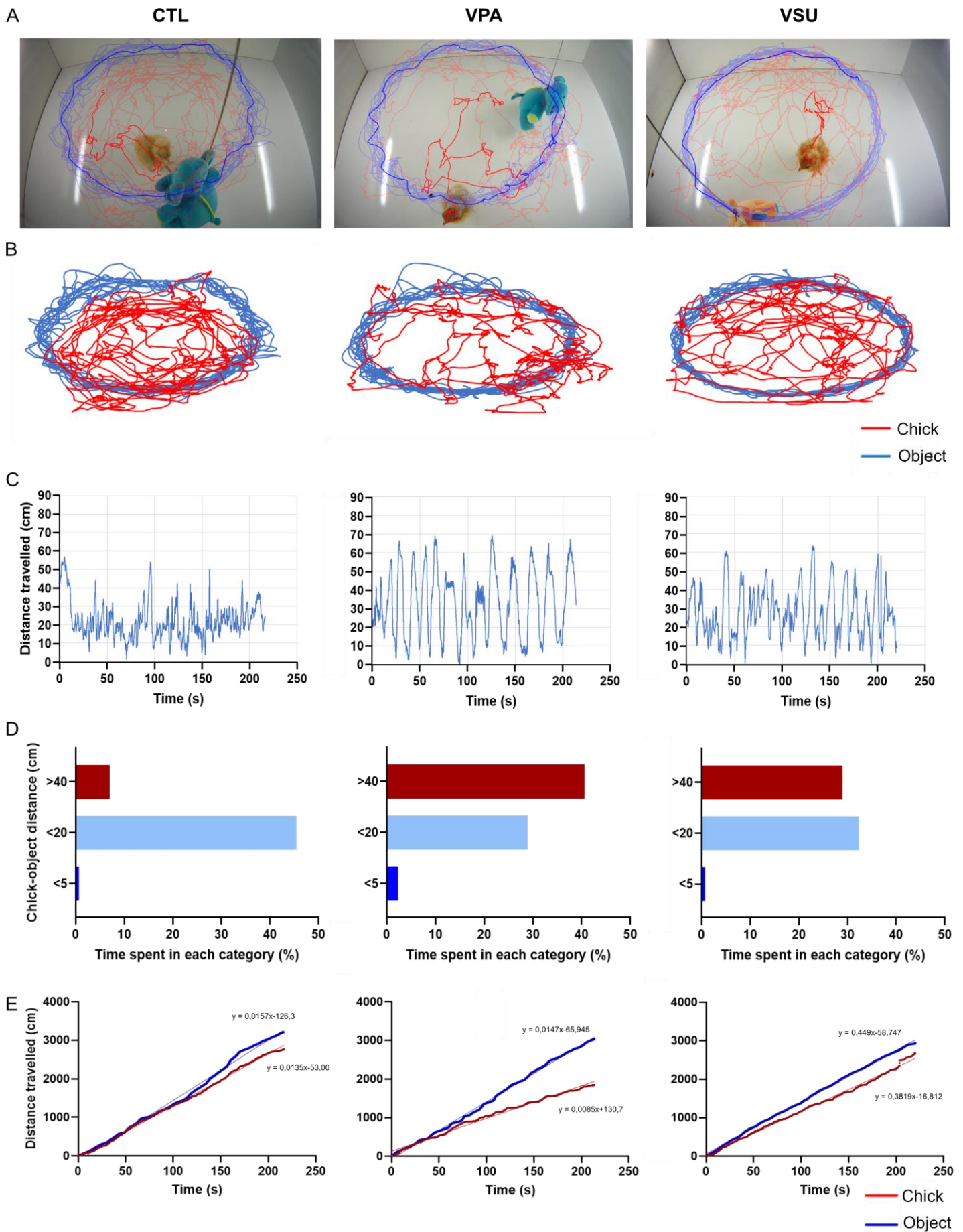


Figure 40. Sunitinib tends to restore social interactions at birth altered by VPA. (A)

The newborn chicks injected at E3,5 with PBS, VPA or VPA+Suni, are placed in an open-field with an object suspended from a wind up mobile and representing the maternal substitute. During the three first postnatal days of the newborn chick, 9 videos of 3,5 min each are filmed per day. The trajectories of the chick (in red) and of the object (in blue) are tracked using the Kinovea software and **(B)** are represented in 2D to analyze the thigmotaxis behavior, corresponding to the red pathway found exterior to the blue circumference. **(C)** The Kinovea software generates the distance between the chick and the object at every second of the video. **(D)** This distance is classified in three categories: above 40 cm referring to a disinterest of the chick towards the object, below 20 cm referring to an attachment of the chick towards the object and below 5 cm referring to a contact between both of them. The control chick spends a majority of its time close to the object (45,5%). The VPA-treated chick spends a majority of its time away from the object (40,6%). The VPA+Suni chick tends to spend more time closer to the object (32,3 %) compared to VPA-treated chicks. **(E)** The total distance travelled by the chick (in red) and by the object (in blue) during each second of the video are referenced using the Kinovea software. The similar distances travelled by both the chick and the object manifest a constant pursuing of the control chick towards the object during the whole behavioral test. The higher distance travelled by the object compared to the VPA-treated chick manifests an absence of motion from the latter, referring to a lack of pursuit towards the object. On the contrary, the similar distances travelled by both the VPA+Suni-treated chick and the object manifest an increase of the pursuit behavior with VPA+Suni compared to VPA-treated chicks.

designated by the object, and exhibits an increased thigmotaxis behavior (**Fig 40B**). When analyzing the distance between the chick and the object at every second of the video, the chick spends more time away from the object, above 40 cm (40,62%), specifying the disinterest of the chick towards the object. Interestingly, the chick spends 2,33% time less than 5 cm away from the object (**Fig 40C,D**), which is due to an increase of aggressive pecking of the chick towards the object.

3. Sunitinib tends to restore social behavior at birth

In an attempt to revert the defective social behavior observed with VPA, we tested the anti-angiogenic molecule, Suni in combination with or without VPA. According to the paradigm, Suni was injected at 21 – 22 HH; embryos were grown until hatching to perform social behavioral tests at birth (**Fig 40A**).

By using the Kinovea software to track the trajectories of both the newborn chick and the object (**Fig 40A,B**), the VPA+Suni-treated chick spends more time in the circumference of the circle designated by the object, resembling the pathway observed with the control chick (**Fig 40B**). When analyzing the distance between the chick and the object at every second of the video, the chick spends more time close to the object, below 20 cm (32,33%). Therefore, the VPA+Suni treated chick is more interested in pursuing the object compared to VPA-treated chicks. However, the chick only spends 0,71% of the time less than 5 cm away from the object (**Fig 40C,D**).

4. Behavioral scoring to study social interactions at birth

In addition to tracking, seven different behaviors of the chick towards the object were scored per second: gaze, pursuit, contact, no look, thigmotaxis, aggressive pecking and self-pecking. For analysis, these behaviors were secondarily grouped

in three main categories. Three positive behaviors attesting the attachment and imprinting towards the object, when the chick is gazing at, or pursuing the object, and in contact with the object. By contrast, the behaviors of the chick paying no attention (no look), and/or standing at distance to avoid contact with the object (here referred as thigmotaxis), and aggressive pecking attested of aversive behaviors. Additionally, another behaviour consisting in iterative self-pecking the object was analyzed as a sign of anxiety and distress.

The control chick expresses high social interactions with the object as it expresses a majority of attachment behaviors, especially notable on the pursuing of the object (**Fig 41A**). In fact, the chick travels almost the same distance as the object during the whole behavioral test (2763,22 cm for the chick versus 3210,55 cm for the object) (**Fig 40E**). Furthermore, a summary of all the behaviors observed by the control chicks (n=10) on a polar chart confirms the majority of attachment behaviors compared to the aversive ones (**Fig 41D**).

These seven behaviors were analyzed, for each chick, throughout 9 tests per day for three days; the first day (D0) corresponding to the day after the chick was born. Overall, the 9 videos of the 3 postnatal days were specifically analyzed on 4 different control chicks. The average of the behaviors shown by the light blue lines show a majority of positive behaviors in the control chicks, especially on the second day after birth (D1) with an increase of the gaze (**Fig 42A**), the pursuit (**Fig 42C**) and the contact (**Fig 43A**). The negative behaviors thigmotaxis (**Fig 42D**) and aggressive pecking (**Fig 43B**), as well as self-pecking (excepting for one control chick on the last day of the behavioral test) (**Fig 43C**) are rarely observed with the control chick.

In fine, as the control chicks exhibit a majority of attachment behaviors towards the object, used as a congener substitute, the process of filial imprinting is therefore validated to model the elaboration of social interactions at birth.

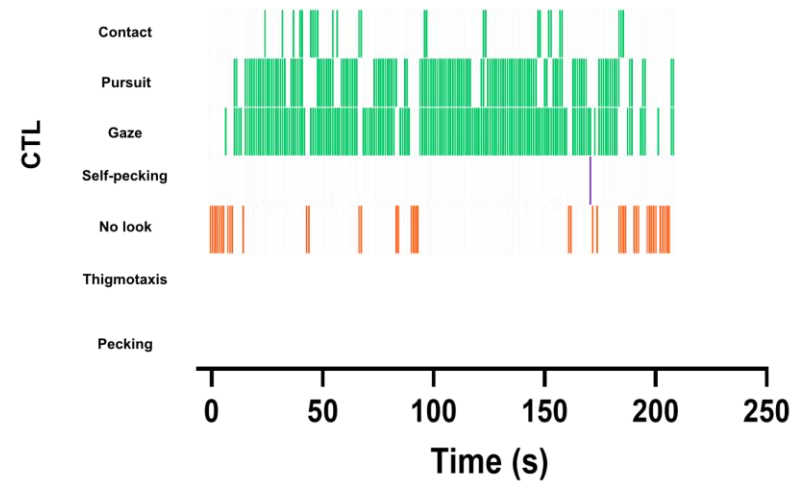
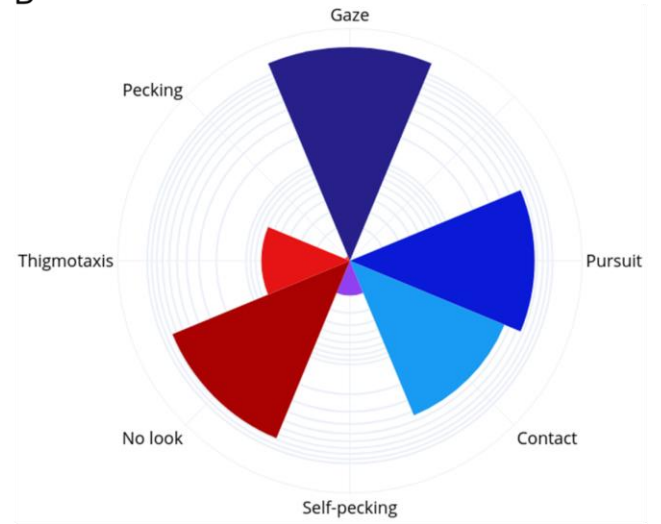
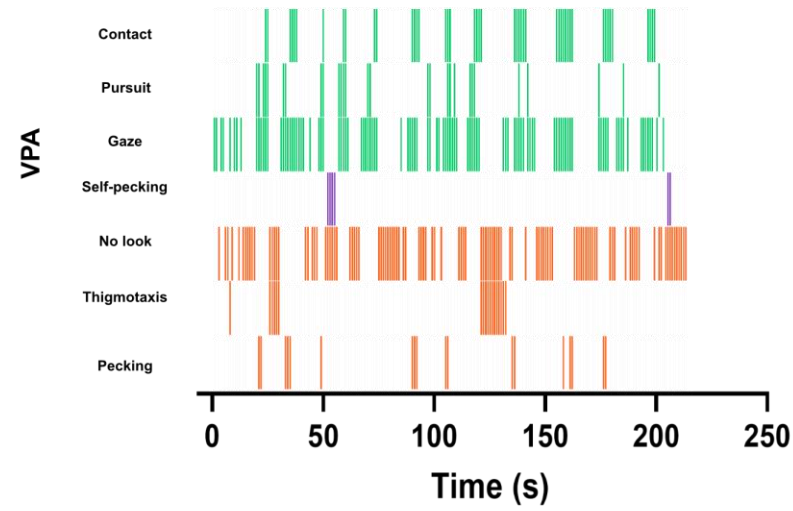
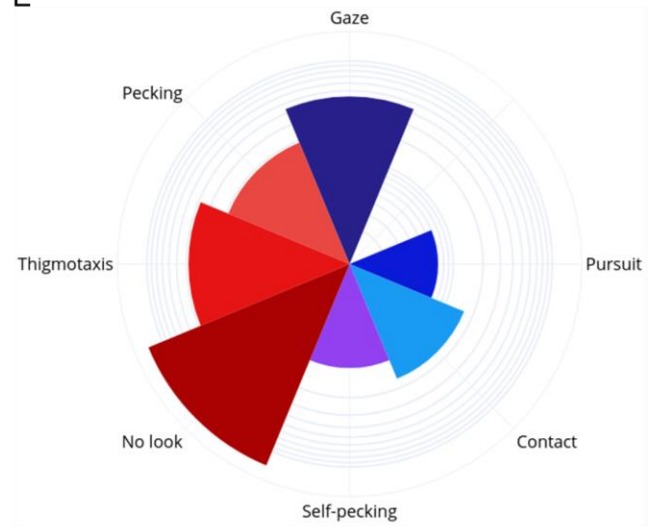
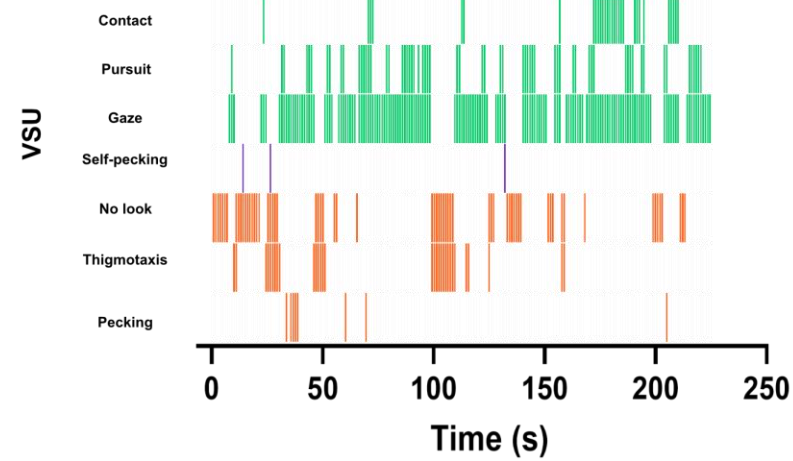
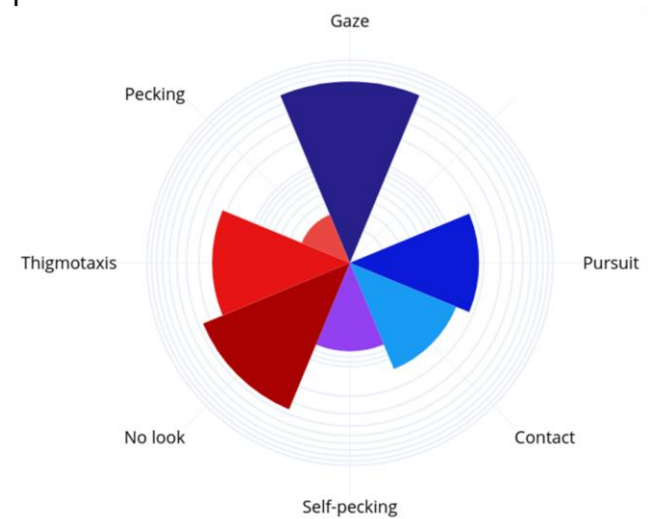
A**D****B****E****C****F**

Figure 41. Sunitinib tends to restore attachment behaviors and reduce aversive behaviors of newborn chicks treated with VPA. (A-C) For each video, 7 behaviors are analyzed every second. Three attachment behaviors (in green) refer to a social interaction of the newborn chick: if the chick is gazing at (gaze), or pursuing the object (pursuit), and if the chick is in contact with the object (contact). A behavior analyzing the anxiety of the chick (in purple): if the chick is self-pecking. Three aversive behaviors (in orange) referring to a social deficit of the newborn chick: if the chick is visually avoiding the object (no look), trying to escape the open-field (thigmotaxis) or aggressively pecking the object (pecking). **(A)** A majority of attachment behaviors is observed compared to the aversive behaviors for control chicks, representing a high social behavior of the newborn chick. **(B)** On the contrary, the VPA-treated chick exhibits more aversive behaviors, representing a deficit social behavior of the newborn chick. **(C)** While the VPA+Suni-treated chick spends time escaping the open-field or aggressively pecking the object, overall, a majority of attachment behaviors is observed compared to the aversive behaviors. Thus, VPA+Suni tends to limit the defective effects of VPA on social interactions at birth. **(D-E)** A polar chart, using the log scale, represents the seven behaviors (attachment behaviors in blue and aversive behaviors in red) summed up on all three postnatal days for all the **(D)** control chicks, the **(E)** VPA-treated chicks and the **(F)** VPA+Suni-treated chicks analyzed. **(D)** A majority of social interaction is observed compared to the social deficit behaviors in control chicks. **(E)** On the contrary, a majority of social deficit behaviors increases compared to control chicks. **(F)** A majority of social interaction behaviors is observed compared to the social deficit behaviors, especially with an increase of the pursuit and a decrease of aggressive pecking compared to VPA-treated chicks.

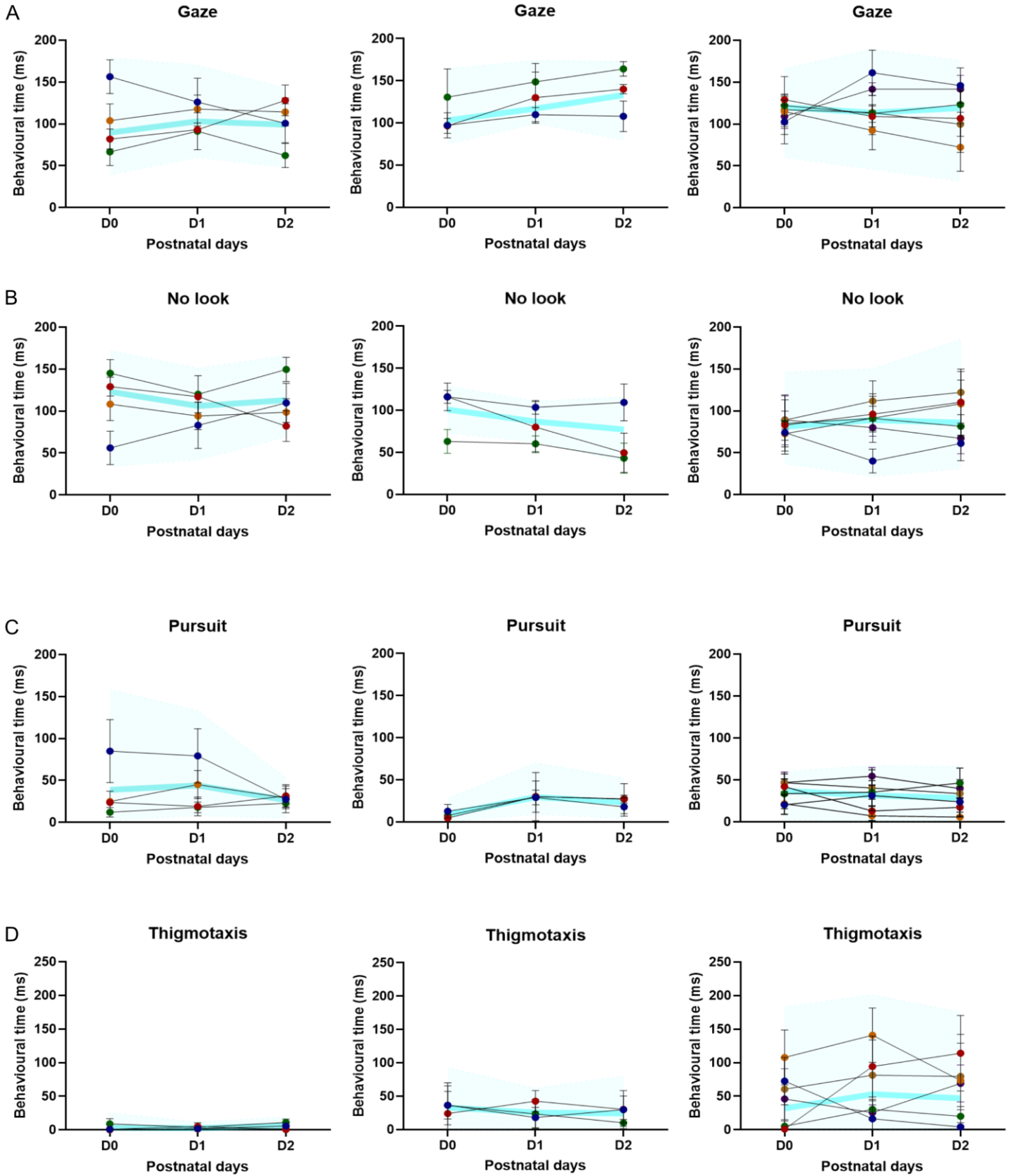
CTL**VPA****VSU**

Figure 42. Sunitinib tends to restore socialization compared to VPA-treated chicks.

During the three first postnatal days of the newborn chicks (D0, D1 and D2), 9 videos of 3,5 min each are filmed per day. For each of the three postnatal days, seven behaviors were separately analyzed for the 9 videos. Among these behaviors, two attachment behaviors refer to a social interaction of the newborn chick: **(A)** if the chick is gazing at (gaze), or **(C)** pursuing the object (pursuit). On the contrary, two aversive behaviors refer to a social deficit of the newborn chick: **(B)** if the chick is visually avoiding the object (no look) or **(D)** trying to escape the open-field (thigmotaxis). Each colored dot represents one newborn chick and the light blue line represents the average of all the chicks for each day. On average, the control chicks exhibit an interest towards the object as they pursue it from D0 and thigmotaxis is rarely observed. While the attachment behavior pursuit is decreased with VPA-treated chicks compared to control chicks, the thigmotaxis behavior increases, notably on D0 and D1. On average, the VPA+Suni-treated chicks exhibit a maximum interest towards the object on the second postnatal day (D1). However, compared to the control and VPA-treated chicks, the thigmotaxis increases. Error bars represent \pm SEM.

CTL

VPA

VSU

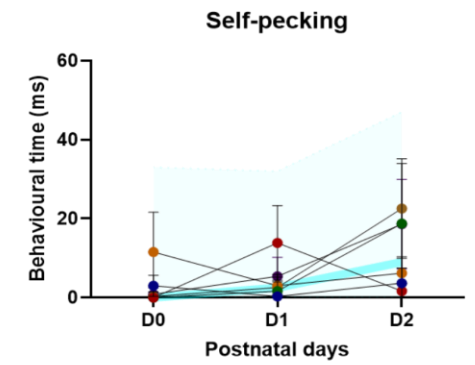
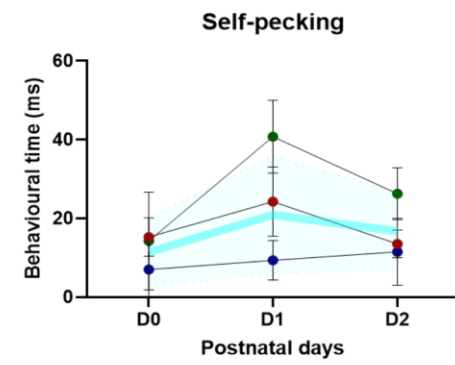
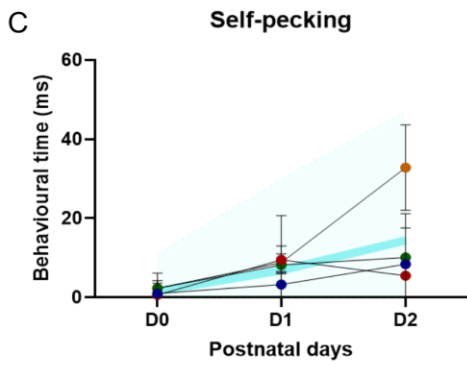
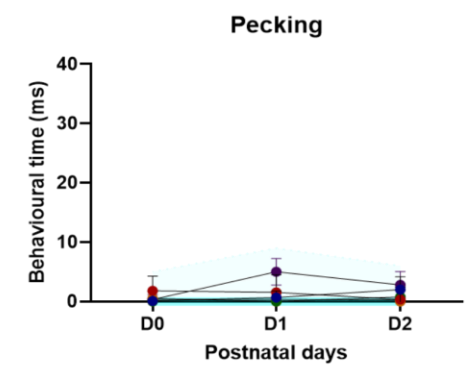
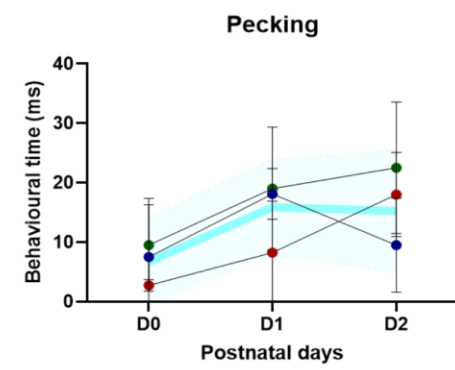
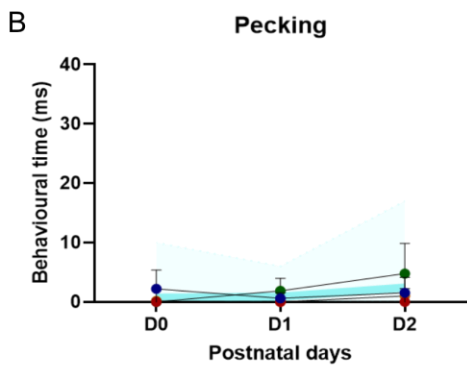
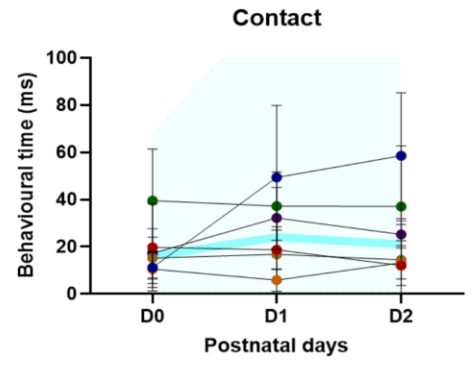
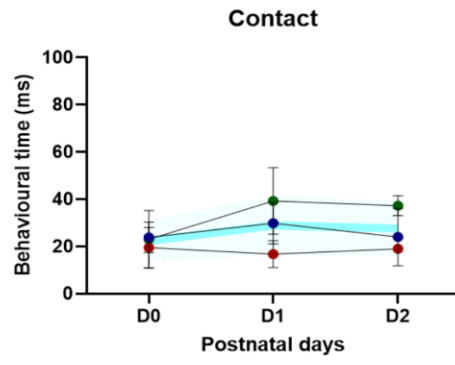
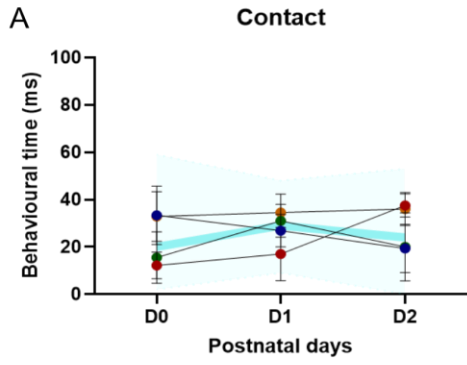


Figure 43. Sunitinib tends to reduce anxiety compared to VPA-treated chicks. During the three first postnatal days of the newborn chicks (D0, D1 and D2), 9 videos of 3,5 min each are filmed per day. For each of the three postnatal days, seven behaviors were separately analyzed for the 9 videos. Among these behaviors, an attachment behavior refers to a social interaction of the newborn chick: **(A)** if the chick is in contact with the object (contact). On the contrary, an aversive behavior refers to a social deficit of the newborn chick: **(B)** if the chick is aggressively pecking the object (pecking). A behavior to analyze the anxiety of the chick is also referred: **(C)** if the chick is self-pecking. Each colored dot represent one newborn chick and the light blue line represent the average of all the chicks for each day. **(A)** While the contact behaviour is relatively similar between control, VPA- and VPA+Suni-treated chicks, **(B)** the high aggressive behaviour of VPA-treated chicks compared to control chicks could explain the observation of similar contact behaviors as the chicks pursue the object in order to aggressively peck it, thus coming into contact with the object. **(C)** Control chicks show little anxiety as the self-pecking behaviour is rarely observed. However, self-pecking is predominant with VPA-treated chicks. A significative decrease of aggressive pecking and self-pecking is observed with VPA+Suni-treated chicks. Error bars represent \pm SEM.

5. VPA increases aversive behaviors at birth

Behavioral scoring reveals a switch from attachment to aversive behaviors with VPA-treated chicks compared to control chicks (**Fig 41A**). For instance, the pursuit behaviour is considerably decreased while thigmotaxis increases. Moreover, VPA-treated chicks trigger aggressive pecking against the object, whereas this behaviour is totally absent with control chicks. Similarly, VPA-treated chicks exhibit anxious behavior as the self-pecking behavior is increased (**Fig 41B**). Overall, a summary of all the behaviors observed by the VPA-treated chicks (n=10) on a polar chart confirms the majority of aversive behaviors compared to attachment behaviors, with an increase of thigmotaxis, aggressive-pecking and self-pecking (**Fig 41B**).

An overall analysis was performed on 3 VPA-treated chicks throughout the 9 tests per day for three days. The average behaviors, shown by the light blue line, confirms the reduced interest of VPA-treated chicks of pursuing the object (**Fig 42C**). However, on average, the VPA-treated remain very aggressive towards the object, compared to control chicks (**Fig 43B**) and are very anxious as they tend to escape the open-field (thigmotaxis) (**Fig 42D**) and perform more self-pecking (**Fig 43C**). The high aggressive behavior could explain the observation of similar contact behavior observed with control chicks (**Fig 43A**) as the VPA-treated chicks pursue the object in order to aggressively peck it, thus coming into contact with the object.

Thus, the process of filial imprinting is therefore altered with VPA treatment as VPA-treated chicks exhibit social impairments at birth.

6. Sunitinib tends to normalize attachment behaviors at birth

By analyzing the seven behaviors, Sunitinib tends to normalize the overall behaviors as more social interactions are observed compared to VPA-treated chicks. It is specifically notable with the pursuit (**Fig 41C**). In fact, the chick travels almost the

same distance as the object during the whole behavioral test (2669,04 cm for the chick versus 2933,64 cm for the object), as observed with the control chick (**Fig 40E**). A summary of all the behaviors observed by the VPA+Suni-treated chicks (n=10) on a polar chart confirms the shift from aversive behaviors observed with VPA- treated chicks to the attachment behaviors. In fine, Suni partially reverses the defective effects of VPA on social behavior at birth (**Fig 41F**).

Overall, the 9 videos of the 3 postnatal days were specifically analyzed on 6 different VPA+Suni-treated chicks. The average of the behaviors shown by the light blue lines show a majority of attachment behaviors. Notably, Suni tends to decrease the aggressive pecking (**Fig 43B**) and self-pecking (**Fig 43C**) behaviors compared to VPA-treated chicks. However, the aversive behavior thigmotaxis remains high. Surprisingly, the VPA+Suni-treated chicks perform more thigmotaxis than VPA-treated chicks (**Fig 42D**).

In fine, Suni partially reverses the defective effects of VPA on social behavior at birth. Consequently, the aberrant meningeal and intracerebral vascular network preceding behavioral disorders at birth suggests that hypervascularization during brain development could be linked to social impairments at birth.

IV. The cephalic neural crest-derived pericytes harbour immune capacities

Given the considerable expansion of the brain vasculature, we postulated that a massive infiltration of leukocytes in the brain parenchyma could ensue and account for the behavioral impairment in VPA-treated chicken. We performed immunolabeling using three macrophage markers found early in development CSF-1R, MAC1 and F4/80. To our surprise, we did not notice leukocyte infiltration

within the parenchyma, but a striking immunostaining of the α SMA-positive pericytes with macrophage markers. These observations suggested that CNC-derived pericytes could harbor macrophagic phenotypes. However, despite a co-localization of both markers, suggesting a macrophagic phenotype of the pericytes, the *in vivo* analysis was limited by autofluorescence of the erythrocytes which are nucleated in avians.

1. Pericytes exhibit high migration capacity *in vitro*, hindered by VPA

To bypass this limitation, *in vitro* cultures were performed in order to specifically target pericytes. In a collaborative work performed in the lab, we demonstrated the stable and robust model of pericytes cell culture since after ten passages, cultures of meningeal pericytes demonstrated nearly 100% preservation of α SMA-positive cells (**Fig. S2**) (Amarante, Bruet, Gorojankina and Creuzet, *in prep.*).

Control pericytes from E8 meninges were exposed to experimental solutions (culture medium, VPA, VPA+Suni or Suni) three days after proliferating in a compartmented well of an insert. Between the day cells were put in culture (D0) and the day inserts were removed to allow migration (D3), the pericytes proliferate to increase their cellular density by 2,42 (from 141,2 cells/mm² to 342,0 cells/mm²) (**Fig 44A**). 24h after removing the insert and allowing cell migration, the cells are fixed and analyzed under an epifluorescence microscope for their morphology, migration capacity into the gap and DNA decondensation process.

Migration capacity of pericytes was analyzed via a migration index by comparing the cellular density in the gap to the cellular density in the lateral well where the cells were proliferating. With the culture medium, the pericytes have a high migration capacity and are able to colonize the gap between the two wells. However, the VPA tends to prevent the migration of the pericytes. The migration

index decreases from 0,2 with the culture medium to 0,09 with VPA. With the application of VPA+Suni or with the only presence of Suni, the cell migration is totally rescued, with respectively a 0,18 and 0,19 migration index. Thus, Suni avoids the limited migration by VPA (**Fig 44B**).

Control pericytes *in vitro* acquire a fibroblastic and star-shaped morphology with several lamellipodia oriented toward the gap between the two wells. Their nuclei are well defined and circumscribed. When in contact with VPA, pericytes become fusiform and bipolar, with long filopodia and few lamellipodia. Their nuclei are deformed, highly stretched and hard to define in the cytoplasm, with a degradation of their nuclear material. Besides, the VPA-induced pericytes have no specific orientation in the gap. While the morphology of the pericytes remain fusiform and bipolar with the exposition of VPA+Suni, their nuclei are better defined than VPA-induced pericytes (**Fig 44C**).

Overall, similarly to immune cells navigating the body toward injury or infected sites ([Guak and Krawczyk, 2020](#)), pericytes exhibit high migration capacities *in vitro*. Even though VPA limits the pericytes' migration capacity *in vitro*, the hypervascularization and invasion of the VZ observed in VPA-treated brains could be due to the interaction between PDGFR β -positive pericytes and PDGF β -positive endothelial cells required for angiogenesis sprouting, as described previously (*cf. introduction, III. 5. b. Platelet-Derived Growth Factor Receptor β*). However, in *in vitro* cultures, the pericytes represent nearly 100% of the cells and the absence of PDGF β /PDGFR β recognition could therefore influence the migration of the pericytes.

2. The pro-immune properties of pericytes are enhanced with VPA

2D mass cultures were also performed on CNC-derived pericytes. Control pericytes from E8 meninges were exposed to experimental solutions (culture

medium, VPA or VPA+Suni) for 24h three days after proliferation. After fixation, the pericytes were stained with early embryonic macrophage markers (CSF-1R, MAC1 and F4/80) and observed under epifluorescence microscopy.

Control pericytes unexpectedly acquire macrophage features as they naturally express all three macrophage markers CSF-1R (with a macrophage marker intensity of 0,786 fluorescence intensity/ μm^2), MAC1 (0,208 fluorescence intensity/ μm^2) and F4/80 (0,385 fluorescence intensity/ μm^2). Moreover, VPA exposition significantly increases MAC1 intensity in pericytes (0,429 fluorescence intensity/ μm^2) and Suni limits the macrophage intensity generated by VPA (0,175). However, no significant difference is observed with CSF-1R and F4/80 between the three groups (**Fig 44D**).

In parallel, in a collaborative work performed in the lab, chick embryos were injected at E3,5 with either PBS for the control condition or VPA for the experimental condition. Cultured pericytes from E8 meninges were then analyzed under flow cytometry using in combination the αSMA marker to distinguish the cells and each of the three macrophage markers (CSF-1R, MAC1 and F4/80). Firstly, the pericytes can express naturally all three macrophage markers (73,0% of the pericytes express CSF-1R, 44,0% of the pericytes express F4/80, and 47,0% of the pericytes express MAC1), confirming the immunocytochemistry results described previously. Secondly, VPA treatment increases the percentage of macrophage cells in CNC-derived pericytes (86,0% of the pericytes express CSF-1R, 64,0% of the pericytes express F4/80, and 76,0% of the pericytes express MAC1). The flow cytometry analysis further confirmed this increase in the percentage of cells expressing macrophage markers in the NC-pericyte cells from VPA-treated embryos (**Fig S3A**).

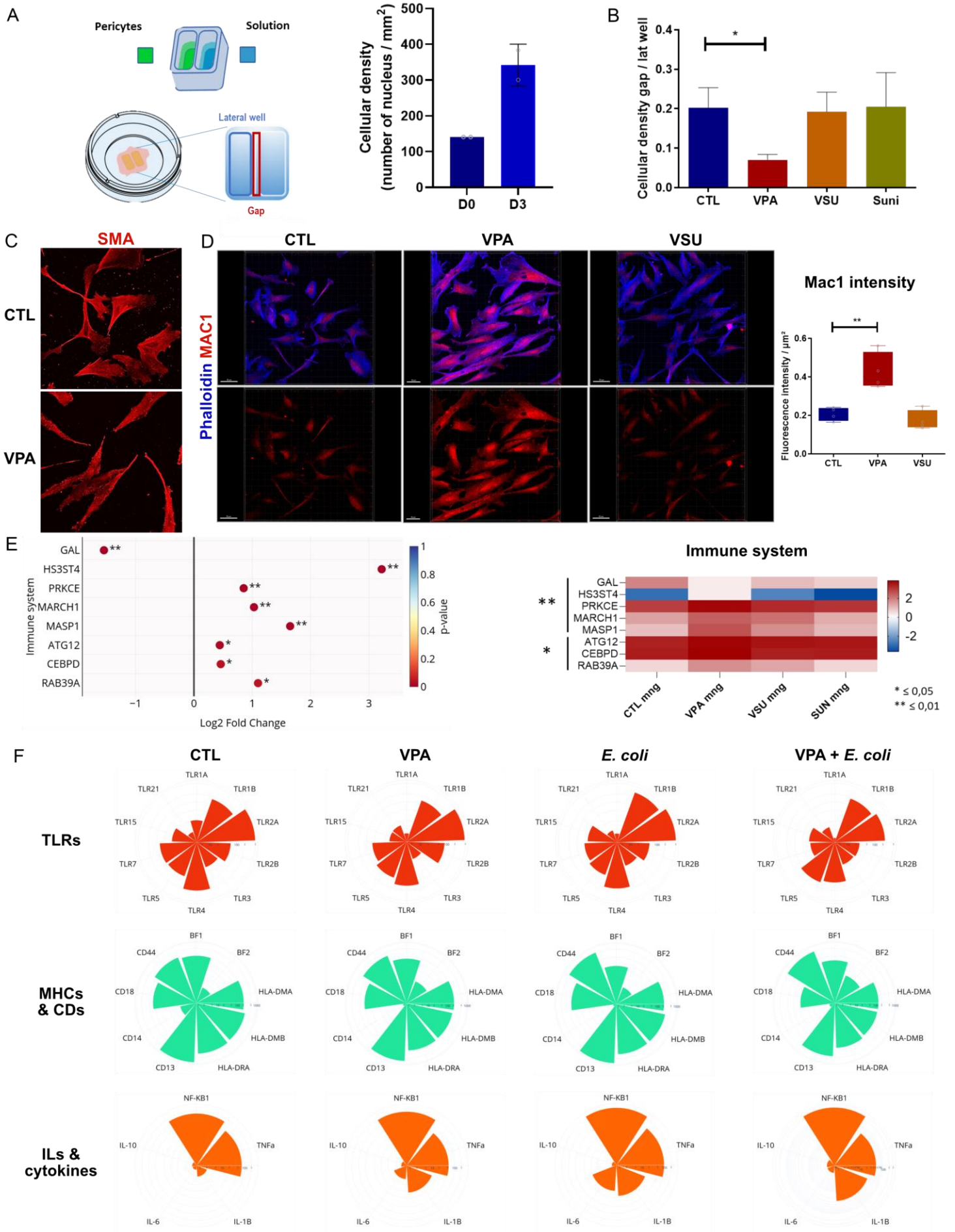


Figure 44. The CNC-derived pericytes harbor immune capacities. (A) Diagram showing *in vitro* cell culture protocol for pericyte isolation from E8 embryo meninges. Pericytes are added in the left well of a 2-well insert and the conditioned solution is placed in the right well (culture medium for control condition, VPA, VPA+Suni (VSU) or Suni alone). After two days of proliferation, the insert is removed to allow contact of the cells with the conditioned solutions (left panel). The cells migrate 24h before formal fixation. The cellular density was calculated to determine pericyte proliferation (right panel). **(B)** Pericyte migration was analyzed in each condition by calculating the cellular density in the gap compared to the cellular density in the left well. VPA significantly limits pericyte migration compared to pericytes exposed to culture medium. No significant difference is observed between the control, VSU and Suni conditions. **(C)** Pericyte cultures exposed to culture medium (CTL) or VPA solution (VPA) visualized under confocal microscopy with the α -SMA marker (in red). Control pericytes *in vitro* acquire a fibroblastic and star-shaped morphology. When in contact with VPA, pericytes become fusiform and bipolar, with long filopodia and few lamellipodia. **(D)** Pericyte cultures visualized under confocal microscopy with the phalloidin marker (in blue) to observe the pericytes and the macrophage marker MAC1 (in red). The left panels represent cell cultures in presence of culture medium, the middle panels represent cell cultures in presence of VPA and the right panels represent cell cultures in presence of VSU. MAC1 intensity was calculated with the ImageJ software by measuring the fluorescence intensity of MAC1 per μm^2 . While control pericytes spontaneously express macrophage markers, VPA increases macrophage marker intensity. VSU tends to normalize the macrophage intensity. **(E)** Bulk RNA sequencing was performed on meninges collected from E8 embryos injected with PBS for control embryos or VPA. VPA deregulates genes expression generally expressed in macrophages (*Prkce* and *Cebpd*) or implicated in phagocytosis (*Atg12* and *Rab39a*). Thus NC-derived pericytes are capable of expressing genes related to macrophages. While VSU tends to normalize the genes expression altered by VPA, Suni alone has no effect of pericytes' genes expression. **(F)** Specific transcriptomic analysis was performed using the Nanostring technology. While pericytes exposed to culture medium spontaneously express immune responsive molecules (TLRs, MHCs and CDs) and inflammatory molecules (interleukins and cytokines), noxious insults (VPA and *E. coli*) increase the expression of these protein-related genes. Error bars represent \pm SEM. ** $p \leq 0.01$; * $p \leq 0.05$; ns not significant.

3. The phagocytosis capacities of pericytes are exacerbated with VPA

To investigate whether NC-derived meningeal pericytes possess functional macrophagic activity, collaborative work in the lab assessed their ability to phagocytose *E. coli* particles using the "pHrodo™ Red *E. coli* BioParticles™ Conjugate for Phagocytosis". When phagocytosed by cells in culture, the inactivated *E. coli* particles become red fluorescent and can be visualized under UV light stimulation. The pericyte cultures were treated with the bacterial particles for up to 3h before being fixed in 4% formaldehyde. Immunocytochemistry images of NC-derived pericyte cultures showed that the cells were capable of phagocytosing bacterial particles within 1h of treatment.

Flow cytometry analysis revealed that after 1h of bacterial particle treatment, 4,6% of cells in the culture were phagocytic pericytes. Furthermore, increasing the treatment time to 3h resulted in a 3.1-fold increase in the percentage of phagocytic pericytes compared to the 1h treatment. After 3h treatment with the bacterial particles, 13,3% of pericytes in the culture were phagocytic. Flow cytometry analysis also showed that the majority of NC-derived pericytes expressing macrophage markers were capable of phagocytosing *E. coli* particles when treated for 1h. This was demonstrated by the increased percentage of phagocytic pericytes expressing CSF-1R, F4/80, or Mac1 (**Fig S3B**).

These observations indicate that meningeal pericytes derived from the NC possess both the expression of macrophage markers and functional macrophagic capabilities, such as the ability to phagocytose bacterial particles. These observations break the traditional view on the professional immune cells, so far perceived as being exclusively mesoderm-derived. In addition, our results support the demonstration that NC-derived pericytes may act as immune cells early in brain development, and cast light on the unexpected and early role of CNC cells in the immune surveillance and modulation in the CNS, before birth.

4. VPA deregulates the expression of macrophage-related genes in pericytes

To identify the gene expression profiling of perivascular cells, bulk RNA sequencing was performed on meninges (*in vivo*) collected from E8 embryos injected with the conditioned solutions (PBS for control embryos, VPA, VPA+Suni and Suni). The samples were then exported to the Novogene company for transcriptomic analysis. Among the 21362 genes identified, 384 genes were significantly up-regulated and 191 genes were significantly down-regulated by VPA compared to the control meninges (**Fig 45A**).

Bulk RNA sequencing of E8 control and VPA-treated meninges reveals significant alterations of genes generally expressed in macrophages including *Prkce* known to mediate LPS signaling in activated macrophages and *Cebpd* generating proteins important for macrophage activation and differentiation. VPA also alters genes implicated in phagocytosis. For instance, *Atg12* coding for a protein involved in autophagy and *Rab39a* coding for a protein involved in phagosome-lysosome fusion are both up-regulated with VPA compared to control meninges. Therefore, NC-derived pericytes are capable of expressing genes related to macrophages, confirming the macrophagic and phagocytosis capacities of the NC-derived pericytes. VPA disrupts the expression of these macrophagic-related genes, suggesting an increase of the pericytes' macrophagic and phagocytotic capacities in presence of noxious toxicities. In presence of Suni, the expression of macrophage-related genes is normalized compared to the control condition (**Fig 44E**).

5. Toxic or septic insults toward pericytes yield distinct immunoresponsive profiles

Specific transcriptomic analysis was performed using the Nanostring technology to decipher immune responses of pericytes on toxic (VPA) or septic (*E. coli*) insults. Gene expression is detected and quantified in each sample from a list of 40 genes (Table 6) by directly counting each barcode linked to a transcript. The Nanostring technology allows an absolute quantification of each condition without comparing the conditions between each other, therefore allowing an exact quantification of the gene profiling expressed by the meninges (*in vivo*) and the cultured pericytes (*in vitro*) collected from E8 embryos harvested from control (PBS-injected) and experimental VPA-, VPA+Suni-, Suni-, *E. coli*- and VPA+*E. coli*-treated series.

Among the list of 40 genes studied, genes specifically related to pericytes were among the most expressed (3471,44 transcripts for α SMA, 2707,08 transcripts for PDGFR β and 857,43 transcripts for CD13), confirming the correct use of the α SMA staining marker.

As predicted, control CNC-derived meninges and cultured pericytes express MHC class I molecules (respectively 205,11 and 189,38 transcripts for BF1). However, a significative collapse of MHC class I is observed when meninges and pericytes are subjected to VPA or *E. coli* particles (respectively 152,06 and 70,81 transcripts for the meninges and 75,52 and 97,88 transcripts for the cultured pericytes). This collapse corresponds to a decrease of self-antigen recognition. On the contrary, VPA and *E. coli* particles highly stimulate the expression of MHC class II genes. These two stimulators trigger non-self-antigen recognition in meninges and pericytes. Moreover, the bulk RNA sequencing reveals an alteration of the *Masp1* gene by VPA. This gene encodes a protein down-regulating the surface expression of MHC class II molecules, therefore VPA alters the expression of MHC class II molecules.

Surprisingly, CNC-derived meninges and cultured pericytes also highly express several TLRs implicated in the stimulation by various pathogens: TLR1, TLR4 and TLR5 stimulated by bacteria, TLR2 and TLR15 stimulated by bacteria and fungi, TLR3 and TLR7 stimulated by viruses, and TLR9 and TLR21 stimulated by bacteria and viruses (for review, Akira and Hemmi, 2003). Exposure to VPA *in vivo* increases transcript quantification of TLR2B (from 59,26 transcripts for control to 82,14 transcripts for VPA). VPA and VPA+*E. coli* exposures *in vivo* increase transcript quantification of TLR5 (from 70,24 transcripts for control to 83,30 transcripts for VPA and 122,19 transcripts for VPA+*E. coli*). VPA and *E. coli* particles alone or together *in vivo* increase transcript quantification of TLR21 (from 8,08 transcripts for control to 14,29 transcripts for VPA, 9,24 transcripts for *E. coli* and 12,61 transcripts for VPA+*E. coli*). *E. coli* particles alone triggers an increase of TLR2A transcripts *in vivo* (from 486,52 transcripts for control to 501,28 transcripts for *E. coli*). *E. coli* particles alone or with VPA triggers an increase of TLR1B transcripts (from 162,71 transcripts for control to 298,26 transcripts for *E. coli* and 170,24 transcripts for VPA+*E. coli*) and TLR 15 transcripts (from 26,52 transcripts for control to 39,49 transcripts for *E. coli* and 28,81 transcripts for VPA+*E. coli*) *in vivo*. *In vitro*, exposure to VPA increases transcript quantification of TLR5 (from 45,89 transcripts for control to 54,9 transcripts for VPA) and TLR21 (from 16,71 transcripts for control to 25,08 transcripts for VPA). TLR3 is stimulated by VPA and VPA+*E. coli* (from 9,79 transcripts for control to 13,30 transcripts for VPA and 10,57 transcripts for VPA+*E. coli*). *E. coli* particles alone or with VPA triggers an increase of TLR15 transcripts (from 75,94 transcripts for control to 351,49 transcripts for *E. coli* and 500,39 transcripts for VPA+*E. coli*). Lastly, TLR7 is stimulated by VPA+*E. coli* (from 65,53 transcripts for control to 91,24 transcripts for VPA+*E. coli*).

CNC-derived meninges and cultured pericytes naturally express various ILs and cytokines. *In vivo* exposure to VPA and/or *E. coli* particles stimulates these ILs such as IL-1B (from 2,21 transcripts for control to 11,45 transcripts for VPA, 16,82

transcripts for *E. coli* and 27,30 transcripts for VPA+*E. coli*), IL-6 (from 1,11 transcripts for control to 2,87 transcripts for VPA, 10,01 transcripts for *E. coli* and 1,52 transcripts for VPA+*E. coli*) and IL-10 (from 1,11 transcripts for control to 1,23 transcripts for VPA, 1,13 transcripts for *E. coli* and 1,52 transcripts for VPA+*E. coli*). *In vitro* exposure to VPA and/or *E. coli* particles also stimulates the interleukins: IL-1B (from 7,56 transcripts for control to 14,12 transcripts for VPA, 1207,92 transcripts for *E. coli* and 1536,72 transcripts for VPA+*E. coli*), IL-6 (from 1,11 transcripts for control to 643,57 transcripts for *E. coli* and 639,66 transcripts for VPA+*E. coli*) and IL-10 (from 1 transcript for control to 1,783 transcripts for VPA, 7,43 transcripts for *E. coli* and 6,72 transcripts for VPA+*E. coli*).

In vivo, VPA and/or *E. coli* particles also stimulate various cytokines such as TNF α (from 72,93 transcripts for control to 95,04 transcripts for *E. coli*), NF- κ B (from 147,65 transcripts for control to 179,05 transcripts for VPA, 256,73 transcripts for *E. coli* and 273,93 transcripts for VPA+*E. coli*), and PDGF β (from 253,38 transcripts for control to 301,33 transcripts for VPA, 315,33 transcripts for *E. coli* and 278,0 transcripts for VPA+*E. coli*). *In vitro* exposure to VPA and/or *E. coli* particles stimulates NF- κ B (from 372,23 transcripts for control to 546,73 transcripts for *E. coli* and 567,27 transcripts for VPA+*E. coli*) and PDGF β (from 151,24 transcripts for control to 181,39 transcripts for VPA, 213,13 transcripts for *E. coli* and 274,03 transcripts for VPA+*E. coli*). However, TNF α is neither stimulated by VPA nor by *E. coli* particles *in vitro* (**Fig 44F**).

Overall, these results suggest that pericytes could participate in the immune defence as immune responsive cells: pathogen recognition and professional antigen-presenting cells. Furthermore, VPA, *E. coli* and VPA+*E. coli* can change this immune profile and potentially lead to neurodevelopmental disorders.

V. The cephalic neural crest-derived pericytes are an active component of the neurovascular unit

This neurovascular unit (NVU) is composed of neurons, neural supporting cells (astrocytes, microglia, oligodendrocytes), and vascular cells (cerebral endothelial cells, pericytes, smooth muscle cells) (Adriani et al., 2017; Neuwelt et al., 2011). In the forebrain, the CNC-derived pericytes are closely linked to the synaptic cleft formed by the neurons as they are an essential component of the NVU (Fig 45B). To our surprise, when analyzing the bulk RNA sequencing performed on NC-derived meninges and cultured pericytes, among the significant genes deregulated by VPA, numerous genes coded for the development, maturation and physiological functions of neurons (Fig 45C) and synapses (Fig 45D).

1. VPA impairs the expression of genes involved in neural control of vasomotricity

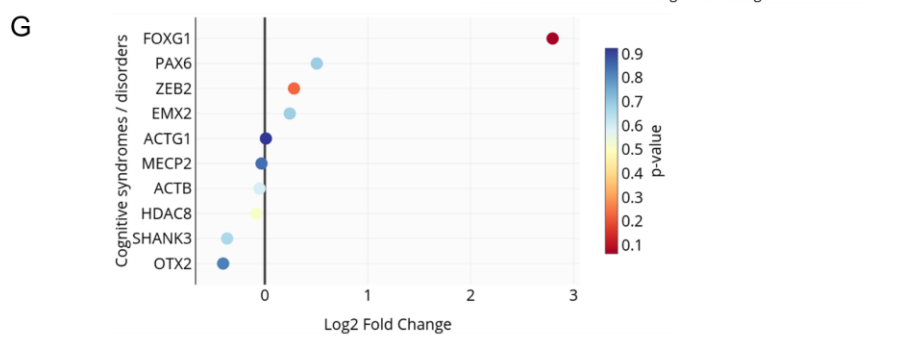
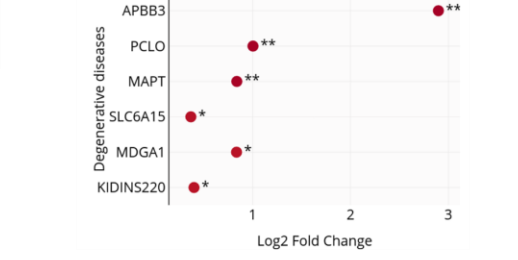
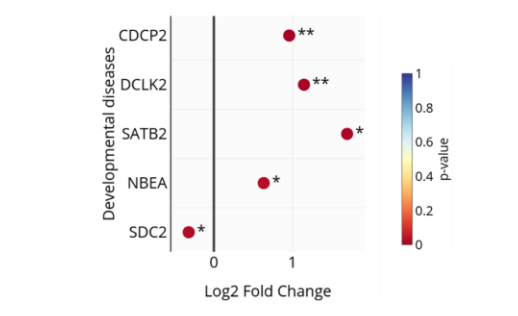
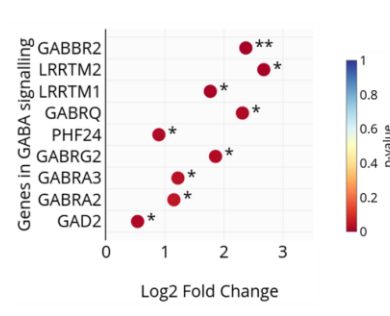
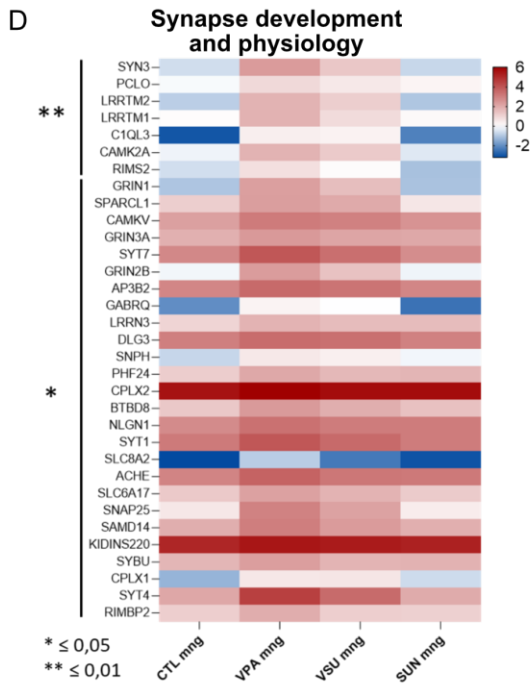
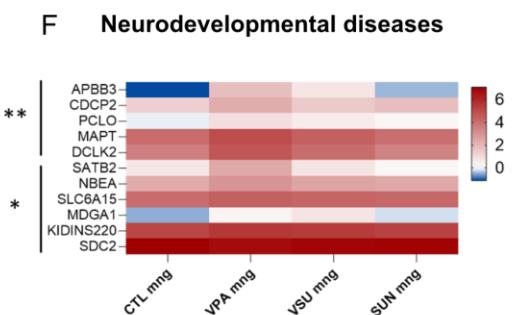
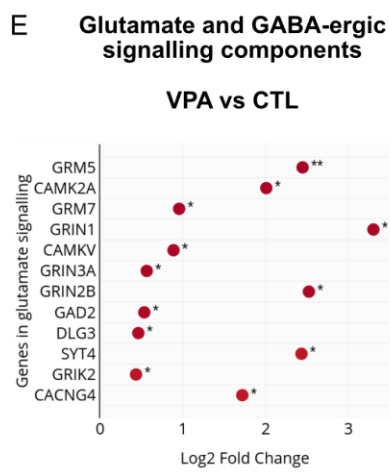
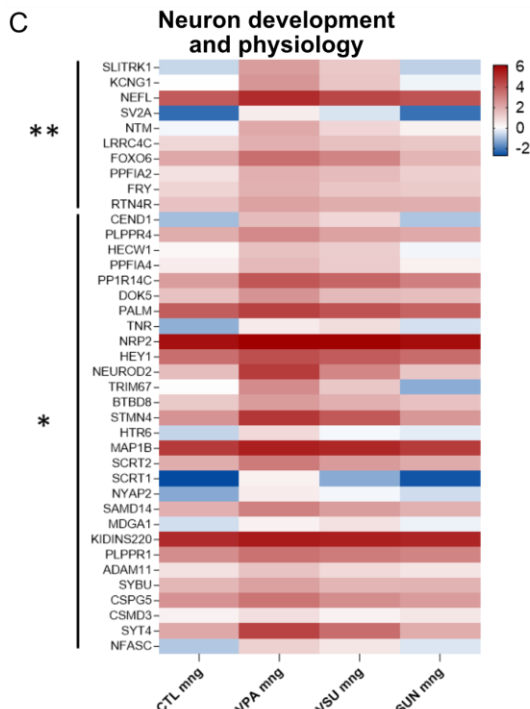
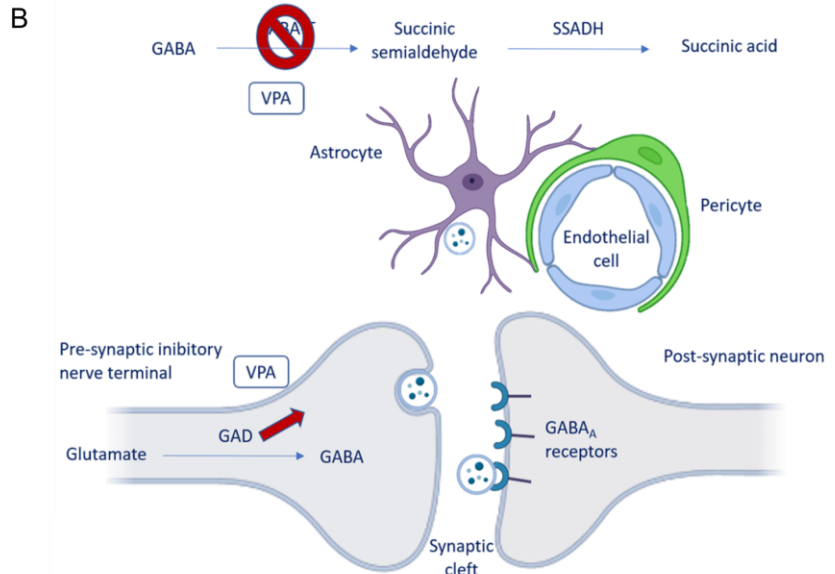
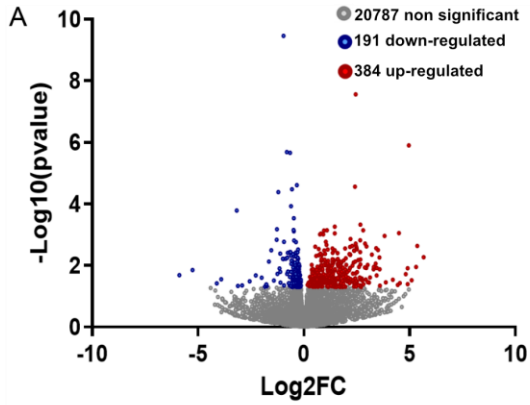
Bulk RNA sequencing shows that VPA significantly affects various genes implicated in the development of neurons via their neurites' outgrowth such as *Slitrk1* and *Ntm*, or in the regulation of neurons including *Scrt2* and *Plppr1* (Fig 45C). Neurons determine the contractility ability of pericytes, due to their smooth muscle actin, via vasodilatation and vasoconstriction signals and indirectly through the release of vasoactive substances from the astrocytes (Simard et al., 2003; Zonta et al., 2003). VPA significantly alters genes implicated in the development of vascular associated smooth muscle cells such as an up-regulation of *Cnn1* and *Gata5*. Similarly, VPA up-regulates genes implicated in the regulation or contraction of smooth muscle cells such as *Kcng1* and *Ndr4*.

2. VPA targets glutamatergic and GABA-ergic signaling

Neurons communicate with astrocytes through the release of glutamate in the synapses, increasing calcium concentration in astrocytes (for review, Sweeney et al., 2016; Zonta et al., 2003). VPA affects numerous genes implicated in the synaptic development such as *Sparcl1* and *Lrrn3* and in the synapse vesicle trafficking including *Syn3*, *Pclo* and *Rims2*. The glutamate signaling is also impacted by VPA up-regulating various genes. For instance, genes giving rise to subunits of the N-methyl-D-aspartate (NMDA), a glutamate receptor, are impacted such as *Grin1*, *Grin3a* and *Grin2b*, as well as metabotropic glutamate receptors including *Grm5* and *Grm7* (Fig 45E).

In 2014, Tyzio and colleagues observed an enhanced glutamatergic activity in hippocampal neurons of VPA-treated rats (Tyzio et al., 2014). Moreover, in 2019, Chiesa and colleagues demonstrated through development an enhanced and persistent glutamatergic activity in CA3 pyramidal neurons of *Shank3*-mutant mice, commonly used models of ASD (Chiesa et al., 2019). Thus, these results confirm the deregulation of VPA on the glutamatergic signaling observed with the RNA sequencing.

As described previously (cf. introduction, XI. 1. VPA, a widely used anticonvulsant), GAD2 catalyses the conversion of glutamate in GABA in pre-synaptic neurons (Kukino and Deguchi, 1977). In the adult brain, GABA is the principal inhibitory neurotransmitter. However, during fetal and post-natal periods, GABA has a depolarizing action and provides the major excitatory synaptic input in immature neurons. GABA's excitatory action is maintained stable by a high concentration of intracellular chloride ions (Cl^-). This excitatory-to-inhibitory shift is triggered shortly before delivery by oxytocin, an essential maternal hormone for labor, by abruptly reducing intracellular Cl^- to exert a



* ≤ 0,05
** ≤ 0,01

Figure 45. The CNC-derived pericytes are an active component of the neurovascular unit. (A) Bulk RNA sequencing was performed on meninges collected from E8 embryos injected with PBS for control embryos or VPA. Out of the 21362 genes identified, 191 genes were down-regulated and 384 genes were up-regulated by VPA compared to control meninges. **(B)** Schematic representation of the neurovascular unit (NVU) observed in late development and after birth. The pre-synaptic neuron transforms glutamate into GABA via the GAD2 enzyme. Both glutamate and GABA are then released in the synaptic cleft and are recaptured by astrocytes. The glutamate entry in astrocytes causes an increase of calcium concentration leading to a chain reaction resulting in the release of the vasoactive substances. These peptides cause contraction of muscular cells and pericytes. Bulk RNA sequencing reveals the deregulation by VPA of several genes implicated in **(C)** neuron and **(D)** synapse developments and physiologies, in **(E)** glutamate and GABA-ergic signaling components. **(F)** The impairment of the NVU components by VPA leads to a deregulation of genes known to have a role in neurodevelopment diseases or neurodegenerative diseases. **(G)** VPA also deregulates genes implicated in diseases with neurocristopathy manifestations taking place during development, before cognitive impairment at birth (Table 1). GAD: glutamic acid decarboxylase, GABA-T: GABA transaminase, SSADH: succinate-semialdehyde dehydrogenase. ** $p \leq 0.01$; * $p \leq 0.05$.

neuroprotective action on newborns (Tyzio et al., 2006; Tyzio et al., 2014). In human and animal models of autism triggered by VPA, the excitatory-to-inhibitory shift is abolished giving rise to an imbalance between excitation and inhibition. For instance, in VPA-induced rat models, increased excitatory GABA is observed in hippocampal neurons. Thus, the alteration of GABA signaling is commonly considered a cause of ASD (Chiesa et al., 2019; Tyzio et al., 2014).

To our surprise, the bulk RNA sequencing reveals the up-regulation of *Gad2* with VPA. It is known that VPA enhances GAD2 (Kukino and Deguchi, 1977), which suggested a positive effect on GABA production. Moreover, our transcriptomic analyses reveal an up-regulation of most genes encoding GABA_A receptor's (GABA_AR) subunits, *Gabra2*, *Gabra3*, *Gabbr2*, *Gabrg2* and *Gabrq* (Fig 45E). These results confirm Tyzio and colleagues' observations of elevated GABA_AR in fetal and early post-natal periods (Tyzio et al., 2014). Thus, a deregulation of NC-derived meninges, due to VPA, could lead to autistic characteristics by interfering in the glutamatergic and GABA-ergic signaling of the NVU.

3. VPA affects gene expression of ion channels regulating vasomotricity

It is known that glutamate entry in astrocytes causes an increase of calcium concentration leading to a chain reaction resulting in the release of the vasoactive substances. These peptides cause contraction of muscular cells and pericytes (for reviews, Muoio et al., 2014; Sweeney et al., 2016; Zonta et al., 2003).

Many ions have a concentration gradient across the membrane, including potassium ions (K⁺), which is at a high concentration inside and a low concentration outside the membrane. Sodium (Na⁺) and Cl⁻ ions are at high concentrations in the extracellular region, and low concentrations in the intracellular regions. The opening of ion transporters at the cellular

membrane actively pushes ions such as K^+ and establish concentration gradients across the membrane. In parallel, ion channels allow ions including Na^+ and Cl^- to passively move across the membrane, reducing its concentration gradient. This membrane permeability leads to the establishment of a voltage, causing the membrane potential. This latter is found in electrically excitable cells such as neurons, skeletal or cardiac muscle cells for generating the propagation of action potentials. Nerves generate depolarizing action potentials to transmit signals along their axons, while skeletal or cardiac muscle cells generate their action potentials, coupled with elevated intracellular calcium ions (Ca^{2+}), in order to contract the muscles (Neher and Sakmann, 1976; Hodgkin and Huxley, 1952; for review, Kadir et al., 2018).

In our study, we show that VPA tends to increase Ca^{2+} /calmodulin-dependent protein kinase genes expression (*Camk2a* and *CamkV*). CAMKs are activated by an increase in the concentration of intracellular Ca^{2+} and calmodulin. When activated, the enzymes are involved in the phosphorylation of transcription factors and therefore, in the regulation of expression of responding genes.

In parallel to the contraction of pericytes due to vasoactive substances, an opening of K^+ channels trigger an influx of K^+ in the intracellular compartment of myocytes, leading to hyperpolarization and vasodilatation (for review, Muoio et al., 2014). VPA alters a group of genes implicated in voltage-gated channels including *Kcns1* and *Kcng1* and in the generation of neurotransmission such as *Sv2a* and *Clcn1*. VPA also up-regulates members of the solute carrier genes (SLC) implicated in the regulation of intracellular ion concentrations. For instance, the *Slc6a17* gene codes for a SLC implicated in the pre-synaptic recapture of neurotransmitters, the *Slc8a2* gene codes for a SLC implicated in the post-synaptic regulation of Ca^{2+} concentration, and the *Slc6a15* gene generates a protein which plays a role in the neuronal transport of amino acids.

Overall, the VPA-induced deregulation of several genes implicated in the generation of membrane potential could emphasize the role of pericytes as electrically excitable cells, capable of conducting the action potential along its membrane. Moreover, due to the proximity of VPA-treated pericytes with the LV and the CSF as they invade the VZ of the brain, a deregulation of transporters and ion channels could lead to an increase of ions or proteins in the CSF. Notably, VPA+Suni tempers the alteration generated by VPA on most genes' expression and Suni does not affect the gene expression profiling.

4. Divergent neurovascular unit in embryos versus adults

As mentioned previously, the main components of the NVU include neurons, astrocytes and pericytes among other cells. However, this NVU composition has precisely been described in the postnatal and adult brains. In fact, in the developing brain of several species, the NVU probably functions differently as the astrocytes appear during late development. For instance, in the developing cortex of mice, from E16 onward, radial glia first give rise to glioblasts which undergo several rounds of division in the SVZ and the cortical plate, resulting in clusters of immature astrocytes. These radial glia also detach from the VZ and give rise to protoplasmic and fibrous astrocytes in the grey and white matters of the cortex respectively ([for review, Akdemir et al., 2020](#)). In the developing telencephalon of rhesus monkeys, the first radial glial cells are first recognized from E48 by their bipolar shape and elongated radial fiber, which terminates with characteristic endfeet on the walls of blood vessels. After E60, some radial glia detach from the VZ and display a range of transitional shapes leading to either fibrous or protoplasmic astrocytes ([Schmechel and Rakic, 1979](#)). During the early postnatal period, after E21 for mice and E165 for rhesus monkeys, differentiated astrocytes in the outer cortical layer undergo symmetrical division and generate daughter astrocytes that exhibit astrocytic morphology and function ([for review, Akdemir et](#)

al., 2020).

Within the chick embryo model, while small clusters of glial precursors were observed from E10 onward in the central canal (Alfei et al., 1999), early stages of gliogenesis begin at E11 in the brain. Domowicz and colleagues observed the presence of glial precursors from E11 onward using the earliest markers: the glutamate aspartate transporter (GLAST), the brain lipid binding protein (BLBP) and Nestin (Domowicz et al., 2008). From E15, several markers reveal the presence of astrocytes: CD44, the glial fibrillary acidic protein (GFAP) and the glutamine synthetase (GLUL) (Alfei et al., 1999; Domowicz et al., 2008; Domowicz et al., 2011). As stated above (*cf. results, V. 1. Pericytes acquire high migration capacity in vitro*), cell cultures demonstrated nearly 100% preservation of α SMA-positive cells. To further corroborate this phenotype, NG2 and PDGFR β markers, conventionally employed to highlight pericytes, were also used to reveal nearly 100% of the pericytes in meningeal cell cultures. Thus, meningeal pericytes appear early in development, as early as in E8 chick embryos, and before the maturation of astrocytes. Therefore, the transcriptomic analyses of neuronal and synaptic development, glutamatergic and GABA-ergic signaling, and membrane potentiality are not attributed to astrocytes but to pericytes during embryonic development. Considering the late arrival of mature astrocytes in the embryonic development, the early NC-derived pericytes could have a larger impact in the NVU and more specifically in their connection with cortical neurons. These observations emphasize the possible leading role played by pericytes in embryonic neurogenesis.

5. VPA impacts neurodevelopmental genes

The neurovascular interaction is essential for normal neurodevelopment as alterations of the vascular network, due to VPA, could impact the regulation of neurodevelopmental genes, leading to neurodevelopmental diseases. For

instance, the bulk RNA sequencing reveals the up-regulation of *Cdcp2* and *Dclk2* known to trigger epilepsy. *Dclk2* also generates lissencephaly. Besides, a deregulation of *Nbea* and *Sdc2* leads to ASD (**Fig 45F**).

In parallel, VPA also deregulates genes implicated in diseases with neurocristopathy manifestations taking place during development, before cognitive impairment at birth (**Table 1**). Indeed, among these genes, VPA deregulates the *Foxg1* gene implicated in atypical RETT syndrome (Aguiar et al., 2014; Papa et al., 2008), *Otx2* implicated in septo-optic dysplasia (Gregory et al., 2021), *Emx2* generating schizencephaly (Brunelli et al., 1996), *Pax6* implicated in Gillespie syndrome (Glaser et al., 1994), *Mecp2* generating RETT syndrome (Jeffrey L. Neul et al., 2010; Kyle et al., 2018), *Shank3* implicated in ASD (Mei et al., 2016), *Zeb2* generating Mowat-Wilson syndrome (Epifanova et al., 2019; Garavelli and Mainardi, 2007), *Hdac8* giving rise to Wilson-Turner syndrome (Harakalova et al., 2012; Wilson and Sullivan, 1994) and either *Actb* or *Actg1* giving rise to Baraitser-Winter syndrome (Rivière et al., 2013; Zhang et al., 2020) (**Fig 45G**).

6. VPA enhances neurodegenerative targets

The hypothetic role of NC-derived pericytes in the cephalic CNS is reinforced by previous works linking the degeneration of pericytes and AD. Indeed, the loss of pericytes due to PDGFR β signaling disruption leads to a decrease of soluble amyloid β -peptide (A β) clearance in the CSF and therefore increases the level of insoluble A β in the brain. Both pericyte loss and insoluble A β increase result in the early development of AD's neuropathology including A β plaques (Sagare et al., 2013; Winkler et al., 2014). Furthermore, from the age of 9 months, pericyte driven vascular injury and A β elevation simultaneously lead to developed tau pathology including neuronal accumulation of hyperphosphorylated tau species, caspase-cleaved tau and tau aggregates (Sagare et al., 2013).

Interestingly, the bulk RNA sequencing underlines the effect of VPA on targets related to AD. For instance, VPA up-regulates the *Apbb3* gene which protein binds to the intracellular domain of AD's amyloid-beta precursor protein (APP) in order to modulate its internalization in the cells. The *Mapt* gene is also up-regulated by VPA. It encodes for the microtubule-associated protein tau (MAPT) and its mutation leads to several neurodegenerative disorders such as AD. Thus, these results emphasize the role of the NC-derived pericytes and meninges in neurodegenerative diseases (**Fig 45F**).

VI. The cephalic neural crest-derived pericytes can promote DNA shedding and generate ETosis to form DNA traps

As mentioned previously (IX.1. *VPA, a widely used anticonvulsant*), VPA generates epigenetic modifications such as histone hyperacetylation by directly inhibiting class I and II HDACs ([Tung and Winn, 2010](#)). Thus, to confirm the VPA effect on DNA modification, specific transcriptomic analyses were performed using the Nanostring technology. Indeed, the transcriptomic analyses demonstrated an increase of *Hdacs* transcription when meninges are exposed to VPA *in vivo*. Transcription of *Hdac1* increases from 959,079 transcripts for control meninges to 1169,441 transcripts for VPA-treated meninges. *Hdac2* increases from 8677,017 to 8820,285 transcripts with VPA, *Hdac3* from 311,938 to 319,733 transcripts and *Hdac8* from 642,659 to 711,432 transcripts (**Fig 46A**).

1. Chromatin decondensation from noxious insults

One specific objective of this project is to understand how CNC cells and meningeal pericytes can mediate their immunosurveillance of the developing embryonic brain. While characterizing the phenotype of these cells, we became

incidentally aware of the propensity of these perivascular CNC cells to decondense their nuclear material and shed extracellular DNA. This process, called neutrophil extracellular trap (NET), was first described for neutrophils and blood circulating cells as a defence mechanism, capable of stopping and trapping circulating pathogens (Brinkmann et al., 2004). However, the process of shedding DNA extracellular traps (or ETosis) characterized in blood circulating cells has never been described in mesenchymal cells, assuming structural function, nor in embryos.

To analyze the capacity of pericytes to decondense their DNA and generate ETosis, control cultured pericytes were put in contact with either culture medium or VPA solution three days after proliferating in a compartmented well of an insert for 3 days. After 24h, the cells were fixed and analyzed for their DNA decondensation process. The Sytox™ green nucleic acid stain marker was used to observe nuclear, cytoplasmic and extracellular DNA. Each cell was categorized in three distinct grades of DNA condensation: 1) a cell containing condensed DNA in the nucleus, 2) a cell containing decondensed DNA present in the nucleus and the cytoplasm, and 3) a cell presenting an ETosis phenotype (Fig 46B).

While a majority of pericytes have condensed DNA in their nucleus when in contact with culture medium (0,25 cells/ μm^2 , corresponding to 75,53%), certain pericytes are capable of spontaneously decondensing their DNA in the cytoplasm (0,08 cells/ μm^2 , corresponding to 24,47%). However, no ETosis process is observed in these cell cultures. On the contrary, in presence of VPA, 0,23 cells/ μm^2 , corresponding to 100% of the cells, pericytes decondense their DNA in the cytoplasm. Besides, 0,02 cells/ μm^2 are capable of generating ETosis in the extracellular compartment. Thus, VPA tends to increase DNA decondensation and ETosis process in pericytes (Fig 46C). Moreover, with pericytes undergoing culture medium, the DNA condensation is positively correlated to its density (the

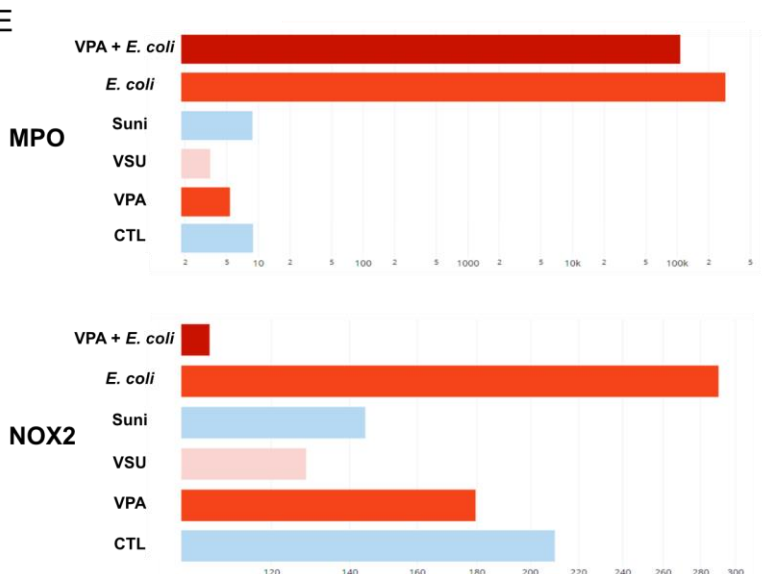
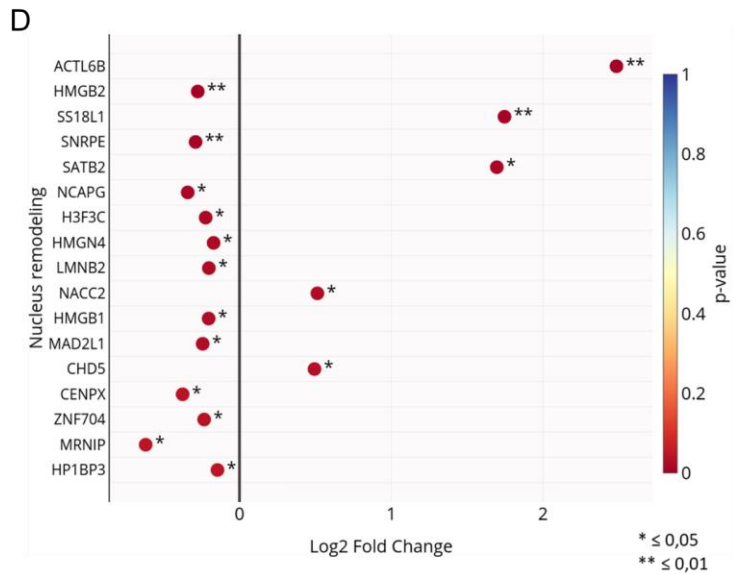
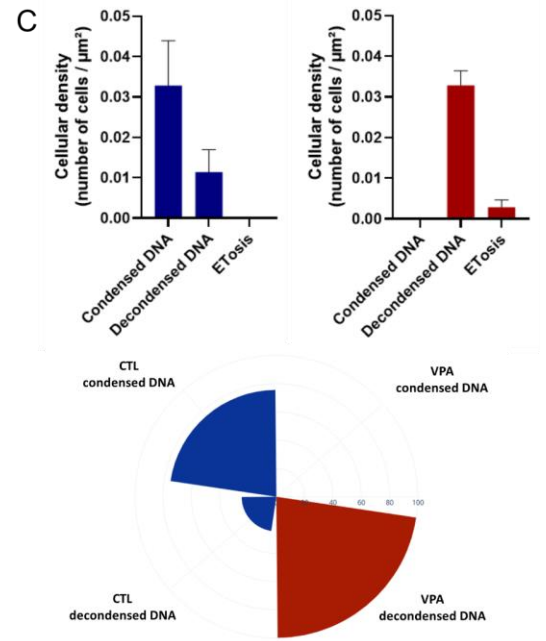
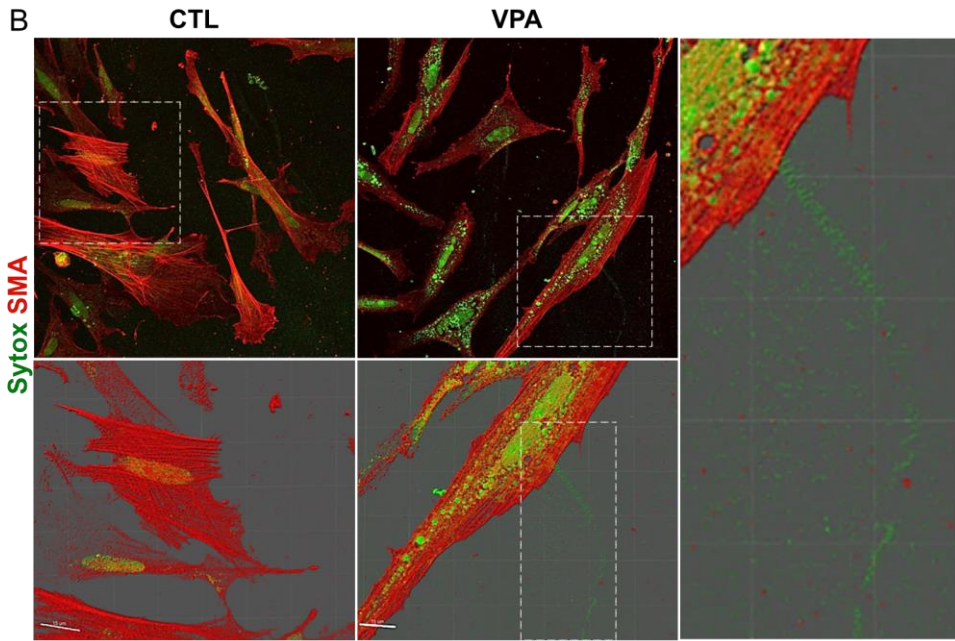
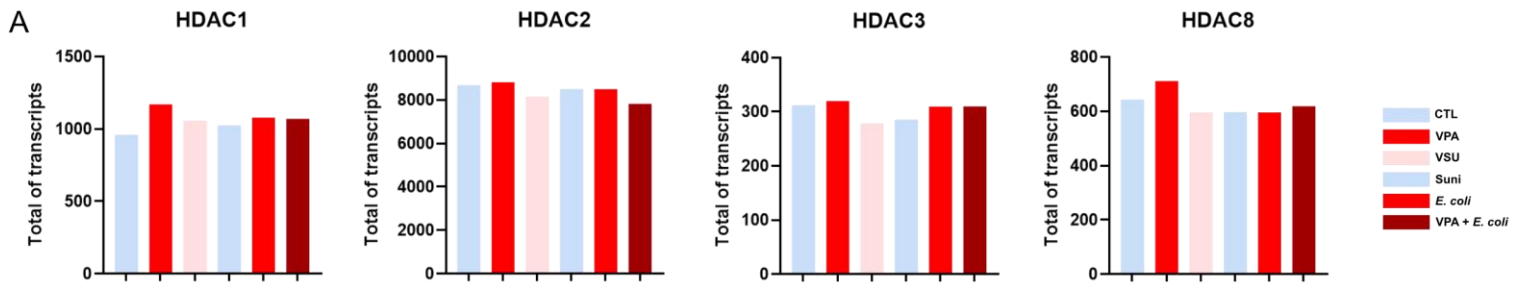


Figure 46. The CNC-derived pericytes promote DNA shedding and generate ETosis to form DNA traps. (A) Specific transcriptomic analysis was performed using the Nanostring technology. An increase of *Hdacs* transcription is observed when meninges are exposed to VPA *in vivo*. **(B)** Pericyte cultures visualized under confocal microscopy with the Sytox™ marker (in green) to observe the DNA and the α -SMA marker (in red) to observe the pericytes. The left panels represent cell cultures in presence of culture medium. The middle and right panels represent cell cultures in presence of VPA. The lower and right images were generated with the Imaris Viewer software 9.7.2. The pericytes in presence of culture medium harbour condensed DNA in their nucleus. The VPA-exposed pericytes contain decondensed DNA in their cytoplasm and generate ETosis (right panel) to form DNA traps. **(C)** Each cell is categorized in three distinct grades of DNA condensation: 1) a cell containing condensed DNA in the nucleus, 2) a cell containing decondensed DNA present in the nucleus and the cytoplasm, and 3) a cell presenting an ETosis phenotype. The cells exposed to culture medium contain a majority of condensed DNA in their nucleus (0,25 cells/ μm^2 , corresponding to 75,53% of the cells), certain pericytes are capable of spontaneously decondensing their DNA in the cytoplasm (0,08 cells/ μm^2 , corresponding to 24,47%). However, no ETosis process is observed in these cell cultures. On the contrary, in presence of VPA, 0,23 cells/ μm^2 , corresponding to 100% of the cells, pericytes decondense their DNA in the cytoplasm. Besides, 0,02 cells/ μm^2 are capable of generating ETosis in the extracellular compartment. **(D)** Bulk RNA sequencing was performed on meninges collected from E8 embryos injected with PBS for control embryos or VPA. VPA deregulates several genes implicated in chromatin remodelling (*Actl6b*, *Ss18l1* and *Satb2*), DNA organization in the nucleus (*Hmgb2*, *Hmgb1* and *Cenpx*), or nuclear membrane organization (*Lmnb4*). **(E)** The specific transcriptomic analysis shows that, *in vivo*, an exposure to *E. coli* increases significantly *Mpo* and *Nox2* transcriptions, two specific markers of ETosis. Error bars represent \pm SEM. ** $p \leq 0.01$; * $p \leq 0.05$.

coefficient of determination R^2 is 0,7687). DNA decondensation is also positively correlated to the cellular density (R^2 is 0,2987). However, with increase of pericyte density, VPA tends to increase DNA decondensation (R^2 is 0,6285). ETosis process is negatively correlated to cellular density in presence of VPA (R^2 is 0,3111).

2. Chromatin decondensation from septic insults

Simultaneously, a collaborative work was performed in the lab to assess DNA decondensation when pericytes are triggered by septic insults. Immunocytochemistry was used to analyze NC-derived pericyte cultures, using DNA markers such as DAPI and Sytox™ green to detect DNA decondensation.

In control condition, 12,0% of the cells in the culture exhibited nuclear DNA decondensation, indicating that NC-derived pericytes are indeed capable of generating ETosis. Furthermore, a significant increase, with 19,3% of cells showing this phenotype, is observed in the cells exhibiting nuclear DNA decondensation following an 1h treatment with E. coli particles treatment (**Fig S5A**).

3. VPA interferes in genes coding for chromatin remodeling proteins

The bulk RNA sequencing emphasizes the effect of VPA on chromatin remodeling. Compared to control meninges, VPA up-regulates various genes whose proteins are known to remodel the chromatin such as *Actl6b*, *Ss18l1* and *Satb2*, or more specifically known to remodel and organize DNA in the nucleus including *Hmgb2*, *Hmgb1* and *Cenpx*. Furthermore, VPA alter genes responsible for the organization of the nuclear membrane (*Lmnb4*) and the regulation of the nucleus size (*Hp1bp3*), suggesting an overall disruption of the nucleus and its components (**Fig 46D**).

4. Noxious insults affect ETosis effectors, PAD4, Cit-H4 and Cit-H3

In eukaryotic cells, genomic DNA exists in the form of chromatin through association with histone proteins, which consist of four core histone (H2A, H2B, H3, and H4) families and one linker histone (H1) family (for review, Zhou and Bai, 2019). H3 and H4 can undergo a post-translational modification called citrullination, which involves the conversion of an arginine into the amino acid citrulline by a peptidyl arginine deiminase, type IV, also known as PAD4. PAD4 converts arginine 2, 8 and 17 of histone H3 and arginine 3 of histone H4 to citrulline. This modification leads to Cit-H3 and Cit-H4, decompacting and shedding the DNA out of the nucleus (Nakashima et al., 2002; Wang et al., 2009). We decided to further investigate this mechanism in depth in order to find out how this process could account for neurodevelopmental defects observed *in vivo*.

Embryos were injected at 21 – 22 HH with either PBS for control models and VPA for experimental models, and mass cultures were performed on pericytes cultivated by harvesting E8 meninges. After 3 days of proliferation, flow cytometry analyses of Sytox™ green and Cit-H3 co-expression were performed to evidence DNA traps. While control pericytes spontaneously release DNA traps, VPA-treated pericytes increase the percentage of ETosis process by 1.2 folds.

To analyze the capacity of pericytes to decondense their DNA and generate ETosis in presence of a septic exposure, *E. coli* particles were added 24h before harvesting E8 control embryos. Flow cytometry analyses of Sytox™ green and Cit-H3 co-expression show that 5,4% of the cultured pericytes release DNA traps spontaneously. The presence of *E. coli* particles significantly increases DNA traps generated by the pericytes by 1,3 (7,3%). TECAN reader analyses were also performed to assess the presence of free Cit-H3/DNA complexes in the supernatants of pericytes to further investigate the DNA traps released by NC-derived pericytes. An increase of the free Cit-H3/DNA complexes by 1,6 was

observed in the supernatants from *E. coli*-treated cultures compared to control cultures (**Fig S5B**).

Further analyses were performed by associating *E. coli* particles with VPA-treated embryos to trigger a double exposure to septic (*E. coli*) and aseptic (VPA) toxicities. The percentage of VPA-treated pericytes presenting DNA decondensation in response to *E. coli* particles increases by 1,7 compared to control pericytes. Furthermore, flow cytometry analyses show an increase by 1,4 of VPA-treated pericytes co-expressing SytoxTM green and Cit-H3 after 1h of *in vitro* treatment to *E. coli* compared to control pericytes. Lastly, consistent with these findings, the conditioned media of pericytes from VPA-treated embryos contained significantly more Cit-H3/DNA complexes than that from CTL (an increase by 1,4) (**Fig S5C**).

5. VPA deregulates the expression of genes coding for ETosis markers

The bulk RNA sequencing performed on E8 embryos' meninges reinforces the effect of VPA on histones. Indeed, VPA alters a group of genes implicated in the transcription of histones such as *H3f3c* or *Snrpe*. The protein encoded by *H3f3c* is a replication-independent histone that is a member of the histone H3 family. *Snrpe* encode for a protein that plays a role in the 3' end processing of histone transcripts. VPA also affect the *Nacc2* gene whose encoded protein enables HDAC binding activity.

Among the 40 genes selected for the Nanostring technology analysis, two genes give rise to specific markers of NETs: MPO linked to extracellular DNA in case of ETosis (Zuo et al., 2020) and NADPH oxidase (NOX) 2. NETs can be divided in NOX2-dependent and NOX2-independent stimuli. In certain cases, NET-inducing stimuli requires the formation of ROS by NOX2 which is therefore considered a specific marker of NETs (Dömer et al., 2021). *In vivo*, an exposure to *E. coli* increases

significantly *MPO* transcription (from 8,839 transcripts for control meninges to 21,351 transcripts with *E. coli*) and *Nox2* transcription (from 209,937 transcripts for control meninges to 290,029 transcripts with *E. coli*) (**Fig 46E**).

Overall, these results suggest that NC-derived pericytes can spontaneously release DNA traps and that septic (*E. coli*) or aseptic toxicities (VPA) during development may trigger higher DNA decondensation and ETosis process, indicating the potential role of NC-derived pericytes in the immune response.

VII. DNA shedding and ETosis occur *in vivo*

1. Pericytes disperse DNA in the parenchyma of VPA-treated brains

E8 whole-mount isolated brains from control, VPA or VPA+Suni-treated embryos at E3,5 were observed under Light sheet microscopy for 3D rendering, using the 3DISCO technique for transparency, The Sytox™ marker was used to observe the extracellular DNA (in green) and the α SMA marker was used to observe the vascularization (in red). While pericytes from control brains spontaneously shed extracellular DNA, VPA increases the ETosis process. However, Suni tends to limit the DNA found extracellularly (**Fig 47A**). Overall, these results confirm the DNA shedding and ETosis process observed in pericyte cultures *in vitro*.

2. Pericytes may disperse DNA and proteins in the CSF of the LV

When observing whole-mount isolated brains from 32 - 34 HH embryos under Light sheet microscopy for 3D rendering, shedding of DNA and Cit-H4 were found linked to the α SMA marker in the LV of the brain. Thus, the DNA extracellular shedding and proteins linked to the ETosis process, found in pericyte cultures, were also observed *in vivo* (**Fig 47B**). Could pericytes therefore disperse extracellular DNA in the CSF of LV through an ETosis process as a defensive

mechanism against noxious insults?

CNC-derived meninges and pericytes are capable of synthesizing various inflammation signals as shown previously. When chick embryos are administrated with VPA, hypervascularization is observed in the brain's parenchyma and specifically in the SVZ and VZ lining the LV, in contact with the CSF. Therefore, pericytes found at the border of the LV could excrete these inflammation molecules in the CSF. Preliminary data on proteomic analyses were performed on the CSF of embryos from several embryonic stages (E8, E10, E12 and E15) for the conditioned solutions injected at E3,5 (control, VPA, VPA+Suni and Suni).

Enzyme-linked immunosorbent assay (ELISA) was performed on all four embryonic stages and for the four conditions. The absorbance detects the presence of several inflammation signals in the CSF such as IL-1 and TNF α . However, while the technique shows biological variations between the series in absorbance, the sensitivity was too low to infer protein concentration.

Mass spectrometry was also performed on CSF collected from E10 embryos. Surprisingly, numerous proteins usually found in the nucleus were present in the CSF. For instance, LAMIN-B1 and LAMIN-B2 initially located at the nuclear envelope, chromatin target of PRMT1 and nuclear factor 1 A-type. Interestingly, nuclear proteins implicated in DNA condensation and decondensation are also found in the CSF in large quantities such as all 6 histones (H1, H2A, H2B, H3, H4 and H5) and HDACs (HDAC2) (**Fig 47C**).

Furthermore, the mass spectrometry analysis reveals several proteins known to be involved in cognitive and neurodevelopmental defects. For instance, FOXP1 is implicated in the atypical form of Rett syndrome and 14q12 microdeletion ([Papa et al., 2008](#)), lissencephaly-1 homolog (LIS-1) mutations give rise to lissencephaly

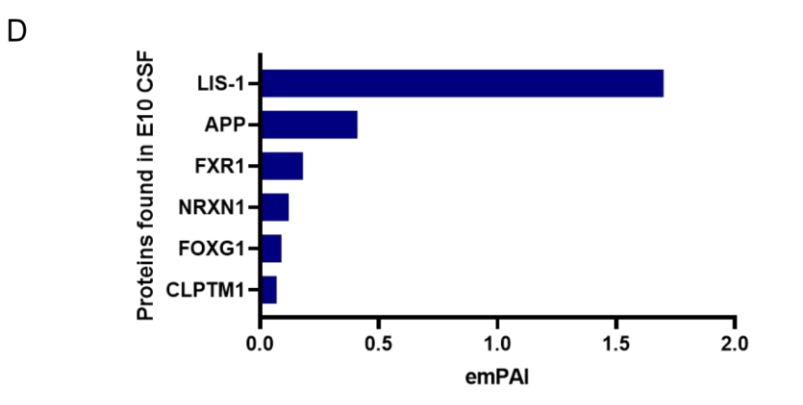
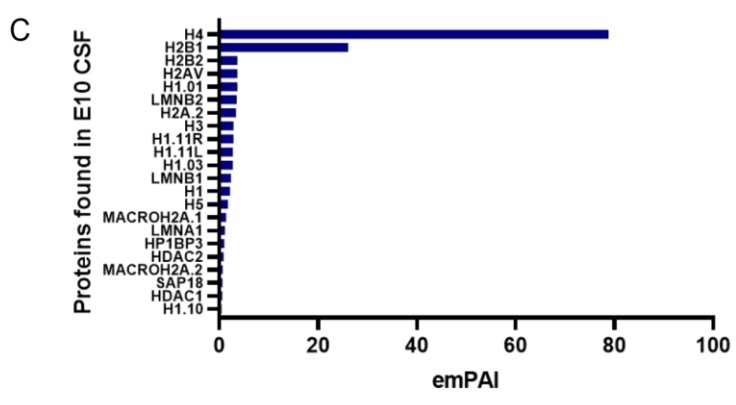
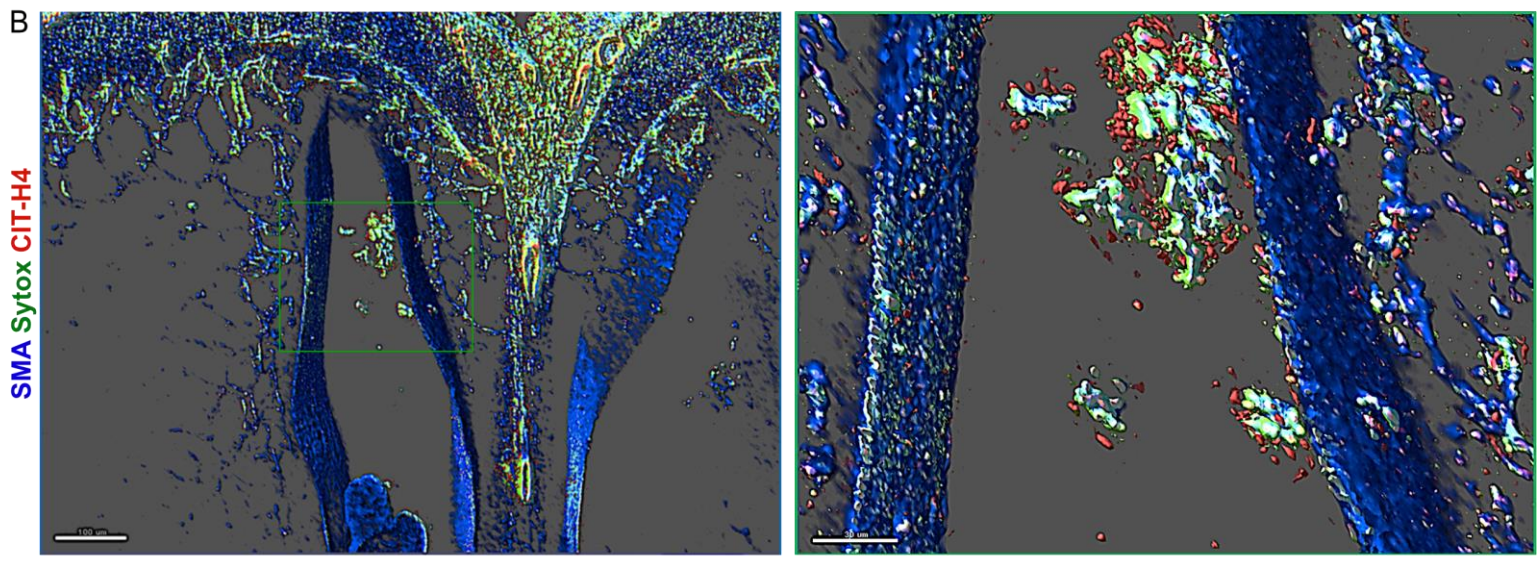
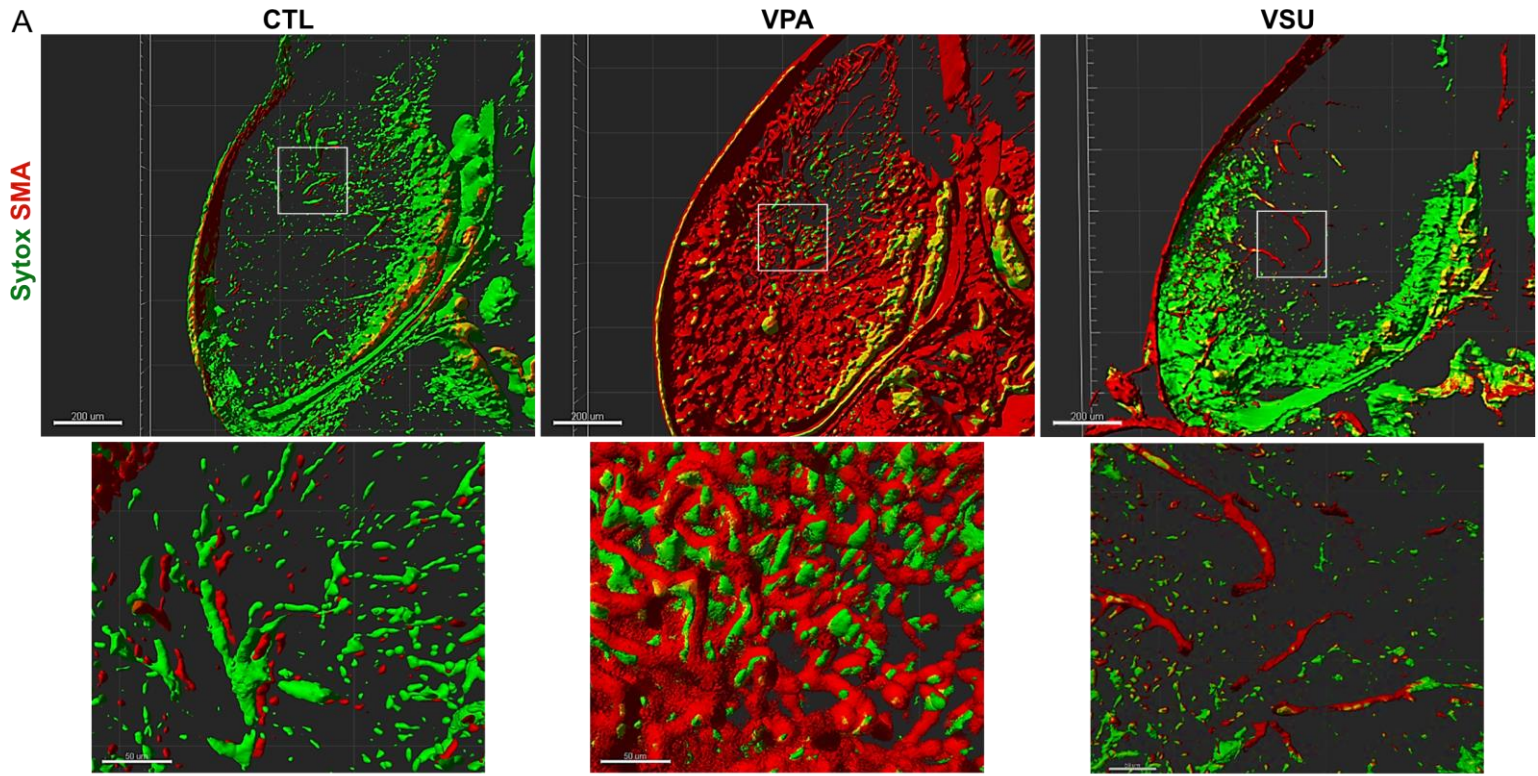


Figure 47. DNA shedding and ETosis occur *in vivo*. **(A)** Light sheet microscopy images of whole-mount E8 chick brains generated with the Imaris Viewer software 9.7.2. DNA is observed with the Sytox™ marker (in green) and vascularization is observed with the α -SMA marker (in red). Chick embryos were injected with conditioned solutions: PBS for control (left panels), VPA (middle panels) or VPA+Suni (VSU, right panels). Scale bars: 200 μ m (in the upper panels) and 50 μ m (in the lower panels). **(B)** Light sheet microscopy image of a control whole-mount E8 chick brain generated with the Imaris Viewer software 9.7.2. Vascularization is observed with the α -SMA marker (in blue), DNA is observed with the Sytox™ marker (in green) and Cit-H4 in red. Shedding of DNA and Cit-H4 is found linked to the α -SMA marker in the CSF of the brain. Scale bars: 100 μ m (in the left panel) and 30 μ m (in the right panel). **(C,D)** Mass spectrometry was performed on CSF collected from E10 embryos. Mass spectrometry analyses reveal **(D)** numerous proteins usually found in the nucleus (histones, lamins and HDACs), and **(C)** several proteins known to be involved in cognitive and neurodevelopmental defects (FOXG1, LIS-1, APP and FXR1).

(for review, Vallee et al., 2000), APP is implicated in AD (for review, Armstrong, 2013), and fragile X mental retardation protein (FMRP) is implicated in Fragile X syndrome (Gothelf et al., 2009) (**Fig 47D**).

3. Choroid plexus may have a role in brain immunity by conditioning the CSF

To analyze a potential role of the CP in brain immunity and to decipher differential expression between the ependyma and the NC-derived stroma of CP in case of noxious insults, ex vivo experiments were performed to isolate the CP on Petri dishes. The CP were either treated with culture medium or with VPA for 24h (**Fig S6A**). E. coli particles are also added 1h or 3h in the Petri dishes before rinsing with PBS 1X, and immunohistochemistry was performed on the CP explants (**Fig S6B**). The CP could be observed by performing z-stacks under an Axio Imager Z1 Upright Trinocular Fluorescence microscope equipped with apotome. To go further, the conditioning of the CSF by the CP could be studied by coupling the CP explants with the microfluidic technology. The CP placed on either side of the μm -scale channels could condition the fluid found in the channels. In fine, the fluid could be analyzed by proteomic analyses to decipher the DNA found during ETosis processes or the proteins secreted by the CP.

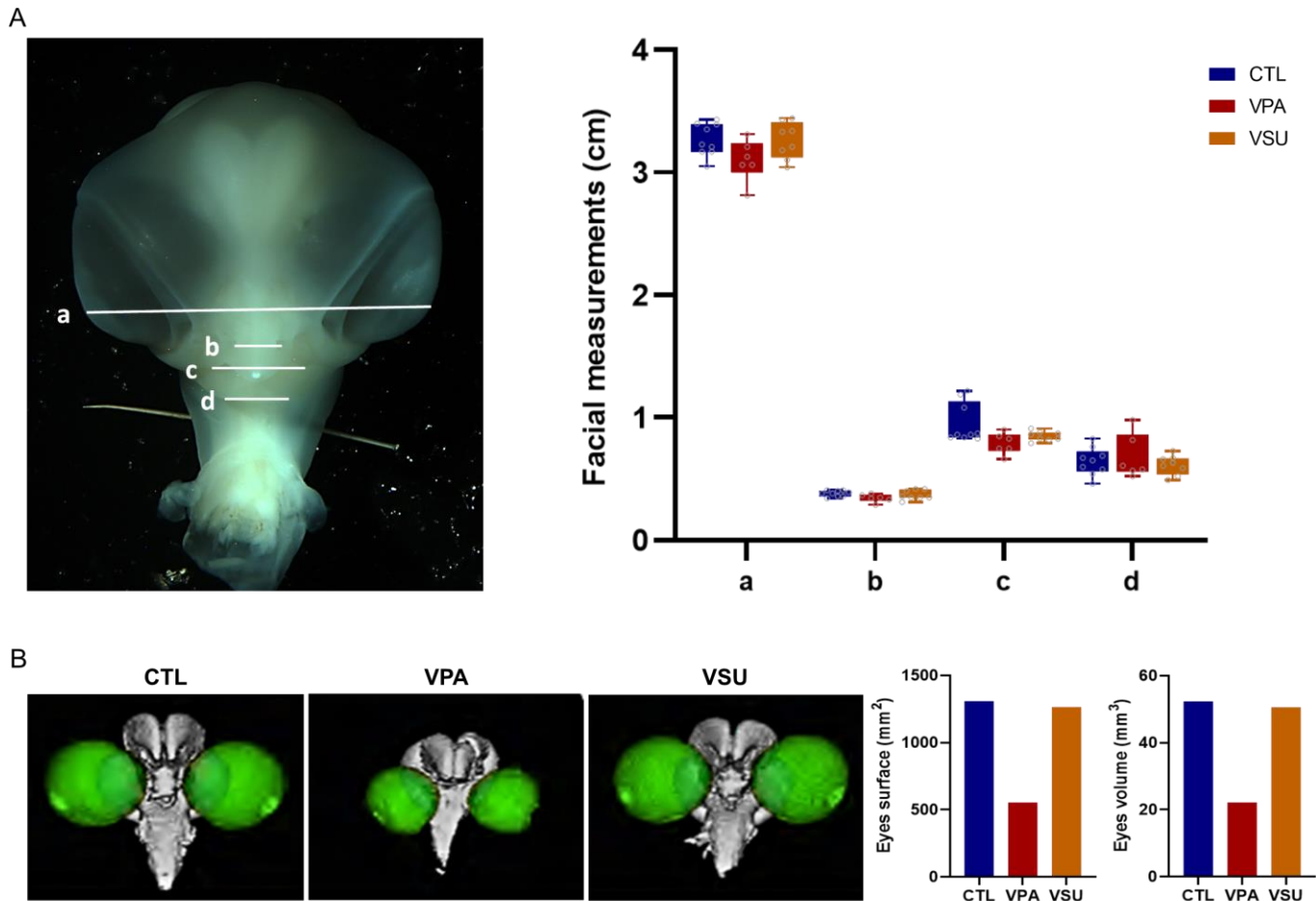


Figure S1. Morphometric analyses of the face. (A) Morphometric analyses of the cerebral morphology on E8 chick heads injected at E3,5 with PBS for control condition, VPA or VPA+Suni (VSU) using ImageJ. a) outer inter-canthal distance, b) inter-alar distance, c) inter-commissural distance, and d) mandibular arch length. **(B)** Micro-computed tomography images of E8 chick embryos injected at E3,5 with PBS for control condition, VPA or VSU: 3D reconstruction on the whole brain and the eyes. The surface and volume of the eyes were measured for each condition. Error bars represent \pm SEM.

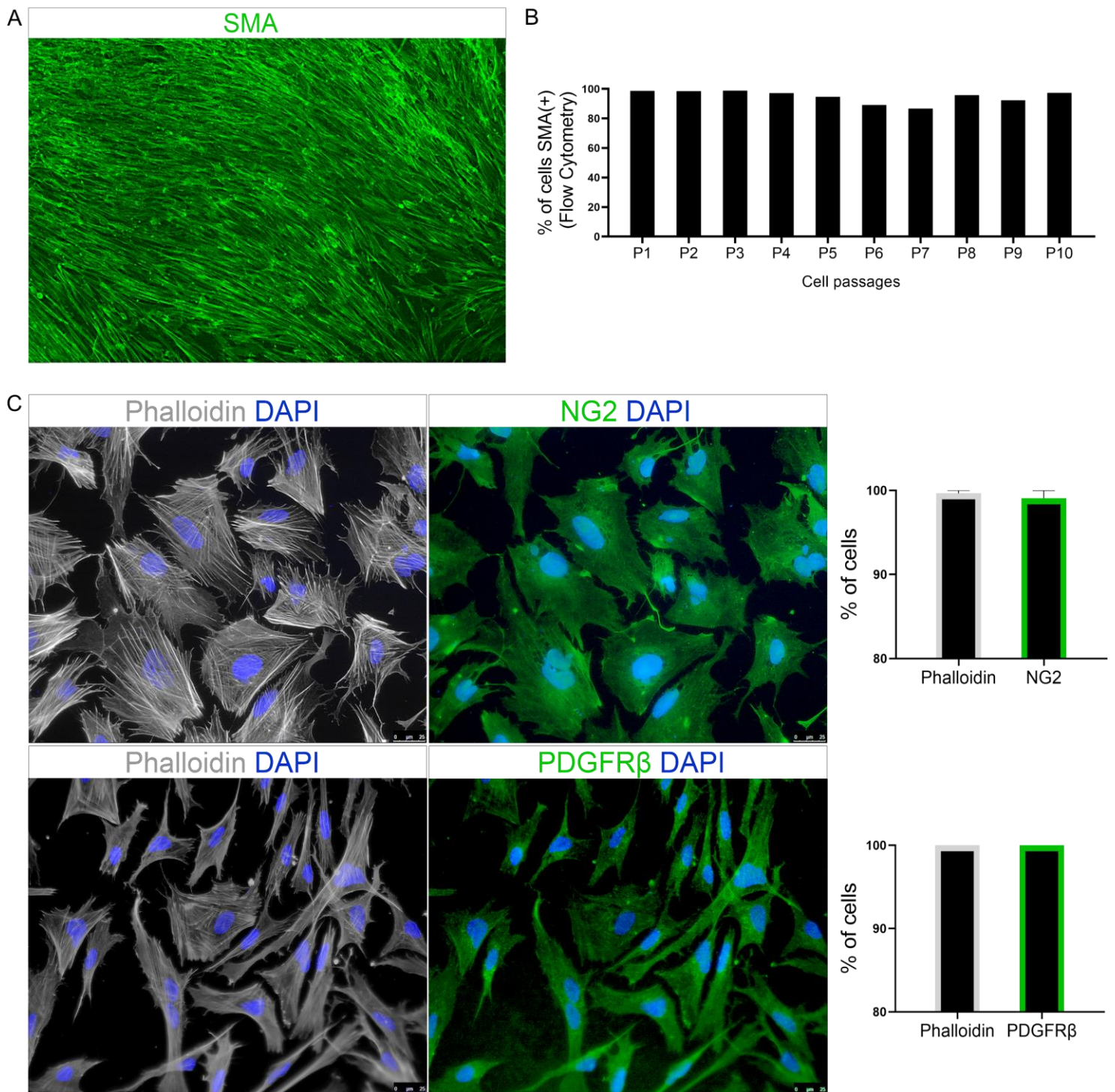


Figure S2. Meningeal NC-derived pericytes provide a homogeneous α SMA(+) cell population under fibronectin-coated cell culture plates and co-express specific pericyte markers. (A) Immunostaining for the pericyte marker α SMA (green) confirms the homogeneity of the meningeal NC-derived pericyte culture *in vitro*. **(B)** Cytometry-determined percentage of α SMA(+) cells in meningeal NC-derived pericytes culture at various passages (up to 10). **(C)** Immunostaining for pericyte markers phalloidin (gray) and NG2 or PDGFR β (green) in meningeal NC-derived pericyte culture. Nuclei are stained with DAPI (blue). Co-expression of both markers is demonstrated. The percentage of cells expressing each marker is quantified using ImageJ software and presented in the graph.

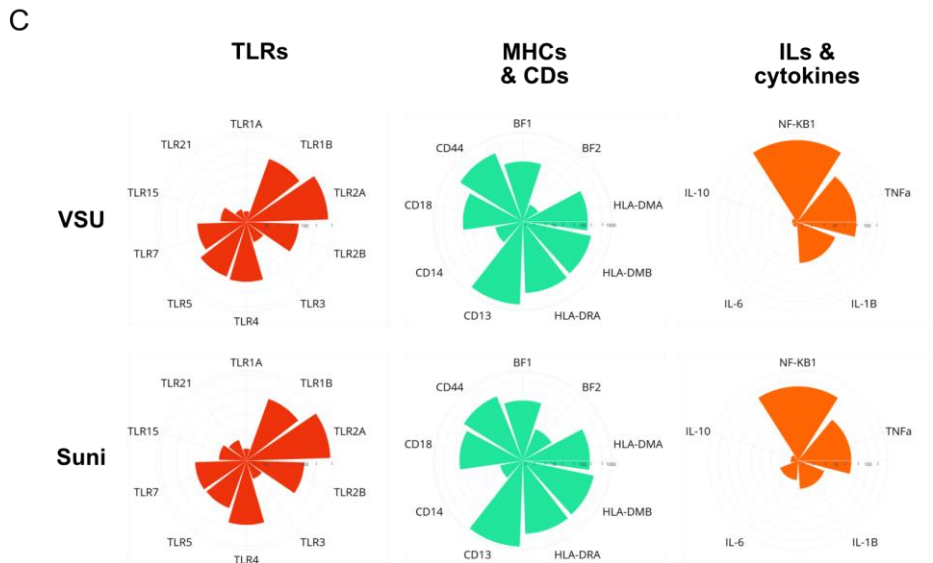
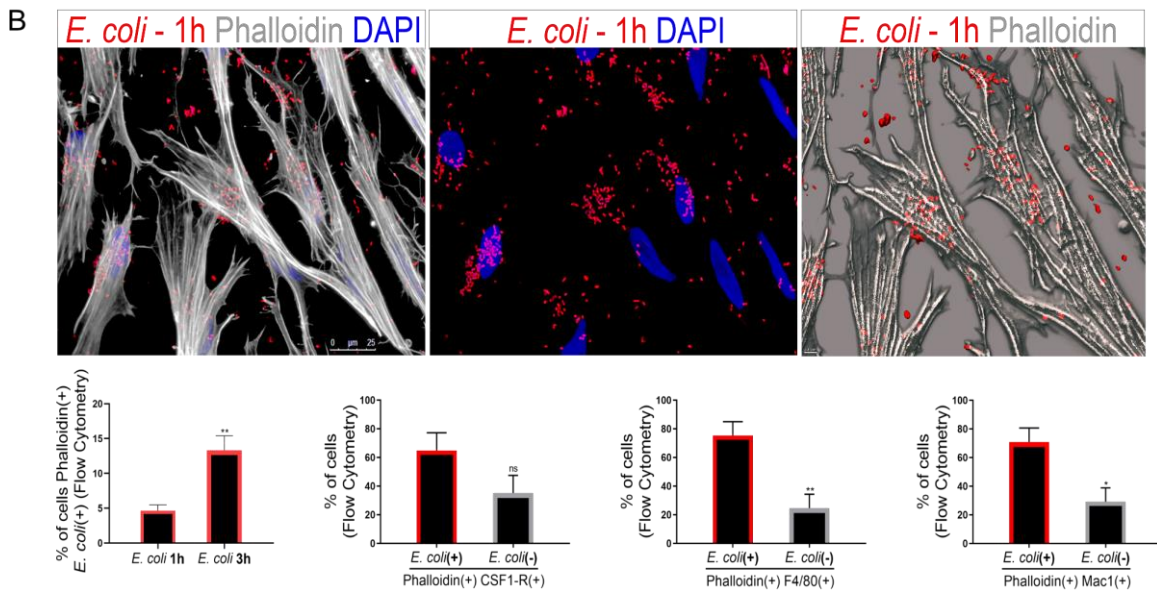
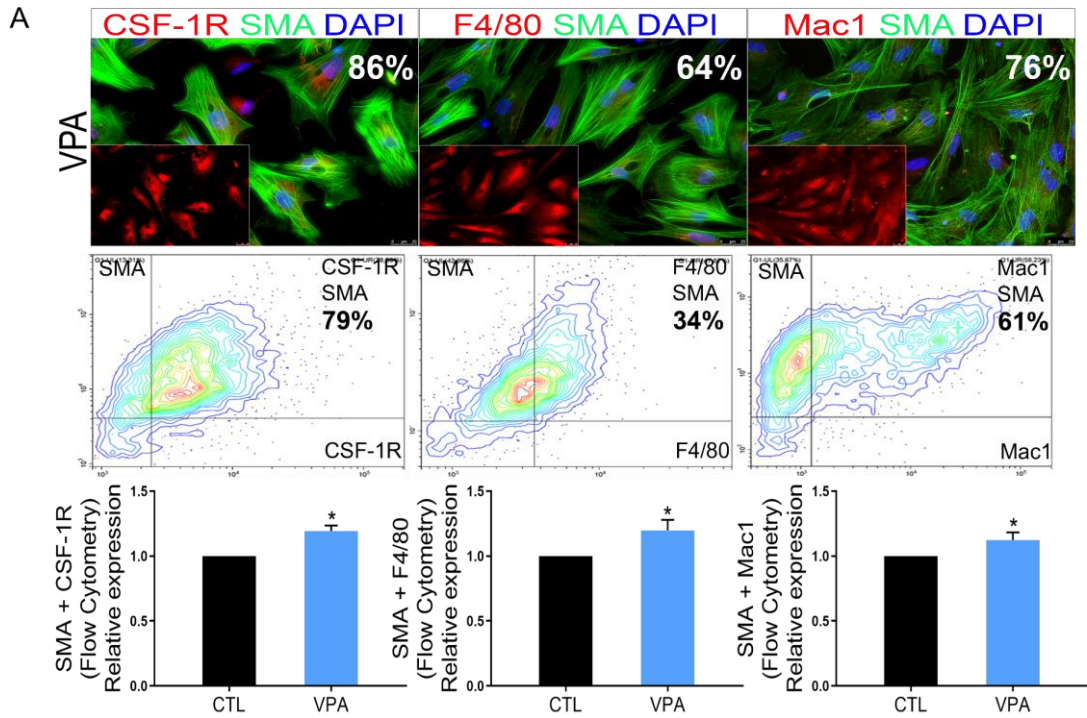


Figure S3. Meningeal NC-derived pericytes present a macrophage-like and immune profile and VPA treatment modulates this profile. (A) Immunostaining showing α SMA(+) (in green) pericytes expressing macrophage markers (CSF-1R, F4/80, and Mac1 respectively, in red) *in vitro*. Nuclei are stained by DAPI (in blue), and insets highlight the expression of macrophage markers alone. The numbers correspond to the mean percentage of double-positive cells quantified with ImageJ software. The center panels below are each marker's respective cytometry analysis and the mean percentage of double-marked cells (pericyte-specific marker α SMA and macrophage markers). The graph panels below compare the relative co-expression of the pericytes-specific marker α SMA and the macrophage markers between CTL cells and VPA cells (cytometry). $*p \leq 0.05$. **(B)** Meningeal NC-derived pericytes (phalloidin(+), in gray) can phagocytose *E. coli* particles (in red) *in vitro* after only 1h of exposure to the bacterial particles. Nuclei are stained by DAPI (in blue). In the lower panels, from the left to the right, cytometry quantification of the percentage of cells expressing the specific pericyte marker phalloidin and fluorescent *E. coli* particles after 1 and 3h of exposure to the bacteria particles; percentage of cells expressing phalloidin, the macrophage markers (CSF-1R, F4/80, and Mac1), and the presence or absence of *E. coli* particles. Error bars represent \pm SEM. $**p \leq 0.01$; $*p \leq 0.05$; ns not significant. **(C)** Specific transcriptomic analysis was performed using the Nanostring technology. While pericytes exposed to culture medium spontaneously express immune responsive molecules (TLRs, MHCs and CDs) and inflammatory molecules (interleukins and cytokines), VPA+Suni (VSU) and Suni normalize the expression emphasized by noxious insults (VPA). Error bars represent \pm SEM. $**p \leq 0.01$; $*p \leq 0.05$; ns not significant.

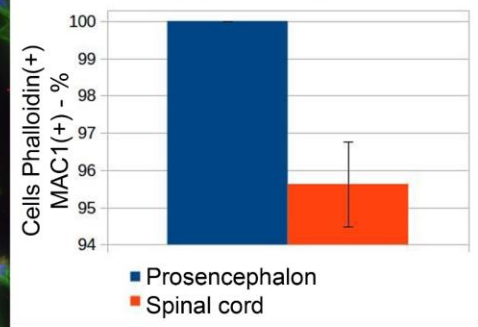
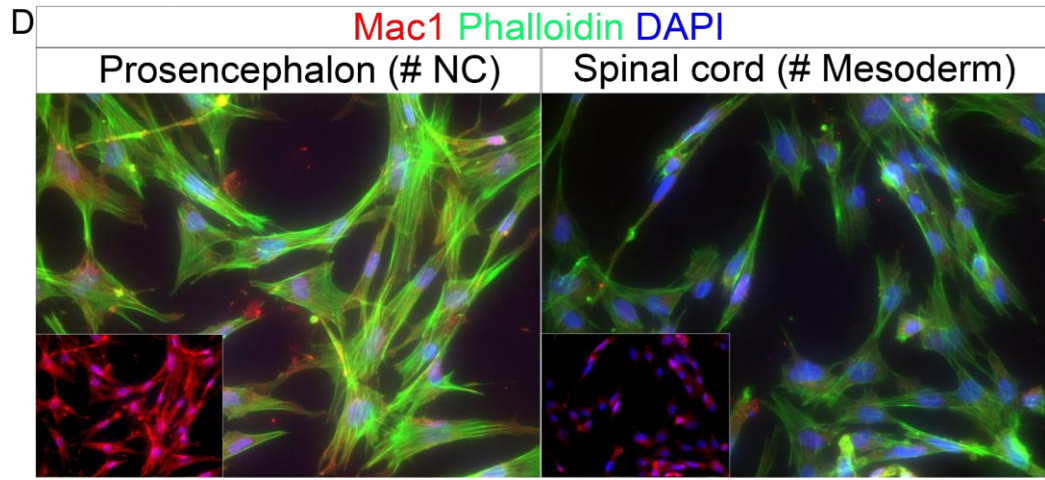
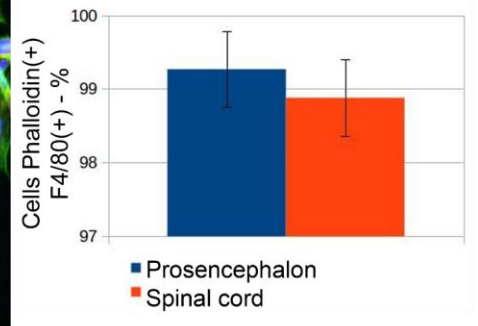
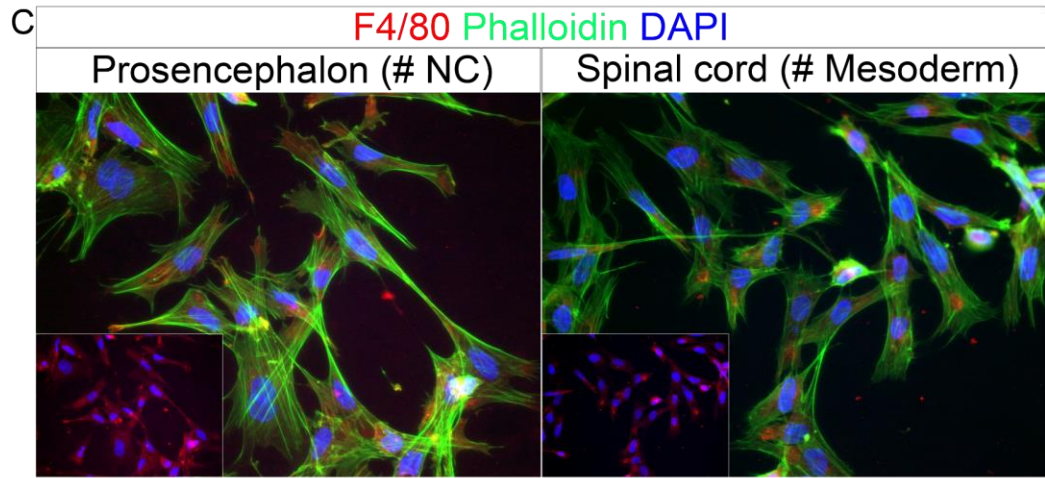
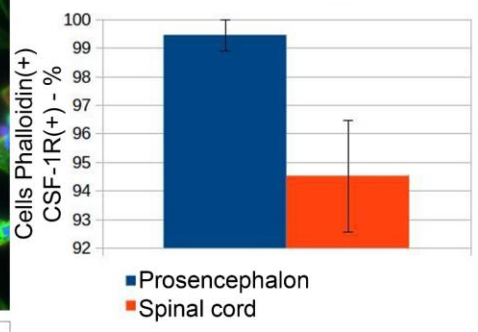
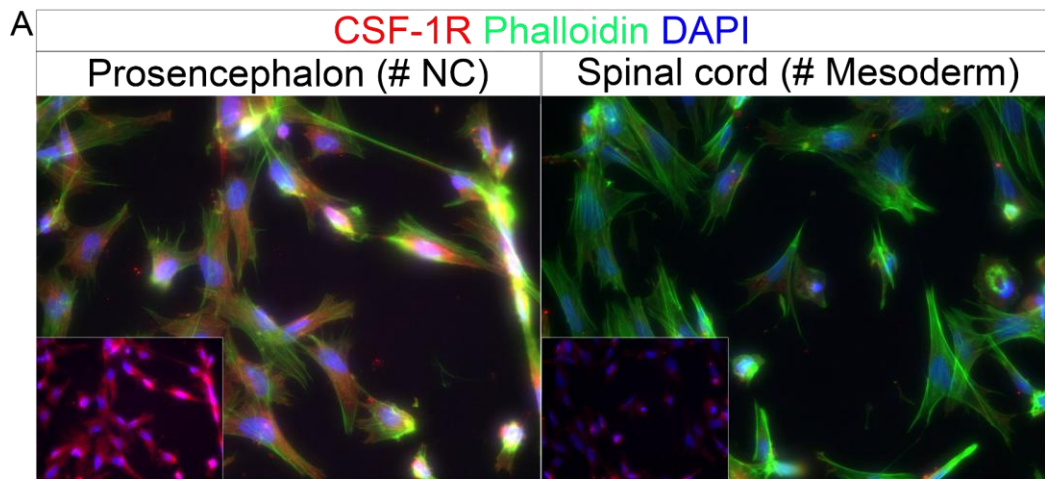


Figure S4. Meningeal spinal cord mesoderm-derived pericytes express macrophage markers at a lower level than meningeal prosencephalon NC-derived pericytes. Immunostaining for the pericyte marker phalloidin (in green) and macrophage markers CSF-1R **(A)**, F4/80 **(C)**, and MAC1 **(D)** (in red) in meningeal NC-derived pericytes from 34HH chicken embryo prosencephalon (left panels) and meningeal mesoderm-derived pericytes from 34HH chicken embryo spinal cord (right panels). Cell nuclei are stained with DAPI (in blue). The insets show the expression of macrophage markers and nuclei. Graphs on the right present the percentage of cells co-expressing pericyte and macrophage markers, as quantified by ImageJ. **(B)** 34HH stage chicken embryo. Dotted lines indicate the region from which the vertebral column was excised. The left panel depicts the isolation of the spinal cord from the vertebral column. The meninges were collected and subjected to tissue dissociation before being seeded in cell culture plates.

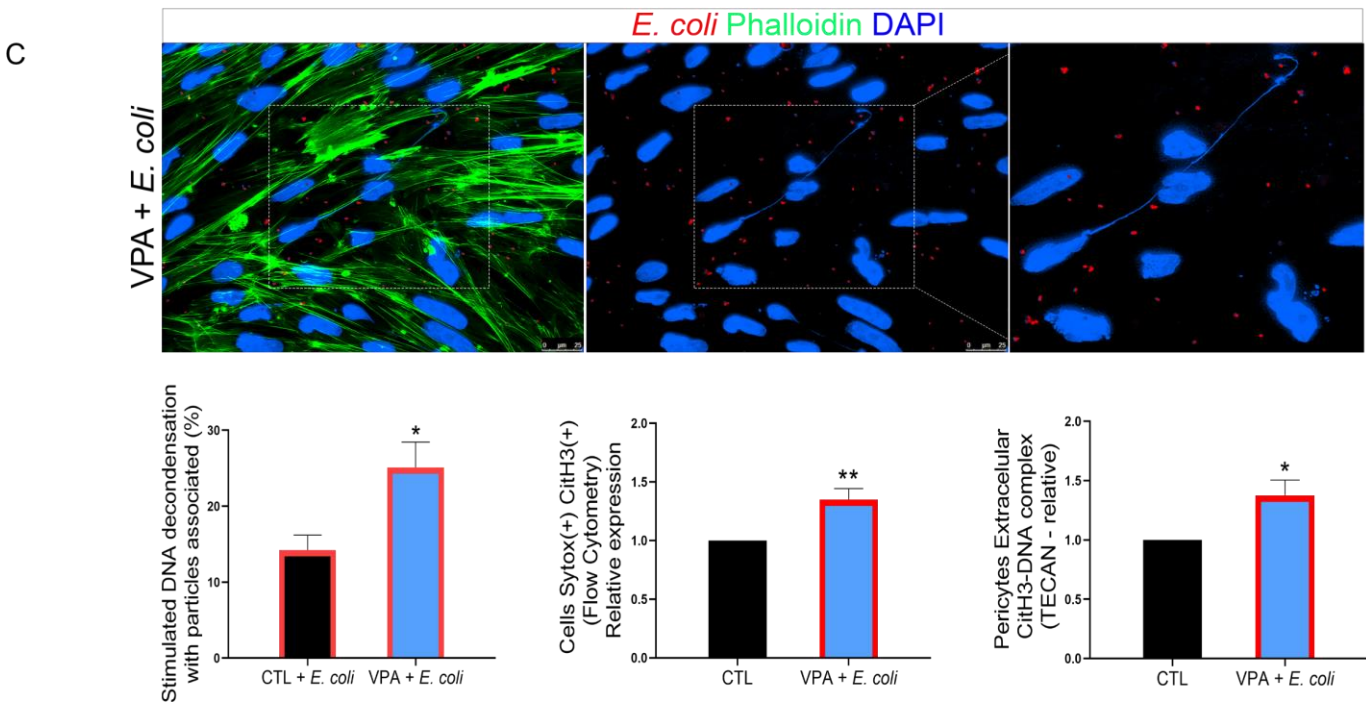
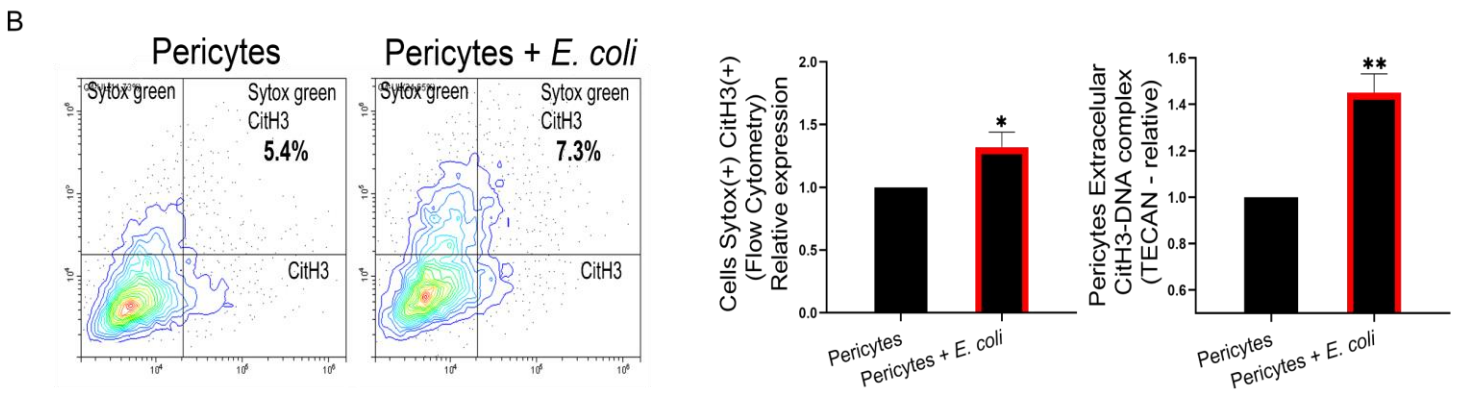
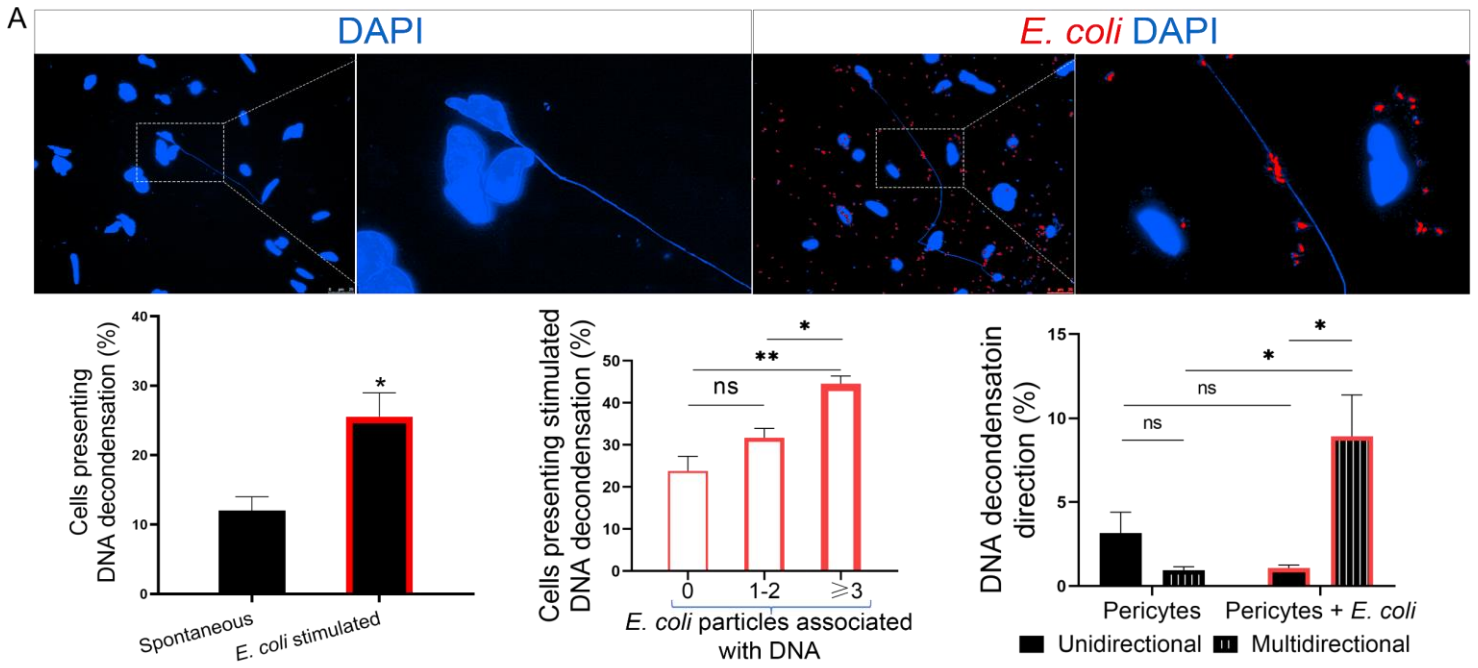


Figure S5. Pericytes present DNA decondensation and produce ETosis *in vitro*. Noxious insults increase the inflammatory profile of pericytes. (A) Pericytes culture illustrating DNA decondensation in both non-treated (spontaneous) and 1h *E. coli*-treated (stimulated) cells. Cell nuclei are represented in blue, and *E. coli* particles in red. The accompanying graphs show the comparison of the percentage of cells displaying DNA decondensation in spontaneous and *E. coli*-stimulated conditions. Additionally, the graphs also show the percentage of *E. coli*-stimulated cells displaying DNA decondensation in association with 0, 1-2, or ≥ 3 *E. coli* particles and the percentage of unidirectional or multidirectional DNA decondensation in spontaneous and *E. coli*-stimulated cells. $**p \leq 0.01$; $*p \leq 0.05$; ns not significant. (B) Double staining of SytoxTM green and Cit-H3 in unfixed pericytes culture treated or not treated with *E. coli* particles for 1h. The numbers in the figure represent the average of double positive cells as determined by cytometry analysis. The first graph illustrates the relative co-expression of SytoxTM green and Cit-H3 in pericytes treated or not treated with *E. coli*. The second graph presents TECAN analysis results, displaying the relative expression of the Cit-H3 / DNA complex in the conditioned media of pericytes treated or not treated with *E. coli* particles. $**p \leq 0.01$; $*p \leq 0.05$. (C) VPA-treated pericyte cell culture illustrating DNA decondensation after 1h of *E. coli* exposure *in vitro*. Cell nuclei are represented in blue, and *E. coli* particles in red. In the graphs below, from left to right, the percentage of cells presenting DNA decondensation with *E. coli* particles associated. In the middle, the graph illustrates the relative co-expression of SytoxTM green and Cit-H3 in pericytes CTL and VPA-treated with *E. coli* particles (cytometry). The last graph presents TECAN analysis results, displaying the relative expression of the Cit-H3 / DNA complex in the conditioned media of CTL and VPA cells treated with *E. coli*. $**p \leq 0.01$, $*p \leq 0.05$; ns not significant.

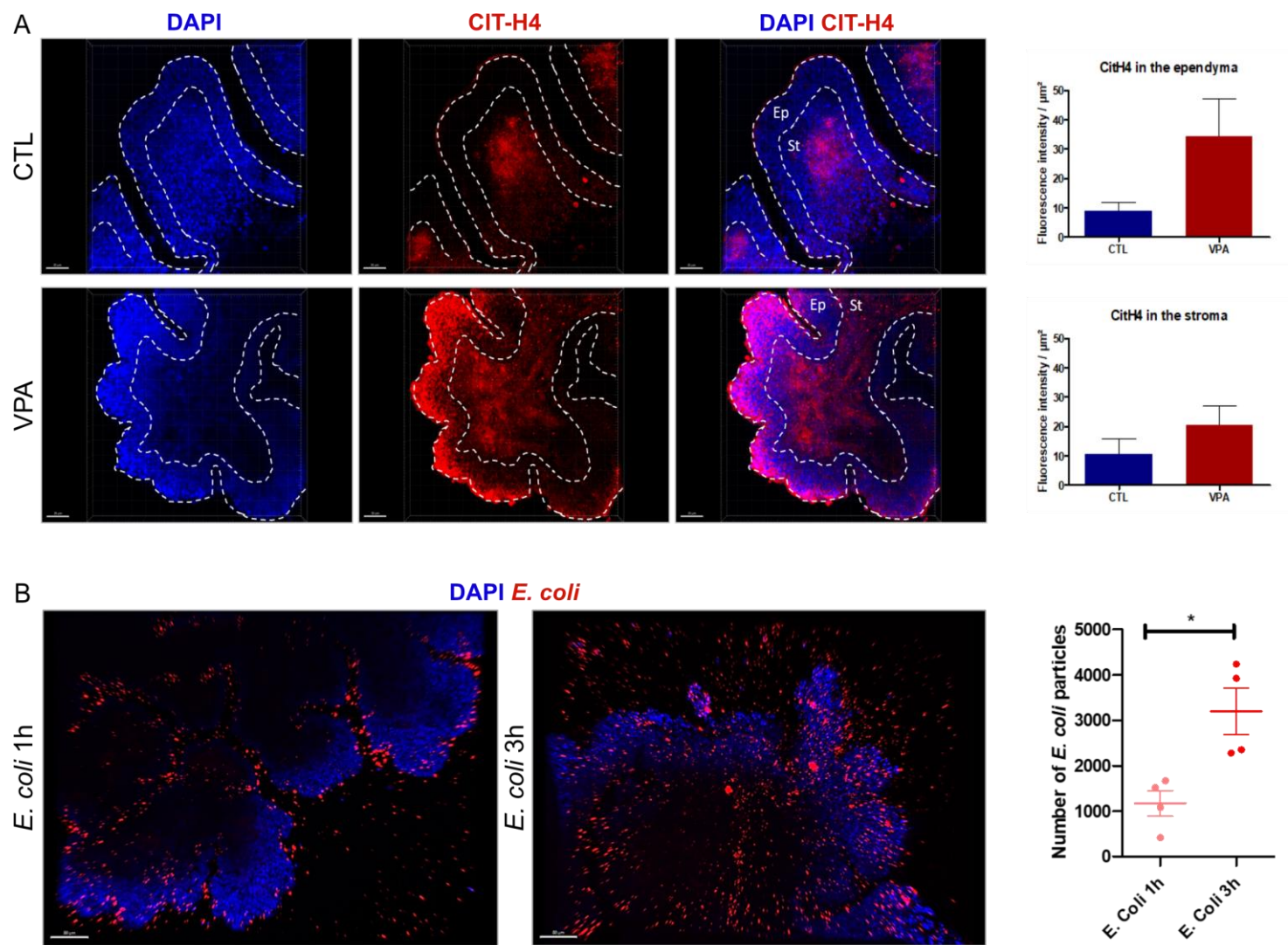


Figure S6. 3D *ex vivo* system to develop CP in a Petri dish. CP were harvested from E8 control embryos and treated with **(A)** conditioned solutions (culture medium for control condition or VPA solution) 24h after fibronectin attachment or with **(B)** *E. coli* during 1h or 3h of treatment. After immunohistochemistry, the CP were observed under an Axio Imager Z1 Upright Trinocular Fluorescence microscope equipped with apotome. The images were visualized and analyzed with the Imaris Viewer software 9.7.2. Ep, ependymal layer, St, stroma. Error bars represent \pm SEM. * $p \leq 0.05$.

DISCUSSION

Previous studies in the lab have investigated the role of the CNC in the formation of the brain and more specifically the morphogenetic and paracrine CNC effect on the development of the brain and sense organs (Aguiar et al., 2014; for review, Creuzet, 2009a; 2009b; Creuzet et al., 2002; 2006; Garcez et al., 2014; Le Douarin et al., 2012). The absence of CNC coincides with brain defects, and leads to the emerging picture that the CNC plays a key role in forebrain development, before birth. These studies documented how the CNC controls brain morphogenesis, hence casting light on the CNC implication in vertebrate encephalization. However, the specific role of CNC in the homeostasis of the brain's development has never been examined. Therefore, the aim of this PhD was to investigate the role of the CNC, which provides the meninges and its pericytes of the forebrain, in brain development and homeostasis, and the later role in cognitive development at birth. During my PhD project, I explored how the CNC-derived meninges can exert an immunosurveillance and protect the brain from noxious, toxic and septic insults. My work points out some key mechanisms.

I. PhD overview: achievements and significance

1. The development of social behavior at birth can be modeled by studying imprinting reflex

I investigated the hypothesis that the deregulation of the CNC may cause neurodevelopmental defects associated with cognitive defects and behavioral impairments at birth. To this end, we use the avian chicken embryo as a model in which the social interactions can be modeled and analyzed using filial imprinting. Our studies on control chicks show that the newborns acquire positive

interactions at birth: these interactions consist of observation, pursuit, and contact with the object, and tend to consolidate over time. When chick embryos are treated with valproic acid (VPA), an anticonvulsant known to cause cognitive disorders in newborns, they exhibit severe alterations in their social interactions after birth. Our results validated the relevance of our model to exploring alterations in social behavior.

2. Aberrant meningeal and intracerebral vascular network precede behavioral disorders

To understand the cellular basis of these behavioral alterations at birth, we analyzed the earliest modifications occurring in the meningeal and intracerebral vascularization at embryonic stages using immunocytochemistry with antibodies directed against proteins and structural markers of perivascular cells. During normal development, at E8, the capillary branches of the meningeal vessels penetrate and vascularize the neural tissue of the pallium from the pial to the ventricular side. However, this vascularization is interrupted at the SVZ, leaving the VZ, avascular ependymal cells. In contrast, VPA-treated embryos show an expansion and densification of the capillary network in the brain parenchyma, and vascular invasion at the expense of VZs flanking the LV, in the dorsal and intermediate pallium, and along the septum. Surprisingly, these defects coincide with the acquisition of macrophage features by meningeal cells, which express markers CSF-1R, MAC1, and F4/80. Therefore, these defects seem to stem from the neuroinflammation of CNC origin.

3. Anti-angiogenic treatments restore social behavior at birth

We challenged to revert these behavioral and vascular defects by treating chicken embryos subjected to the noxious effects of VPA, using Suni as an antiangiogenic drug. A significant rescue of social behavior and hypervascularization in the brain

was observed, indicating that the defects can be tamed with drugs preventing vascular and pro-inflammatory progression.

4. Embryonic perivascular cells are endowed with immune properties

The phenotypical changes of CNC-meninges and pericytes were confirmed by bulk RNAseq transcriptomic analysis. We also performed profiling of both meninges (*in vivo*) and cultured pericytes (*in vitro*), stimulated or not by toxic (VPA) or septic (*E.coli*) insults using the Nanostring® strategy. This technique allows an actual quantification without amplification of transcripts using barcoded riboprobes which allows a refined cell profiling in the different experimental situations.

We show that, during early embryogenesis, pericytes express different MHC class II molecules when stimulated with VPA or *E. coli*. Pericytes also express TLRs and various cytokines. Altogether, these results indicate that pericytes are professional immune cells, capable of pathogen recognition and antigen presentation.

5. Perivascular cells develop DNA traps in response to pathogenic stimuli

Our work also reveals that pericytes mediate their immunosurveillance of the developing brain by decondensing their nuclear material and forming extracellular DNA traps upon noxious insults. This process, initiated by the enzyme Peptidyl Arginine Deiminase4 (PAD4), causes citrullination of histones 3 and 4, which lead the nuclear DNA to be to unfolded and shed outside the cell. In fine, this process leads to the formation of extracellular traps (ETs), which act as an “alert system” for potentially noxious modifications of brain homeostasis. Light sheet microscopy was used to visualize whole-mount brains and confirm the DNA decondensation as well as ETosis *in vivo*: shedding of DNA and citrullinated histones were observed in the CSF of the LV and indicate possible cytogenetic imprinting of CNC meninges on the CSF. When subjected to a VPA toxic non-septic shock, the pericytes showed exacerbated macrophagic traits, together with an incoercible capacity to form and

shed extracellular DNA web: these processes are associated with behavioral impairments and autistic manifestations in the neonate.

Overall, my work has deciphered a multi-systemic role of the CNC-derived meninges and pericytes **(Fig. 48)**:

- a role in social behavior at birth
- a role in craniofacial development
- a pro-neurogenic role
- a role in immune surveillance
- a role in carbohydrate metabolism.

II. NC-derived meninges' role in social behavior at birth

In 2004, Michaelis and colleagues demonstrated an anti-angiogenic effect of VPA in *in vitro* experiments as they show an inhibition of endothelial cells proliferation, migration and tube formation in the human umbilical vein (Michaelis et al., 2004). *In vivo* experiments showed disturbance of vessel formation in mice embryos and angiogenesis inhibition in the chicken chorioallantoic membrane assay both treated with VPA. However, in contrast, our results demonstrated hypervascularization of the brain when embryos are treated with VPA. Both vasculogenesis, forming new blood vessels, and angiogenesis, developing new capillaries from pre-existing blood vessels (Egginton and Gerritsen, 2003), were observed in VPA-treated brains. Vasculogenesis was observed particularly in the brain parenchyma as new blood vessels are formed by ramification. The number of branches and their length increased compared to control brains, forming more anastomosis. Angiogenesis was particularly observed by capillaries sprouting in

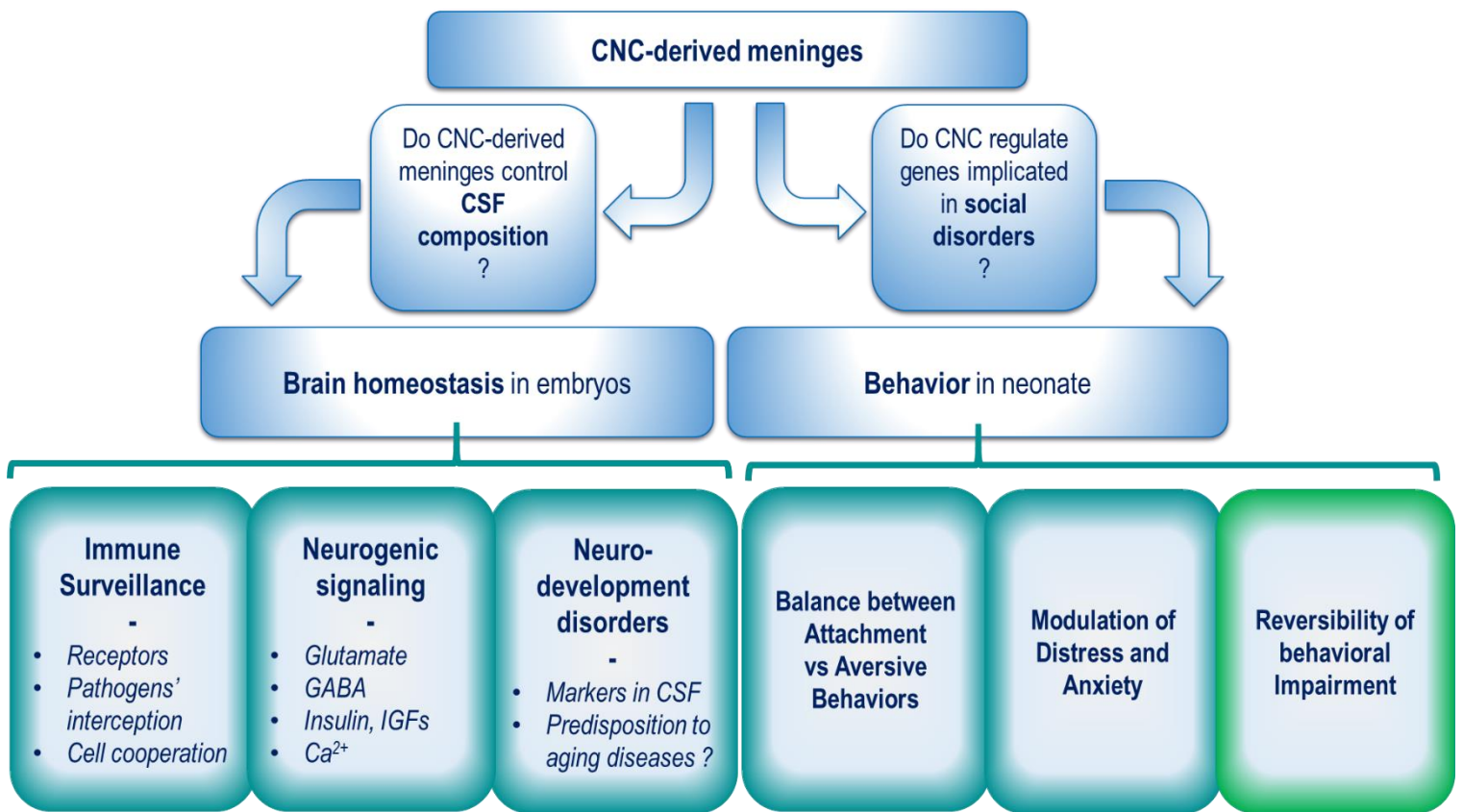


Figure 48. The CNC-derived meninges and pericytes' roles in brain homeostasis during development and in neonate behavior

the VZ of the brain.

During embryonic development, neurogenesis initiates in the VZ adjacent to the LV, where neural stem cells differentiate into new neurons that will migrate to the proximity of their final destination (Nottebohm, 2002). Neurogenesis requires a hypoxic environment, crucial for self-renewal properties and pluripotency of neural stem cells. Hypoxia allows proliferation, migration and maturation of neural stem cells (for review, Li et al. 2021). The limit of the blood vessels bringing oxygen at the border of the VZ therefore generates an hypoxic environment at the level of the VZ, allowing normal development of the neural stem cells. In case of VPA exposure, hypervascularization leads to the presence of blood vessels in the VZ, thus generating a normoxia environment during early embryonic development. This could lead to accelerated neuronal differentiation and exhaustion of neural stem cell niche, resulting in decreased brain size. In fine, VPA could lead to a deregulation of neurogenesis, observed with bulk RNA sequencing, and generate social impairment at birth.

The diagnosis of ASD clinically relies on behavioral impairments characterized by three symptom domains: social deficit interaction, repetitive behavior and impaired communication (American Psychiatric Association, 2013; Nicolini and Fahnstock, 2018). VPA exposure *in utero* in mice leads to ASD in newborn pups as they acquire deficit social functioning, communication deficits and increased repetitive behavior. They present delayed neurodevelopment and impaired cognitive functions (Nicolini and Fahnstock, 2018), reduced distress pup calls (Gandal et al., 2010; Gąssowska-Dobrowolska et al., 2020), decreased exploration, increased anxiety (Gąssowska-Dobrowolska et al., 2020; Markram et al., 2008; Schneider and Przewłocki, 2005; Schneider et al., 2006; Schneider et al., 2008), and abnormal fear processing (Markram et al., 2008).

Besides, the BTBR T+ tf/J mouse is studied as a model of autism as they acquire

these three symptom domains. These mice lack social interactions, have unusual spontaneous repetitive behavior patterns with high level of repetitive self-grooming and lack in communication (McFarlane et al., 2008). Interestingly, they are also characterized by an abnormal development of the meninges, with meningeal extension atrophied in adult mice. This malformation leads to shrunk LV, reduced CP in length and enlarged arteries in the ventral extremity of the falx cerebri (Mercier et al., 2011). Thus, the malformation of the falx cerebri, and more generally of the meninges, could impact social behavior at birth, leading to autistic symptoms.

During this PhD project the newborn chick was used as our model to study social behavior at birth. The chick model offers numerous advantages. Firstly, the chick embryo model allows precise space-specific and time-specific microinjections of conditioned solutions. Indeed, microinjections are performed in a space-specific manner as they are directly performed in the brains' vesicles of the CNS and microsurgery is performed in a stage-specific manner due to the accessibility of the avian embryo at any stage of its development. Secondly, with the chick model, the "filial imprinting" can be modeled and used for behavioral studies (Bateson, 1969; 1979; 1990), allowing us to isolate the newborn chick from its congener at birth and avoiding any social interaction before the behavioral tests. On the contrary, pup mice are only separated from their congeners after three weeks, during the weaning process. While newborn chicks acquire accurate vision and walking movement from the first day of birth, pup mice are blind at birth, they crawl from birth to 5 days and only start walking from 5 to 10 days old. However, while newborn chicks were treated with VPA at E3,5 by direct micro-injection in the three vesicles of the brain, behavioral tests were not possible with septic insult via *E. coli* particles as chick embryos could not survive more than 24h of *E. coli* exposure.

During the behavioral tests performed on newborn chicks with an object substituting their congener, the first step was to confirm the use of filial imprinting with our newborn chick models. Indeed, control chicks, treated with PBS at E3,5 presented high interactions with the decoy. However, while control chicks showed attachment towards the object, VPA-treated chicks at E3,5 presented aversive behavior as observed with other organism models previously. For instance, two major behaviors considered as symptoms of ASD were observed in VPA-treated chicks: 1) social deficit interaction as they were less interested by the object. Indeed, they spent less time observing the object compared to control chicks, they rarely pursued the object and their contact with the object was due to an active aggressivity of the newborn chick. 2) repetitive behavior as they constantly pecked the object aggressively during the whole test. In addition, two other behaviors reinforce an autistic manifestation of the VPA-treated chicks as they showed higher anxiety and abnormal fear compared to control chicks. Unlike newborn pup mice, VPA-treated chicks increase distress calls and increase exploration as thigmotaxis is worsened compared to control chicks. Finally, increased anxiety was observed with high self-pecking in VPA-treated chicks compared to control chicks.

These observations are reinforced by the use of the anti-angiogenic drug Suni. Firstly, Suni rescues the vascularization of the brain by limiting hypervascularization triggered by VPA, especially at the level of the VZ. Then, this limited vascular development observed *in vivo* improves social behavior at birth, confirming the role of NC-derived meninges in cognitive development at birth.

III. NC-derived meninges' role in craniofacial development

As mentioned above, previous studies in the lab had demonstrated the role of CNC in craniofacial development ([for review, Creuzet, 2009a](#); [Creuzet et al., 2002](#),

2006; for review, Le Douarin et al., 2012; Garcez et al., 2014). However, the role of the CNC-derived meninges in craniofacial development remained elusive. Furthermore, published studies have shown that VPA exposure during the first trimester of pregnancy could lead to an increased risk of congenital malformations, especially affecting the developing nervous system, resulting in NT defects leading to spina bifida aperta and exencephaly or microcephaly (for reviews, Nau et al., 1991; Ornoy, 2009). Other organs are also affected by VPA, leading to craniofacial abnormalities such as craniosynostosis and cleft palate (Jentink et al., 2010; for review, Nau et al., 1991; Werler et al., 2011) or eye defects (Gurvich et al., 2005).

By analyzing the effect of VPA on NC-derived meninges and performing cerebral and facial morphometric analyses on E8 chick embryos, our results confirmed the effect of VPA on craniofacial malformation as microcephaly. Moreover, a reduction of the size of the eyes were observed in VPA-treated embryos compared to control embryos. Besides, bulk RNA sequencing data reinforce the role of the NC-derived meninges in craniofacial development as VPA targets many genes implicated in skull development. For instance, VPA down-regulates the *Fgf6* gene, coding for the FGF6 protein which is known to activate FGFR2. Several cases of *Fgfr2* mutations combined with a form of craniosynostosis called acrocephaly have been reported in Apert syndrome (Premalatha et al., 2010; Yu et al., 2000). VPA also deregulates other genes giving rise to craniosynostosis in case of mutation (*Nell1*, *Epha1*, *Nbea* and *Stab2*).

Interestingly, while Suni rescues brain vascularization and improves social behavior at birth in case of VPA exposure, it does not rescue craniofacial malformations generated by VPA.

In 2021, Naqvi and colleagues developed a theoretical approach based on genomic analyses to discover striking convergence of common genetic variation affecting brain and face shape, at least in part mediated by regulatory regions active in CNC cells and their derivatives (Naqvi et al., 2021). Brain T1-weighted magnetic resonance imaging (MRI) scans were used on a cohort of 21,780 subjects composed of an adult population (40 to 70 years old). The MRI was focused on the mid-cortical surface (midway between the white-grey matter interface and the pial surface). In addition, the Adolescent Brain Cognitive Development Study (ABCD) was performed on a total of 11,411 children between 8.9 and 11 years old.

Surprisingly, while much of the shared genetic variation between brain and face shape is mediated by CNCs, they claim that these shared genetic effects do not appear to significantly impact neuropsychiatric disorder risk or cognitive functions. In our studies, consistent with the conclusions in Naqvi's article, even though craniofacial malformations are not rescued with Suni, we observe a rescue of social behavior at birth.

However, even though craniofacial malformations are not rescued, a normalization of the vascular network with Suni is observed prior to a rescue of cognitive behavior at birth. Therefore, we postulate that NC-derived meninges, among other causes, could have an impact in cognitive behavior at birth.

Furthermore, unlike the conclusion of Naqvi and colleagues, numerous studies have registered the appearance of cognitive disorders and syndromes taking place after craniofacial malformations during development (Table 1), thus suggesting a link between craniofacial malformations and cognitive impairments at birth (Aguiar et al., 2014; Harakalova et al., 2012; Kyle et al., 2018; Mei et al., 2016; Zhang et al., 2020). More specifically, these malformations seem to derive from neurocristopathy manifestations, therefore originating from NCCs.

In their study, Naqvi and colleagues used a theoretical approach based on genomics analyses. They base their observations and conclusions using imaging

analyses such as MRI and genetic studies. They do not consider any environmental factors that could have an impact on craniofacial malformations during development. In our studies, we decipher the effect of environmental factors giving rise to craniofacial malformations before cognitive impairments at birth, with the use of toxic (VPA) and septic (*E. coli*) insults.

Finally, as cited in their study due to a limited cohort sample, Naqvi and colleagues do not exclude a correlation between genetic variation between brain and face shape and behavioral–cognitive traits at birth.

IV. NC-derived meninges' pro-neurogenic role

After birth, the NVU is composed of neurons, astrocytes and pericytes, among other cells. The main role of this NVU is assuring the proper transmission of neuronal signals in order to insure regulation of vascular pressure. ([Adriani et al., 2017](#); [Neuwelt et al., 2011](#)). However, during embryonic development, astrocytes appear during late development. For example, during chick development, glial precursors start emerging from E11 onward and functional astrocytes differentiate from E15 onwards ([Domowicz et al., 2008](#); [Domowicz et al., 2011](#)). Therefore, since the NVU composition differs from embryonic stage to adult stage by the absence of astrocytes, the NC-derived pericytes could have a greater role in the neurovascular system, probably directly interacting with neurons, during early development. Bulk RNA sequencing reveals the impact of VPA-treated meninges and pericytes as VPA targets numerous genes implicated in several mechanisms of the NVU system. These observations indicate that VPA insult may severely impact the neurogenesis and neurovascular system in development.

V. NC-derived meninges' role in immune surveillance

In the postnatal BBB, astrocytes play an important role in the immune defense against environmental pathogens. However, as described previously, astrocytes and microglial cells appear during late development (for review, [Abbott et al., 2010](#); [Daneman and Prat, 2015](#)). Thus, the composition of the BBB differs during embryogenesis and after birth and the early immune defense is ensured by NC-derived pericytes. Especially at the level of the CP, the absence of BBB could lead to an entrance of the pathogens, infecting the developing CNS. The stromal pericytes could have an important role in immune surveillance during early embryogenesis. Moreover, the lymphoid organs at the origin of the lymphoid cells are only fully developed during the late stages of embryonic development. For instance, the first lymphoid organ to develop is the thymus, located around the pharynx and involved in the formation of the T cell repertoire. The thymic rudiment first appears at E3 and the organ is fully developed by E12. T cells are only detected from E10 and are fully immunocompetent by E18. Meanwhile, for the second lymphoid organ specific to birds, the bursa of Fabricius, its rudiment appears at E4 and is a well-organized lymphoid structure by E18. B cells develop in the bursa of Fabricius from E11 and are fully immunocompetent by E18 ([Garcia et al., 2021](#)).

The vascular vessels are composed of an inner layer of endothelial cells, interacting with an outer sheath of mural cells. Among these mural cells, the NC-derived pericytes project their cytoplasmic protrusions around the endothelial cells to ensure a double structural role by maintaining the blood vessels circular and by controlling the hemodynamic stress on blood circulation ([Appaix, 2014](#)). However, the CNC-derived pericytes have never been characterized as immune cells in embryos.

In vitro experiments and RNA sequencing have evidenced a novel role of CNC-derived pericytes: their macrophagic characteristics and role in immune surveillance at an early embryonic stage. Indeed, cultured pericytes spontaneously express macrophagic and inflammatory markers. Interestingly, in case of noxious insults such as VPA or *E. coli* exposure, these immune characteristics are highly emphasized. These macrophagic features are specific to pericytes deriving from the CNC as immunohistochemistry results have shown that meningeal spinal cord mesoderm-derived pericytes express macrophage markers at a lower level than meningeal prosencephalon NC-derived pericytes (Fig. S4). Moreover, by using 2-well inserts in cell cultures, we have demonstrated that CNC-derived pericytes exhibit high migration capacities and are capable of bacterial phagocytosis like the professional immune cells. In these experiments, the pericytes stimulated by noxious insults keep their fibroblastic form, confirming that these cells could not be activated microglia which become amyloid in the case of activation. Overall, we hypothesize that while the stimulated cells could be considered as recruiting cells expressing inflammatory molecules and phagocytosing *E. coli* particles, the control cells are considered as cooperating cells migrating towards the site of infection, like typical immune cells. Along with the immune characteristics described previously, this PhD project has also evidenced a new immune defense system in CNC-derived pericytes, the ETosis process that has never been discovered previously in embryonic, perivascular or mesenchymal cells.

During embryonic development, specific macrophages have been described to defend the CNS against pathogens: 1) microglia colonizing the parenchymal brain and 2) non-parenchymal CNS-associated macrophages (CAMs). Interestingly, similarly to NC-derived pericytes, CAMs are located in the CNS interfaces such as the perivascular space, the meninges, and the CP of the brain (Faraco et al., 2017; Gerganova et al., 2022; Karam et al., 2022). Moreover, the CAMs can be discriminated from parenchymal microglia by their high expression of CD11b (also

known as MAC1), F4/80 and CSF-1R (Gerganova et al., 2022). These three surface markers were also observed in NC-derived pericytes using immunohistochemistry techniques. However, CAMs only start colonizing the brain as progenitors from E9,5 in mice and start maturing at E12,5 (Goldmann et al., 2016; Mehl et al., 2022), whereas mature NC-derived pericytes can be observed during early development. Moreover, the origin of CAMs and pericytes differ as CAMs derive from EMPs originated from the yolk sack whereas cranial pericytes derive from NCCs. Therefore, NC-derived pericytes and CAMs are probably different cell types ensuring the immune defense of the CNS at different stages of the embryonic development: the NC-derived pericytes could ensure the immune defense during early embryogenesis and CAMs could take over their immune role during late embryogenesis.

In 1953, specific cells found at the ventricle border of the ependymal CP, the epiplexus cells or Kolmer's cells, present similar characteristics to the stromal pericytes observed during this PhD project. In particular, Kolmer's cells and NC-derived pericytes both display cytoplasmic processes surrounding the ependymal cells and the endothelial cells respectively. Moreover, they both are actively recruited, play a significant role in inflammation in case of infection, and have phagocytic behavior. Lastly, Kolmer's cells and pericytes are polymorphic based on their activated state, ranging from round to polar and stellar or from stellar to fibroblastic respectively. However, even though the role of Kolmer's cells in immune defence has been studied since the 1950s, the origin of these cells has not yet been identified and could probably derive from NCC, similarly to stromal pericytes.

To ensure the origin of the pericytes studied *in vitro*, meninges were collected from E8 chick embryos, before the emergence of microglial cells. Moreover, after ten passages, cultures of meningeal pericytes demonstrate nearly 100% preservation

of α SMA-positive cells (**Fig. S2B**). To further corroborate this phenotype, NG2 and PDGFR β markers, which are conventionally employed to highlight pericytes, stained nearly 100% of the cells found in meningeal cultures (**Fig. S2C**). Indeed, the fibronectin used for cell cultures precisely retains perivascular cells rich in actin, such as pericytes. By contrast, leukocyte and circulating cells do not adhere to the fibronectin: experiments confirmed the characteristic of this fibronectin as chick blood cultures on fibronectin-coated dish did not show any cellular staining. Finally, the Nanostring analyses on E8 chick meninges confirmed the high expression of specific pericyte markers (α SMA, PDGFR β and CD13).

VI. NC-derived meninges' plausible role in carbohydrate metabolism

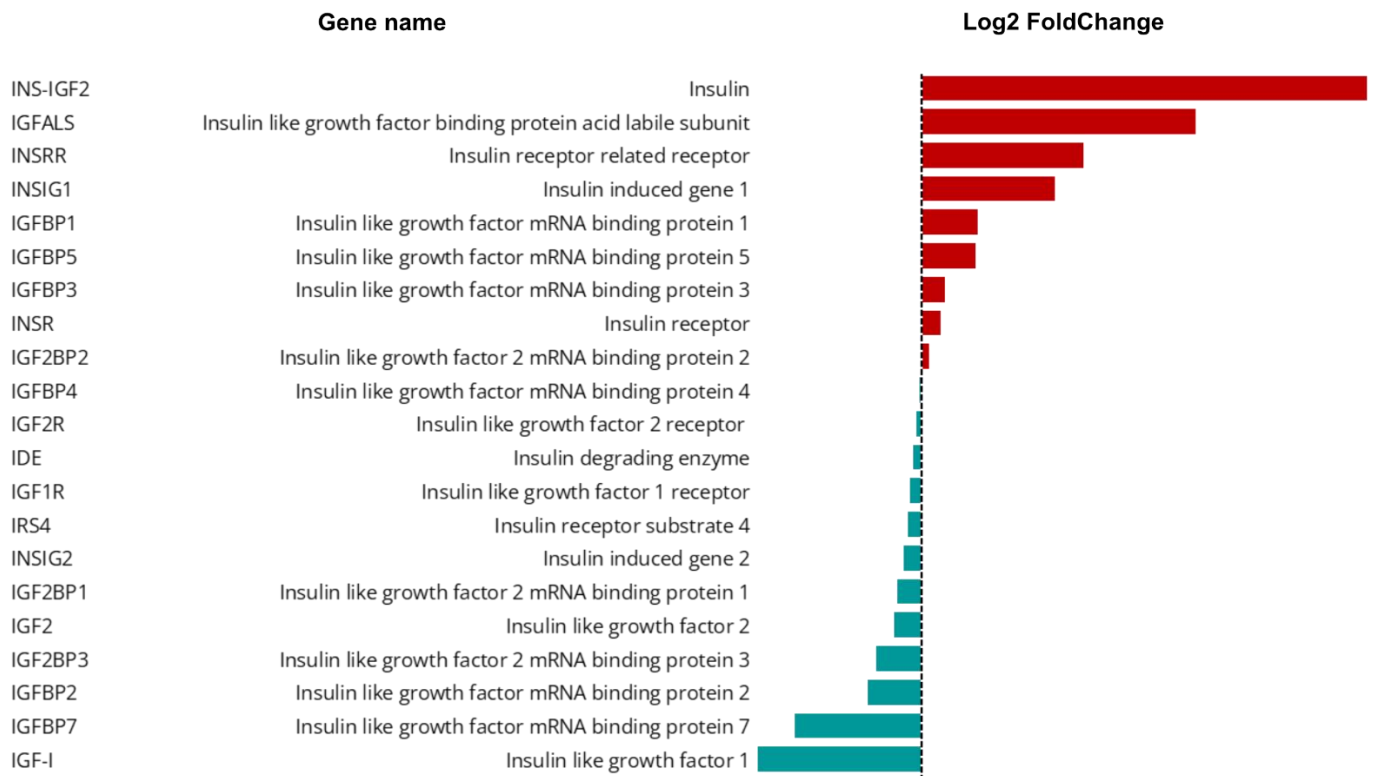
The role of the NC-derived meninges in carbohydrate metabolism has never been previously studied and was not the aim of my PhD project. However, interestingly, the bulk RNA sequencing performed on E8 chick meninges revealed the effect of VPA on several targets of the insulin pathway (**Fig. 49A**). The String-db.org site gathers bibliographic data connecting all these genes (**Fig. 49B**).

The insulin pathway regulating the glucose concentration in the blood (glycemia) also affects the concentration of glucose found in the CSF (glycorrachia). In fact, both glycemia and glycorrachia are linked as the latter correspond to 0,6 times the glycemia. In case of bacterial infection, particularly during a meningo-encephalitis, the glycorrachia decreases, giving rise to hypoglycorrachia ([Cabral et al., 2008](#); [Fang et al., 1997](#); [Hurmuzache et al., 2012](#)). By regulating the insulin pathway and specifically by regulating targets related to insulin growth factor (IGF), embryonic NC-derived meninges could therefore control glucose level in the CSF. IGF-1 could have a role in neural development and more specifically in axon myelination and synaptogenesis. Therefore, a deficiency of IGF-1 could prevent

normal neurogenesis ([Steinman and Mankuta, 2013](#)). Even though glycorrachia hasn't been precisely documented in autistic patients, many studies have discovered a potential connection between the levels of IGF-1 and ASD ([Riikonen, 2016](#); [Steinman, 2019](#); [Steinman and Mankuta, 2013](#)). Thus, one could expect to also reveal hypoglycorrachia.

A

VPA vs CTL



B

Homo sapiens

Gallus gallus

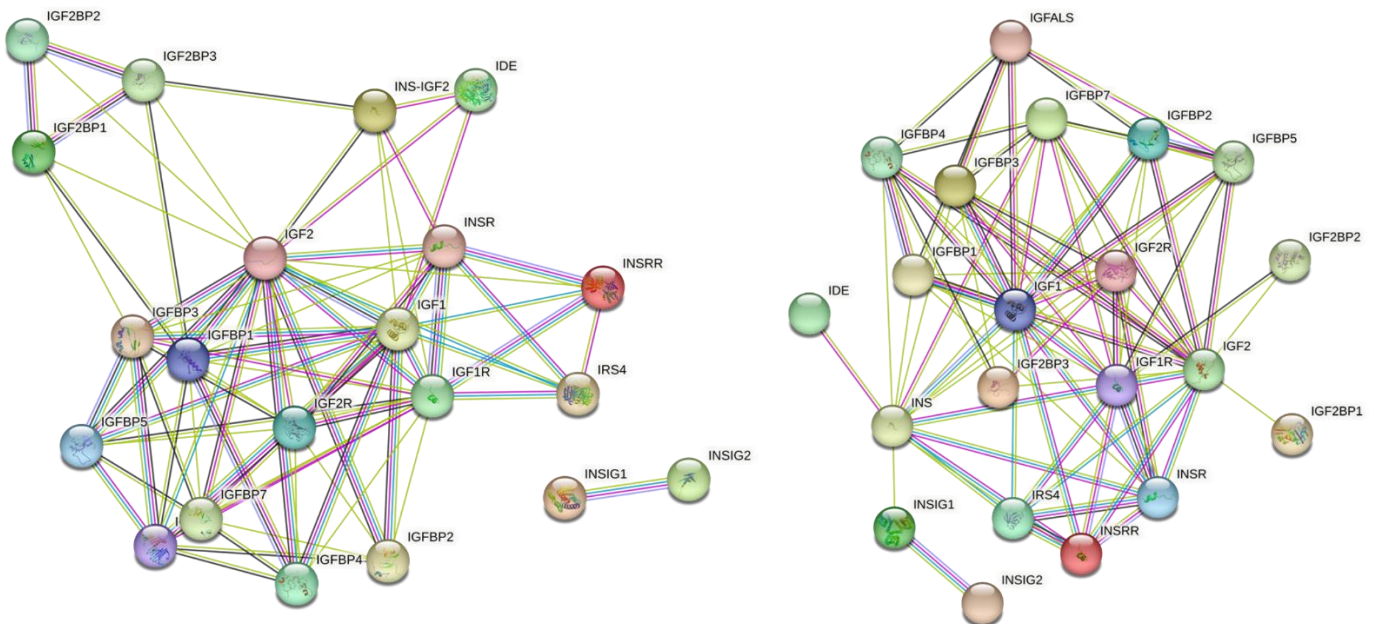


Figure 49. The CNC-derived meninges regulate the insulin pathway and VPA modulates this pathway. (A) Bulk RNA sequencing performed on E8 chick meninges reveal a differential expression of the insulin pathway with VPA treatment. **(B)** String graphs performed on the insulin pathway's molecules in the Homo sapiens / human (left panel) and the Gallus gallus / chicken (right panel) species.

CONCLUSION AND FUTURE DIRECTIONS

Overall, my PhD project has demonstrated the importance of the NC-derived meninges and its pericytes during embryonic development as a hub for social behaviour at birth, for craniofacial development, for pro-neurogenesis and pro-immune checkpoints, and possibly for carbohydrate metabolism. Further studies in proteomic analyses, already initiated in the lab, would reinforce the role of the NC-derived meninges and its stromal pericytes in CSF conditioning during embryogenesis, and specifically in presence of noxious insults. Moreover, to decipher the specific role of NC-derived meninges on neurogenesis, E8,5 forebrain samples injected with the conditioned solutions at E3,5 (PBS for the control condition, VPA or VPA+Suni) and/or exposed to *E. coli* were collected to perform RNAseq analyses.

This work promises to include meningeal tissue in the clinical picture of neurodevelopmental pathologies. Furthermore, this work also paves the way for documenting the biological significance of extracellular DNA in CSF and the pathophysiological importance of this mechanism in the etiology of neurodevelopmental disorders.

Significant changes in the nuclei accompany massive exposure to pathogens. In cells where phagocytosis is active, we observe nuclear DNA decondensation, accompanying the presentation of bacterial particles on the cell surface. This mechanism, initially demonstrated for neutrophil cells, has just now been described for cells that play a structural role in tissues, such as perivascular meningeal cells. Our observations indicate that perivascular cells, in cooperation with a few adjacent cells, can assemble large DNA traps that massively intercept pathogenic particles.

In this context, the training of ETosis appears to be essential to:

1. collectively halt the spread of pathogens
2. present phagocytized infectious particles in the extracellular space,
3. alert the perivascular cellular network and recruit adjacent perivascular cells.

CNC-derived cells can participate via phagocytosis and ETosis in brain defense, which is a promising avenue for understanding the origins of neurodevelopmental deficits.

Characterizing DNA secretion in CSF raises the question of its possible activating or inhibiting effect on embryonic neurogenesis. We intend to pursue our research by discovering the biological significance of this process during development in the embryo and fetus.

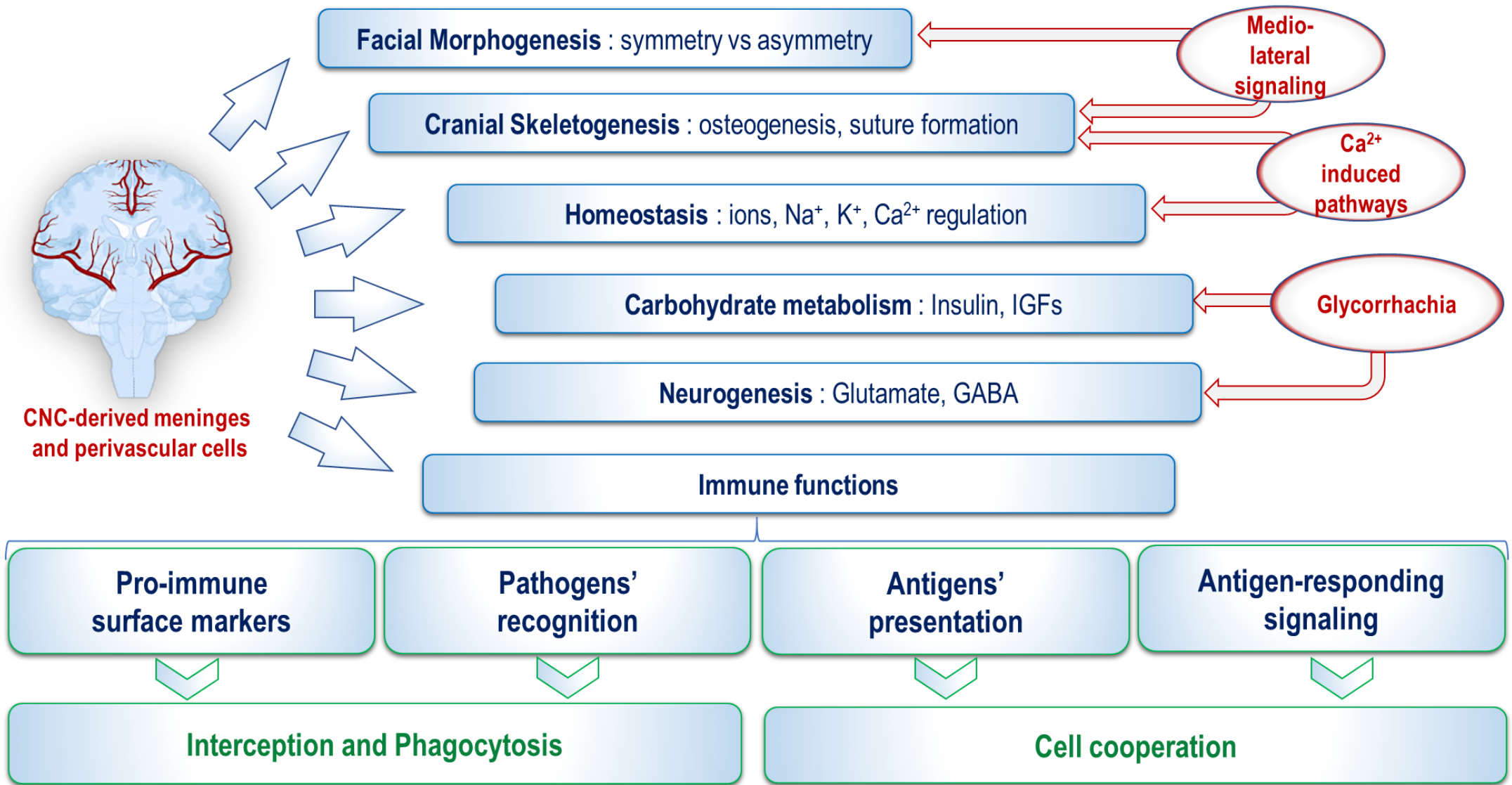


Figure 50. Multi-systemic role of the CNC-derived meninges and pericytes

REFERENCES

- Abbott, N. J., Patabendige, A. A. K., Dolman, D. E. M., Yusof, S. R. and Begley, D. J.** (2010). Structure and function of the blood-brain barrier. *Neurobiol. Dis.* **37**, 13–25.
- Abbott, N. J., Pizzo, M. E., Preston, J. E., Janigro, D. and Thorne, R. G.** (2018). The role of brain barriers in fluid movement in the CNS: is there a 'glymphatic' system? *Acta Neuropathol.* **135**, 387–407.
- Adler, S. P., Nigro, G. and Pereira, L.** (2007). Recent Advances in the Prevention and Treatment of Congenital Cytomegalovirus Infections. *Semin. Perinatol.* **31**, 10–18.
- Adriani, G., Ma, D., Pavesi, A., Kamm, R. D. and Goh, E. L. K.** (2017). A 3D neurovascular microfluidic model consisting of neurons, astrocytes and cerebral endothelial cells as a blood-brain barrier. *Lab Chip* **17**, 448–459.
- Aguiar, D. P., Sghari, S. and Creuzet, S.** (2014). The facial neural crest controls fore- and midbrain patterning by regulating Foxg1 expression through Smad1 activity. *Development* **141**, 2494–2505.
- Akdemir, E. S., Huang, A. Y. and Deneen, B.** (2020). Astrocytogenesis: where, when, and how. *F1000Research* **9**,.
- Akira, S. and Hemmi, H.** (2003). Recognition of pathogen-associated molecular patterns by TLR family. *Immunol. Lett.* **85**, 85–95.
- Alappat, S., Zhang, Z. Y. and Chen, Y. P.** (2003). Msx homeobox gene family and craniofacial development. *Cell Res.* **13**, 429–442.
- Alfei, L., Aita, M., Caronti, B., De Vita, R., Margotta, V., Albani, L. M. and Valente, A.** (1999). Hyaluronate receptor CD44 is expressed by astrocytes in the adult chicken and in astrocyte cell precursors in early development of the chick spinal cord. *Eur J Histochem* **43**, 29–38.
- Alliot, F., Rutin, J., Leenen, P. J. M. and Pessac, B.** (1999). Pericytes and periendothelial cells of brain parenchyma vessels co-express aminopeptidase N, aminopeptidase A, and nestin. *J. Neurosci. Res.* **58**, 367–378.
- Alrajeh, M.** (2018). Embryologie de la neurofibromatose de type I: morphogénèse craniofaciale et régulations du gène NF1 dans la crête neurale.
- Alrajeh, M., Vavrusova, Z. and Creuzet, S. E.** (2019). Deciphering the Neural Crest Contribution to Cephalic Development with Avian Embryos. *Methods Mol. Biol.* **1976**, 55–70.

- American Psychiatric Association** (2013). Diagnostic and statistical manual of mental disorders (5th ed.).
- Appaix, F.** (2014). Brain mesenchymal stem cells: The other stem cells of the brain? *World J. Stem Cells* **6**, 134.
- Armati, P. J. and Mathey, E. K.** (2013). An update on Schwann cell biology - Immunomodulation, neural regulation and other surprises. *J. Neurol. Sci.* **333**, 68–72.
- Armstrong, R. A.** (2013). What causes Alzheimer's disease? *Folia Neuropathol.* **51**, 169–188.
- Armulik, A., Genové, G., Mäe, M., Nisancioglu, M. H., Wallgard, E., Niaudet, C., He, L., Norlin, J., Lindblom, P., Strittmatter, K., et al.** (2010). Pericytes regulate the blood-brain barrier. *Nature* **468**, 557–561.
- Armulik, A., Genové, G. and Betsholtz, C.** (2011). Pericytes: Developmental, Physiological, and Pathological Perspectives, Problems, and Promises. *Dev. Cell* **21**, 193–215.
- Asaga, H., Nakashima, K., Senshu, T., Ishigami, A. and Yamada, M.** (2001). Immunocytochemical localization of peptidylarginine deiminase in human eosinophils and neutrophils. *J. Leukoc. Biol.* **70**, 46–51.
- Bailey, R.** (2021). Function and Layers of the Meninges in the Brain. *ThoughtCo*.
- Bair, M. M. and Munakomi, S.** (2022). *Neuroanatomy, Falx Cerebri*.
- Baker, C. V.** (2008). The evolution and elaboration of vertebrate neural crest cells. *Curr. Opin. Genet. Dev.* **18**, 536–543.
- Baker, C. V. H. and Bronner-fraser, M.** (1997). The origins of the neural crest . Part I : embryonic induction. **69**, 3–11.
- Baker, C. V. H. and Bronner-Fraser, M.** (1997). The origin of the neural crest. Part II: an evolutionary perspective. *Mech. Dev.* **69**, 13–29.
- Baltz, T., de Lima, A. D. and Voigt, T.** (2010). Contribution of GABAergic interneurons to the development of spontaneous activity patterns in cultured neocortical networks. *Front. Cell. Neurosci.* **4**,.
- Bassuk, A. G. and Kibar, Z.** (2009). Genetic Basis of Neural Tube Defects. *Semin. Pediatr. Neurol.* **16**, 101–110.
- Bateson, P. P.** (1969). The development of social attachments in birds and man. *Adv. Sci.* **25**, 279–88.
- Bateson, P.** (1979). Brief exposure to a novel stimulus during imprinting in chicks and its influence on subsequent preferences. **7**, 259–262.

- Bateson, P.** (1990). Is Imprinting Such a Special Case? 125–131.
- Bayot, M. L., Reddy, V. and Zabel, M. K.** (2022). *Neuroanatomy, Dural Venous Sinuses*.
- Beall, A. C. and Rosenquist, T. H.** (1990). Smooth muscle cells of neural crest origin form the aorticopulmonary septum in the avian embryo. *Anat. Rec.* **226**, 360–366.
- Bell, L. A., Wallis, G. J. and Wilcox, K. S.** (2020). Reactivity and increased proliferation of NG2 cells following central nervous system infection with Theiler's murine encephalomyelitis virus. *J. Neuroinflammation* **17**, 1–14.
- Ben-Ari, Y., Gaiarsa, J. L., Tyzio, R. and Khazipov, R.** (2007). GABA: A pioneer transmitter that excites immature neurons and generates primitive oscillations. *Physiol. Rev.* **87**, 1215–1284.
- Berger, S. L.** (2007). The complex language of chromatin regulation during transcription. *Nature* **447**, 407–412.
- Biondi, G.** (1934). Zur Histopathologie des menschlichen Plexus chorioideus und des Ependyms. *Arch. Psychiat. Nervenkr.* **101**, 666–728.
- Blatt, G. J. and Fatemi, S. H.** (2011). Alterations in GABAergic biomarkers in the autism brain: Research findings and clinical implications. *Anat. Rec.* **294**, 1646–1652.
- Bolton, P. F., Dennis, N. R., Browne, C. E., Thomas, N. S., Veltman, M. W. M., Thompson, R. J. and Jacobs, P.** (2001). The phenotypic manifestations of interstitial duplications of proximal 15q with special reference to the autistic spectrum disorders. *Am. J. Med. Genet. - Neuropsychiatr. Genet.* **105**, 675–685.
- Bourassa, P., Tremblay, C., Schneider, J. A., Bennett, D. A. and Calon, F.** (2020). Brain mural cell loss in the parietal cortex in Alzheimer's disease correlates with cognitive decline and TDP-43 pathology. *Neuropathol. Appl. Neurobiol.* **46**, 458–477.
- Boutrus, M., Gilani, S. Z., Alvares, G. A., Maybery, M. T., Tan, D. W., Mian, A. and Whitehouse, A. J. O.** (2019). Increased facial asymmetry in autism spectrum conditions is associated with symptom presentation. *Autism Res.* **12**, 1774–1783.
- Bowden, C. L.** (2009). Anticonvulsants in bipolar disorders: current research and practice and future directions. *Bipolar Disord.* **11**, 20–33.
- Bozec, A., Sudaka, A., Toussan, N., Fischel, J. L., Etienne-Grimaldi, M. C. and Milano, G.** (2009). Combination of sunitinib, cetuximab and irradiation in an orthotopic head and neck cancer model. *Ann. Oncol.* **20**, 1703–1707.
- Bräutigam, K., Vakis, A. and Tsitsipanis, C.** (2019). Pathogenesis of idiopathic Normal Pressure Hydrocephalus: A review of knowledge. *J. Clin. Neurosci.* **61**, 10–13.
- Breier, G. and Risau, W.** (1996). The role of vascular endothelial growth factor in blood vessel formation. *Trends Cell Biol.* **6**, 454–456.

- Brierley, J. B. and Field, E. J.** (1948). The connexions of the spinal sub-arachnoid space with the lymphatic system. *J. Anat.* **82**, 153–66.
- Brinkmann, V.** (2018). Neutrophil Extracellular Traps in the Second Decade. *J. Innate Immun.* **10**, 414–421.
- Brinkmann, V., Reichard, U., Goosmann, C., Fauler, B., Uhlemann, Y., Weiss, D. S., Weinrauch, Y. and Zychlinsky, A.** (2004). Neutrophil Extracellular Traps Kill Bacteria. *Science (80-.).* **303**, 1532–1535.
- Bronner, M. E. and LeDouarin, N. M.** (2012). Development and evolution of the neural crest: An overview. *Dev. Biol.* **366**, 2–9.
- Brown, D. T., Izard, T. and Misteli, T.** (2006). Mapping the interaction surface of linker histone H10 with the nucleosome of native chromatin in vivo. *Nat. Struct. Mol. Biol.* **13**, 250–255.
- Brunelli, S., Faiella, A., Capra, V., Nigro, V., Simeone, A., Cama, A. and Boncinelli, E.** (1996). Germline mutations in the homeobox gene EMX2 in patients with severe schizencephaly. *Nat. Genet.* **12**, 94–96.
- Burri, P. H. and Djonov, V.** (2002). Intussusceptive angiogenesis - The alternative to capillary sprouting. *Mol. Aspects Med.* **23**, 1–27.
- Cabral, D. B. C., Bezerra, P. C., Miranda Filho, D. D. B. and Mendizabal, M. D. F. M. A.** (2008). Importância do exame do liquor de controle em meningite bacteriana como critério de alta. *Rev. Soc. Bras. Med. Trop.* **41**, 189–192.
- Cao, B. J. and Peng, N. A.** (1993). Magnesium valporoate attenuates hyperactivity induced by dexamphetamine-chlordiazepoxide mixture in rodents. *Eur. J. Pharmacol.* **237**, 177–181.
- Carpenter, S. J., McCarthy, L. E. and Borison, H. L.** (1970). Electron microscopic study on the epiplexus (Kolmer) cells of the cat choroid plexus. *Zeitschrift für Zellforsch. und Mikroskopische Anat.* **110**, 471–486.
- Casaca-Carreira, J., Temel, Y., Heschem, S. A. and Jahanshahi, A.** (2018). Transependymal Cerebrospinal Fluid Flow: Opportunity for Drug Delivery? *Mol. Neurobiol.* **55**, 2780–2788.
- Catala, M.** (1998). Embryonic and fetal development of structures associated with the cerebro-spinal fluid in man and other species. Part I: The ventricular system, meninges and choroid plexuses. *Arch. Anat. Cytol. Pathol.* **46**, 153–69.
- Cayea, P. D., Balcar, I., Alberti, O. and Jones, T. B.** (1984). Prenatal diagnosis of semilobar holoprosencephaly. *Am. J. Roentgenol.* **142**, 401–402.
- Charrier, J., Teillet, M., Lapointe, F. and Douarin, N. M. Le** (1999). Defining subregions of Hensen ' s node essential for caudalward movement , midline development and

cell survival. **4783**, 4771–4783.

- Chau, K. F., Springel, M. W., Broadbelt, K. G., Park, H. yeon, Topal, S., Lun, M. P., Mullan, H., Maynard, T., Steen, H., LaMantia, A. S., et al.** (2015). Progressive Differentiation and Instructive Capacities of Amniotic Fluid and Cerebrospinal Fluid Proteomes following Neural Tube Closure. *Dev. Cell* **35**, 789–802.
- Chau, K. F., Shannon, M. L., Fame, R. M., Fonseca, E., Mullan, H., Johnson, M. B., Sendamarai, A. K., Springel, M. W., Laurent, B. and Lehtinen, M. K.** (2018). Downregulation of ribosome biogenesis during early forebrain development. *Elife* **7**, 1–26.
- Cheeran, M. C. J., Lokensgard, J. R. and Schleiss, M. R.** (2009). Neuropathogenesis of congenital cytomegalovirus infection: Disease mechanisms and prospects for intervention. *Clin. Microbiol. Rev.* **22**, 99–126.
- Chen, V. S., Morrison, J. P., Southwell, M. F., Foley, J. F., Bolon, B. and Elmore, S. A.** (2017). Histology Atlas of the Developing Prenatal and Postnatal Mouse Central Nervous System, with Emphasis on Prenatal Days E7.5 to E18.5. *Toxicol. Pathol.* **45**, 705–744.
- Chess, S.** (1971). Autism in children with congenital rubella. *J. Autism Child. Schizophr.* **1**, 33–47.
- Chibon, P.** (1964). Analyse par la méthode de marquage nucléaire à la thymidine tritiée des dérivés de la crête neurale céphalique chez l'Urodèle *Pleurodeles waltlii* Michah. *C. R. Hebd. Seances Acad. Sci.* **259**, 3624–7.
- Chiesa, M., Nardou, R., Lozovaya, N., Eftekhari, S., Tyzio, R., Guimond, D., Ferrari, D. C. and Ben-Ari, Y.** (2019). Enhanced Glutamatergic Currents at Birth in Shank3 KO Mice. *Neural Plast.* **2019**, 1–11.
- Chow, B. W. and Gu, C.** (2015). The Molecular Constituents of the Blood–Brain Barrier. *Trends Neurosci.* **38**, 598–608.
- Christensen, J., Grønberg, T. K., Sørensen, M. J., Schendel, D., Parner, E. T., Pedersen, L. H. and Vestergaard, M.** (2013). Prenatal Valproate Exposure and Risk of Autism Spectrum Disorders and Childhood Autism. *JAMA* **309**, 1696.
- Christianson, A. L., Chesler, N. and Kromberg, J. G.** (1994). Fetal valproate syndrome: clinical and neuro-developmental features in two sibling pairs. *Dev. Med. Child Neurol.* **36**, 361–9.
- Clayton-Smith, J. and Donnai, D.** (1995). Syndrome of the month Fetal valproate syndrome. *JMed Genet* **32**, 724–727.
- Cobos, I., Shimamura, K., Rubenstein, J. L. R., Martínez, S. and Puelles, L.** (2001). Fate map of the avian anterior forebrain at the four-somite stage, based on the analysis of quail-chick chimeras. *Dev. Biol.* **239**, 46–67.

- Colville-Nash, P. R. and Willoughby, D. A.** (1997). Growth factors in angiogenesis: Current interest and therapeutic potential. *Mol. Med. Today* **3**, 14–23.
- Couly, G. F. and Le Douarin, N. M.** (1985). Mapping of the early neural primordium in quail-chick chimeras. I. Developmental relationships between placodes, facial ectoderm, and prosencephalon. *Dev. Biol.* **110**, 422–439.
- Couly, G., Coltey, P., Eichmann, A. and Le Douarin, N. M.** (1995). The angiogenic potentials of the cephalic mesoderm and the origin of brain and head blood vessels. *Mech. Dev.* **53**, 97–112.
- Creuzet, S. E.** (2009a). Neural crest contribution to forebrain development. *Semin. Cell Dev. Biol.* **20**, 751–759.
- Creuzet, S. E.** (2009b). Regulation of pre-otic brain development by the cephalic neural crest. *Proc. Natl. Acad. Sci. U. S. A.* **106**, 15774–15779.
- Creuzet, S., Couly, G., Vincent, C. and Le Douarin, N. M.** (2002). Negative effect of Hox gene expression on the development of the neural crest-derived facial skeleton. *Development* **129**, 4301–4313.
- Creuzet, S., Vincent, C. and Couly, G.** (2005). Neural crest derivatives in ocular and periocular structures. *Int. J. Dev. Biol.* **49**, 161–171.
- Creuzet, S. E., Martinez, S. and Le Douarin, N. M.** (2006). The cephalic neural crest exerts a critical effect on forebrain and midbrain development. *Proc. Natl. Acad. Sci. U. S. A.* **103**, 14033–14038.
- Crossley, P. H., Martinez, S., Ohkubo, Y. and Rubenstein, J. L. R.** (2001). Coordinate expression of Fgf8, Otx2, Bmp4, and Shh in the rostral prosencephalon during development of the telencephalic and optic vesicles. *Neuroscience* **108**, 183–206.
- Cserr, H. F., Harling-Berg, C. J. and Knopf, P. M.** (1992). Drainage of Brain Extracellular Fluid into Blood and Deep Cervical Lymph and its Immunological Significance. *Brain Pathol.* **2**, 269–276.
- Cui, J., Shipley, F. B., Shannon, M. L., Alturkistani, O., Dani, N., Webb, M. D., Sugden, A. U., Andermann, M. L. and Lehtinen, M. K.** (2020). Inflammation of the Embryonic Choroid Plexus Barrier following Maternal Immune Activation. *Dev. Cell* **55**, 617–628.e6.
- Currle, D. S., Cheng, X., Hsu, C. M. and Monuki, E. S.** (2005). Direct and indirect roles of CNS dorsal midline cells in choroid plexus epithelia formation. *Development* **132**, 3549–3559.
- Cushing, H.** (1914). Studies on the Cerebro-Spinal Fluid : I. Introduction. *J. Med. Res.* **31**, 1–19.
- Dandy, W. E.** (1919). Experimental Hydrocephalus. *Ann. Surg.* **70**, 129–142.

- Daneman, R. and Prat, A.** (2015). The Blood–Brain Barrier. *Cold Spring Harb. Perspect. Biol.* **7**, a020412.
- Dani, N., Herbst, R. H., McCabe, C., Green, G. S., Kaiser, K., Head, J. P., Cui, J., Shipley, F. B., Jang, A., Dionne, D., et al.** (2021). A cellular and spatial map of the choroid plexus across brain ventricles and ages. *Cell* **184**, 3056-3074.e21.
- De Morsier, G.** (1956). Studies on malformation of cranio-encephalic sutures. III. Agenesis of the septum lucidum with malformation of the optic tract. *Schweiz. Arch. Neurol. Psychiatr.* **77**, 267–92.
- Delahanty, R. J., Kang, J. Q., Brune, C. W., Kistner, E. O., Courchesne, E., Cox, N. J., Cook, E. H., Macdonald, R. L. and Sutcliffe, J. S.** (2011). Maternal transmission of a rare GABRB3 signal peptide variant is associated with autism. *Mol. Psychiatry* **16**, 86–96.
- Detwiler, S. R.** (1937). Application of Vital Dyes to the Study of Sheath Cell Origin. *Proc. Soc. Exp. Biol. Med.* **37**, 380–382.
- Di Gregorio, A.** (2020). *The notochord gene regulatory network in chordate evolution: Conservation and divergence from Ciona to vertebrates*. 1st ed. Elsevier Inc.
- Dib, M., Scharf, C. and Busch, C.** (2022). Recapitulating the Pharmacological Interactions of Cetuximab with Sunitinib and Cisplatin in Head and Neck Carcinoma Cells in vitro.
- Ding, R., Darland, D. C., Parmacek, M. S. and Amore, P. A. D.** (2004). Reveal Molecular Mechanisms of Smooth Muscle / Pericyte Differentiation. **520**, 509–520.
- Dömer, D., Walther, T., Möller, S., Behnen, M. and Laskay, T.** (2021). Neutrophil Extracellular Traps Activate Proinflammatory Functions of Human Neutrophils. *Front. Immunol.* **12**, 1–15.
- Domowicz, M. S., Sanders, T. A., Ragsdale, C. W. and Schwartz, N. B.** (2008). Aggrecan is expressed by embryonic brain glia and regulates astrocyte development. *Dev. Biol.* **315**, 114–124.
- Domowicz, M. S., Henry, J. G., Wadlington, N., Navarro, A., Kraig, R. P. and Schwartz, N. B.** (2011). Astrocyte precursor response to embryonic brain injury. *Brain Res.* **1389**, 35–49.
- Donoghue, P. C. J., Graham, A. and Kelsh, R. N.** (2008). The origin and evolution of the neural crest. *BioEssays* **30**, 530–541.
- Dore-Duffy, P. and Cleary, K.** (2011). Morphology and Properties of Pericytes. In *Methods in Molecular Biology*, pp. 49–68.
- Dorris, F.** (1938). The production of pigment in vitro by chick neural crest. *Wilhelm Roux. Arch. Entwickl. Mech. Org.* **138**, 323–334.

- DuShane, G. P.** (1935). An experimental study of the origin of pigment cells in Amphibia. *J. Exptl. Zool.* **72**, 1–31.
- Eberharter, A. and Becker, P. B.** (2002). Histone acetylation: A switch between repressive and permissive chromatin. Second in review on chromatin dynamics. *EMBO Rep.* **3**, 224–229.
- Echevarría, D., Vieira, C., Gimeno, L. and Martí, S.** (2003). Neuroepithelial secondary organizers and cell fate specification in the developing brain. **43**, 179–191.
- Egginton, S. and Gerritsen, M.** (2003). Lumen formation. In vivo versus in vitro observations. *Microcirculation* **10**, 45–61.
- Emrich, H. M., Zerssen, D., Kissling, W., Müller, H.-J. and Windorfer, A.** (1980). Effect of sodium valproate on mania. *Arch. Psychiatr. Nervenkr.* **229**, 1–16.
- Engelhardt, B. and Ransohoff, R. M.** (2005). The ins and outs of T-lymphocyte trafficking to the CNS: Anatomical sites and molecular mechanisms. *Trends Immunol.* **26**, 485–495.
- Epifanova, E., Babaev, A., Newman, A. G. and Tarabykin, V.** (2019). Role of Zeb2 / Sip1 in neuronal development. *Brain Res.* **1705**, 24–31.
- Erwin Neher and Bert Sakmann** (1976). Single-channel currents recorded from membrane of denervated frog muscle fibres. *Nature* **260**, 799–802.
- Estes, M. L. and McAllister, A. K.** (2016). Maternal immune activation: Implications for neuropsychiatric disorders. *Science (80-.).* **353**, 772–777.
- Etchevers, H., Couly, G., Vincent, C. and Le Douarin, N.** (1999). Anterior cephalic neural crest is required for forebrain viability. *Development* **126**, 3533–3543.
- Etchevers, H. C., Vincent, C., Le Douarin, N. M. and Couly, G. F.** (2001). The cephalic neural crest provides pericytes and smooth muscle cells to all blood vessels of the face and forebrain. *Development* **128**, 1059–1068.
- Etchevers, H. C., Couly, G. and Le Douarin, N. M.** (2002). Morphogenesis of the branchial vascular sector. *Trends Cardiovasc. Med.* **12**, 299–304.
- Evers, S.** (2008). Treatment of migraine with prophylactic drugs. *Expert Opin. Pharmacother.* **9**, 2565–2573.
- Faivre, S., Djelloul, S. and Raymond, E.** (2006). New Paradigms in Anticancer Therapy: Targeting Multiple Signaling Pathways With Kinase Inhibitors. *Semin. Oncol.* **33**, 407–420.
- Fame, R. M. and Lehtinen, M. K.** (2020). Emergence and Developmental Roles of the Cerebrospinal Fluid System. *Dev. Cell* **52**, 261–275.

- Fame, R. M., Chang, J. T., Hong, A., Aponte-Santiago, N. A. and Sive, H.** (2016). Directional cerebrospinal fluid movement between brain ventricles in larval zebrafish. *Fluids Barriers CNS* **13**.
- Fang, C. T., Ferng, W. F., Hwang, J. J., Yu, C. J., Chen, Y. C., Wang, M. H., Chang, S. C. and Hsieh, W. C.** (1997). *Life-threatening scrub typhus with meningoencephalitis and acute respiratory distress syndrome.*
- Faraco, G., Park, L., Anrather, J. and Iadecola, C.** (2017). Brain perivascular macrophages: characterization and functional roles in health and disease. *J. Mol. Med.* **95**, 1143–1152.
- Ferrara, N. and Alitalo, K.** (1999). Clinical applications of angiogenic growth factors and their inhibitors. *Nat. Med.* **5**, 1359–1364.
- Fruttiger, M.** (2002). Development of the mouse retinal vasculature: Angiogenesis versus vasculogenesis. *Investig. Ophthalmol. Vis. Sci.* **43**, 522–527.
- Fuchs, T. A., Abed, U., Goosmann, C., Hurwitz, R., Schulze, I., Wahn, V., Weinrauch, Y., Brinkmann, V. and Zychlinsky, A.** (2007). Novel cell death program leads to neutrophil extracellular traps. *J. Cell Biol.* **176**, 231–241.
- Fujimoto, T. and Singer, S. J.** (1987). Immunocytochemical studies of desmin and vimentin in pericapillary cells of chicken. *J. Histochem. Cytochem.* **35**, 1105–15.
- Fujimoto, T., Tokuyasu, K. T. and Singer, S. J.** (1987). Direct morphological demonstration of the coexistence of vimentin and desmin in the same intermediate filaments of vascular smooth muscle cells. *J. Submicrosc. Cytol.* **19**, 1–9.
- Gabbiani, G., Schmid, E., Winter, S., Chaponnier, C., de Ckhashtonay, C., Vandekerckhove, J., Weber, K. and Franke, W. W.** (1981). Vascular smooth muscle cells differ from other smooth muscle cells: Predominance of vimentin filaments and a specific α -type actin. *Proc. Natl. Acad. Sci. U. S. A.* **78**, 298–302.
- Gandal, M. J., Edgar, J. C., Ehrlichman, R. S., Mehta, M., Roberts, T. P. L. and Siegel, S. J.** (2010). Validating γ oscillations and delayed auditory responses as translational biomarkers of autism. *Biol. Psychiatry* **68**, 1100–1106.
- Ganguli, S. and Chavali, P. L.** (2021). Intrauterine Viral Infections: Impact of Inflammation on Fetal Neurodevelopment. *Front. Neurosci.* **15**, 1–14.
- Gans, C. and Northcutt, R. G.** (1983). Neural crest and the origin of vertebrates: A new head. *Science (80-)*. **220**, 268–274.
- Garavelli, L. and Mainardi, P. C.** (2007). Mowat-Wilson syndrome. **12**, 1–12.
- Garcez, R. C., Le Douarin, N. M. and Creuzet, S. E.** (2014). Combinatorial activity of Six1-2-4 genes in cephalic neural crest cells controls craniofacial and brain development. *Cell. Mol. Life Sci.* **71**, 2149–2164.

- Gardener, H., Spiegelman, D. and Buka, S. L.** (2011). Perinatal and neonatal risk factors for autism: A comprehensive meta-analysis. *Pediatrics* **128**, 344–355.
- Gąssowska-Dobrowolska, M., Cieślik, M., Czapski, G. A., Jęsko, H., Frontczak-Baniewicz, M., Gewartowska, M., Dominiak, A., Polowy, R., Filipkowski, R. K., Babiec, L., et al.** (2020). Prenatal exposure to valproic acid affects microglia and synaptic ultrastructure in a brain-region-specific manner in young-adult male rats: Relevance to autism spectrum disorders. *Int. J. Mol. Sci.* **21**,.
- Gato, Á., Moro, J. A., Alonso, M. I., Bueno, D., De La Mano, A. and Martín, C.** (2005). Embryonic cerebrospinal fluid regulates neuroepithelial survival, proliferation, and neurogenesis in chick embryos. *Anat. Rec. - Part A Discov. Mol. Cell. Evol. Biol.* **284**, 475–484.
- Gerganova, G., Riddell, A. and Miller, A. A.** (2022). CNS border-associated macrophages in the homeostatic and ischaemic brain. *Pharmacol. Ther.* **240**, 108220.
- Gerlai, R.** (2014). Social behavior of zebrafish: From synthetic images to biological mechanisms of shoaling. *J. Neurosci. Methods* **234**, 59–65.
- Ghafouri, M., Amini, S., Khalili, K. and Sawaya, B. E.** (2006). HIV-1 associated dementia: Symptoms and causes. *Retrovirology* **3**, 1–11.
- Gherzi-Egea, J. F., Strazielle, N., Catala, M., Silva-Vargas, V., Doetsch, F. and Engelhardt, B.** (2018). Molecular anatomy and functions of the choroidal blood-cerebrospinal fluid barrier in health and disease. *Acta Neuropathol.* **135**, 337–361.
- Gilbert, B. &** (2019). *Developmental Biology*.
- Ginhoux, F., Greter, M., Leboeuf, M., Nandi, S., See, P., Gokhan, S., Mehler, M. F., Conway, S. J., Ng, L. G., Stanley, E. R., et al.** (2010). Fate Mapping Analysis Reveals That Adult Microglia Derive from Primitive Macrophages. *Science (80-.)*. **330**, 841–845.
- Girolamo, F., de Trizio, I., Errede, M., Longo, G., d’Amati, A. and Virgintino, D.** (2021). Neural crest cell-derived pericytes act as pro-angiogenic cells in human neocortex development and gliomas. *Fluids Barriers CNS* **18**, 1–26.
- Glaser, T., Ton, C. C. T., Mueller, R., Petzl-Erler, M. L., Oliver, C., Nevin, N. C., Housman, D. E. and Maas, R. L.** (1994). Absence of PAX6 Gene Mutations in Gillespie Syndrome (Partial Aniridia, Cerebellar Ataxia, and Mental Retardation). *Genomics* **19**, 145–148.
- Glynn, M. W., Elmer, B. M., Garay, P. A., Liu, X., Leigh, A., El-sabeawy, F. and Mcallister, A. K.** (2012). Establishment of Cortical Connections. **14**, 442–451.
- Goldmann, T., Wieghofer, P., Prutek, F., Hagemeyer, N., Frenzel, K., Staszewski, O., Kierdorf, K., Amann, L., Krueger, M., Locatelli, G., et al.** (2016). Origin, fate and dynamics of macrophages at CNS interfaces Tobias. **17**, 797–805.
- Goronowitsch, N.** (1893). Untersuchungen über die Entwicklung der

sog.“Ganglienleisten“ im Kopfe der Vögelembryonen. *Morph Jahrb* **20**, 187–259.

Gothelf, D., Furfaro, J. A., Hoeft, F., Eckert, M. A., Hall, S. S., Hara, R. O., Erba, H. W., Ringel, J., Hayashi, K. M., Patnaik, S., et al. (2009). Neuroanatomy of fragile X syndrome is associated with aberrant behavior and the fragile X mental retardation protein (FMRP). *NIH Public Access* **63**, 40–51.

Gräff, J. and Mansuy, I. M. (2008). Epigenetic codes in cognition and behaviour. *Behav. Brain Res.* **192**, 70–87.

Grant, P. A., Eberharter, A., John, S., Cook, R. G., Turner, B. M. and Workman, J. L. (1999). Expanded lysine acetylation specificity of Gcn5 in native complexes. *J. Biol. Chem.* **274**, 5895–5900.

Grapin-botton, A., Bonnin, M., Sieweke, M. and Douarin, N. M. Le (1998). Defined concentrations of a posteriorizing signal are critical for MafB / Kreisler segmental expression in the hindbrain. **1181**, 1173–1181.

Grassé, P.-P. (1975). Le système nerveux des insectes. *Trait Zool.* **3**, 321–510.

Gregory, L. C., Gergics, P., Nakaguma, M., Bando, H., Patti, G., McCabe, M. J., Fang, Q., Ma, Q., Ozel, A. B., Li, J. Z., et al. (2021). The phenotypic spectrum associated with OTX2 mutations in humans.

Gridelli, C., Maione, P., Del Gaizo, F., Colantuoni, G., Guerriero, C., Ferrara, C., Nicoletta, D., Comunale, D., De Vita, A. and Rossi, A. (2007). Sorafenib and Sunitinib in the Treatment of Advanced Non-Small Cell Lung Cancer. *Oncologist* **12**, 191–200.

Grzadzinski, R., Huerta, M. and Lord, C. (2013). DSM-5 and autism spectrum disorders (ASDs): An opportunity for identifying ASD subtypes. *Mol. Autism* **4**, 2–7.

Guak, H. and Krawczyk, C. M. (2020). Implications of cellular metabolism for immune cell migration. *Immunology* **161**, 200–208.

Güntürkün, O., von Eugen, K., Packheiser, J. and Pusch, R. (2021). Avian pallial circuits and cognition: A comparison to mammals. *Curr. Opin. Neurobiol.* **71**, 29–36.

Guo, J., Marcotte, P. A., McCall, J. O., Dai, Y., Pease, L. J., Michaelides, M. R., Davidsen, S. K. and Glaser, K. B. (2006). Inhibition of phosphorylation of the colony-stimulating factor-1 receptor (c-Fms) tyrosine kinase in transfected cells by ABT-869 and other tyrosine kinase inhibitors. *Mol. Cancer Ther.* **5**, 1007–1013.

Gupta, R. and Sen, N. (2016). Traumatic brain injury: a risk factor for neurodegenerative diseases. **27**, 93–100.

Gurvich, N., Berman, M. G., Wittner, B. S., Gentleman, R. C., Klein, P. S. and Green, J. B. A. (2005). Association of valproate-induced teratogenesis with histone deacetylase inhibition in vivo. *FASEB J.* **19**, 1166–1168.

- Hall, B. K.** (1999). Chordate and Vertebrate Origins and Diversification. *Evol. Dev. Biol.*
- Hall, A. C., Brennan, A., Goold, R. G., Cleverley, K., Lucas, F. R., Gordon-Weeks, P. R. and Salinas, P. C.** (2002). Valproate regulates GSK-3-mediated axonal remodeling and synapsin I clustering in developing neurons. *Mol. Cell. Neurosci.* **20**, 257–270.
- Hamburger, V. and Hamilton, H. L.** (1951). A series of normal stages in the development of the chick embryo. *Dev. Dyn.* **88**, 49–92.
- Hammond, W. S. and Yntema, C. L.** (1947). Depletions in the thoraco-lumbar sympathetic system following removal of neural crest in the chick. *J. Comp. Neurol.* **86**, 237–265.
- Harakalova, M., Boogaard, M. Van Den, Sinke, R., Lieshout, S. Van, Tuil, M. C. Van, Duran, K., Renkens, I., Terhal, P. A., Kovel, C. De, Nijman, I. J., et al.** (2012). X-exome sequencing identifies a HDAC8 variant in a large pedigree with X-linked intellectual disability, truncal obesity, gynaecomastia, hypogonadism and unusual face. 539–543.
- Harrison, R. G.** (1924). Neuroblast versus sheath cell in the development of peripheral nerves. *J. Comp. Neurol.* **37**, 123–205.
- He, Y., Li, Z., Shi, X., Ding, J. and Wang, X.** (2022). Roles of NG2 Glia in Cerebral Small Vessel Disease. *Neurosci. Bull.*
- Hellström, M., Kalén, M., Lindahl, P., Abramsson, A. and Betsholtz, C.** (1999). Role of PDGF-B and PDGFR- β in recruitment of vascular smooth muscle cells and pericytes during embryonic blood vessel formation in the mouse. *Development* **126**, 3047–3055.
- Hensen, V.** (1876). Beobachtungen über die Befruchtung und Entwicklung des Kaninchens and Meerschweinchens. *Zool. Anat. Entwickl. Gesch.* **1**, 353–423.
- Hilber, H.** (1942). Experimentelle Studien zum Schicksal des Rumpfganglienleistenmaterials.
- Hirose, T., Hamaguchi, S., Matsumoto, N., Irisawa, T., Seki, M., Tasaki, O., Hosotsubo, H., Yamamoto, N., Yamamoto, K., Akeda, Y., et al.** (2014). Presence of neutrophil extracellular traps and citrullinated histone H3 in the bloodstream of critically ill patients. *PLoS One* **9**, 1–9.
- His, W.** (1868). Untersuchungen über die erste Anlage des Wirbelthierleibes: die erste Entwicklung des Hühnchens im Ei. *F.C.W. Vogel, Leipzig.*
- Hodgkin, A. L. and Huxley, A. F.** (1952). The components of membrane conductance in the giant axon of *Loligo*. *J. Physiol.* **116**, 473–496.
- Holland, L. Z. and Holland, N. D.** (2001). Evolution of neural crest and placodes: Amphioxus as a model for the ancestral vertebrate? *J. Anat.* **199**, 85–98.

- Hörstadius, S. and Sellman, S.** (1946). Experimentelle Untersuchungen über die Determination des Knorpeligen Kopfskelettes bei Urodellen. *Almqvist & Wiksell*.
- Hosoya, Y. and Fujita, T.** (1973). Scanning electron microscope observation of intraventricular macrophages (kolmer cells) in the rat brain. *Arch. Histol. Jpn.* **35**, 133–140.
- Huang, F.-J., You, W., Bonaldo, P., Seyfried, T. N., Pasquale, E. B. and Stallcup, W. B.** (2011). Pericyte Deficiencies Lead To Aberrant Tumor. *Dev. Biol.* **344**, 1035–1046.
- Hunter, N. L. and Dymecki, S. M.** (2007). Molecularly and temporally separable lineages form the hindbrain roof plate and contribute differentially to the choroid plexus. *Development* **134**, 3449–3460.
- Hurmuzache, Luca, C., Lovin, I. and Dorobat, C.** (2012). *Tuberculosis meningo-encephalitis with positive csf for KB and slowly favourable evolution. Case report.*
- Iizuka, N., Morita, A., Kawano, C., Mori, A., Sakamoto, K., Kuroyama, M., Ishii, K. and Nakahara, T.** (2018). Anti-angiogenic effects of valproic acid in a mouse model of oxygen-induced retinopathy. *J. Pharmacol. Sci.* **138**, 203–208.
- Jeffrey L. Neul, Kaufmann, W. E., Glaze, D. G., Christodoulou, J., Clarke, A. J., Bahi-Buisson, N., Leonard, H., Bailey, M. E. S., Schanen, N. C., Zappella, M., et al.** (2010). Rett syndrome: Revised diagnostic criteria and nomenclature. *Ann. Neurol.* **68**, 944–950.
- Jentink, J., Loane, M. A., Dolk, H., Barisic, I., Garne, E., Morris, J. K. and Den Berg, L. T. W. D. J. Van** (2010). Valproic acid monotherapy in pregnancy and major congenital malformations. *Obstet. Gynecol. Surv.* **65**, 619–620.
- Jessen, N. A., Munk, A. S. F., Lundgaard, I. and Nedergaard, M.** (2015). The Glymphatic System: A Beginner's Guide. *Neurochem. Res.* **40**, 2583–2599.
- Jindatip, D., Fujiwara, K., Kouki, T. and Yashiro, T.** (2012). Transmission and scanning electron microscopy study of the characteristics and morphology of pericytes and novel desmin-immunopositive perivascular cells before and after castration in rat anterior pituitary gland. *Anat. Sci. Int.* **87**, 165–173.
- Joel D Boerckel, Devon E Mason, Anna M McDermott, E. A.** (2014). Microcomputed tomography: approaches and applications in bioengineering. *Stem Cell Res. Ther.* **5**, 144.
- Johnston, M. C.** (1966). A radioautographic study of the migration and fate of cranial neural crest cells in the chick embryo. *Anat. Rec.* **156**, 143–155.
- Joukal, M., Klusáková, I., Solár, P., Kuklová, A. and Dubový, P.** (2016). Cellular reactions of the choroid plexus induced by peripheral nerve injury. *Neurosci. Lett.* **628**, 73–77.
- Jung, G. A., Yoon, J. Y., Moon, B. S., Yang, D. H., Kim, H. Y., Lee, S. H., Bryja, V., Arenas,**

- E. and Choi, K. Y.** (2008). Valproic acid induces differentiation and inhibition of proliferation in neural progenitor cells via the beta-catenin-Ras-ERK- p21 Cip/WAF1 pathway. *BMC Cell Biol.* **9**, 1–12.
- Kadir, L. A., Stacey, M. and Barrett-Jolley, R.** (2018). Emerging roles of the membrane potential: Action beyond the action potential. *Front. Physiol.* **9**, 1–10.
- Kalueff, A. V., Stewart, A. M. and Gerlai, R.** (2014). Zebrafish as an emerging model for studying complex brain disorders. *Trends Pharmacol. Sci.* **35**, 63–75.
- Karam, M., Janbon, H., Malkinson, G. and Brunet, I.** (2022). Heterogeneity and developmental dynamics of LYVE-1 perivascular macrophages distribution in the mouse brain. *J. Cereb. Blood Flow Metab.* **42**, 1797–1812.
- Karimy, J. K., Duran, D., Hu, J. K. J. K., Gavankar, C., Gaillard, J. R., Bayri, Y., Rice, H., DiLuna, M. L., Gerzanich, V., Simard, J. M., et al.** (2016). Cerebrospinal fluid hypersecretion in pediatric hydrocephalus. *Neurosurg. Focus* **41**, 1–11.
- Kastschenko, N.** (1888). Zur Entwicklungsgeschichte des Selachierembryos. *Anat. Anz.* **3**, 445–467.
- Kataoka, S., Takuma, K., Hara, Y., Maeda, Y., Ago, Y. and Matsuda, T.** (2013). Autism-like behaviours with transient histone hyperacetylation in mice treated prenatally with valproic acid. *Int. J. Neuropsychopharmacol.* **16**, 91–103.
- Keep, R. F. and Jones, H. C.** (1990). A morphometric study on the development of the lateral ventricle choroid plexus, choroid plexus capillaries and ventricular ependyma in the rat. *Dev. Brain Res.* **56**, 47–53.
- Kelley, C., D'Amore, P., Hechtman, H. B. and Shepro, D.** (1987). Microvascular pericyte contractility in vitro: Comparison with other cells of the vascular wall. *J. Cell Biol.* **104**, 483–490.
- Kendell, R. E.** (1989). Maternal Influenza in the Etiology of Schizophrenia. *Arch. Gen. Psychiatry* **46**, 878.
- Kierdorf, K., Masuda, T., Jordão, M. J. C. and Prinz, M.** (2019). Macrophages at CNS interfaces: ontogeny and function in health and disease. *Nat. Rev. Neurosci.* **20**, 547–562.
- King, L. S. and Keeler, C. E.** (1932). Absence of Corpus Callosum, a Hereditary Brain Anomaly of the House Mouse. Preliminary Report. *Proc. Natl. Acad. Sci.* **18**, 525–528.
- Kirby, M. L.** (1988). Nodose placode contributes autonomic neurons to the heart in the absence of cardiac neural crest. *J. Neurosci.* **8**, 1089–1095.
- Kirby, M. L. and Waldo, K. L.** (1990). Role of neural crest in congenital heart disease. *Circulation* **82**, 332–340.

- Koduri, S., Daou, B., Hua, Y., Keep, R., Xi, G. and Pandey, A. S.** (2020). Mechanisms of Post-Hemorrhagic Stroke Hydrocephalus Development: The Role of Kolmer Epiplexus Cells. *World Neurosurg.* **144**, 256–257.
- Koecke, H. U.** (1960). Untersuchungen über die regionalen Potenzen der Neuralleiste zur Bildung von Melanoblasten bei der Hausente (*Anas domestica*). *Arch. Entwicklungsmech. Organ.* **151**, 612–659.
- Kokovay, E., Wang, Y., Kusek, G., Wurster, R., Lederman, P., Lowry, N., Shen, Q. and Temple, S.** (2012). VCAM1 is essential to maintain the structure of the SVZ niche and acts as an environmental sensor to regulate SVZ lineage progression. *Cell Stem Cell* **11**, 220–230.
- Kostecki, K., De Jesus, O. and Pearson-Shaver, A. L.** (2022). *Subfalcine Herniation*.
- Krauer, F., Riesen, M., Reveiz, L., Oladapo, O. T., Martínez-Vega, R., Porgo, T. V., Haefliger, A., Broutet, N. J. and Low, N.** (2017). Zika Virus Infection as a Cause of Congenital Brain Abnormalities and Guillain–Barré Syndrome: Systematic Review. *PLOS Med.* **14**, e1002203.
- Kukino, K. and Deguchi, T.** (1977). Effects of sodium dipropylacetate on gamma-aminobutyric acid and biogenic amines in rat brain. *Chem. Pharm. Bull. (Tokyo)*. **25**, 2257–62.
- Kunz, J., Krause, D., Kremer, M. and Dermietzel, R.** (1994). The 140-kDa Protein of Blood-Brain Barrier-Associated Pericytes Is Identical to Aminopeptidase N. *J. Neurochem.* **62**, 2375–2386.
- Kupffer, C.** (1868). Beobachtungen fiber die Entwicklung. *Anatomie* 209–272.
- Kyle, S. M., Vashi, N. and Justice, M. J.** (2018). Rett syndrome : a neurological disorder with metabolic components.
- Lambert, P. A., Carraz, G., Borselli, S. and Bouchardy, M.** (1975). Dipropylacetamide in the treatment of manic-depressive psychosis. *Encephale.* **1**, 25–31.
- Langford, M. B., O’Leary, C. J., Veeraval, L., White, A., Lanoue, V. and Cooper, H. M.** (2020). WNT5a Regulates Epithelial Morphogenesis in the Developing Choroid Plexus. *Cereb. Cortex* **30**, 3617–3631.
- Le Douarin, N. M.** (1969). Details of the interphase nucleus in Japanese quail (*Cortunix cortunix japonica*). *Bull. Biol. Fr. Belg.* **103**, 435–452.
- Le Douarin, N. M.** (1982). *The Neural Crest*. Cambridge Univ. Press. Cambridge.
- Le Douarin, N. M. and Dupin, E.** (2018). The “beginnings” of the neural crest. *Dev. Biol.* **444**, S3–S13.
- Le Douarin, N. and Kalcheim, C.** (1999). *The Neural Crest*. Cambridge University Press.

- Le Douarin, N. M. and Teillet, M. A. M.** (1974). Experimental analysis of the migration and differentiation of neuroblasts of the autonomic nervous system and of neuroectodermal mesenchymal derivatives, using a biological cell marking technique. *Dev. Biol.* **41**, 162–184.
- Le Douarin, N. M., Couly, G. and Creuzet, S. E.** (2012). The neural crest is a powerful regulator of pre-otic brain development. *Dev. Biol.* **366**, 74–82.
- Le Douarin N.M., Creuzet, S., Couly, G., and Dupin, E.** (2004). Neural crest cell plasticity and its limits. *Development* **131**, 4637–4650.
- Le Lievre, C. S.** (1976). Contribution des crêtes neurales à la genèse des structures céphaliques et cervicales chez les Oiseaux.
- Le Lievre, C. S. and Le Douarin, N. M.** (1975). Mesenchymal derivatives of the neural crest: analysis of chimaeric quail and chick embryos. *J. Embryol. Exp. Morphol.* **34**, 125–154.
- Lemche, E.** (2020). Research evidence from studies on filial imprinting , attachment , and early life stress : a new route for scientific integration. 127–133.
- Levéen, P., Pekny, M., Gebre-Medhin, S., Swolin, B., Larsson, E. and Betsholtz, C.** (1994). Mice deficient for PDGF B show renal, cardiovascular, and hematological abnormalities. *Genes Dev.* **8**, 1875–1887.
- Levine, J. M. and Card, J. P.** (1987). Light and electron microscopic localization of a cell surface antigen (NG2) in the rat cerebellum: association with smooth protoplasmic astrocytes. *J. Neurosci.* **7**, 2711–2720.
- Li, P., Li, M., Lindberg, M. R., Kennett, M. J., Xiong, N. and Wang, Y.** (2010). PAD4 is essential for antibacterial innate immunity mediated by neutrophil extracellular traps. *J. Exp. Med.* **207**, 1853–1862.
- Li, M., Lin, C., Leso, A. and Nefedova, Y.** (2020). Quantification of citrullinated histone h3 bound dna for detection of neutrophil extracellular traps. *Cancers (Basel)*. **12**, 1–11.
- Li, G., Liu, J., Guan, Y. and Ji, X.** (2021). The role of hypoxia in stem cell regulation of the central nervous system: From embryonic development to adult proliferation. *CNS Neurosci. Ther.* **27**, 1446–1457.
- Lindahl, P., Johansson, B. R., Levéen, P. and Betsholtz, C.** (1997). Pericyte loss and microaneurysm formation in PDGF-B-deficient mice. *Science (80-)*. **277**, 242–245.
- Lindvall, M., Edvinsson, L. and Owman, C.** (1978). Sympathetic nervous control of cerebrospinal fluid production from the choroid plexus. *Science (80-)*. **201**, 176–178.
- Llovera, G., Benakis, C., Enzmann, G., Cai, R., Arzberger, T., Ghasemigharagoz, A., Mao, X., Malik, R., Lazarevic, I., Liebscher, S., et al.** (2017). The choroid plexus is a key cerebral invasion route for T cells after stroke. *Acta Neuropathol.* **134**, 851–868.

- Lood, C., Blanco, L. P., Purmalek, M. M., Carmona-Rivera, C., De Ravin, S. S., Smith, C. K., Malech, H. L., Ledbetter, J. A., Elkon, K. B. and Kaplan, M. J.** (2016). Neutrophil extracellular traps enriched in oxidized mitochondrial DNA are interferogenic and contribute to lupus-like disease. *Nat. Med.* **22**, 146–153.
- Lorenz, K.** (1935). Der Kumpan in der Umwelt des Vogels – Der Artgenosse als auslösendes Moment sozialer Verhaltensweisen. 115–282.
- Löscher, W.** (2002). Basic Pharmacology of Valproate. *CNS Drugs* **16**, 669–694.
- Louveau, A., Smirnov, I., Keyes, T. J., Eccles, J. D., Rouhani, S. J., Peske, J. D., Derecki, N. C., Castle, D., Mandell, J. W., Lee, K. S., et al.** (2015). Structural and functional features of central nervous system lymphatic vessels. *Nature* **523**, 337–341.
- Louveau, A., Plog, B. A., Antila, S., Alitalo, K., Nedergaard, M. and Kipnis, J.** (2017). Understanding the functions and relationships of the glymphatic system and meningeal lymphatics. *J. Clin. Invest.* **127**, 3210–3219.
- Ma, D. Q., Whitehead, P. L., Menold, M. M., Martin, E. R., Ashley-Koch, A. E., Mei, H., Ritchie, M. D., DeLong, G. R., Abramson, R. K., Wright, H. H., et al.** (2005). Identification of significant association and gene-gene interaction of GABA receptor subunit genes in autism. *Am. J. Hum. Genet.* **77**, 377–388.
- Ma, Q., Ries, M., Decker, Y., Müller, A., Riner, C., Bücker, A., Fassbender, K., Detmar, M. and Proulx, S. T.** (2019). Rapid lymphatic efflux limits cerebrospinal fluid flow to the brain. *Acta Neuropathol.* **137**, 151–165.
- MacDonald, B. T., Tamai, K. and He, X.** (2009). Wnt/ β -Catenin Signaling: Components, Mechanisms, and Diseases. *Dev. Cell* **17**, 9–26.
- Markram, H., Rinaldi, T. and Markram, K.** (2007). The intense world syndrome--an alternative hypothesis for autism. *Front. Neurosci.*
- Markram, K., Rinaldi, T., Mendola, D. La, Sandi, C. and Markram, H.** (2008). Abnormal fear conditioning and amygdala processing in an animal model of autism. *Neuropsychopharmacology* **33**, 901–912.
- Marshall, M.** (1879). The morphology of the vertebrate olfactory organ.
- Martik, M. L. and Bronner, M. E.** (2017). Regulatory Logic Underlying Diversification of the Neural Crest. *Trends Genet.* **33**, 715–727.
- Martínez-Cerdeño, V., García-Moreno, F., Tosches, M. A., Csillag, A., Manger, P. R. and Molnár, Z.** (2018). Update on forebrain evolution: From neurogenesis to thermogenesis. *Semin. Cell Dev. Biol.* **76**, 15–22.
- Martinsen, B. J.** (2005). Reference guide to the stages of chick heart embryology. *Dev. Dyn.* **233**, 1217–1237.

- Mast, T. J., Cukierski, M. A., Nau, H. and Hendrickx, A. G.** (1986). Predicting the human teratogenic potential of the anticonvulsant, valproic acid, from a non-human primate model. *Toxicology* **39**, 111–119.
- McFarlane, H. G., Kusek, G. K., Yang, M., Phoenix, J. L., Bolivar, V. J. and Crawley, J. N.** (2008). Autism-like behavioral phenotypes in BTBR T+tf/J mice. *Genes, Brain Behav.* **7**, 152–163.
- Medeiros, D. M.** (2013). The evolution of the neural crest: New perspectives from lamprey and invertebrate neural crest-like cells. *Wiley Interdiscip. Rev. Dev. Biol.* **2**, 1–15.
- Mednick, S. A.** (1988). Adult Schizophrenia Following Prenatal Exposure to an Influenza Epidemic. *Arch. Gen. Psychiatry* **45**, 189.
- Mehl, L. C., Manjally, A. V., Bouadi, O., Gibson, E. M. and Tay, T. L.** (2022). Microglia in brain development and regeneration. *Dev.* **149**, 1–14.
- Mei, Y., Monteiro, P., Zhou, Y., Kim, J.-A., Gao, X., Fu, Z. and Feng, G.** (2016). Adult restoration of Shank3 expression rescues selective autistic-like phenotypes. *Nature* **530**, 481–484.
- Melo, A. I., Lovic, V., Gonzalez, A., Madden, M., Sinopoli, K. and Fleming, A. S.** (2006). Maternal and littermate deprivation disrupts maternal behavior and social-learning of food preference in adulthood: Tactile stimulation, nest odor, and social rearing prevent these effects. *Dev. Psychobiol.* **48**, 209–219.
- Mendel, D. B., Laird, A. D., Xin, X., Louie, S. G., Christensen, J. G., Li, G., Schreck, R. E., Abrams, T. J., Ngai, T. J., Lee, L. B., et al.** (2003). In vivo antitumor activity of SU11248, a novel tyrosine kinase inhibitor targeting vascular endothelial growth factor and platelet-derived growth factor receptors: determination of a pharmacokinetic/pharmacodynamic relationship. *Clin. Cancer Res.* **9**, 327–37.
- Mercier, F., Cho Kwon, Y. and Kodama, R.** (2011). Meningeal/vascular alterations and loss of extracellular matrix in the neurogenic zone of adult BTBR T+ tf/J mice, animal model for autism. *Neurosci. Lett.* **498**, 173–178.
- Meulemans, D. and Bronner-Fraser, M.** (2004). Gene-regulatory interactions in neural crest evolution and development. *Dev. Cell* **7**, 291–299.
- Michaelis, M., Michaelis, U. R., Fleming, I., Suhan, T., Cinatl, J., Blaheta, R. A., Hoffmann, K., Kotchetkov, R., Busse, R., Nau, H., et al.** (2004). Valproic Acid Inhibits Angiogenesis in Vitro and in Vivo. *Mol. Pharmacol.* **65**, 520–527.
- Miles, J. H.** (2011). Autism spectrum disorders-A genetics review. *Genet. Med.* **13**, 278–294.
- Mohanam, S., Cherrington, B. D., Horibata, S., McElwee, J. L., Thompson, P. R. and Coonrod, S. A.** (2012). Potential role of peptidylarginine deiminase enzymes and protein citrullination in cancer pathogenesis. *Biochem. Res. Int.* **2012**,.

- Moldrich, R. X., Leanage, G., She, D., Dolan-Evans, E., Nelson, M., Reza, N. and Reutens, D. C.** (2013). Inhibition of histone deacetylase in utero causes sociability deficits in postnatal mice. *Behav. Brain Res.* **257**, 253–264.
- Mollanji, R., Bozanovic-Sosic, R., Zakharov, A., Makarian, L. and Johnston, M. G.** (2002). Blocking cerebrospinal fluid absorption through the cribriform plate increases resting intracranial pressure. *Am. J. Physiol. - Regul. Integr. Comp. Physiol.* **282**, 1593–1599.
- Monuki, E. S., Porter, F. D. and Walsh, C. A.** (2001). Patterning of the dorsal telencephalon and cerebral cortex by a roof plate-lhx2 pathway. *Neuron* **32**, 591–604.
- Morrison, B. M., Lee, Y. and Rothstein, J. D.** (2013). Oligodendroglia: metabolic supporters of axons. *Trends Cell Biol.* **23**, 644–651.
- Mrdjen, D., Pavlovic, A., Hartmann, F. J., Schreiner, B., Utz, S. G., Leung, B. P., Lelios, I., Heppner, F. L., Kipnis, J., Merkler, D., et al.** (2018). High-Dimensional Single-Cell Mapping of Central Nervous System Immune Cells Reveals Distinct Myeloid Subsets in Health, Aging, and Disease. *Immunity* **48**, 380-395.e6.
- Muoio, V., Persson, P. B. and Sendeski, M. M.** (2014). The neurovascular unit - concept review. *Acta Physiol.* **210**, 790–798.
- Nakahara, T., Morita, A., Yagasaki, R., Mori, A. and Sakamoto, K.** (2017). Mammalian Target of Rapamycin (mTOR) as a Potential Therapeutic Target in Pathological Ocular Angiogenesis. *Biol. Pharm. Bull.* **40**, 2045–2049.
- Nakamura, S., Koga, N. and Moriyasu, N.** (1982). Epilexus cell (Kolmer cell) and its reaction against foreign bodies. *No To Shinkei* **34**, 895–907.
- Nakashima, K., Hagiwara, T., Ishigami, A., Nagata, S., Asaga, H., Kuramotot, M., Senshu, T. and Yamada, M.** (1999). Molecular characterization of peptidylarginine deiminase in HL-60 cells induced by retinoic acid and 1 α ,25-dihydroxyvitamin D3. *J. Biol. Chem.* **274**, 27786–27792.
- Nakashima, K., Hagiwara, T. and Yamada, M.** (2002). Nuclear localization of peptidylarginine deiminase V and histone deimination in granulocytes. *J. Biol. Chem.* **277**, 49562–49568.
- Nakatsu, T.** (2000). Neural tube closure in humans initiates at multiple sites: Evidence from human embryos and implications for the pathogenesis of neural tube defects. *Anat. Embryol. (Berl)*. **201**, 455–466.
- Nau, H., Hauck, R. -S and Ehlers, K.** (1991). Valproic Acid-Induced Neural Tube Defects in Mouse and Human: Aspects of Chirality, Alternative Drug Development, Pharmacokinetics and Possible Mechanisms. *Pharmacol. Toxicol.* **69**, 310–321.
- Nawar, G.** (1956). Experimental analysis of the origin of the autonomic ganglia in the chick embryo. *Am. J. Anat.* **99**, 473–505.

- Neeli, I., Khan, S. N. and Radic, M.** (2008). Histone Deimination As a Response to Inflammatory Stimuli in Neutrophils. *J. Immunol.* **180**, 1895–1902.
- Nehls, V. and Drenckhahn, D.** (1993). The versatility of microvascular pericytes: from mesenchyme to smooth muscle? *Histochemistry* **99**, 1–12.
- Neuwelt, E. A., Bauer, B., Fahlke, C., Fricker, G., Iadecola, C., Janigro, D., Leybaert, L., Molnár, Z., O'Donnell, M. E., Powlischock, J. T., et al.** (2011). Engaging neuroscience to advance translational research in brain barrier biology. *Nat. Rev. Neurosci.* **12**, 169–182.
- Nevo, N., Lecourt, S., Bièche, I., Kucia, M., Cras, A., Blandinieres, A., Vacher, S., Gendron, N., Guerin, C. L., Ratajczak, M. Z., et al.** (2020). Valproic Acid Decreases Endothelial Colony Forming Cells Differentiation and Induces Endothelial-to-Mesenchymal Transition-like Process. *Stem Cell Rev. Reports* **16**, 357–368.
- Nicolini, C. and Fahnstock, M.** (2018). The valproic acid-induced rodent model of autism. *Exp. Neurol.* **299**, 217–227.
- Nielsen, C. M. and Dymecki, S. M.** (2010). Sonic hedgehog is required for vascular outgrowth in the hindbrain choroid plexus. *Dev. Biol.* **340**, 430–437.
- Nilubol, N., Merkel, R., Yang, L., Patel, D., Reynolds, J. C., Sadowski, S. M., Neychev, V. and Kebebew, E.** (2017). A phase II trial of valproic acid in patients with advanced, radioiodine-resistant thyroid cancers of follicular cell origin. *Clin. Endocrinol. (Oxf)*. **86**, 128–133.
- Nishibatake, M., Kirby, M. L. and Van Mierop, L. H. S.** (1987). Pathogenesis of persistent truncus arteriosus and dextroposed aorta in the chick embryo after neural crest ablation. *Circulation* **75**, 255–264.
- Northcutt, R. G.** (2002). Understanding vertebrate brain evolution. *Integr. Comp. Biol.* **42**, 743–756.
- Nottebohm, F.** (2002). Neuronal replacement in adult brain. *Brain Res. Bull.* **57**, 737–749.
- O'Farrell, A. M., Abrams, T. J., Yuen, H. A., Ngai, T. J., Louie, S. G., Yee, K. W. H., Wong, L. M., Hong, W., Lee, L. B., Town, A., et al.** (2003). SU11248 is a novel FLT3 tyrosine kinase inhibitor with potent activity in vitro and in vivo. *Blood* **101**, 3597–3605.
- Olsen, J. J., Pohl, S. Ö., Deshmukh, A., Visweswaran, M. and Natalie, C.** (2017). The Role of Wnt Signalling in Angiogenesis. **1**, 131–142.
- O'Rahilly, R. and Müller, F.** (1990). Ventricular system and choroid plexuses of the human brain during the embryonic period proper. *Am. J. Anat.* **189**, 285–302.
- O'Rahilly, R. and Müller, F.** (2002). The two sites of fusion of the neural folds and the two neuropores in the human embryo. *Teratology* **65**, 162–170.

- Ornoy, A.** (2009). Valproic acid in pregnancy: How much are we endangering the embryo and fetus? *Reprod. Toxicol.* **28**, 1–10.
- Oschwald, A., Petry, P., Kierdorf, K. and Erny, D.** (2020). CNS Macrophages and Infant Infections. *Front. Immunol.* **11**, 1–21.
- Ozderdem, U., Grako, K. A., Dahlin-Huppe, K., Monosov, E. and Stallcup, W. B.** (2001). NG2 proteoglycan is expressed exclusively by mural cells during vascular morphogenesis. *Dev. Dyn.* **222**, 218–227.
- Papa, F. T., Mencarelli, M. A., Caselli, R., Katzaki, E., Sampieri, K., Meloni, I., Ariani, F., Longo, I., Maggio, A., Balestri, P., et al.** (2008). Clinical Report A 3 Mb Deletion in 14q12 Causes Severe Mental Retardation , Mild Facial Dysmorphisms and Rett-like Features. **1998**, 1994–1998.
- Papayannopoulos, V.** (2018). Neutrophil extracellular traps in immunity and disease. *Nat. Rev. Immunol.* **18**, 134–147.
- Paridaen, J. T. M. L., Wilsch-Bräuninger, M. and Huttner, W. B.** (2013). Asymmetric inheritance of centrosome-associated primary cilium membrane directs ciliogenesis after cell division. *Cell* **155**, 333.
- Pate, K. T., Stringari, C., Sprowl-tanio, S., Wang, K., Teslaa, T., Hoverter, N. P., Mcquade, M. M., Garner, C., Digman, M. A., Teitell, M. A., et al.** (2014). Wnt signaling directs a metabolic program of glycolysis and angiogenesis in colon cancer. **33**, 1454–1473.
- Patterson, P. H.** (2009). Immune involvement in schizophrenia and autism: Etiology, pathology and animal models. *Behav. Brain Res.* **204**, 313–321.
- Paul, G., Özen, I., Christophersen, N. S., Reinbothe, T., Bengzon, J., Visse, E., Jansson, K., Dannaeus, K., Henriques-Oliveira, C., Roybon, L., et al.** (2012). The adult human brain harbors multipotent perivascular mesenchymal stem cells. *PLoS One* **7**,.
- Peter, I. S.** (2017). Regulatory states in the developmental control of gene expression. *Brief. Funct. Genomics* **16**, 281–287.
- Platt, J. B.** (1893). Ectodermic Origin of the Cartilages of the Head.
- Platt, J. B.** (1897). The Development of the Cartilaginous Skull and of the Branchial and Hypoglossal Musculature in Necturus.
- Pollay, M.** (2010). The function and structure of the cerebrospinal fluid outflow system. *Cerebrospinal Fluid Res.* **7**, 1–20.
- Pollock, J. A. and Newton, T. H.** (1968). The anterior falx artery: normal and pathologic anatomy. *Radiology* **91**, 1089–1095.
- Posokhova, E., Shukla, A., Seaman, S., Volate, S., Beth, M., Wu, B., Morris, H., Swing,**

- D. A., Zhou, M., Zudaire, E., et al.** (2016). GPR124 Functions as a WNT7-Specific Co-Activator of Canonical β -Catenin Signaling. **10**, 123–130.
- Praetorius, J. and Damkier, H. H.** (2017). Transport across the choroid plexus epithelium. *Am. J. Physiol. - Cell Physiol.* **312**, C673–C686.
- Premalatha, Kannan, V. P. and Madhu** (2010). Apert syndrome. *J. Indian Soc. Pedod. Prev. Dent.* **28**, 322–325.
- Ragge, N. K., Subak-Sharpe, I. D. and Collin, J. R. O.** (2007). A practical guide to the management of anophthalmia and microphthalmia. *Eye* **21**, 1290–1300.
- Raper, D., Louveau, A. and Kipnis, J.** (2016). How Do Meningeal Lymphatic Vessels Drain the CNS? *Trends Neurosci.* **39**, 581–586.
- Rasmussen, S. A., Jamieson, D. J., Honein, M. A. and Petersen, L. R.** (2016). Zika Virus and Birth Defects — Reviewing the Evidence for Causality. *N. Engl. J. Med.* **374**, 1981–1987.
- Raven, C. P.** (1936). Zur Entwicklung der Ganglienleiste. V. Über die Differenzierung des Rumpfganglienleistenmaterials. *Wilhelm Roux' Arch. Fur Entwicklungsmechanik Der Org.* **134**, 122–145.
- Rawles, M. E.** (1940). The Pigment-Forming Potency of Early Chick Blastoderms. *Proc. Natl. Acad. Sci. U. S. A.* **26**, 86–94.
- Reeves, B. C., Karimy, J. K., Kundishora, A. J., Mestre, H., Cerci, H. M., Matouk, C., Alper, S. L., Lundgaard, I., Nedergaard, M. and Kahle, K. T.** (2020). Glymphatic System Impairment in Alzheimer's Disease and Idiopathic Normal Pressure Hydrocephalus. *Trends Mol. Med.* **26**, 285–295.
- Remijnsen, Q., Kuijpers, T. W., Wirawan, E., Lippens, S., Vandenabeele, P. and Vanden Berghe, T.** (2011). Dying for a cause: NETosis, mechanisms behind an antimicrobial cell death modality. *Cell Death Differ.* **18**, 581–588.
- Reynolds, R. and Hardy, R.** (1997). Oligodendroglial progenitors labeled with the O4 antibody persist in the adult rat cerebral cortex in vivo. *J. Neurosci. Res.* **47**, 455–470.
- Richmond, T. J. and Davey, C. A.** (2003). The structure of DNA in the nucleosome core. *Nature* **423**, 145–150.
- Riikonen, R.** (2016). Treatment of autistic spectrum disorder with insulin-like growth factors. *Eur. J. Paediatr. Neurol.* **20**, 816–823.
- Risau, W.** (1997). Mechanisms of angiogenesis. *Nature* **386**, 671–4.
- Rivière, J.-B., M van Bon, B. W., Hoischen, A., Kholmanskikh, S. S., O, B. J., Gilissen, C., Gijssen, S., Sullivan, C. T., Christian, S. L., Abdul-Rahman, O. A., et al.** (2013). De novo mutations in the actin genes ACTB and ACTG1 cause Baraitser-Winter syndrome

HHS Public Access Author manuscript. *Nat Genet* **44**, 440–442.

- Rodier, P. M., Ingram, J. L., Tisdale, B., Nelson, S. and Romano, J.** (1996). Embryological origin for autism: Developmental anomalies of the cranial nerve motor nuclei. *J. Comp. Neurol.* **370**, 247–261.
- Rothstein, M., Bhattacharya, D. and Simoes-Costa, M.** (2018). The molecular basis of neural crest axial identity. *Dev. Biol.* **444**, S170–S180.
- Rustenhoven, J., Jansson, D., Smyth, L. C. and Dragunow, M.** (2017). Brain Pericytes As Mediators of Neuroinflammation. **38**, 291–304.
- Ryu, C. W.** (2010). Persistent falcine sinus: Is it really rare? *Am. J. Neuroradiol.* **31**, 367–369.
- Sagare, A. P., Bell, R. D., Zhao, Z., Ma, Q., Winkler, E. A., Ramanathan, A. and Zlokovic, B. V** (2013). Pericyte loss influences Alzheimer-like neurodegeneration in mice. *Nat. Commun.* **4**, 2932.
- Sauka-Spengler, T. and Bronner-Fraser, M.** (2008). A gene regulatory network orchestrates neural crest formation. *Nat. Rev. Mol. Cell Biol.* **9**, 557–568.
- Saunders, N. R., Dziegielewska, K. M., Møllgård, K. and Habgood, M. D.** (2018). Physiology and molecular biology of barrier mechanisms in the fetal and neonatal brain. *J. Physiol.* **596**, 5723–5756.
- Saverino, C. and Gerlai, R.** (2008). The social zebrafish: Behavioral responses to conspecific, heterospecific, and computer animated fish. *Behav. Brain Res.* **191**, 77–87.
- Schmechel, D. E. and Rakic, P.** (1979). A golgi study of radial glial cells in developing monkey telencephalon: Morphogenesis and transformation into astrocytes. *Anat. Embryol. (Berl).* **156**, 115–152.
- Schmid, E., Osborn, M., Rungger-brandl, E., Gabbiani, G., Weberz, K. and Franke, W. W.** (1982). Distribution of vimentin and desmin filaments in smooth muscle tissue of mammalian and avian aorta.
- Schneider, T. and Przewłocki, R.** (2005). Behavioral alterations in rats prenatally to valproic acid: Animal model of autism. *Neuropsychopharmacology* **30**, 80–89.
- Schneider, T., Turczak, J. and Przewłocki, R.** (2006). Environmental enrichment reverses behavioral alterations in rats prenatally exposed to valproic acid: Issues for a therapeutic approach in autism. *Neuropsychopharmacology* **31**, 36–46.
- Schneider, T., Roman, A., Basta-Kaim, A., Kubera, M., Budziszewska, B., Schneider, K. and Przewłocki, R.** (2008). Gender-specific behavioral and immunological alterations in an animal model of autism induced by prenatal exposure to valproic acid. *Psychoneuroendocrinology* **33**, 728–740.

- Scholz, B., Korn, C., Wojtarowicz, J., Boutros, M., Niehrs, C. and Augustin, H. G.** (2016). Endothelial RSPO3 Controls Vascular Stability and Pruning through Non-canonical. *Dev. Cell* **36**, 79–93.
- Schor, A. M. and Schor, S. L.** (1986). The isolation and culture of endothelial cells and pericytes from the bovine retinal microvasculature: A comparative study with large vessel vascular cells. *Microvasc. Res.* **32**, 21–38.
- Scola, G. and Duong, A.** (2017). Prenatal maternal immune activation and brain development with relevance to psychiatric disorders. *Neuroscience* **346**, 403–408.
- Scott, J. P.** (1962). Critical Periods in Behavioral Development. *Science (80-.)*. **138**, 949–958.
- Seiwert, T. Y. and Cohen, E. E. W.** (2008). Targeting Angiogenesis in Head and Neck Cancer. *Semin. Oncol.* **35**, 274–285.
- Sekar, A., Bialas, A. R., De Rivera, H., Davis, A., Hammond, T. R., Kamitaki, N., Tooley, K., Presumey, J., Baum, M., Doren, V. Van, et al.** (2016). Schizophrenia risk from complex variation of complement component 4 Schizophrenia Working Group of the Psychiatric Genomics Consortium HHS Public Access. *Nature. Febr.* **11**, 177–183.
- Sernagor, E., Chabrol, F., Bony, G. and Cancedda, L.** (2010). Gabaergic control of neurite outgrowth and remodeling during development and adult neurogenesis: General rules and differences in diverse systems. *Front. Cell. Neurosci.* **4**, 1–11.
- Shah, A., Oxley, G., Lovic, V. and Fleming, A. S.** (2002). Effects of preweaning exposure to novel maternal odors on maternal responsiveness and selectivity in adulthood. *Dev. Psychobiol.* **41**, 187–196.
- Shalaby, F., Rossant, J., Yamaguchi, T. P., Gertsenstein, M., Wu, X. F., Breitman, M. L. and Schuh, A. C.** (1995). Failure of blood-island formation and vasculogenesis in Flk-1-deficient mice. *Nature* **376**, 62–6.
- Shatz, C. J.** (2009). MHC Class I: An Unexpected Role in Neuronal Plasticity. *Neuron* **64**, 40–45.
- Shen, M. D., Nordahl, C. W., Young, G. S., Wootton-Gorges, S. L., Lee, A., Liston, S. E., Harrington, K. R., Ozonoff, S. and Amaral, D. G.** (2013). Early brain enlargement and elevated extra-axial fluid in infants who develop autism spectrum disorder. *Brain* **136**, 2825–2835.
- Shiraishi, N., Nakashima, T., Yamada, S., Uwabe, C., Kose, K. and Takakuwa, T.** (2013). Morphogenesis of lateral choroid plexus during human embryonic period. *Anat. Rec. (Hoboken)*. **296**, 692–700.
- Silva-Vargas, V., Maldonado-Soto, A. R., Mizrak, D., Codega, P. and Doetsch, F.** (2016). Age-Dependent Niche Signals from the Choroid Plexus Regulate Adult Neural Stem Cells. *Cell Stem Cell* **19**, 643–652.

- Simard, M., Arcuino, G., Takano, T., Liu, Q. S. and Nedergaard, M.** (2003). Signaling at the gliovascular interface. *J. Neurosci.* **23**, 9254–9262.
- Sizarov, A., Lamers, W. H., Mohun, T. J., Brown, N. A., Anderson, R. H. and Moorman, A. F. M.** (2012). Three-dimensional and molecular analysis of the arterial pole of the developing human heart. *J. Anat.* **220**, 336–349.
- Skalli, O., Ropraz, P., Trzeciak, A., Benzouana, G., Gillesen, D. and Gabbiani, G.** (1986). A monoclonal antibody against α -smooth muscle actin: A new probe for smooth muscle differentiation. *J. Cell Biol.* **103**, 2787–2796.
- Skalli, O., Pelte, M. F., Peclet, M. C., Gabbiani, G., Gugliotta, P., Bussolati, G., Ravazzola, M. and Orci, L.** (1989). α -Smooth muscle actin, a differentiation marker of smooth muscle cells, is present in microfilamentous bundles of pericytes. *J. Histochem. Cytochem.* **37**, 315–321.
- Smyth, L. C. D., Rustenhoven, J., Scotter, E. L., Schweder, P., Faull, R. L. M., Park, T. I. H. and Dragunow, M.** (2018). Markers for human brain pericytes and smooth muscle cells. *J. Chem. Neuroanat.* **92**, 48–60.
- Soriano, P.** (1994). Abnormal kidney development and hematological disorders in PDGF β -receptor mutant mice. *Genes Dev.* **8**, 1888–1896.
- Spassky, N. and Meunier, A.** (2017). The development and functions of multiciliated epithelia. *Nat. Rev. Mol. Cell Biol.* **18**, 423–436.
- Spemann, H.** (1924). Facsimile reproduction of the cover of an original reprint of the 1924 article by Hans Spemann and Hilde Mangold, with a handwritten dedication by H. Spemann which reads "With best regards, H.S." (Courtesy of K. Sander, Freiburg). *Archiv.*
- Steinman, G.** (2019). IGF – Autism prevention/amelioration. *Med. Hypotheses* **122**, 45–47.
- Steinman, G. and Mankuta, D.** (2013). Insulin-like growth factor and the etiology of autism. *Med. Hypotheses* **80**, 475–480.
- Stern, H., Booth, J. C., Elek, S. D. and Fleck, D. G.** (1969). Microbial causes of mental retardation. The role of prenatal infections with cytomegalovirus, rubella virus, and toxoplasma. *Lancet* **294**, 443–448.
- Steventon, B., Carmona-Fontaine, C. and Mayor, R.** (2005). Genetic network during neural crest induction: From cell specification to cell survival. *Semin. Cell Dev. Biol.* **16**, 647–654.
- Straface, G., Selmin, A., Zanardo, V., De Santis, M., Ercoli, A. and Scambia, G.** (2012). Herpes simplex virus infection in pregnancy. *Infect. Dis. Obstet. Gynecol.* **2012**,.
- Sweeney, M. D., Ayyadurai, S. and Zlokovic, B. V.** (2016). Pericytes of the neurovascular unit: Key functions and signaling pathways. *Nat. Neurosci.* **19**, 771–783.

- Tamega, O. J., Tirapelli, L. F. and Petroni, S.** (2000). Scanning electron microscopy study of the choroid plexus in the monkey (*Cebus apella apella*). *Arq. Neuropsiquiatr.* **58**, 820–825.
- Tan, D. W., Gilani, S. Z., Boutrus, M., Alvares, G. A., Whitehouse, A. J. O., Mian, A., Suter, D. and Maybery, M. T.** (2021). Facial asymmetry in parents of children on the autism spectrum. *Autism Res.* **14**, 2260–2269.
- Thanseem, I., Anitha, A., Nakamura, K., Suda, S., Iwata, K., Matsuzaki, H., Ohtsubo, M., Ueki, T., Katayama, T., Iwata, Y., et al.** (2012). Elevated transcription factor specificity protein 1 in autistic brains alters the expression of autism candidate genes. *Biol. Psychiatry* **71**, 410–418.
- Thomas, R. H.** (2018). Valproate: life-saving, life-changing. *Clin. Med. (Northfield. Il).* **18**, s1–s8.
- Tilton, R. G., Kilo, C., Williamson, J. R. and Murch, D. W.** (1979). Differences in pericyte contractile function in rat cardiac and skeletal muscle microvasculatures. *Microvasc. Res.* **18**, 336–352.
- Tojais, N. F., Peghaire, C., Franzl, N., Reynaud, A., Dufourcq, P., Moreau, C. and Couffinal, T.** (2014). Frizzled7 controls vascular permeability through the Wnt-canonical pathway and cross-talk with endothelial cell junction complexes. **7**, 291–303.
- Tomson, T., Battino, D., Bonizzoni, E., Craig, J., Lindhout, D., Perucca, E., Sabers, A., Thomas, S. V. and Vajda, F.** (2018). Comparative risk of major congenital malformations with eight different antiepileptic drugs: a prospective cohort study of the EURAP registry. *Lancet Neurol.* **17**, 530–538.
- Tung, E. W. Y. and Winn, L. M.** (2010). Epigenetic modifications in valproic acid-induced teratogenesis. *Toxicol. Appl. Pharmacol.* **248**, 201–209.
- Tyzio, R., Cossart, R., Khalilov, I., Minlebaev, M., Hübner, C. A., Represa, A., Ben-Ari, Y. and Khazipov, R.** (2006). Maternal Oxytocin Triggers a Transient Inhibitory Switch in GABA Signaling in the Fetal Brain During Delivery. *Science (80-.).* **314**, 1788–1792.
- Tyzio, R., Nardou, R., Ferrari, D. C., Tsintsadze, T., Shahrokhi, A., Eftekhari, S., Khalilov, I., Tsintsadze, V., Brouchoud, C., Chazal, G., et al.** (2014). Oxytocin-mediated GABA inhibition during delivery attenuates autism pathogenesis in rodent offspring. *Science (80-.).* **343**, 675–679.
- Uzunalli, G., Herr, S., Dieterly, A. M., Shi, R. and Lyle, L. T.** (2021). Structural disruption of the blood–brain barrier in repetitive primary blast injury. *Fluids Barriers CNS* **18**, 1–13.
- Vallee, R. B., Faulkner, N. E. and Tai, C. Y.** (2000). The role of cytoplasmic dynein in the human brain developmental disease lissencephaly. *Biochim. Biophys. Acta - Mol. Cell*

Res. **1496**, 89–98.

- Van Rie, A., Mupuala, A. and Dow, A.** (2008). Impact of the HIV/AIDS Epidemic on the Neurodevelopment of Preschool-Aged Children in Kinshasa, Democratic Republic of the Congo. *Pediatrics* **122**, e123–e128.
- Vandekerckhove, J. and Weber, K.** (1978a). Mammalian cytoplasmic actins are the products of at least two genes and differ in primary structure in at least 25 identified positions from skeletal muscle actins. *Proc. Natl. Acad. Sci. U. S. A.* **75**, 1106–1110.
- Vandekerckhove, J. and Weber, K.** (1978b). At least six different actins are expressed in a higher mammal: An analysis based on the amino acid sequence of the amino-terminal tryptic peptide. *J. Mol. Biol.* **126**, 783–802.
- Vandekerckhove, J. and Weber, K.** (1981). Actin Typing on Total Cellular Extracts: A Highly Sensitive Protein-Chemical Procedure Able to Distinguish Different Actins. *Eur. J. Biochem.* **113**, 595–603.
- Vanhollebeke, B., Stone, O. A., Bostaille, N., Cho, C., Zhou, Y., Maquet, E., Gauquier, A. and Cabochette, P.** (2015). Tip cell-specific requirement for an atypical Gpr124- and Reck-dependent Wnt / β -catenin pathway during brain angiogenesis. 1–25.
- Vélez, C., Aránega, A. E., Marchal, J. A., Melguizo, C., Prados, J. C., Carrillo, E. and Aránega, A.** (2000). Development of chick cardiomyocytes: Modulation of intermediate filaments by basic fibroblast and platelet-derived growth factors. *Cells Tissues Organs* **167**, 163–170.
- Vidal, C. N., Nicolson, R., Boire, J.-Y., Barra, V., DeVito, T. J., Hayashi, K. M., Geaga, J. A., Drost, D. J., Williamson, P. C., Rajakumar, N., et al.** (2008). Three-dimensional mapping of the lateral ventricles in autism. *Psychiatry Res. Neuroimaging* **163**, 106–115.
- Vigouroux, R. J., Belle, M. and Chédotal, A.** (2017). Neuroscience in the third dimension: Shedding new light on the brain with tissue clearing. *Mol. Brain* **10**, 1–10.
- Vossenaar, E. R., Zendman, A. J. W., Van Venrooij, W. J. and Pruijn, G. J. M.** (2003). PAD, a growing family of citrullinating enzymes: Genes, features and involvement in disease. *BioEssays* **25**, 1106–1118.
- Wahlsten, D., Metten, P. and Crabbe, J. C.** (2003). Survey of 21 inbred mouse strains in two laboratories reveals that BTBR T/+ tf/tf has severely reduced hippocampal commissure and absent corpus callosum. *Brain Res.* **971**, 47–54.
- Waldo, K., Miyagawa-Tomita, S., Kumiski, D. and Kirby, M. L.** (1998). Cardiac neural crest cells provide new insight into septation of the cardiac outflow tract: Aortic sac to ventricular septal closure. *Dev. Biol.* **196**, 129–144.
- Walz, N., Mühlberger, A. and Pauli, P.** (2016). A Human Open Field Test Reveals Thigmotaxis Related to Agoraphobic Fear. *Biol. Psychiatry* **80**, 390–397.

- Wang, Y., Li, M., Stadler, S., Correll, S., Li, P., Wang, D., Hayama, R., Leonelli, L., Han, H., Grigoryev, S. A., et al.** (2009). Histone hypercitrullination mediates chromatin decondensation and neutrophil extracellular trap formation. *J. Cell Biol.* **184**, 205–213.
- Weed, L. H.** (1914). Studies on Cerebro-Spinal Fluid. No. III : The pathways of escape from the Subarachnoid Spaces with particular reference to the Arachnoid Villi. *J. Med. Res.* **31**, 51–91.
- Welikala, A. H. N.** (1947). Extensive Calcification of the Falx Cerebri. *Br. J. Radiol.* **20**, 295–296.
- Werler, M. M., Ahrens, K. A., Bosco, J. L. F., Mitchell, A. A., Anderka, M. T., Gilboa, S. M. and Holmes, L. B.** (2011). Use of Antiepileptic Medications in Pregnancy in Relation to Risks of Birth Defects. *Ann. Epidemiol.* **21**, 842–850.
- Weston, J. A.** (1963). A radioautographic analysis of the migration and localization of trunk neural crest cells in the chick. *Dev. Biol.* **6**, 279–310.
- Williams, P. G. and Hersh, J. H.** (1997). A male with fetal valproate syndrome and autism. *Dev. Med. Child Neurol.* **39**, 632–4.
- Williams, G., King, J., Cunningham, M., Stephan, M., Kerr, B. and Hersh, J. H.** (2001). Fetal valproate syndrome and autism: additional evidence of an association. *Dev. Med. Child Neurol.* **43**, 202–6.
- Williams, R. M., Lukoseviciute, M., Sauka-Spengler, T. and Bronner, M. E.** (2022). Single-cell atlas of early chick development reveals gradual segregation of neural crest lineage from the neural plate border during neurulation. *Elife* **11**, 1–21.
- Willier, B. H. and Rawles, M. E.** (1940). The Control of Feather Color Pattern by Melanophores Grafted from One Embryo to Another of a Different Breed of Fowl. *Physiol. Zool.* **13**, 177–201.
- Wilson, D. A. and Sullivan, R. M.** (1994). Neurobiology of associative learning in the neonate: Early olfactory learning. *Behav. Neural Biol.* **61**, 1–18.
- Winkler, E. A., Sagare, A. P. and Zlokovic, B. V.** (2014). The pericyte: A forgotten cell type with important implications for alzheimer's disease? *Brain Pathol.* **24**, 371–386.
- Yntema, C. L. and Hammond, W. S.** (1945). Depletions and abnormalities in the cervical sympathetic system of the chick following extirpation of neural crest. *J. Exp. Zool.* **100**, 237–263.
- York, J. R., Mccauley, D. W. and Mccauley, D. W.** (2020). The origin and evolution of vertebrate neural crest cells.
- Yost, C. C., Cody, M. J., Harris, E. S., Thornton, N. L., McInturff, A. M., Martinez, M. L., Chandler, N. B., Rodesch, C. K., Albertine, K. H., Petti, C. A., et al.** (2009). Impaired neutrophil extracellular trap (NET) formation: A novel innate immune deficiency of

human neonates. *Blood* **113**, 6419–6427.

Yu, K., Herr, A. B., Waksman, G. and Ornitz, D. M. (2000). Loss of fibroblast growth factor receptor 2 ligand-binding specificity in Apert syndrome. *Proc. Natl. Acad. Sci. U. S. A.* **97**, 14536–14541.

Zalc, B. (2016). The acquisition of myelin : An evolutionary perspective. **1641**, 4–10.

Zalc, B. and Colman, D. R. (2000). Origins of Vertebrate Success. *Science (80-.)*. **288**, 271–271.

Zhang, K., Cox, E., Strom, S., Xu, Z. L., Disilvestro, A. and Usrey, K. (2020). Prenatal presentation and diagnosis of Baraitser-Winter syndrome using exome sequencing. *Am. J. Med. Genet. Part A* **182**, 2124–2128.

Zhou, Y. and Nathans, J. (2015). Gpr124 controls CNS angiogenesis and blood-brain barrier integrity by promoting ligand-specific canonical Wnt signaling. **31**, 248–256.

Zhou, B. R. and Bai, Y. (2019). Chromatin structures condensed by linker histones. *Essays Biochem.* **63**, 75–87.

Zhu, D., Zhang, Y. and Wang, S. (2021). Histone citrullination: a new target for tumors. *Mol. Cancer* **20**, 1–17.

Zimmermann, F. F., Gaspary, K. V., Leite, C. E., De Paula Cognato, G. and Bonan, C. D. (2015). Embryological exposure to valproic acid induces social interaction deficits in zebrafish (*Danio rerio*): A developmental behavior analysis. *Neurotoxicol. Teratol.* **52**, 36–41.

Zohn, I. E. (2012). Mouse as a model for multifactorial inheritance of neural tube defects. *Birth Defects Res. Part C - Embryo Today Rev.* **96**, 193–205.

Zonta, M., Angulo, M. C., Gobbo, S., Rosengarten, B., Hossmann, K. A., Pozzan, T. and Carmignoto, G. (2003). Neuron-to-astrocyte signaling is central to the dynamic control of brain microcirculation. *Nat. Neurosci.* **6**, 43–50.

Zuo, Y., Yalavarthi, S., Shi, H., Gockman, K., Zuo, M., Madison, J. A., Blair, C. N., Weber, A., Barnes, B. J., Egeblad, M., et al. (2020). Neutrophil extracellular traps in COVID-19. *JCI Insight* **9**, 1–11.



Review

The Emerging Roles of the Cephalic Neural Crest in Brain Development and Developmental Encephalopathies

Emmanuel Bruet [†], Diego Amarante-Silva [†], Tatiana Gorojankina and Sophie Creuzet ^{*}

Paris-Saclay Institute of Neuroscience, NeuroPSI, CNRS, Paris-Saclay University, Campus CEA Saclay, Bât 151, 151 Route de la Rotonde, 91400 Saclay, France

^{*} Correspondence: sophie.creuzet@cnrs.fr

[†] These authors contributed equally to this work.

Abstract: The neural crest, a unique cell population originating from the primitive neural field, has a multi-systemic and structural contribution to vertebrate development. At the cephalic level, the neural crest generates most of the skeletal tissues encasing the developing forebrain and provides the prosencephalon with functional vasculature and meninges. Over the last decade, we have demonstrated that the cephalic neural crest (CNC) exerts an autonomous and prominent control on the development of the forebrain and sense organs. The present paper reviews the primary mechanisms by which CNC can orchestrate vertebrate encephalization. Demonstrating the role of the CNC as an exogenous source of patterning for the forebrain provides a novel conceptual framework with profound implications for understanding neurodevelopment. From a biomedical standpoint, these data suggest that the spectrum of neurocristopathies is broader than expected and that some neurological disorders may stem from CNC dysfunctions.

Keywords: neural crest; mesectoderm; embryology; evolution; forebrain development



Citation: Bruet, E.; Amarante-Silva, D.; Gorojankina, T.; Creuzet, S. The Emerging Roles of the Cephalic Neural Crest in Brain Development and Developmental Encephalopathies. *Int. J. Mol. Sci.* **2023**, *24*, 9844. <https://doi.org/10.3390/ijms24129844>

Academic Editor: Nicolas Pilon

Received: 7 March 2023

Revised: 23 May 2023

Accepted: 25 May 2023

Published: 7 June 2023



Copyright: © 2023 by the authors. Licensee MDPI, Basel, Switzerland. This article is an open access article distributed under the terms and conditions of the Creative Commons Attribution (CC BY) license (<https://creativecommons.org/licenses/by/4.0/>).

1. Introduction

The face and the brain are phylogenetic organs that formed during vertebrate evolution. Their development coincided with the emergence of a multipotent cell population in the vertebrate embryo, the neural crest (NC). This structure represents an essential asset in the evolution of the chordate phylum since specific vertebrate traits (peripheral nervous system, cephalic skeletal tissues, and head development) are linked to the NC and its derivatives [1,2]. The NC first develops from the neural fold, bulging from the lateral borders of the neural plate at the neurula stage. At the time of neural tube closure, NC cells delaminate and migrate from the neural primordium to colonize elected sites, where they differentiate into a large variety of cell types. NC derivatives include the neurons and glial cells of the peripheral nervous system, the pigment cells, and endocrine cells, such as the adrenal medulla and calcitonin-producing cells [2].

Anteriorly, the cephalic NC (CNC) forms the mesectoderm, a vast, multipotent, and plastic mesenchyme which differentiates into connective tissues, chondrogenic and osteogenic cells. Consequently, CNC cells form much of the craniofacial skeleton, including the skull, the upper and lower jaws, and the hypobranchial skeleton [3]. In addition to skeletal derivatives, the CNC also contributes to the elaboration of the facial and cerebral vascular tree: CNC cells give rise to the pericytes lining the facial and cerebral capillaries in the forebrain and the adventitial peri-vascular cells of the aortic arches. Its contribution to the functional vasculature in the anterior part of the body extends down to the heart, where the CNC cells form the conotruncus and the sigmoid valves [4,5]. Therefore, the cardiovascular CNC derivatives participate in the homeostasis of the craniofacial structures and support the requisite demands in the oxygenation of the developing forebrain. Thus, from a developmental standpoint, the CNC exerts an essential structural role in building skeletal, vascular, and cephalic structures.

As an echo of the multiple and diverse contributions of NC cells, the spectrum of NC dysfunctions is broad and encompass a multiplicity of pathogenic conditions. The cohort of disorders (like melanoma, congenital melanocytic naevus, Hirschsprung disease, neurofibromatosis, and Merkel cell carcinoma) and malformative syndromes (Waardenburg, CHARGE, DiGeorge, Goldenhar, Axenfeld–Rieger, cranio-frontonasal syndromes, and congenital heart defects) arising from NC defects are collectively referred to as neurocristopathies [6,7]. The congenital disorders and craniofacial dysmorphisms that stem from NC defects illustrate how the basic embryological mechanisms and aberrant variations in molecular network activity may diverge from the normal developmental program. The conservation of cell interactions and signaling pathways across species justifies the importance of experimental animal studies to enlighten the etiology of human diseases. Over the last decade, investigations using developmental models have shown that the CNC, besides its structural role in head development, also exerts a potent morphogenetic “paracrine” effect on the brain and sense organs. Here, we review the primary pathway by which CNC cells control vertebrate encephalization. The evidence indicate that the spectrum of neural crest disorders is broader than expected and suggest that some neurodevelopmental defects and encephalopathies are neurocristopathies.

2. Vertebrate Neurulation: Ontogenesis of the Central Nervous System and the Neural Crest

The formation of the nervous system in vertebrate embryos begins at the late stage of gastrulation with a thickening of the superficial sheet. It leads to the formation of a neural plate, a specification of the dorsal ectoderm, which, under the induction of the underlying axial mesoderm and the notochord/prechordal plate complex, thickens along the midline and delimits the future neural ectoderm or neurectoderm, and initiates the formation of the central nervous system (CNS; Figure 1A).

At this stage, a neural fold bilaterally flanks the neural plate and accompanies the growth, elevation, and folding of the neural plate towards the midline. During this process, the neurectoderm separates from the superficial ectoderm, destined to form the skin. As the edges of the plate curve and form a neural groove, the neural bulges tend to converge along the dorsal midline. This complex growth-convergence process results in the fusion of the lateral edges of the neurectoderm and leads to neural tube closure [8–10].

Neural tube formation starts at the cephalic level before progressing to the more caudal levels. In neurula-stage embryos, while the anterior part of the embryo sees the progressive formation of the CNS, in the posterior part, gastrulation is still very active at the primitive streak. However, this folding and closing dynamic, characteristic of primary neurulation, only concerns the anterior 2/3 of the neuraxis. More caudally, secondary neurulation occurs due to the cavitation of a neural cord [11,12].

Anteriorly, soon after neural tube closure, the organization of the encephalon into three vesicles is fixed: the anterior brain or prosencephalon, the midbrain or mesencephalon, and the posterior brain or rhombencephalon (Figure 1A). More caudally, the neural tube is the origin of the spinal cord. Later on, the prosencephalon subdivides secondarily into the telencephalon and diencephalon. The telencephalon gives rise to the cerebral hemispheres, the olfactory bulbs, and the hippocampus. From the diencephalon comes the thalamus, the epithalamus, and the hypothalamus.

Parallel to the formation of the CNS, neurulation also leads to the formation of a population of pluripotent cells, the NC, which appears at the edge of the neural plate as bilateral neural bulges interposed between the neural and superficial ectoderm. As the two neural bulges fuse to form the neural tube, NC cells undergo an epithelial–mesenchymal transition: they detach from the neural plate and become mesenchymal. At the same time, NC cells acquire migratory properties and disperse throughout the embryo to give various derivatives, such as neurons, glial, pigmentary, and endocrine cells, but also cartilaginous and bony skeletal tissue [2]. Due to its neural and glial derivatives, NC is

essential for forming the enteric nervous system (ENS) and developing the peripheral nervous system (PNS).

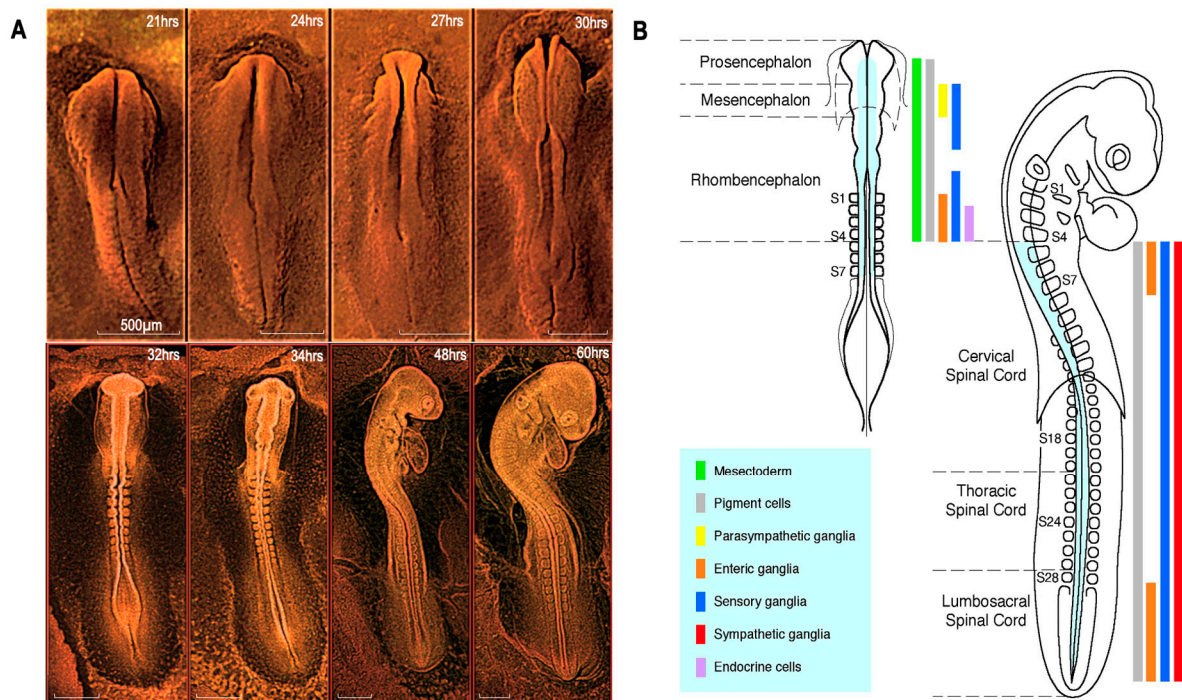


Figure 1. Development of the nervous system in the bird embryo. (A) Embryos showing the dynamics of early and then late stages of neurulation. From left to right, the cephalic development of chicken embryos after 21 h, 24 h, 27 h (showing the closure of the mesencephalic neural tube), 32 h (showing the first constrictions individualizing the anterior, middle, and posterior brain), 34 h (showing the segmentation of the rhombencephalon into rhombomeres is apparent), 48 h of incubation (showing the subdivision of the prosencephalon into the telencephalon and diencephalon) and 60 h. (B) Derivatives of the NC according to their level of origin along the anteroposterior axis. At the cephalic level, the NC forms mesectodermal derivatives (green) comprising skeletogenic, connective, adipose and perivascular cells. Glial and melanocytic phenotypes represent a basic trait produced throughout the neuraxis. The rhombencephalic and sacral NC provides the enteric neurons. As for the neuroendocrine, calcitonin and adrenomedullary cells, they derive from the posterior rhombencephalic (r8) and thoracic levels, respectively. Scale bars: 500 μm . Adapted from [13].

3. Neural Crest Discovery and Ontogenic Contribution

The NC “emerged” only recently in the history of biology. A German anatomist, His W., discovered NC cells originating from the edges of the neural tube in the chicken embryo, which migrated to form the spinal ganglia [14] and coined the term “ganglion crest”. A few years later, Kastschenko N., who described the mesenchymal contribution of NC cells to branchial arches in selachian embryos, first reported the role of NC in the formation of facial cartilages and branchial arches, and Goronowitsch N. extended this notion to birds and teleost fish [15,16]. Notably, Platt J.B., an American researcher who, based on her observations in the newt, *Necturus*, claimed that the NC was at the origin of the “visceral” (i.e., gill) cartilages and assigned the origin of dentin to the NC [17,18]. Moreover, she ascribed the term “mesectoderm” or “ectomesenchyme” to the NC-derived mesenchyme in order to distinguish it from the mesoderm-derived mesenchyme. At that time, the “three germ layers” theory prevailed, which assigned an exclusive mesodermal origin to skeletal tissue in vertebrates; these observations were particularly disputed. The experimental demonstration came later, during the first half of the 20th century, by experiments essentially based on ablation, xenograft, and cell tracing experiments carried out in lower vertebrates, amphibians, and fish [19–26]. During the second half of the 20th

century, these notions were extended to higher vertebrates, birds, and mammals. At the beginning of the 1960s, the work on the chicken embryo regained interest and intensity, such as applying tritiated thymidine to elective embryonic territories which allowed a precise cell marking [27]. This approach allowed to trace the dissemination of the NC cells from the neural primordium to the facial processes and branchial arches [28]. At the end of this decade, the quail–chick chimera technique made a breakthrough in experimental embryology [29]. It used interphase heterochromatin distribution as a differential structural character between two bird species. This character enables the discrimination of discrete cell territory to follow the fate of its progenies in an interspecific environment. While in chicken heterochromatin evenly disperses in the nucleoplasm, in quail, it condenses to the nucleolus; this structural distinction allowed tracing the respective contribution of tissues from each species, which later on, benefited from developing an antibody (Ab) directed against an antigen carried by quail cell nuclei, QCPN Ab (Carlson & Carlson, 1984; University of Michigan), to ease the histological analysis of chimeric tissues. Because of its stability and resolution, irrespective of the cell state of differentiation, this technique became an important tool well-adapted to the systematic exploration of NC cells' fate (for review [3,30]). By combining the micromanipulation of tissue Anlagen and gene expression, this technique becomes a resourceful model for functional studies. This model offers the prospect of unraveling cell interactions to identify the mechanisms underlying cell specification and differentiation with unparalleled spatiotemporal accuracy. It became decisive for the systematic explorations of the NC to understand the complexity of the NC cell population, to decipher the bidirectional interactions with the adjacent tissues, and more specifically to understand the developmental crosstalk with the developing brain [31].

4. CNC: A Source of Mesenchyme for the Face and Pharynx

The NC has the dual characteristics of being transient and multipotent. Although it disappears as an anatomical structure, undergoing an epithelial–mesenchymal transition, it produces highly invasive cells that have a lasting impact on vertebrate ontogeny through their derivatives. The NC has a multisystemic contribution. On one hand, it is at the origin of various derivatives, such as neurons of the peripheral nervous system, glial, pigmentary, and endocrine cells. However, the nature of the derivatives it generates varies at the level of the anteroposterior axis from which its cells originate (Figure 1B).

In birds, the migration of the CNC begins in the midbrain, when the neural bulges meet at the dorsal midline. Before resorbing into a population of migratory and mesenchymal cells, the NC cells form two easily identifiable bilateral masses. Their complete emigration at the cephalic level covers about 10 h (from 6 to 13 somite stage). In the early stages of their migration, the cells express genes that allow them to be distinguished from the neural primordium, from which they originate, and from the surface ectoderm. These include transcription factors, such as *Slug/Snail2*; genes of the *Sry-related HMG box (Sox)* family, notably *Sox8*, *Sox9* and *Sox10*; *Paired box (Pax)3*; *Pax7*; and *Forkhead box (Fox)d3* [32–37]. During this period, they also acquire surface antigens and, in particular, a glycoprotein recognized by a monoclonal antibody, Human natural killer-1 (HNK1) is widely used to follow the initial stages of their migration [38]. However, none of these genes used as markers can completely characterize the whole population of NC cells; moreover, their expression is usually transient. The chimera system provided a reliable approach for short- and long-term tracing. According to quail–chick fate maps, NC cells from the posterior diencephalon (located caudally to the pineal gland anlage) colonize the upper face primordium, corresponding to the nasofrontal and nasolateral buds (Figure 2A). The NC cells from the mesencephalon and the first two rhombomeres r1–r2, fill the first branchial arch (BA1; Figure 2A). In the more posterior branchial arches (BA2–BA4–6), cells originate from the middle and posterior rhombencephalon. NC cells from r4 provide the mesectodermal cells in BA2, with a small contribution from adjacent rhombomeres r3 and r5. NC cells from r6 to r8 colonize BA3 and BA4–6. These notions were primarily

observed in birds but were extended to mammals via the development of specific transgenic models [39–47].

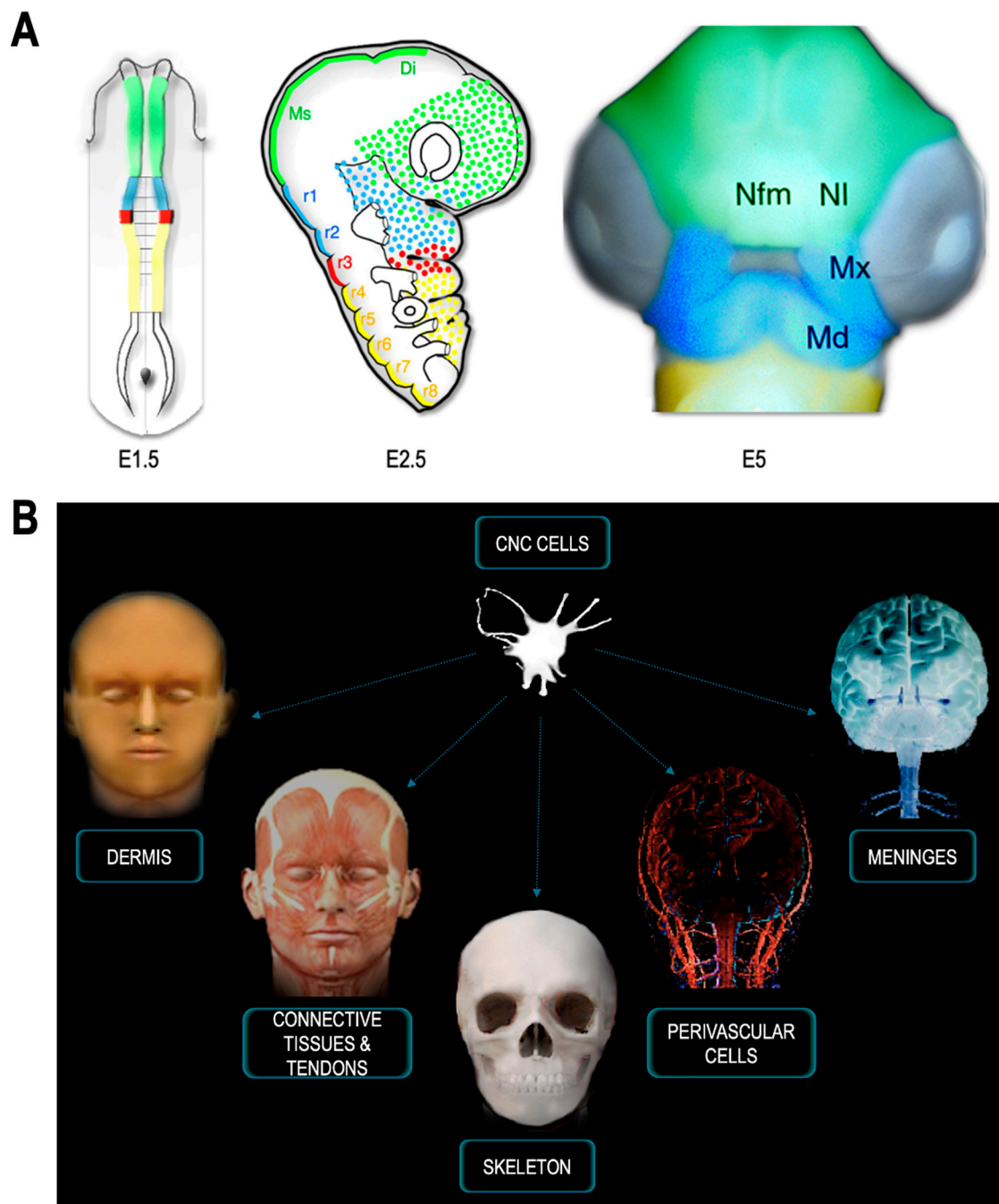


Figure 2. Contribution of the CNC to head formation and craniofacial structures. **(A)** Diencephalic and mesencephalic CNC cells colonize the medial nasofrontal (Nfm) and nasolateral (NI) buds. The anterior rhombencephalic NC (blue) provides most of the mesenchyme for the maxillary (Mx) and mandibular (Md) processes. **(B)** CNC cells differentiate into the dermis, the connective tissue, and tendons of the extraocular, facial and gill striated muscles, the skull and jaw skeleton. The CNC is also the origin of the perivascular cells that accompany the vascular network for vascularization of the face and forebrain, as well as the meninges of the telencephalon and thalamus. Adapted from [48].

The migration of the NC cells primarily depends on the extracellular matrix where fibronectin, collagens, and laminins, delimit permissive migration pathways [49–51]. Repellent signals are produced along the migration pathways, whereas chemoattractant

molecules are present within the migration pathways and at their destination site. In particular, the interaction between the molecule Semaphorin 3A and its receptor Neuropilin2 exerts a potent role in segregating migration currents from the rhombencephalic NC to the posterior arches [52,53]. However, Semaphorin acts in conjunction with other molecules to define “crest-free zones”, where NC cells are absent. The combination of permissive versus repellent signals confers a segmental distribution to the migration of these highly invasive and pluripotent cells. When the genes encoding the transcription factor *Twist*, or the neuregulin receptor, *ErbB4*, are mutated, an abnormal and invasive migratory phenotype of crest-free zones occurs [54–56].

Similarly, when the binding of Ephrin molecules to their receptors is inhibited, directional migration of NC cells is impaired with long-term consequences of craniofacial malformations [57]. In addition, local foci of cell death also refine the migration of NC cells derived from r3 and r5, which undergo massive apoptosis under the control of adjacent rhombomeres through the production of the factor Bone Morphogenetic Protein 4 (Bmp4). This results in a depletion of mesectodermal cells at the interface between the 1st and 2nd BAs and the 2nd and 3rd BAs, which restricts r4 cell migration to BA2, whose mesenchymal contribution is thus isolated from the adjacent arches [58–60]. Together, these mechanisms contribute to the restriction of a cell population in the second arch with a robust molecular identity inherent to its exclusive expression of *Homeobox (Hox)a2* gene, whose activity is potentially deleterious for the differentiation of more rostral structures. Furthermore, some molecules can guide CNC cell migration. They belong to the families of stromal cell-derived factors (Sdf), vascular endothelium growth factors (Vegf), Fibroblasts growth factors (Fgf), and Glial cell-derived neurotrophic factor (Gdnf) (for review [61]). Most of these guiding molecules exert a dual role: on one hand, they pave the way for NC cell migration, and on the other hand, they control NC cell differentiation. Their dual action provides a functional link between the multiple morphogenetic solicitations at the early stages of NC cell migration and the multisystemic contribution of NC derivatives to morphogenesis.

5. The CNC and Craniofacial Skeletogenesis: A Vertebrate Synapomorphy

The craniofacial skeleton represents a complex system of interconnected skeletal pieces presenting tremendous morphological variety. Moreover, the craniofacial skeletal system is also composite, consisting of various tissues, cartilage, endochondral bone, and membrane bone. In addition to the anatomical and histological complexity of its components which is challenging to study, this system develops according to a global organization plan which fulfills multiple functions and requirements. They include the protection of the brain, the support of the sense organs, the formation of the organs of predation, and the anchoring point of the digestive and superior respiratory tracts. From these varied needs, distinct skeletogenic processes are engaged: in the upper face that includes, on one hand, the elaboration of the cranium and the organization of the sensory capsules, which collectively form the neurocranium, and, on the other hand, includes the construction of the jaws and the hypobranchial skeleton, which together compose the visceral skeleton or viscerocranium, also referred to as splanchnocranium. These ontogenic processes follow their intrinsic morphogenetic logic, resulting from distinct developmental strategies initiated from isolated skeletogenic foci. As their differentiation progresses, these different skeletogenic foci become confluent and inter-dependent. Despite their apparent complexity, craniofacial structures share the common feature of being derived from the CNC. Cell tracing investigations in the chicken [28,62–66] revealed that most of the cranial skeleton is NC-derived. They are at the origin of the bones and cartilage of the upper and lower jaws, the nasal capsule, and the periorbital skeleton [63,66], along with the visceral, maxillo-mandibular, and hyoid skeleton [67,68]. In addition, in mammals, NC cells are also at the origin of the dentin, cementum, and dental pulp [39]. In contrast, only the occipital region, the basi-post-sphenoid, and part of the otic capsule are of mesodermal origin. The contribution of mesoderm to the cephalic structures of vertebrates is also to form

the vascular endothelium of the blood vessels, necessary for nutrition and oxygenation and the striated muscles of the face. Dorsally, the boundary between mesectodermal and mesodermal components of the cranial skeleton lies at the interface between the parietal and occipital bone. Ventrally, the boundary coincides with the anterior end of the notochord, which projects to the level of the sella turcica housing the ventral face of the pituitary gland, where the basi-post-sphenoid of mesodermal origin abuts to the basi-pre-sphenoid of NC origin.

6. Functional Partition in CNC Skeleton and Molecular Identities

Long-term tracing studies revealed different capacities in CNC cells to form skeletal tissues along the neuraxis. The ability to form cartilage and endochondral bone is shared by all CNC cells, regardless of their level of origin. However, the ability to form dermal bone is limited to the CNC cells present in the face, the nasofrontal and lateral buds, and the maxillomandibular processes. The CNC can therefore be subdivided into two functional areas. One area is rostral, extending from the middle diencephalon down to r2, which is the origin of the facial and cranial skeleton. Therefore, this region of the CNC is considered as the “facial NC” (or FNC [69]; Figure 2A). The other is more caudal, from r4 to r8, which allows the cells to form much of the hyoid bone. At the interface between these two territories, the cells of r3 correspond to an intermediate zone where NC cells participate in the first arch, facial, and the second arch, hyoid [69]. The functional demarcation within the CNC correlates with distinct molecular identities: anteriorly, the CNC cells originating from the diencephalon down to r2 do not express *Hox* genes, while CNC cells from r4 down to r8 express a sophisticated code of *Hox* genes. During development, the activation of *Hox* genes governs tissue segmentation and the antero-posterior patterning of the CNS. The expression of *Hox* genes is also intimately linked to the specification of the rhombencephalic NCC cells destined to fill the pharyngeal arches, and restrict the skeletogenic capacities to endochondral cartilage and bone derivatives in the gill region [70–72]. Anteriorly, in the frontonasal and maxillomandibular region, *Hox* genes are not expressed.

Ectopic transpositions of CNC demonstrated that within the *Hox*-negative domain, the cells of the facial NC behave as an “equivalence group”, i.e., a morphogenetic territory whose different levels are endowed with comparable developmental capacities. Each portion of the FNC is equally capable of generating the whole facial and mandibular skeletal components. In contrast, the transposition of the *Hox*-positive cells into the *Hox*-negative domain could not modify their *Hox* code. These cells migrate and colonize the facial buds, but are unable to form any appropriate skeletal, nasofrontal and maxillomandibular structures [70,73]. In mice, null mutation of the *Hox* genes perturb the formation of skeletal structures derived from the CNC [71,72,74], and results in duplication of the lower jaw, at the expense of BA2 skeleton [71,72]. Similarly, heterotopic grafts or ectopic expression of *Hoxa2* demonstrate the incompatibility between *Hox* gene expression and the development of maxillo-mandibular structures: *Hox*-positive cells in BA1 cannot generate a mandibular skeleton [69,73,75–77].

7. Contribution of CNC to Cardio-Vascular and Peri-Ocular Structures

In addition to the head skeleton, CNC massively contributes to connective tissues and tendons of the facial striated musculature (Figure 2A,B). The CNC forms the smooth musculature of the arrector pili muscles and the subcutaneous adipose tissue [62]: it provides the attachment points and connective sheaths for the muscle bundles, and dictates the arrangement of the hyoid, maxillomandibular, and extraocular skeletal musculature [45,67].

The CNC cells also contribute to the singularity of the anterior vascular arborescence: they form the perivascular cells which line the arterial tree from its emergence in the conotruncus to the capillary network irrigating the face and the forebrain. CNC cells migrating from r6 to r8, build the interventricular septum and the sigmoid valves [34,40,78–81]. In addition, they participate in the vasa vasorum in the ascending aorta and the tunica media of the coronary arteries [82]. When these cells are absent or deficient, irreversible

defects affect the septation of the heart and the systolic ejection chambers [78,79,81,83]. These defects stem from the aberrant proliferation of cardiomyocytes and compromise the formation of myofibers. Secondarily, such defects are complicated by extensive coronary atresia of the entire myocardium [84–88]. Given the vital importance of the CNC in cardiac development and physiology, the territory extending from r6 to r8 is classically considered as the “cardiac NC”.

In the face and the brain, the FNC has a musculo-connective contribution to the vasculature: its cells differentiate into pericytes and can be readily distinguished from endothelial cells by the accumulation of smooth muscle actin filament in their cytoplasm [4,5]. In the forebrain, pericytes derived from the CNC cells line the capillary network forming a very dense choroidal veil that prefigures the formation of the leptomeninges [4,66]. The meninges of the telencephalic hemispheres and thalamus thus originate from the CNC (Figure 2B). More caudally, from the optic tectum down to the tip of the spinal cord, meninges form the mesoderm. The transition between the vascular sectors, lined by CNC and mesoderm, occurs in the Circle of Willis, around the pituitary gland (Figure 3).

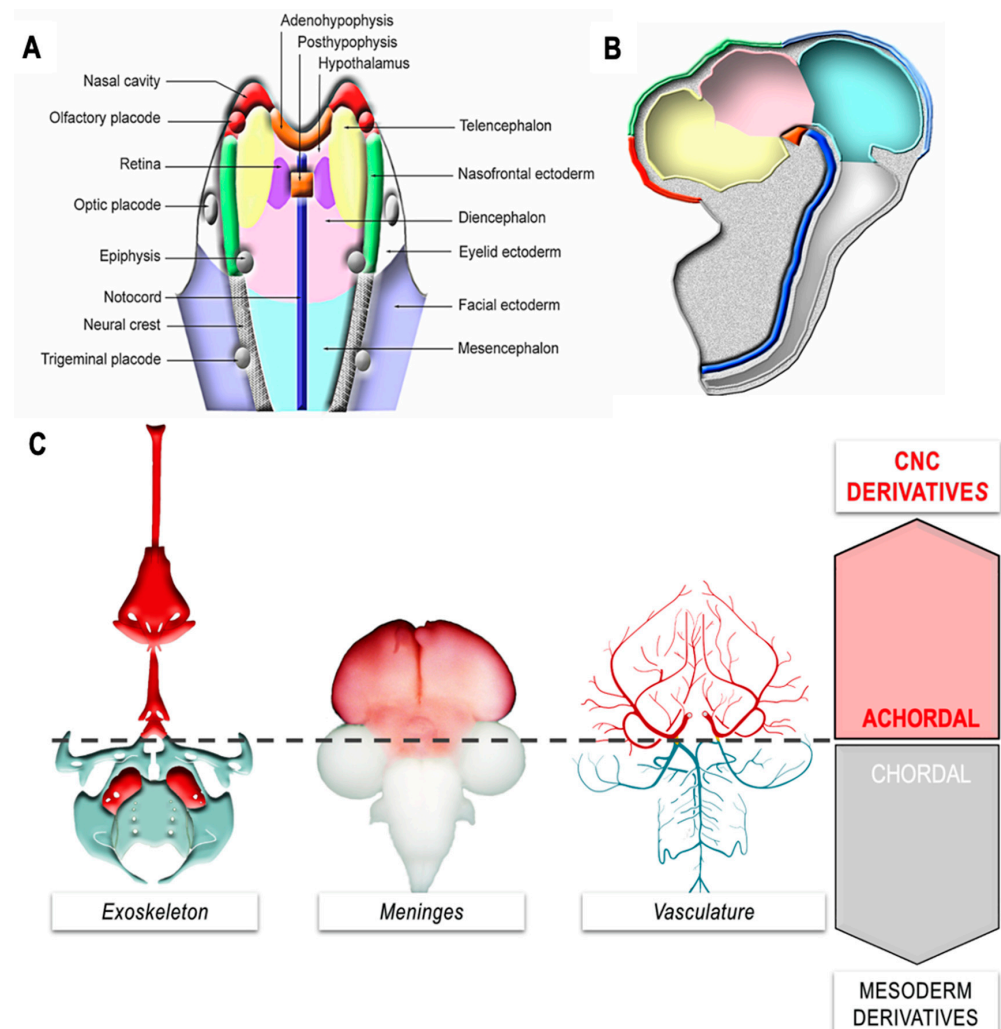


Figure 3. Development of the achordal segment (A) Projection of presumptive territories at the neural plate stage, showing the outline of the pituitary (orange), nasal muscularis (red), nasofrontal ectoderm (green) and telencephalon (yellow). In projection, the notochord appears in blue. (B) Fate of neuroectodermal derivatives at E5. (C) Derivatives of the CNC and emergence of the achordal segment. The skeletal, meningeal, and perivascular derivatives of the CNC that accompany the growth of the anterior cerebrum develop anterior to the tip of the notochord. Adapted from [89].

Laterally, the CNC also produces a tissue similar to the pia mater around the ocular anlage, the choroid membrane, which lines the outer surface of the retina, thus organizing the posterior uvea. In the choroid membrane, CNC cells differentiate into pericytes and melanocytes [4,64,66,86]. The CNC phenotype consists of perivascular cells in the periocular mesectodermal layer intimately associated with the pigmented retina. It also forms the cartilaginous skeleton of the sclera, the membranous bones that form the scleral ossicles. In the anterior periocular region, the abundant mesenchymal tissue derived from CNC also yields smooth muscle cells in the ciliary bodies and around Schlemm's canal, as well as the striated muscle myofibers of the iris (for review [86]). The contiguous relationship between these smooth and striated muscles derived from the CNC extends to the stroma of the nictitating membrane and the eyelids [86]. Lining the anterior chamber, the CNC form the corneal endothelium and keratocytes of the corneal stroma [64], which in many respects is suggestive of a cartilaginous-like structure. At the interface between the sclera and the cornea, CNC cells persist in an undifferentiated state in adults and form a stem cell niche within the scleral-corneal lamina. Altogether, the periocular CNC derivatives contribute to visual function by providing ocular structures with refraction media (cornea, and ossicles) and by participating in their homeostasis, both at the level of the anterior chamber (ciliary body and muscles, Schlemm's canal), and the posterior chamber (choroidal membrane; for review [86]).

8. CNC Contribution to the Emergence of an Achordal Segment: The “New Head”

During evolution, the transition from protochordates to vertebrates was marked by the appearance of a new structure, the NC. Absent in protochordates, the NC is a vertebrate innovation, a synapomorphic character unique to this group: given the diversity of lineages it generates, the NC can be considered as a fourth germ layer, making vertebrates quadroblastic organisms [90–92].

Anterior to the pineal anlage, the neural fold does not produce migrating CNC [90,93,94], but gives rise to the pituitary anlage medially (Figure 3A–C), which is contiguous with the rostral end of the notochord in early neurula. From the mesio-lateral territories of the neural fold, the nasal mucosa, the olfactory placodes, as well as the ectoderm destined to cover the naso-frontal bud and the phyltrum region develop. In contrast, at this stage, the telencephalon is located more caudally in the cephalic neural plate, laterally flanking the presumptive territory of the retina and the diencephalon (Figure 3A,B). It is important to note that all of the skeletal, perivascular, and meningeal derivatives of the facial CNC that accompany the development and growth of the forebrain develop anteriorly to the rostral end of the notochord (Figure 3A,B), whose anatomical projection onto the CNS corresponds to the level of the hypophysis.

From a phylogenetic standpoint, the CNC cells have allowed the emergence of a new territory, the achordal segment characterized by innovative facial and cerebral structures (Figure 3C). The transition from cephalochordates to vertebrates was marked by the sophistication of the brain and its associated sense organs—vision, smell, hearing—along with the development of facial structures and predatory organs. While cephalochordate fed by filtering organic marine particles, the vertebrates became predators. These transformations were accompanied by a change in lifestyle, a change in behavior that involved the acquisition of predatory organs, and the sophistication of sense organs and associative nerve centers. This change coincided with a considerable increase in the volume and complexity of cephalic vesicles in vertebrates, associated with the development of cognitive functions.

The importance of CNC in the construction of the vertebrate head, revealed in experimental embryology studies, paved the way for the hypothesis presented by Gans and Northcutt in a 1983 paper entitled “Neural Crest and the Origin of Vertebrates: A New Head” [1]. The authors argue that the appearance of the CNC in the embryo of the first vertebrates was a decisive step, playing a key role in the formation of a “new head”, an innovative addition to the pre-existing chordate organizational plan. This “new head” was the site of the development of a brain associated with sensory organs (absent in protochor-

dates) and a predatory organ, the jaw, whose skeleton is entirely derived from the CNC (for review [91]).

9. CNC Regulation of Pre-Otic Brain Morphogenesis

The hypothesis that CNC could play a prime evolutionary role in the process of cephalization has been investigated over the last years. To this end, ablation and rescue experiments were designed and extensively performed to explore the specific input of CNC cells on forebrain development.

The absence of FNC, which results in dramatic facial phenotype, is also harmful to the brain. Microsurgical ablation of FNC led to severe anencephaly along the territories where the FNC was excised (Figure 4H). Ablated embryos showed irreversible neural tube defects, and further extended rostrally to the telencephalon [73,92,95]. Furthermore, FNC-dependent anencephaly was correlated with the loss of *Fgf8* expression in the anterior neural ridge (ANR) and of the *Wingless (Wnt)*, *Wnt1*, *Wnt3a*, and *Wnt8* genes in the dorsal part of the thalamus and the midbrain. This resulted in agenesis of the dorsal thalamic nuclei. In parallel, profound perturbations in the expression pattern of *Empty spiracles homeobox (Emx2)*, *Pax6*, and *Distal-less homeobox (Dlx2)* [96–98] accompanied the developmental defects of cerebral hemispheres [95]. Exogenous supply of *Fgf8* allows the regeneration of the development of the cerebral hemispheres (telencephalon), the thalamus (diencephalon), and the optic roof (midbrain). *Fgf8* stimulates the rostral progression of CNC cells located at the limit of the excised territory (i.e., r3), which then migrate along the anterior neural plate, and promote fusion of the prosencephalic neuroepithelium (Figure 4I). At the same time, the expression of the transcription factors *Emx2*, *Pax6*, and *Dlx2*, involved in the specification of the cephalic neuroepithelium is restored [95].

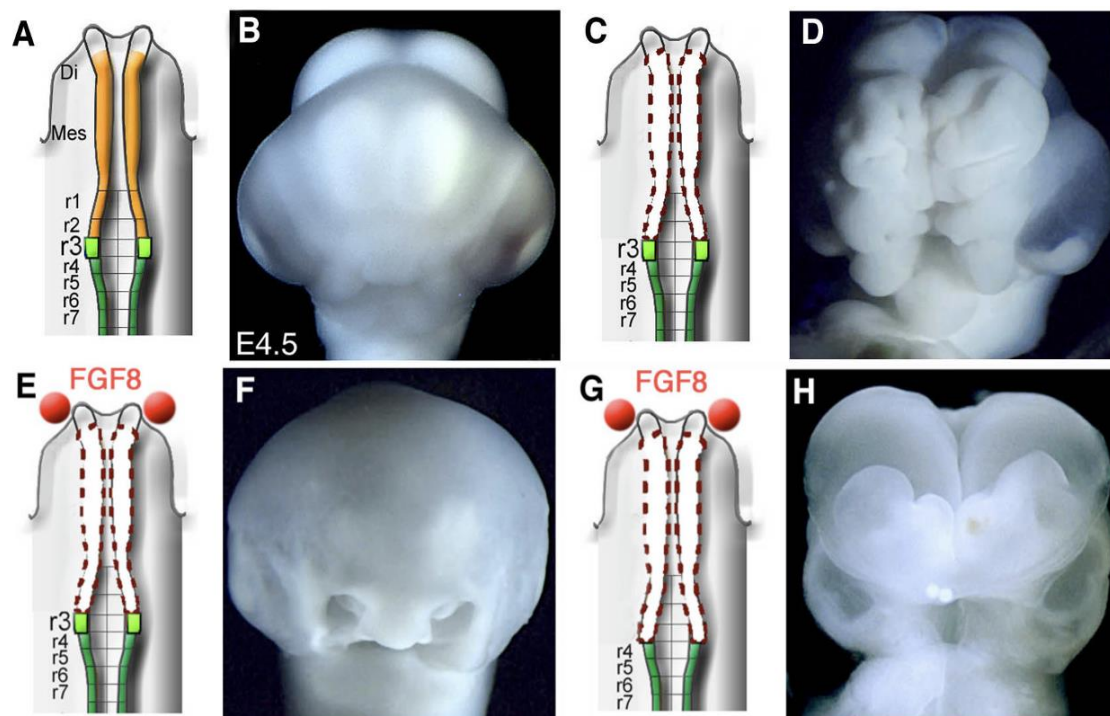


Figure 4. Cont.

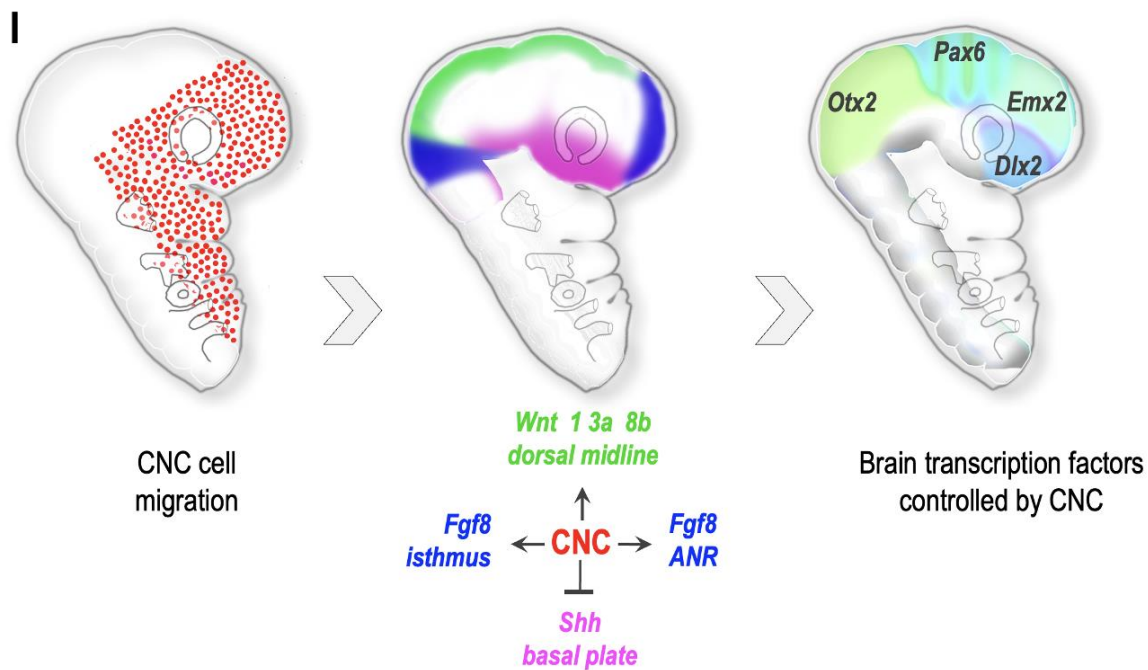


Figure 4. FNC controls cephalic neural tube closure. (A,B) At E5, when the facial NC ((A), in yellow) is intact (B) anterior and middle cephalic vesicle formation is normal. (C,D) Removal of the facial NC (C), from the middle diencephalon to r2, leads to extensive anencephaly (D). (E,F) Implantation of *Fgf8* beads ((E), in red) allows closure of the tube (F). (G,H) When ablation is extended to r3, the embryos are anencephalic, despite *Fgf8* bead implantation. (I) The facial NC regulates the morphogenetic activity of brain organizing centers. (I) During their migration, NC cells stimulate *Fgf8* activity in the RNA and isthmus, as well as *Wnt* activity along the dorsal midline. At the same time, they limit *Shh* expression to the basal lamina and repress its dorsal expansion. Scale bars: 500 μ m. Adapted from [99].

Therefore, the absence of CNC generates deficits in the brain comparable to the most severe congenital malformations of the brain; these consist of partial or total absence of the cerebral hemispheres and neural tube closure defects. These observations suggest that deregulations of CNC may be at the origin of such congenital malformations, the latter considered until now as intrinsic defects of the brain tissue.

These observations suggested the existence of NC cell-dependent signaling essential for (i) neural tube closure, (ii) roof plate development, and (iii) the molecular identity of the prosencephalic lamina. By controlling the expression of *Fgf8* in the ANR, the CNC exerts a “dorsalizing” action, to shape the telencephalon, and repress the ventralizing signals mediated by the *Sonic hedgehog* (*Shh*) morphogen (Figure 4I).

10. CNC Control of Brain Growth by Opposing *Bmp* Action

Bmps molecules are known to negatively regulate *Fgf8* production in this region [99,100]. Two primary sources of *Bmps* exist in the anterior region of the embryo at the phylogenesis stages. One, active in the early embryo at E1.5–2, is located in the pre-chordal plate (PCP) and produces *Bmp7*; the other, located in the prosencephalic neuroepithelium and surface ectoderm, produces *Bmp4* from E2 [101]. Factors expressed in the Spemann organizer, *Chordin* and *Noggin*, antagonists of *Bmps*, are involved in the control of forebrain development in the mouse [102,103]. However, CNC cells, during their migration, are a source of *Bmps* antagonistic factors, notably *Gremlin* and *Noggin* [104,105].

When the expression of the *Bmp4* gene is driven by a retroviral vector electroporated into the ANR, its activation prevents the deployment of CNC cells in the facial processes and along the prosencephalic vesicles. This results in brain defects mainly in the absence of rhinencephalon. These deficits can be reproduced either by surgical ablation of the

ANR or by locally silencing *Fgf8*. Depletion of *Fgf8* in the ANR was accompanied by drastic reductions in upper face structures (nasal capsule and upper jaw; [106]). The significant reduction in prosencephalic size indicates that the amount of *Bmp4* produced regulates the production of *Fgf8* in ANR and, consequently, the volume of lateral and dorsal forebrain structures.

Both *Gremlin* and *Noggin* are expressed in CNC cells. When these two BMP antagonists are inactivated simultaneously by bilateral electroporation with double-stranded RNAs, and then grafted onto a non-transfected host embryo, these experiments lead to a drastic reduction of *Fgf8* expression in the ANR, and result in microcephaly. Conversely, when *Gremlin* and *Noggin* genes are overexpressed, *Fgf8* expression in the ANR is expanded, leading to macrocephaly with a brain size augmented by up to 30% (Figure 5; [106]).

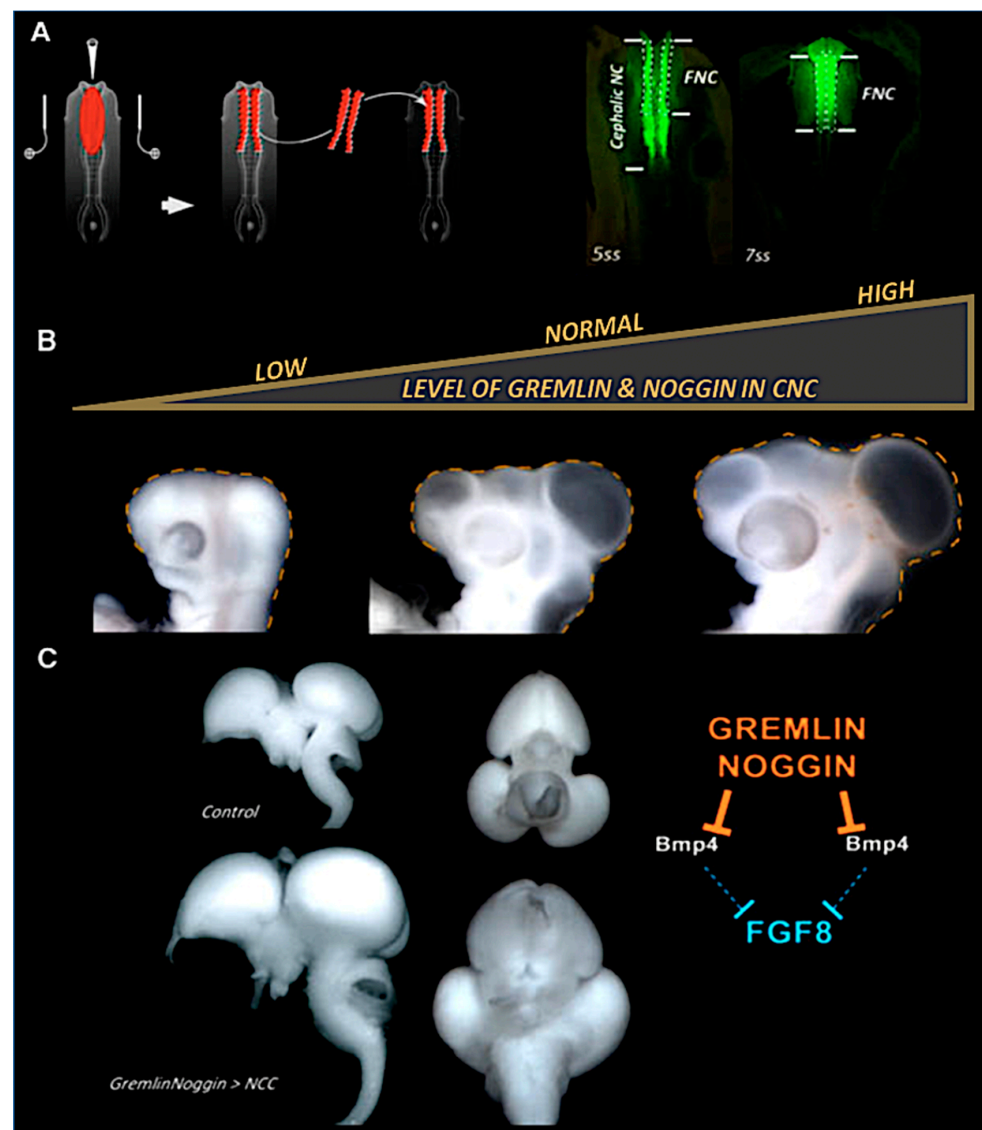


Figure 5. FNC regulates brain growth through the action of *Gremlin* and *Noggin*. (A) Bilateral transfection and grafting of the CNC. Expression of GFP to attest the transfection efficiency. (B) Joint inhibition of *Gremlin* and *Noggin* activity results in microcephaly (left, dotted line), whereas their overexpression results in macrocephaly (right, dotted line). (C) In macrocephalic embryos, brain size increases by nearly 30% more than normal. Adapted from [107,108].

11. Role of Six Genes in CNC Cells for Forebrain Development

The combined expression of the *Hox* genes constitutes a phylogenetically ancient program that underlies the organizational plan of all Bilateria. In the head, the CNC and its derivatives develop independently of *Hox* gene activity. Activation of the *Hoxa2* gene in *Hox*-negative CNC leads to major craniofacial and cerebral defects: these reproduce the malformations generated by the ablation of CNC, i.e., the absence of a face and an extended anencephaly [70,73].

Along this line, ectopic expression of *Hoxa2* in the FNC was used to unmask the molecular mechanisms by which CNC coordinates facial and brain development. These data demonstrated that in the pharyngeal region, *Hoxa2* directly targets *Sine oculis* homeobox (*Six*)₂ expression and represses its activity in mesenchyme destined to form the structures in BA2 [109].

In the head, forced expression of *Hoxa2* in the facial CNC leads to a reduction in the expression of the *Six1*, *Six2*, and *Six4* genes. These genes have a similar expression pattern in premigratory CNC cells and those colonizing the nasofrontal bud and the maxillomandibular complex. However, selective inactivation of their expression by silencing generated various deficits, ranging from a global reduction in facial skeleton size to partial truncations. Under these conditions, brain alterations in the choroid plexus agenesis, moderate defects of the septal region, and alobar holoprosencephaly, are also observed. In contrast, simultaneous inactivation of these three genes reproduced the malformations caused by *Hoxa2* and led to anencephaly. In addition, it turned out that both ectopic *Hoxa2* gene expression and inactivation of *Six* genes expanded Bmp signaling. Under these conditions, overexpression of Bmp antagonists, *Noggin*, *Gremlin* and *Dan*, was sufficient to counteract the deleterious effects of ectopic *Hoxa2* expression on brain morphogenesis. These experiments revealed that the *Six* gene family, including *Six1*, *Six2*, and *Six4*, cooperate to achieve normal brain development. The identification and detailed analysis of the impact of this molecular cascade on brain morphogenesis documents the mechanisms mobilized by the CNC to promote the sophistication of anterior brain vesicles [110]. These results suggest that during evolution, the diversification of *Six* gene function in *Hox*-negative CNC cells has enabled the elaboration and development of complex craniofacial and cerebral structures.

12. Integration of Fgf, Wnt and Bmp Signaling by the CNC for Forebrain Development

Surface Plasmon Resonance analysis revealed that Fgf8 is a high-affinity ligand for Cubulin (Cubn) and that Fgf8–Cubn binding is required for Fgf pathway transduction by the signaling mediators *Mitogen-activated protein kinase* (*Mapk*) and *Mothers against decapentaplegic homolog 1* (*Smad1*). Gene expression pattern shows that *FgfR1*, *FgfR3*, and, to a lesser extent, *FgfR2*, are expressed in CNC cells to a pattern similar to Cubn. Silencing of *FgfR3* at the neurulation stage results in microcephaly and facial hypoplasia, which is as severe as the effects following Cubn inactivation, whereas inactivation of *FgfR1* or *FgfR2* does not affect head development. Simultaneous inactivation of *Cubn* and *FgfR3* worsens the microcephaly phenotype: the addition of the deficits indicates that Cubn and FgfR3 are partners in Fgf8 signaling at these early stages. Together, they are required for integration of Fgf8 signals into CNC cells to orchestrate face and brain development [92,95,111]. These experiments showed how the highly conserved function of this receptor maintains the survival of the anterior neural plate and allows specification of the prosencephalon.

To further highlight the role of CNC on forebrain development, we analyzed whether CNC cells control the expression of transcription factor *Foxg1*, the earliest telencephalic marker [107,112]. *Foxg1* activity is known to regulate neuronal maturation: mutations in this gene in humans are associated with microcephaly and mental retardation [108,113]. Previous work demonstrated that *Foxg1* expression in the telencephalon is linked to Fgf8 activity in the ANR [114–117]. To explore the link between CNC and *Foxg1* expression, the activity of the *Smad1* was modulated in FNC. *Smad1* is an intracellular transduction factor for Fgf, Bmp, and Wnt signaling, which is transiently expressed by CNC cells just before

their migration. To unmask the mechanisms by which CNC exerts its trophic role on the telencephalon, *Smad1* activation was blocked: CNC cells became insensitive to Bmp, Fgf, and Wnt signaling and stopped their morphogenetic activity on the brain.

Inactivation of *Smad1* led to the loss of *Fgf8* and *Foxg1* expression. This resulted in severe microcephaly and partial holoprosencephaly observed from E4 to E8. Transfection of CNC cells with constructs that drive expression of constitutively active forms of *Smad1*, mimicking the activation of the Fgf and Wnt pathways [118], recovers *Foxg1* expression and rescues telencephalon development. Furthermore, the loss of *Foxg1* function in the telencephalon affected the development of the thalamus and optic roof by deregulating gene expression at their level: *Orthodenticle homeobox (Otx2)* was reduced dorsally, and conversely, *Foxa2* significantly increased in the basal plate, meaning that this part of the brain is ventralized in the absence of telencephalic development (Figure 6). In addition, downstream of *Smad1* activity in CNC cells, *Dickkopf-related protein (Dkk1)*, an antagonist of Wnt signals, was shown to control the induction of telencephalon specification through *Foxg1* activation [119]. Moreover, *Cerberus*, an antagonist of the Bmp pathway, was also required, and acted synergistically with *Dkk1* to control *Foxg1* expression, maintain *Otx2* expression, and repress the ventral expansion of *Foxa2* ([119]; Figure 6).

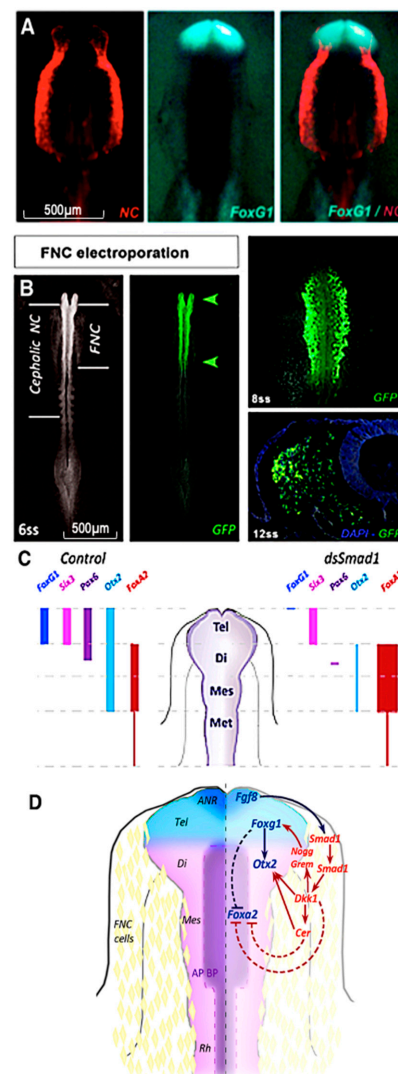


Figure 6. FNC controls *Foxg1* expression. (A) NC cell migration (red) coincides with *Foxg1* activation (cyan). (B) RNAi electroporation against *Smad1* in the NC inhibits (C) expression of *Foxg1*, *Otx2*, and *Pax6*. (D) Regulation of *Foxg1* by FNC mobilizing *Dkk1* to control *Gremlin* and *Noggin* activity, and of *Otx2* by *Cerberus* that enhances *Foxg1* expression. Adapted from [120].

13. Concluding Remarks and Perspectives

Developmental studies in embryos point to the CNC cells' role in brain growth and specification and highlight the molecular mechanisms by which CNC exerts a "paracrine" pro-encephalic control on brain regionalization. Altogether, these data show that the FNC plays a crucial role in controlling *Foxg1*, *Otx2*, *Emx2*, and *Dlx2* genes' expression, which is essential for early brain development [99,120]. They shed new light on the molecular control of these transcription factors crucial for forebrain development and the development of cognitive function at birth.

In humans, mutations in *Foxg1* and 14q12 microdeletion are responsible for microcephaly, mental retardation, language and manual skills' regression [108,113]. Epidemiologic studies in humans have highlighted that several neurodevelopmental syndromes or disorders have neurocristopathy manifestations before cognitive impairment at birth. For instance, *Foxg1* mutations are responsible for microcephaly and mild facial dysmorphisms in the atypical form of Rett syndrome and 14q12 microdeletion [108]. Septo-Optic Dysplasia [121], caused by mutations in *Otx2*, triggers syndromic phenotypes, including midline defects. These include agenesis of the interhemispheric septum and/or corpus callosum and lead to cortical malformations, microphthalmia or anophthalmia, and intellectual deficits [122,123]. Mutations in the homeobox gene *Emx2* led to severe schizencephaly in humans, characterized by full-thickness cleft within the cerebral hemispheres [120]. Additionally, both *Pax6* and *Dlx2* have been linked to the pathogenesis of autism spectrum disorders. Some studies emphasized the role of the *Pax6* gene as a chromatin modulator of autism-related genes [124], and *Dlx2* is associated with an increased susceptibility to autism [125]. Overall, studies by Creuzet and coworkers showed that FNC plays a crucial role in controlling *Foxg1*, *Otx2*, *Emx2*, and *Dlx2* genes' expression, which is crucial for early brain development [99,120], suggesting a possible role of CNC dysfunctions in the etiology of some neurodevelopmental defects and encephalopathies.

Funding: This research was funded by the Centre National de la Recherche Scientifique (CNRS) and grants from the Foundation for Medical Research (FRM-EQUIPE-2017), the National Research Funding Agency (ANR-MCORGLAUC-2020), and the National Institute for Health and Medical Research (3R-INSERM-2019). EB holds a fellowship from IDEX-Paris-Saclay University, and DAS held fellowships from FRM, INSERM, and ANR grants.

Institutional Review Board Statement: Not applicable.

Informed Consent Statement: Not applicable.

Data Availability Statement: Not applicable.

Conflicts of Interest: The authors declare no conflict of interest.

References

1. Gans, C.; Northcutt, R.G. Neural crest and the origin of vertebrates: A new head. *Science* **1983**, *220*, 268–274. [[CrossRef](#)] [[PubMed](#)]
2. Le Douarin, N.M. *The Neural Crest*; Cambridge University Press: Cambridge, UK, 1982.
3. Le Douarin, N.; Kalcheim, C. *The Neural Crest*; Cambridge University Press: Cambridge, UK, 1999; ISBN 9780521620109.
4. Etchevers, H.; Couly, G.; Vincent, C.; Le Douarin, N. Anterior cephalic neural crest is required for forebrain viability. *Development* **1999**, *126*, 3533–3543. [[CrossRef](#)] [[PubMed](#)]
5. Etchevers, H.; Vincent, C.; Le Douarin, N.; Couly, G. The cephalic neural crest provides pericytes and smooth muscle cells to all blood vessels of the face and forebrain. *Development* **2001**, *128*, 1059–1068. [[CrossRef](#)] [[PubMed](#)]
6. Etchevers, H.C.; Amiel, J.; Lyonnet, S. Molecular bases of human neurocristopathies. *Adv. Exp. Med. Biol.* **2006**, *589*, 213–234. [[CrossRef](#)]
7. Bolande, R.P. The neurocristopathies. A unifying concept of disease arising in neural crest maldevelopment. *Hum. Pathol.* **1974**, *5*, 409–429. [[CrossRef](#)]
8. Langman, J.; Guerrant, R.L.; Freeman, B.G. Behavior of neuro-epithelial cells during closure of the neural tube. *J. Comp. Neurol.* **1966**, *127*, 399–411. [[CrossRef](#)]
9. di Virgilio, G.; Lavenda, N.; Worden, J.L. Sequence of events in neural tube closure and the formation of neural crest in the chick embryo. *Cells Tissues Organs* **1967**, *68*, 127–146. [[CrossRef](#)]

10. Smith, J.L.; Schoenwolf, G.C.; Quan, J. Quantitative analyses of neuroepithelial cell shapes during bending of the mouse neural plate. *J. Comp. Neurol.* **1994**, *342*, 144–151. [[CrossRef](#)]
11. Gont, L.K.; Steinbeisser, H.; Blumberg, B.; De Robertis, E.M. Tail formation as a continuation of gastrulation: The multiple cell populations of the *Xenopus* tailbud derive from the late blastopore lip. *Development* **1993**, *119*, 991–1004. [[CrossRef](#)]
12. Catala, M.; Teillet, M.; De Robertis, E.M.; Le Douarin, M.L. A spinal cord fate map in the avian embryo: While regressing, Hensen's node lays down the notochord and floor plate thus joining the spinal cord lateral walls. *Development* **1996**, *122*, 2599–2610. [[CrossRef](#)]
13. Le Douarin, N.M.; Creuzet, S.E.; Couly, G.; Dupin, E. Neural Crest Cell Plasticity and its Limits. *Development* **2004**, *131*, 4637–4650. [[CrossRef](#)] [[PubMed](#)]
14. His, W. *Untersuchungen über die erste Anlage des Wirbelthierleibes: Die erste Entwicklung des Hühnchens im Ei*; F.C.W. Vogel: Leipzig, Germany, 1868.
15. Goronowitsch, N. Untersuchungen über die Entwicklung der sog. "Ganglienleisten" im Kopfe der Vögelebryonen. *Morph. Jahrb.* **1893**, *20*, 187–259.
16. Kastschenko, N. Zur Entwicklungsgeschichte des Selachierembryos. *Anat. Anz.* **1888**, *3*, 445–467.
17. Platt, J.B. Ectodermic Origin of the Cartilages of the Head. *Anat. Anz.* **1893**, *8*, 506–509.
18. Platt, J.B. The Development of the Cartilaginous Skull and of the Branchial and Hypoglossal Musculature in *Necturus*. *Morph. Jahrb.* **1897**, *25*, 377–464.
19. Detwiler, S.R. Observations upon the migration of neural crest cells, and upon the development of the spinal ganglia and vertebral arches in *Amblystoma*. *Am. J. Anat.* **1937**, *61*, 63–94. [[CrossRef](#)]
20. Detwiler, S.R. Application of Vital Dyes to the Study of Sheath Cell Origin. *Proc. Soc. Exp. Biol. Med.* **1937**, *37*, 380–382. [[CrossRef](#)]
21. Hörstadius, S.; Sellman, S. Experimental studies on the determination of the chondrocranium in *Amblystoma mexicanum*. *Ark. Zool. A* **1941**, *33*, 1–8.
22. Hörstadius, S.; Sellman, S. *Experimentelle Untersuchungen über die Determination des Knorpeligen Kopfskelettes bei Urodellen*; Almquist & Wiksell: Stockholm, Sweden, 1946.
23. Raven, C.P. Zur Entwicklung der Ganglienleiste III. Die Induktionsfähigkeit des Kopfganglienleistenmaterials von *Rana fusca*. *Wilhelm Roux' Arch. Entwickl. Org.* **1933**, *130*, 517–561. [[CrossRef](#)]
24. Raven, C.P. Experiments on the origin of the sheath cells and sympathetic neuroblasts in amphibia. *J. Comp. Neurol.* **1937**, *67*, 221–240. [[CrossRef](#)]
25. Stone, L.S. Further experiments on the extirpation and transplantation of mesectoderm in *Amblystoma punctatum*. *J. Exp. Zool.* **1926**, *44*, 95–131. [[CrossRef](#)]
26. Stone, L.S. Experiments showing the role of migrating neural crest (mesectoderm) in the formation of head skeleton and loose connective tissue in *Rana palustris*. *Wilhelm Roux' Arch. Entwickl. Org.* **1929**, *118*, 40–77. [[CrossRef](#)] [[PubMed](#)]
27. Weston, J.A. A radioautographic analysis of the migration and localization of trunk neural crest cells in the chick. *Dev. Biol.* **1963**, *6*, 279–310. [[CrossRef](#)] [[PubMed](#)]
28. Johnston, M.C. A radioautographic study of the migration and fate of cranial neural crest cells in the chick embryo. *Anat. Rec.* **1966**, *156*, 143–155. [[CrossRef](#)] [[PubMed](#)]
29. Le Douarin, N.M. Details of the interphase nucleus in Japanese quail (*Coturnix coturnix japonica*). *Bull. Biol. Fr. Belg.* **1969**, *103*, 435–452.
30. Le Douarin, N. A biological cell labeling technique and its use in experimental embryology. *Dev. Biol.* **1973**, *30*, 217–222. [[CrossRef](#)]
31. Alrajeh, M.; Vavrusova, Z.; Creuzet, S. Deciphering the Neural Crest Contribution to Cephalic Development with Avian Embryos. *Methods Mol. Biol.* **2019**, *1976*, 55–70. [[CrossRef](#)]
32. Meulemans, D.; Bronner-Fraser, M. Gene-regulatory interactions in neural crest evolution and development. *Dev. Cell* **2004**, *7*, 291–299. [[CrossRef](#)]
33. Nieto, M.A.; Sargent, M.G.; Wilkinson, D.G.; Cooke, J. Control of cell behavior during vertebrate development by *Slug*, a zinc finger gene. *Science* **1994**, *264*, 835–839. [[CrossRef](#)]
34. Epstein, J.A. Pax3, neural crest and cardiovascular development. *Trends Cardiovasc. Med.* **1996**, *6*, 255–260. [[CrossRef](#)]
35. Kos, R.; Reedy, M.V.; Johnson, R.L.; Erickson, C.A. The winged-helix transcription factor FoxD3 is important for establishing the neural crest lineage and repressing melanogenesis in avian embryos. *Development* **2001**, *128*, 1467–1479. [[CrossRef](#)] [[PubMed](#)]
36. Sasai, N.; Mizuseki, K.; Sasai, Y. Requirement of FoxD3-class signaling for neural crest determination in *Xenopus*. *Development* **2001**, *128*, 2525–2536. [[CrossRef](#)] [[PubMed](#)]
37. Hong, C.S.; Saint-Jeannet, J.P. Sox proteins and neural crest development. *Semin. Cell Dev. Biol.* **2005**, *16*, 694–703. [[CrossRef](#)] [[PubMed](#)]
38. Tucker, R.P.; Erickson, C.A. Morphology and behavior of quail neural crest cells in artificial three-dimensional extracellular matrices. *Dev. Biol.* **1984**, *104*, 390–405. [[CrossRef](#)]
39. Chai, Y.; Jiang, X.; Ito, Y.; Bringas, P.; Han, J.; Rowitch, D.H.; Soriano, P.; McMahon, A.P.; Sucov, H.M. Fate of the mammalian cranial neural crest during tooth and mandibular morphogenesis. *Development* **2000**, *127*, 1671–1679. [[CrossRef](#)]
40. Jiang, X.; Rowitch, D.H.; Soriano, P.; McMahon, A.P.; Sucov, H.M. Fate of the mammalian cardiac neural crest. *Development* **2000**, *127*, 1607–1616. [[CrossRef](#)]

41. Jiang, X.; Iseki, S.; Maxson, R.E.; Sucov, H.M.; Morriss-Kay, G.M. Tissue origins and interactions in the mammalian skull vault. *Dev. Biol.* **2002**, *241*, 106–116. [[CrossRef](#)]
42. Ito, Y.; Yeo, J.Y.; Chytil, A.; Han, J.; Bringas, P.; Nakajima, A.; Shuler, C.F.; Moses, H.L.; Chai, Y. Conditional inactivation of *Tgfb2* in cranial neural crest causes cleft palate and calvaria defects. *Development* **2003**, *130*, 5269–5280. [[CrossRef](#)]
43. Tallquist, M.D.; Soriano, P. Cell autonomous requirement for PDGFR α in populations of cranial and cardiac neural crest cells. *Development* **2003**, *130*, 507–518. [[CrossRef](#)]
44. Brewer, S.; Feng, W.; Huang, J.; Sullivan, S.; Williams, T. Wnt1-Cre-mediated deletion of AP-2 α causes multiple neural crest-related defects. *Dev. Biol.* **2004**, *267*, 135–152. [[CrossRef](#)]
45. Matsuoka, T.; Ahlberg, P.E.; Kassarlis, N.; Iannarelli, R.; Dennehy, U.; Richardson, W.D.; McMahon, A.P.; Koentges, G. Neural crest origins of the neck and shoulder. *Nature* **2005**, *436*, 347–355. [[CrossRef](#)] [[PubMed](#)]
46. Lewis, A.E.; Vasudevan, H.N.; O'Neill, A.K.; Soriano, P.; Bush, J.O. The widely used Wnt1-Cre transgene causes developmental phenotypes by ectopic activation of Wnt signaling. *Dev. Biol.* **2013**, *379*, 229–234. [[CrossRef](#)] [[PubMed](#)]
47. Pietri, T.; Eder, O.; Blanche, M.; Thiery, J.P.; Dufour, S. The human tissue plasminogen activator-Cre mouse: A new tool for targeting specifically neural crest cells and their derivatives in vivo. *Dev. Biol.* **2003**, *259*, 176–187. [[CrossRef](#)] [[PubMed](#)]
48. Le Douarin, N.M.; Brito, J.M.; Creuzet, S. The Role of the Neural Crest in Face and Brain Development. *Brain Res. Rev.* **2007**, *55*, 237–247. [[CrossRef](#)]
49. Duband, J.L.; Thiery, J.P. Distribution of laminin and collagens during avian neural crest development. *Development* **1987**, *101*, 461–478. [[CrossRef](#)]
50. Tucker, G.C.; Duband, J.L.; Dufour, S.; Thiery, J.P. Cell-adhesion and substrate-adhesion molecules: Their instructive roles in neural crest cell migration. *Development* **1988**, *103*, 81–94. [[CrossRef](#)]
51. Perris, R.; Perissinotto, D. Role of the extracellular matrix during neural crest cell migration. *Mech. Dev.* **2000**, *95*, 3–21. [[CrossRef](#)]
52. Osborne, N.J.; Begbie, J.; Chilton, J.K.; Schmidt, H.; Eickholt, B.J. Semaphorin/neuropilin signaling influences the positioning of migratory neural crest cells within the hindbrain region of the chick. *Dev. Dyn.* **2005**, *232*, 939–949. [[CrossRef](#)]
53. Yu, H.H.; Moens, C.B. Semaphorin signaling guides cranial neural crest cell migration in zebrafish. *Dev. Biol.* **2005**, *280*, 373–385. [[CrossRef](#)]
54. Soo, K.; O'Rourke, M.P.; Khoo, P.L.; Steiner, K.A.; Wong, N.; Behringer, R.R.; Tam, P.P.L. Twist function is required for the morphogenesis of the cephalic neural tube and the differentiation of the cranial neural crest cells in the mouse embryo. *Dev. Biol.* **2002**, *247*, 251–270. [[CrossRef](#)]
55. Golding, J.P.; Trainor, P.; Krumlauf, R.; Gassmann, M. Defects in pathfinding by cranial neural crest cells in mice lacking the neuregulin receptor erbB4. *Nat. Cell Biol.* **2000**, *2*, 103–109. [[CrossRef](#)] [[PubMed](#)]
56. Golding, J.P.; Sobieszczuk, D.; Dixon, M.; Coles, E.; Christiansen, J.; Wilkinson, D.; Gassmann, M. Roles of erbB4, rhombomere-specific, and rhombomere-independent cues in maintaining neural crest-free zones in the embryonic head. *Dev. Biol.* **2004**, *266*, 361–372. [[CrossRef](#)] [[PubMed](#)]
57. Davy, A.; Aubin, J.; Soriano, P. Ephrin-B1 forward and reverse signaling are required during mouse development. *Genes Dev.* **2004**, *18*, 572–583. [[CrossRef](#)]
58. Lumsden, A.; Sprawson, N.; Graham, A. Segmental origin and migration of neural crest cells in the hindbrain region of the chick embryo. *Development* **1991**, *113*, 1281–1291. [[CrossRef](#)] [[PubMed](#)]
59. Graham, A.; Heyman, I.; Lumsden, A. Even-numbered rhombomeres control the apoptotic elimination of neural crest cells from odd-numbered rhombomeres in the chick hindbrain. *Development* **1993**, *119*, 233–245. [[CrossRef](#)] [[PubMed](#)]
60. Graham, A.; Francis-West, P.; Brickell, P.; Lumsden, A. The signalling molecule BMP4 mediates apoptosis in the rhombencephalic neural crest. *Nature* **1994**, *372*, 684–686. [[CrossRef](#)] [[PubMed](#)]
61. Theveneau, E.; Mayor, R. Collective cell migration of the cephalic neural crest: The art of integrating information. *Genesis* **2011**, *49*, 164–176. [[CrossRef](#)]
62. Le Lievre, C.S.; Le Douarin, N.M. Mesenchymal derivatives of the neural crest: Analysis of chimaeric quail and chick embryos. *J. Embryol. Exp. Morphol.* **1975**, *34*, 125–154. [[CrossRef](#)]
63. Couly, G.F.; Coltey, P.M.; Le Douarin, N.M. The triple origin of skull in higher vertebrates: A study in quail-chick chimeras. *Development* **1993**, *117*, 409–429. [[CrossRef](#)]
64. Johnston, M.C.; Noden, D.M.; Hazelton, R.D.; Coulombre, J.L.; Coulombre, A.J. Origins of avian ocular and periocular tissues. *Exp. Eye Res.* **1979**, *29*, 27–43. [[CrossRef](#)]
65. Le Lievre, C. Rôle des cellules méséctodermiques issues des crêtes neurales céphaliques dans la formation des arcs branchiaux et du squelette viscéral. *Development* **1974**, *31*, 453–477. [[CrossRef](#)]
66. Le Lievre, C.S. Participation of neural crest-derived cells in the genesis of the skull in birds. *J. Embryol. Exp. Morphol.* **1978**, *47*, 17–37. [[CrossRef](#)] [[PubMed](#)]
67. Köntges, G.; Lumsden, A. Rhombencephalic neural crest segmentation is preserved throughout craniofacial ontogeny. *Development* **1996**, *122*, 3229–3242. [[CrossRef](#)]
68. Couly, G.; Grapin-botton, A.; Coltey, P.; Douarin, N.M. Le Couly-1996 The regeneration of the cephalic neural crest a problem revisited. *Development* **1996**, *3407*, 3393–3407. [[CrossRef](#)] [[PubMed](#)]
69. Creuzet, S.; Schuler, B.; Couly, G.; Le Douarin, N.M. Reciprocal relationships between *Fgf8* and neural crest cells in facial and forebrain development. *Proc. Natl. Acad. Sci. USA* **2004**, *101*, 4843–4847. [[CrossRef](#)] [[PubMed](#)]

70. Hunt, P.; Gulisano, M.; Cook, M.; Sham, M.-H.; Faiella, A.; Wilkinson, D.; Boncinelli, E.; Krumlauf, R. A Distinct Hox Code for the Branchial Region of the Vertebrate Head. *Nature* **1991**, *353*, 861–864. [[CrossRef](#)] [[PubMed](#)]
71. Krumlauf, R. Hox Genes in Vertebrate Development. *Cell* **1994**, *78*, 191–201. [[CrossRef](#)]
72. Prince, V.; Lumsden, A. Hoxa-2 Expression in Normal and Transposed Rhombomeres: Independent Regulation in the Neural Tube and Neural Crest. *Development* **1994**, *120*, 911–923. [[CrossRef](#)]
73. Couly, G.; Grapin-Botton, A.; Coltey, P.; Ruhin, B.; Le Douarin, N.M. Determination of the identity of the derivatives of the cephalic neural crest: Incompatibility between Hox gene expression and lower jaw development. *Development* **1998**, *125*, 3445–3459. [[CrossRef](#)]
74. Creuzet, S.; Couly, G.; Vincent, C.; Le Douarin, N.M. Negative Effect of Hox Gene Expression on the Development of the Neural Crest-Derived Facial Skeleton. *Development* **2002**, *129*, 4301–4313. [[CrossRef](#)]
75. Couly, G.; Creuzet, S.; Bennaceur, S.; Vincent, C.; Le Douarin, N.M. Interactions between Hox-Negative Cephalic Neural Crest Cells and the Foregut Endoderm in Patterning the Facial Skeleton in the Vertebrate Head. *Development* **2002**, *129*, 1061–1073. [[CrossRef](#)] [[PubMed](#)]
76. Gendron-Maguire, M.; Mallo, M.; Zhang, M.; Gridley, T. Hoxa-2 mutant mice exhibit homeotic transformation of skeletal elements derived from cranial neural crest. *Cell* **1993**, *75*, 1317–1331. [[CrossRef](#)]
77. Rijli, F.M.; Mark, M.; Lakkaraju, S.; Dierich, A.; Dollé, P.; Chambon, P. A homeotic transformation is generated in the rostral branchial region of the head by disruption of Hoxa-2, which acts as a selector gene. *Cell* **1993**, *75*, 1333–1349. [[CrossRef](#)] [[PubMed](#)]
78. Ramírez-Solis, R.; Zheng, H.; Whiting, J.; Krumlauf, R.; Bradley, A. Hoxb-4 (Hox-2.6) mutant mice show homeotic transformation of a cervical vertebra and defects in the closure of the sternal rudiments. *Cell* **1993**, *73*, 279–294. [[CrossRef](#)] [[PubMed](#)]
79. Santagati, F.; Rijli, F.M. Cranial neural crest and the building of the vertebrate head. *Nat. Rev. Neurosci.* **2003**, *4*, 806–818. [[CrossRef](#)] [[PubMed](#)]
80. Grammatopoulos, G.A.; Bell, E.; Toole, L.; Lumsden, A.; Tucker, A.S. Homeotic transformation of branchial arch identity after Hoxa2 overexpression. *Development* **2000**, *127*, 5355–5365. [[CrossRef](#)]
81. Pasqualetti, M.; Ori, M.; Nardi, I.; Rijli, F.M. Ectopic Hoxa2 induction after neural crest migration results in homeosis of jaw elements in *Xenopus*. *Development* **2000**, *127*, 5367–5378. [[CrossRef](#)]
82. Kirby, M.L.; Stewart, D.E. Neural crest origin of cardiac ganglion cells in the chick embryo: Identification and extirpation. *Dev. Biol.* **1983**, *97*, 433–443. [[CrossRef](#)]
83. Kirby, M.L.; Gale, T.F.; Stewart, D.E. Neural Crest Contribute to the APSpdf. *Science* **1983**, *220*, 1059–1061. [[CrossRef](#)]
84. Creazzo, T.L.; Godt, R.E.; Leatherbury, L.; Conway, S.J.; Kirby, M.L. Role of cardiac neural crest cells in cardiovascular development. *Annu. Rev. Physiol.* **1998**, *60*, 267–286. [[CrossRef](#)]
85. Kirby, M.L.; Turnage, K.L.; Hays, B.M. Characterization of conotruncal malformations following ablation of “cardiac” neural crest. *Anat. Rec.* **1985**, *213*, 87–93. [[CrossRef](#)] [[PubMed](#)]
86. Waldo, K.L.; Kumiski, D.H.; Kirby, M.L. Association of the cardiac neural crest with development of the coronary arteries in the chick embryo. *Anat. Rec.* **1994**, *239*, 315–331. [[CrossRef](#)]
87. Escot, S.; Blavet, C.; Härtle, S.; Duband, J.L.; Fournier-Thibault, C. Misregulation of SDF1-CXCR4 signaling impairs early cardiac neural crest cell migration leading to conotruncal defects. *Circ. Res.* **2013**, *113*, 505–516. [[CrossRef](#)] [[PubMed](#)]
88. Waldo, K.; Zdanowicz, M.; Burch, J.; Kumiski, D.H.; Stadt, H.A.; Godt, R.E.; Creazzo, T.L.; Kirby, M.L. A novel role for cardiac neural crest in heart development. *J. Clin. Investig.* **1999**, *103*, 1499–1507. [[CrossRef](#)] [[PubMed](#)]
89. Creuzet, S.E. Neural Crest Contribution to Forebrain Development. *Semin. Cell Dev. Biol.* **2009**, *20*, 751–759. [[CrossRef](#)] [[PubMed](#)]
90. Hall, B. The neural crest as a fourth germ layer and vertebrate as a quadroblastic not triploblastic. *Evol. Dev.* **2000**, *2*, 3–5. [[CrossRef](#)]
91. Baker, C.V. The Evolution and Elaboration of Vertebrate Neural Crest Cells. *Curr. Opin. Genet. Dev.* **2008**, *18*, 536–543. [[CrossRef](#)]
92. Hall, B.K. Germ Layers and the Germ-Layer Theory Revisited. *Evol. Biol.* **1998**, *30*, 121–186. [[CrossRef](#)]
93. Hanato, T.; Nakagawa, M.; Okamoto, N.; Nishijima, S.; Fujino, H.; Shimada, M.; Takeuchi, Y.; Imanaka-Yoshida, K. Developmental defects of coronary vasculature in rat embryos administered bis-diamine. *Birth Defects Res. Part B-Dev. Reprod. Toxicol.* **2011**, *92*, 10–16. [[CrossRef](#)]
94. Creuzet, S.; Vincent, C.; Couly, G. Neural crest derivatives in ocular and periocular structures. *Int. J. Dev. Biol.* **2005**, *49*, 161–171. [[CrossRef](#)]
95. Couly, G.F.; Le Douarin, N.M. Mapping of the early neural primordium in quail-chick chimeras. I. Developmental relationships between placodes, facial ectoderm, and prosencephalon. *Dev. Biol.* **1985**, *110*, 422–439. [[CrossRef](#)] [[PubMed](#)]
96. Couly, G.F.; Le Douarin, N.M. Mapping of the early neural primordium in quail-chick chimeras. II. The prosencephalic neural plate and neural folds: Implications for the genesis of cephalic human congenital abnormalities. *Dev. Biol.* **1987**, *120*, 198–214. [[CrossRef](#)] [[PubMed](#)]
97. Couly, G.; Le Douarin, N.M. The fate map of the cephalic neural primordium at the presomitic to the 3-somite stage in the avian embryo. *Development* **1988**, *103*, 101–113. [[CrossRef](#)] [[PubMed](#)]
98. Manzanares, M.; Nieto, M.Á. A Celebration of the New Head and an Evaluation of the New Mouth. *Neuron* **2003**, *37*, 895–898. [[CrossRef](#)] [[PubMed](#)]

99. Creuzet, S.E.; Martinez, S.; Le Douarin, N.M. The cephalic neural crest exerts a critical effect on forebrain and midbrain development. *Proc. Natl. Acad. Sci. USA* **2006**, *103*, 14033–14038. [[CrossRef](#)]
100. Simeone, A.; Acampora, D.; Gulisano, M.; Stornaiuolo, A.; Boncinelli, E. Nested expression domains of four homeobox genes in developing rostral brain. *Nature* **1992**, *358*, 687–690. [[CrossRef](#)]
101. Rhinn, M.; Dierich, A.; Shawlot, W.; Behringer, R.R.; Le Meur, M.; Ang, S.L. Sequential roles for Otx2 in visceral endoderm and neuroectoderm for forebrain and midbrain induction and specification. *Development* **1998**, *125*, 845–856. [[CrossRef](#)]
102. Fernandez, A.S.; Pieau, C.; Repérant, J.; Boncinelli, E.; Wassef, M. Expression of the Emx-1 and Dlx-1 homeobox genes define three molecularly distinct domains in the telencephalon of mouse, chick, turtle and frog embryos: Implications for the evolution of telencephalic subdivisions in amniotes. *Development* **1998**, *2111*, 2099–2111. [[CrossRef](#)]
103. Aoto, K.; Nishimura, T.; Eto, K.; Motoyama, J. Mouse GLI3 regulates Fgf8 expression and apoptosis in the developing neural tube, face, and limb bud. *Dev. Biol.* **2002**, *251*, 320–332. [[CrossRef](#)]
104. Ohkubo, Y.; Chiang, C.; Rubenstein, J.L.R. Coordinate regulation and synergistic actions of BMP4, SHH and FGF8 in the rostral prosencephalon regulate morphogenesis of the telencephalic and optic vesicles. *Neuroscience* **2002**, *111*, 1–17. [[CrossRef](#)]
105. Crossley, P.H.; Martinez, S.; Ohkubo, Y.; Rubenstein, J.L.R. Coordinate expression of Fgf8, Otx2, Bmp4, and Shh in the rostral prosencephalon during development of the telencephalic and optic vesicles. *Neuroscience* **2001**, *108*, 183–206. [[CrossRef](#)] [[PubMed](#)]
106. Bachiller, D.; Klingensmith, J.; Kemp, C.; Belo, J.A.; Anderson, R.M.; May, S.R.; McMahon, J.A.; McMahon, A.P.; Harland, R.M.; Rossant, J.; et al. The organizer factors Chordin and Noggin are required for mouse forebrain development. *Nature* **2000**, *403*, 658–661. [[CrossRef](#)] [[PubMed](#)]
107. Creuzet, S.E. Regulation of pre-otic brain development by the cephalic neural crest. *Proc. Natl. Acad. Sci. USA* **2009**, *106*, 15774–15779. [[CrossRef](#)] [[PubMed](#)]
108. Garcez, R.C.; Le Douarin, N.M.; Creuzet, S.E. Combinatorial activity of Six1-2-4 genes in cephalic neural crest cells controls craniofacial and brain development. *Cell. Mol. Life Sci.* **2014**, *71*, 2149–2164. [[CrossRef](#)] [[PubMed](#)]
109. Anderson, R.M.; Lawrence, A.R.; Stottmann, R.W.; Bachiller, D.; Klingensmith, J. Chd and Nog promote organising centres of forebrain development in the mouse. *Development* **2002**, *4987*, 4975–4987. [[CrossRef](#)] [[PubMed](#)]
110. Bardot, B.; Lecoin, L.; Huillard, E.; Calothy, G.; Marx, M. Expression pattern of the *drm/gremlin* gene during chicken embryonic development. *Mech. Dev.* **2001**, *101*, 263–265. [[CrossRef](#)] [[PubMed](#)]
111. Tzahor, E.; Kempf, H.; Mootosamy, R.C.; Poon, A.C.; Abzhanov, A.; Tabin, C.J.; Dietrich, S.; Lassar, A.B. Antagonists of Wnt and BMP signaling promote the formation of vertebrate head muscle. *Genes Dev.* **2003**, *17*, 3087–3099. [[CrossRef](#)] [[PubMed](#)]
112. Kutejova, E.; Engist, B.; Mallo, M.; Kanzler, B.; Bobola, N. *Hoxa2* downregulates *Six2* in the neural crest-derived mesenchyme. *Development* **2005**, *132*, 469–478. [[CrossRef](#)]
113. Cases, O.; Perea-Gomez, A.; Aguiar, D.P.; Nykjaer, A.; Amsellem, S.; Chandellier, J.; Umbhauer, M.; Cereghini, S.; Madsen, M.; Collignon, J.; et al. Cubilin, a high affinity receptor for fibroblast growth factor 8, is required for cell survival in the developing vertebrate head. *J. Biol. Chem.* **2013**, *288*, 16655–16670. [[CrossRef](#)]
114. Xuan, S.; Baptista, C.A.; Balas, G.; Tao, W.; Soares, V.C.; Lai, E. Winged helix transcription factor BF-1 is essential for the development of the cerebral hemispheres. *Neuron* **1995**, *14*, 1141–1152. [[CrossRef](#)]
115. Tao, W.; Lai, E. Telencephalon-restricted expression of BF-1, a new member of the HNF-3/fork head gene family, in the developing rat brain. *Neuron* **1992**, *8*, 957–966. [[CrossRef](#)] [[PubMed](#)]
116. Papa, F.T.; Mencarelli, M.A.; Caselli, R.; Katzaki, E.; Sampieri, K.; Meloni, I.; Ariani, F.; Longo, I.; Maggio, A.; Balestri, P.; et al. Clinical Report A 3 Mb Deletion in 14q12 Causes Severe Mental Retardation, Mild Facial Dysmorphisms and Rett-like Features. *Am. J. Med. Genet. Part A* **2008**, *1998*, 1994–1998. [[CrossRef](#)] [[PubMed](#)]
117. Allou, L.; Lambert, L.; Amsellem, D.; Bieth, E.; Edery, P.; Destrée, A.; Rivier, F.; Amor, D.; Thompson, E.; Nicholl, J.; et al. 14q12 and severe Rett-like phenotypes: New clinical insights and physical mapping of FOXP1-regulatory elements. *Eur. J. Hum. Genet.* **2012**, *20*, 1216–1223. [[CrossRef](#)] [[PubMed](#)]
118. Shimamura, K.; Rubenstein, J.L.R. Inductive interactions direct early regionalization of the mouse forebrain. *Development* **1997**, *124*, 2709–2718. [[CrossRef](#)]
119. Houart, C.; Westerfield, M.; Wilson, S.W. A small population of anterior cells patterns the forebrain during zebrafish gastrulation. *Nature* **1998**, *391*, 788–792. [[CrossRef](#)]
120. Aguiar, D.P.; Sghari, S.; Creuzet, S. The facial neural crest controls fore- and midbrain patterning by regulating *Foxg1* expression through *Smad1* activity. *Development* **2014**, *141*, 2494–2505. [[CrossRef](#)]
121. Shanmugalingam, S.; Houart, C.; Picker, A.; Reifers, F.; Macdonald, R.; Barth, A.; Griffin, K.; Brand, M.; Wilson, S.W. *Ace/Fgf8* is required for forebrain commissure formation and patterning of the telencephalon. *Development* **2000**, *127*, 2549–2561. [[CrossRef](#)]
122. Storm, E.E.; Garel, S.; Borello, U.; Hebert, J.M.; Martinez, S.; McConnel, S.K.; Martin, G.R.; Rubenstein, J.L.R. Dose-dependent functions fo *Fgf8* in regulating telencephalic patterning centers. *Development* **2006**, *133*, 1831–1844. [[CrossRef](#)]
123. Fuentealba, L.C.; Eivers, E.; Ikeda, A.; Hurtado, C.; Kuroda, H.; Pera, E.M.; De Robertis, E.M. Integrating Patterning Signals: Wnt/GSK3 Regulates the Duration of the BMP/Smad1 Signal. *Cell* **2007**, *131*, 980–993. [[CrossRef](#)]

124. De Morsier, G. Studies on malformation of cranio-encephalic sutures. III. Agenesis of the septum lucidum with malformation of the optic tract. *Schweiz. Arch. Neurol. Psychiatr.* **1956**, *77*, 267–292.
125. Gregory, L.C.; Gergics, P.; Nakaguma, M.; Bando, H.; Patti, G.; McCabe, M.J.; Fang, Q.; Ma, Q.; Ozel, A.B.; Li, J.Z.; et al. The phenotypic spectrum associated with OTX2 mutations in humans. *Eur. J. Endocrinol.* **2021**, *185*, 121–135. [[CrossRef](#)] [[PubMed](#)]

Disclaimer/Publisher’s Note: The statements, opinions and data contained in all publications are solely those of the individual author(s) and contributor(s) and not of MDPI and/or the editor(s). MDPI and/or the editor(s) disclaim responsibility for any injury to people or property resulting from any ideas, methods, instructions or products referred to in the content.

RESUME

La crête neurale (CN) est une population de cellules multipotentes issues du neurectoderme, à la neurulation, à l'origine de nombreux lignages. Au niveau céphalique, la CN céphalique (CNC) forme les péricytes qui composent les méninges et le stroma des plexus choroïdes (PC) du cerveau antérieur. Les travaux antérieurs de l'équipe ont montré que l'absence de CNC coïncide avec des anomalies cérébrales, consistant en une anencéphalie sévère et une absence de PC. De plus, certains gènes liés chez l'homme à des syndromes neurodéveloppementaux sont soit régulés précocement par la CNC, soit exprimés par les méninges dérivées de la CNC.

Nous avons exploré le lien entre les altérations de méninges et les troubles du comportement à la naissance, et posé l'hypothèse que la CNC contrôle l'homéostasie et l'immunité intra-cérébrale du cerveau antérieur. Pour explorer ces questions, nous utilisons l'embryon de poulet comme modèle : nous avons mis au point un ensemble de tests comportementaux reposant sur le réflexe de "l'empreinte filiale". Grâce à l'accessibilité de l'embryon aviaire à tous les stades de développement, des expériences de micro-injection ont été réalisées et analysées par immunohistochimie sur des coupes histologiques, et sur cerveaux entiers clarifiés, en utilisant la microscopie à feuillets de lumière. Un profil transcriptomique a également été réalisé sur des méninges et des péricytes, cultivés in vitro.

Lorsque des embryons de poussins sont traités au VPA, un anticonvulsivant connu pour provoquer des troubles cognitifs de type autistiques, ils présentent des altérations sévères de leurs interactions sociales après la naissance et une hypervascularisation dans le cerveau. De plus, nous montrons l'implication de cellules dérivées de la CNC dans la veille immunitaire du cerveau en

développement : ces cellules sont capables d'intercepter des agents pathogènes, et confèrent un privilège immunitaire au cerveau. Nos analyses fonctionnelles révèlent que les péricytes dérivés de la CNC sont des cellules immunitaires professionnelles qui expriment des récepteurs immunitaires et des molécules inflammatoires. Une dérégulation de cette fonction immunitaire par le VPA entraîne des effets néfastes sur l'élaboration des fonctions cognitives. De plus, nous montrons que les cellules périvasculaires sont capables de former des pièges d'ADN qui peuvent s'avérer nocifs en provoquant une réaction inflammatoire incoercible. Les péricytes entrant en contact avec le VPA génèrent une décondensation de leur ADN qui se retrouve en grande proportion dans le cytoplasme. Des filaments d'ADN sont aussi observés dans le compartiment extracellulaire. Le VPA tend également à empêcher la migration des péricytes, conduisant à des cellules coopérantes qui produisent des cytokines et aident les cellules affectées par le VPA.

L'utilisation d'un médicament antiangiogénique, le Sunitinib (Suni) permet un sauvetage significatif du comportement social, de l'hypervascularisation dans le cerveau, et de la fonction immunitaire des cellules méningées.

En révélant que ces cellules sont dotées de capacités macrophagiques, et capable de phagocyter des agents pathogènes, nous montrons l'implication des péricytes comme cellules immunocompétentes dans la surveillance immunitaire du cerveau en développement. Nos travaux introduisent un nouvel acteur cellulaire, les cellules périvasculaires dérivées de la CNC, dans la défense du cerveau contre les intrusions pathogènes. Comprendre ces mécanismes présente des implications biomédicales qui revêtent une importance toute particulière pour éclairer l'origine de troubles du comportement, considérés jusqu'à présent comme « cerveau autonome » mais dont nous montrons qu'ils peuvent impliquer des cellules méningées défectueuses.